Intrinsic effects of ubiquitin and SUMO on protein phase separation

Dissertation

Zur Erlangung des Grades

„Doktor der Naturwissenschaften“

(Dr. rer. nat.)

am Fachbereich Biologie

der Johannes Gutenberg Universität Mainz

Philipp Christian Schönberger

Geboren am 08.05.1994 in Mainz

JOHANNES GUTENBERG UNIVERSITÄT MAINZ

Januar 2025

1st examiner:

2nd examiner:

Date of defense: 26.02.2025

Declaration

I, Philipp Schönberger, declare that the work presented in this thesis is my own. I confirm that any information or data obtained from other sources is appropriately indicated in the thesis.

Abstract

Proteins can prefer self-interaction over solvent-interaction, which leads to the formation of protein-enriched biomolecular condensates. This phenomenon is known as phase separation, which controls cellular organization and proteostasis. Aberrant phase separation can result in the formation of cytotoxic aggregates that are hallmarks of several neurodegenerative diseases. The post-translational modifiers (PTM) ubiquitin and SUMO can control phase separation by mediating protein-protein interactions (classical effect), but also by directly changing the biophysical properties of proteins undergoing phase separation (intrinsic effect).

As this intrinsic effect is rather unexplored, I performed an *in vitro* screening to investigate how PTMs alter phase separation of several internally disordered regions (IDRs) derived from neurodegenerative disease-relevant hallmark proteins. I could show that both ubiquitin and SUMO2 generally enhance condensate formation, while SUMO1 has an ambivalent role that depends on the targeted IDR and can act both as an enhancer, but strikingly also as an inhibitor of phase separation. By combining biochemistry methods, structural mass-spectrometry and mammalian cell culture, I was able to reveal how the SUMO1 N-terminus and β_2-sheet inhibit phase separation of the TDP-43 low-complexity domain (LCD) by blocking its self-assembly site. In contrast, I discovered that the SUMO2 N-terminus can switch from a *cis*-interaction with its surface to a *trans*-interaction on another molecule when being attached to a self-assembling protein, which explains the unspecific effect of enhancing condensate formation by SUMO2.

Lastly, I started to investigate the physiological consequences of ubiquitylation and SUMOylation on TDP-43 in a cellular context. I was able to establish a high-throughput platform for screening the effects of distinct PTM-deficiencies on TDP-43 LLPS. Furthermore, I studied the effect of TDP-43 mutants deficient in self-interaction on ubiquitylation and SUMOylation. In summary, these experiments can contribute to an understanding of how ubiquitin and SUMO engage with aberrant TDP-43 phase separation.

Zusammenfassung

Phasenseparierung entsteht, wenn Proteine eine stärkere Präferenz zur Selbstinteraktion statt zur Interaktion mit ihrem Lösungsmittel aufweisen. Dieses Phänomen trägt zur Organisation zellulärer Komponenten bei und steuert die Proteinhomöostase durch die Bildung von biomolekularen Kondensaten. Störungen in der Phasenseparierung können zur Entstehung cytotoxischer Aggregate führen, welche ein entscheidender Faktor für die Entwicklung zahlreicher neurodegenerativer Krankheiten sind. Die post-translationalen Modifikationen Ubiquitin und SUMO können Phasenseparierung regulieren, indem sie Protein-Protein Interaktionen herstellen (klassischer Effekt). Des Weiteren haben sie einen direkten Einfluss auf die biophysikalischen Eigenschaften von phasenseparierenden Proteinen (intrinsischer Effekt).

Diesen intrinsischen Effekt habe ich untersucht, indem ich die Fähigkeit zur Phasenseparierung ungefalteter Domänen aus krankheitsrelevanten Proteinen in Konjugation mit Ubiquitin und SUMO getestet habe. Ich konnte demonstrieren, dass Ubiquitin und SUMO2 Phasenseparierung verstärken, während SUMO1 abhängig vom konjugierten Protein sowohl verstärkend als auch hemmend auf die Phasenseparierung wirken kann. Durch die Anwendung biochemischer Methoden, Massenspektrometrie und humaner Zellkultur konnte ich zeigen, dass N-Terminus und β_2-Faltblatt von SUMO1 die Selbstinteraktionsdomäne eines TDP-43-Fragments blockieren und somit dessen Phasenseparierung inhibiert wird. Im Gegensatz dazu kann der N-Terminus von SUMO2 von einer *cis*-Interaktion mit dessen Oberfläche zu einer *trans*-Interaktion auf einem weiteren SUMO2-Molekül wechseln, was die Phasenseparierung unabhängig des konjugierten Proteins verstärken kann.

Zuletzt habe ich die physiologischen Folgen der Modifikation von TDP-43 mit Ubiquitin und SUMO in einem zellulären Kontext untersucht. Dazu etablierte ich eine Hochdurchsatz-Plattform zur Ermittlung der Konsequenzen fehlender post-translationaler Modifikationen unter zellulärem Stress. Außerdem analysierte ich die Modifikation von TDP-43 mit Ubiquitin und SUMO, wenn Mutanten dessen Phasenseparierung verändern. Insgesamt können diese Experimente zu einem besseren Verständnis der krankhaften Aggregation von TDP-43 in einem neurotoxischen Kontext beitragen.

Content

List of figures

List of tables

1 Introduction

Proteins are fundamental macromolecules defining cells as living matter. Cellular organization of proteins is the key requirement for biological processes. This relies on the ability of proteins to adopt precise structures, building catalytic units and forming binding sites that promote interactions. While these processes often occur in organelles enclosed by membranes, the formation of biomolecular condensates by phase separation can also provide a defined reaction environment. In any case, proteins are further regulated by post-translational modifications (PTMs). PTMs are of diverse nature, reaching from the attachment of a small chemical group as for phosphorylation or acetylation, up to the conjugation of whole proteins like the well-studied proteins ubiquitin and SUMO. As a sum of these complex factors, cells require a tight regulation of protein integrity to maintain a stable environment for the physiological execution of cellular processes. In the following sections, I will introduce the ubiquitin/SUMO system with a particular focus on structural aspects, and the physical process of phase separation in a biological context. The interconnection between these topics and their physiological and pathological relevance is the foundation of this work, aiming to contribute to the better understanding of the development of neurodegenerative diseases.

1.1 Ubiquitin and SUMO

Ubiquitin is an essential protein with the size of 8.6 kDa that is attached as a PTM to lysines and other target sites on a broad range of substrate proteins, leading to the regulation of various cellular processes. The discovery of ubiquitin in 1975 led to the establishment of a whole research field, highlighting its significance with the award of the Nobel Prize in Chemistry in 2004 to Aaron Ciechanover, Avram Hershko and Irwin Rose (Goldstein *et al.* 1975). The complexity of the ubiquitin system originates in the diversity of ubiquitin-like proteins (UbLs) and their ability to be modified with themselves via internal lysines. As a result, polymeric chains of various geometries and compositions with distinct functions can form (Cappadocia and Lima 2018). A simplified set of possible arrangements is shown in **Figure 1**. The most prominent member of the UbL-family is the Small Ubiquitin-like Modifier (SUMO), which has a similar fold like ubiquitin but exists in several isoforms in mammals.

Post-translational modification of targets with ubiquitin and UbLs is a dynamic process that is tightly controlled by dedicated enzymes, called “writers” and “erasers” of the ubiquitin

code. The functional outcome relies on binding partners with dedicated interaction sites that recognize the PTM in a highly specific manner, the so called “readers” (Dikic and Schulman 2023). This can regulate both modified proteins or PTM-interacting proteins, for example by functional activation or inhibition, translocalization throughout the cell, or by affecting protein stability. (Komander and Rape 2012; Flotho and Melchior 2013).

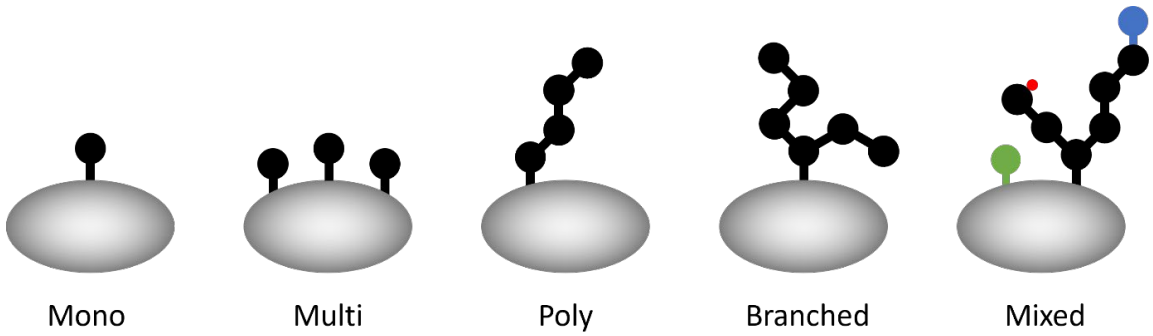

Figure 1: Post-translational protein modification with Ubiquitin and UbLs. Substrates can be conjugated with a single modifier (mono), multiple modifiers (multi), polymeric chains (poly), branched and in a mixed manner, including further modifications like e.g. phosphorylation and acetylation of Ub and UbLs.

1.1.1 Structural and biophysical properties

Ubiquitin and UbLs share a common globular fold, consisting of a β-grasp arrangement and an α-helix (Cappadocia and Lima 2018). While ubiquitin is highly conserved throughout all eukaryotic organisms, SUMO can exist in different isoforms depending on the organism. A single SUMO protein Smt3 exists in *Saccharomyces cerevisiae*, but in contrast, eight SUMO isoforms have been identified in *Arabidopsis thaliana* (Morrell and Sadanandom 2019). In mammalian cells, SUMO1, SUMO2 and SUMO3 are well-studied, while SUMO4 and SUMO5 are often considered as pseudogenes, as their expression is still debated (Celen and Sahin 2020). While SUMO2 and SUMO3 are 98% identical and often considered as SUMO2/3, they only share less than 50% of amino acid sequence identity with SUMO1 (**Figure 2** B). All SUMO isoforms have a sequence identity of less than 20% with ubiquitin (Flotho and Melchior 2013).

SUMO differs from ubiquitin by its flexible and intrinsically disordered N-terminus (**Figure 2** D). The size of the globular core of each modifier is 25-30 Å in diameter, but the flexible N-terminus of SUMO adds an additional element of another 25-30 Å stretched length. Both N-terminus of SUMO1 and SUMO2/3 are rich in charged amino acids and slightly differ in their length (**Figure 2** A).

The secondary structural elements of the core fold are positioned in a comparable arrangement, consisting of β_1-β_2-α-β_3-β_4 that are connected by short unstructured loops. Additional minor secondary structural elements are shown in **Figure 2** A. The last two β-sheets are connected by a largely disordered loop that is negatively charged in case of SUMO. In general, all SUMO isoforms have a higher number of charged amino acid compared to ubiquitin, and furthermore having an overall negative net charge (**Figure 2** C). Ubiquitin has a few well-defined surface patches that mediate protein-protein interactions, as for example the hydrophobic I44- and I36-patches. In contrast, the SUMO α-helix and β_2-sheet provide a large groove as protein binding site (Perry *et al.* 2008; Komander and Rape 2012). The mechanism of ubiquitin and SUMO recognition is further described in **section 1.1.3**. All modifiers are rich in exposed lysines, which can contribute to the formation of polymeric ubiquitin- and SUMO-chains (Ulrich 2008; Li and Ye 2008).

A common C-terminal GG-motif is shared between the modifiers, required for the attachment to substrate proteins. The C-terminal region is exposed and flexible, enabling interaction with the conjugation machinery, which is further elaborated in the next **section 1.1.2**. While the ubiquitin C-terminus is positively charged, SUMO1 harbors a single negatively charged glutamate and SUMO2/3 is largely polar.

Both ubiquitin and SUMO are generally considered as stable and highly soluble proteins under various conditions. These properties led to their usage as fusion partners for recombinant protein production by heterologous overexpression (Panavas *et al.* 2009). Indeed, even the stability and solubility of the fusion target can be altered due to a direct modulation of its biophysical properties (Morimoto *et al.* 2016). This mostly relies on the ability of the modifiers to act as solubilizer that stabilize the fold of aggregation-prone proteins, similar to the maltose-binding protein (MBP), while the exact mechanism has not been elucidated so far (Butt *et al.* 2005).

Sequence alignments and identity, structures and biophysical properties were extracted from publicly available sequences and structures using common bioinformatic tools (Gasteiger *et al.* 2005; Schrödinger and DeLano 2020; The UniProt Consortium 2024).

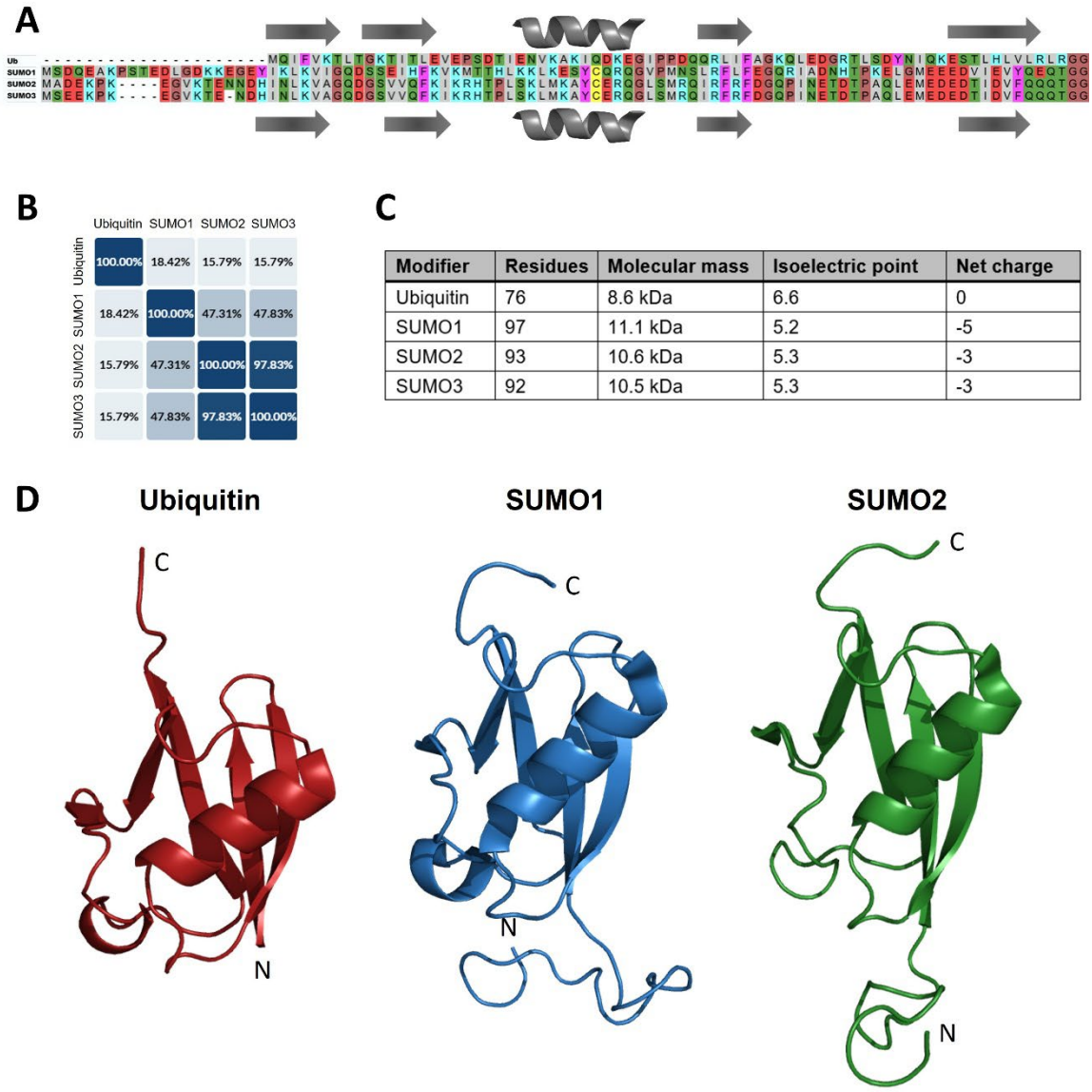

Modifier	Residues	Molecular mass	Isoelectric point	Net charge
Ubiquitin	76	8.6 kDa	6.6	0
SUMO1	97	11.1 kDa	5.2	-5
SUMO2	93	10.6 kDa	5.3	-3
SUMO3	92	10.5 kDa	5.3	-3

Figure 2: Structural overview of ubiquitin and SUMO. (**A**) Sequence alignment of human ubiquitin and SUMO isoforms generated with the Unitprot align tool. (**B**) Sequence identity calculated with the Uniprot align tool. (**C**) Biophysical properties of SUMO. (**D**) Structures of ubiquitin and SUMO visualized with PyMOL. Ubiquitin (PDB:1ubq), SUMO1 (PDB:2kqs), SUMO2 (PDB:2n1w).

1.1.2 Enzymatic machinery for conjugation and deconjugation

Ubiquitin and SUMO are conjugated to target proteins by a dedicated enzymatic cascade (**Figure 3**). This results in their attachment via the C-terminal GG-motif to the ε-amino group of a substrate through the formation of an isopeptide bond. The general process is conserved amongst ubiquitin and UbLs, whereas significant differences between both systems will be highlighted. Ubiquitin is expressed as linear fusions to ribosomal proteins

or as a linear polypeptide chain consisting out of several moieties (Finley *et al.* 1989). In comparison, SUMO is expressed in an immature form, harboring a C-terminal extension of 2-11 amino acid residues that highly differ between the isoforms (Xu and Au 2005). These precursors are processed by specific proteases that are later described in this section, which results in the exposure of the C-terminal GG-motif, which is the attachment site to target proteins.

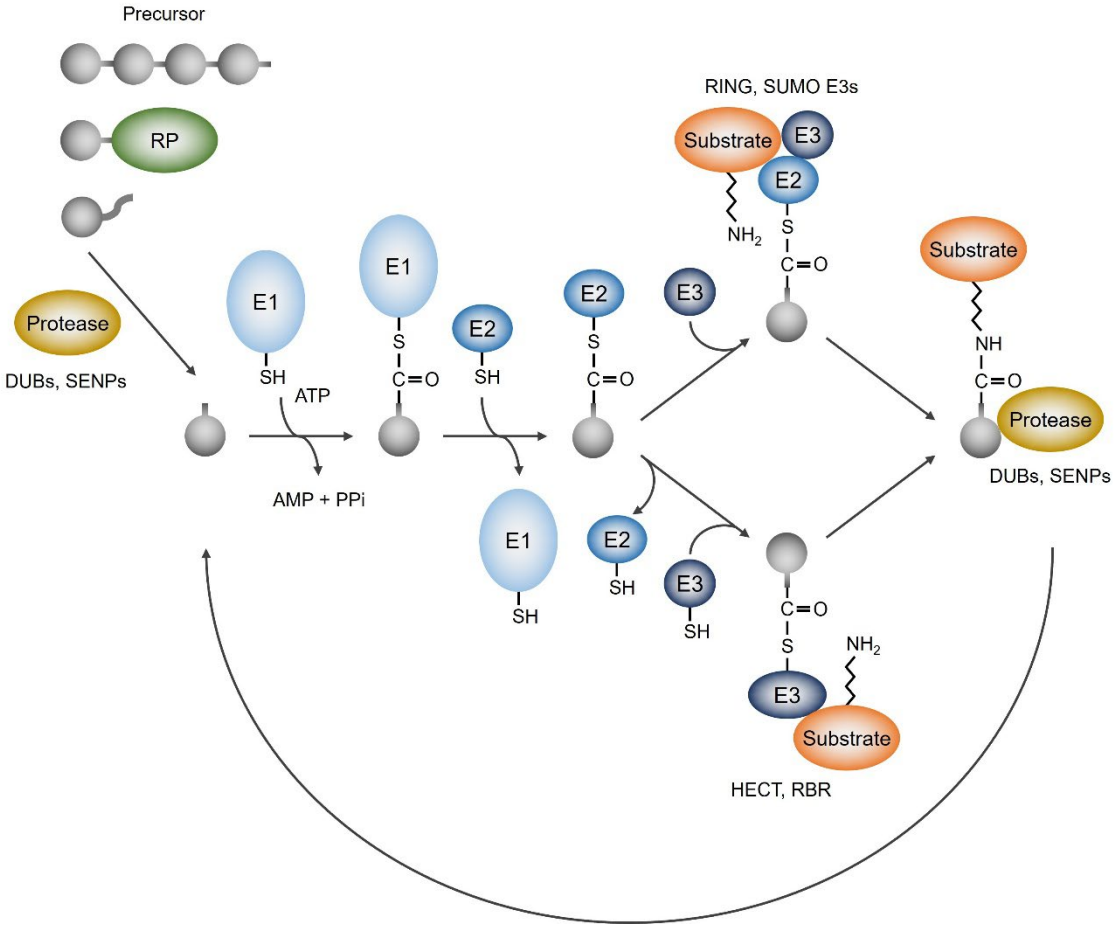

Figure 3: Conjugation and deconjugation of ubiquitin and SUMO. Precursor forms of ubiquitin and SUMO are processed by specific proteases. The modifier gets activated by E1s and transferred to a substrate by E2s. Ligation to the substrate can occur in two different mechanisms depending on the class of E3s. Proteases remove the modifier from the substrate. This figure is adapted from different reviews to combine both the ubiquitin and the SUMO system in one scheme (Pichler *et al.* 2017; Damgaard 2021).

A multi-domain activating enzyme (E1) catalyzes adenylation of the glycine carboxyl-group under the consumption of ATP and forms a highly reactive Ub/SUMO~E1 thioester with a conserved cysteine at the catalytic side of the E1. All E1s have a conserved fold but still show substantial differences. In contrast to the monomeric ubiquitin E1s UBA1 and UBA6, the SUMO E1 SAE1/UBA2 is a heterodimeric protein consisting of separate subunits for

adenylation and thioester. The activated modifier is then transferred to the catalytic cysteine of a conjugating enzyme (E2) via transthiolation, leading to the formation of an Ub/SUMO~E2 thioester bond (Lois and Lima 2005; Schulman and Harper 2009).

Most E2s belong to the UBC-family that share a highly conserved fold. Specific binding sites enable interactions with E1, substrate and ligating enzymes (E3). More than 30 human E2 enzymes have been identified for ubiquitin and there are often distinct combinations of E2s and E3s for targeting a particular substrate or generating a certain type of polyubiquitin linkage (Stewart *et al.* 2016). This is classified into two major mechanisms that depend on the class of E3 enzymes. HECT-type E3s have a catalytic cysteine, which allows transthiolation from the charged E2, resulting in a direct ubiquitin transfer from the E3 to the substrate. Really Interesting New Gene (RING) E3s catalyze the ubiquitin transfer by mediating interactions between Ub~E2 and the substrate. The mechanism of RING between RING (RBR) E3s is an intermediate of both other E3 classes, as this kind of E3 harbors the positioning RING domains and an active site cysteine. This generates a broad variety of enzymes, whereas to this date more than 600 E3 ligases have been identified (Licchesi *et al.* 2020; Yang *et al.* 2021).

The combination of E2s and E3s govern the formation of distinct polyubiquitin chains. This highly depends on the positioning of the enzymatic machinery in relation to the target lysine within ubiquitin. Anchor points can be K6, K11, K27, K29, K33, K48, K63 and the N-terminal methionine. An existing chain of a certain linkage type can be elongated on additional lysines on ubiquitin, resulting in the formation of branched chains. The chain geometry is defined by the position of the linked lysine, leading to different spacings between the ubiquitin moieties. Differently linked polyubiquitin chains are often associated with distinct cellular functions (Fushman and Walker 2010; Akutsu *et al.* 2016; Ivanova *et al.* 2024).

In contrast to ubiquitin, only Ubc9 is known as the sole E2 enzyme in the SUMO system, which is in principle sufficient for the attachment of SUMO to substrates. Ubc9 directly interacts with SUMO consensus motifs (SCMs) consisting of ΨKxE (Ψ = hydrophobic residue) on its substrates. This interaction is based on a weak affinity and the efficiency of the SUMO transfer to its substrate is usually highly enhanced by E3 ligases. Most E3s do so by stabilization of the interaction between SUMO~Ubc9 and the target, or by arranging the components to enhance reactivity for a more effective transfer of SUMO to the acceptor lysine. Since there is no preference of Ubc9 for one SUMO isoform, specificity is mediated by E3 ligases. An exception of this mechanism is the nuclear pore protein RanGAP1 that harbors a unique Ubc9 interaction site and is efficiently modified with SUMO in the

absence of an E3 ligase (Bernier-Villamor *et al.* 2002; Yunus and Lima 2006; Plechanovová *et al.* 2012). In contrast to the ubiquitin system, polymeric SUMO chains have a lower correlation between geometry and function. Both SUMO1 and SUMO2/3 possess internal lysines that participate in chain formation. The most prominent polySUMOylation site is a SCM localized around K11 in SUMO2/3. Moreover, the distal SUMO can be capped with either SUMO1 or further modified with polyubiquitin (Xu *et al.* 2014; Hendriks *et al.* 2018; Sriramachandran *et al.* 2019).

Removal of ubiquitin and SUMO from substrates and depolymerization of chains is accomplished by a set of dedicated proteases, deubiquitinating enzymes (DUBs) and SUMO proteases that cleave between the C-terminal GG-motif and the lysine residue on the target. Hydrolyzation of the isopeptide bond relies on various mechanisms. Cysteine proteases like ubiquitin-specific proteases (USPs) and Sentrin-specific proteases (SENPs) have an active site with a His-Asp-Cys catalytic triad. Proteins of the SENP family can participate both in deSUMOylation and processing of the SUMO precursor. Another DUB family are Zn^{2+}-dependent metalloproteases with a catalytic serine, as for example the K63-linked polyubiquitin-selective DUB AMSH. In any case, deubiquitylation and deSUMOylation lead to release of intact modifiers to the cellular pool, enabling recycling of ubiquitin and SUMO, either as a physiological procedure or in response to stress. The opposing interplay of conjugation and deconjugation machinery and the variety of deconjugating enzymes makes ubiquitylation with all related UbLs a highly dynamic system that enables tight regulation of cellular processes. (Hickey *et al.* 2012; Clague *et al.* 2019; Lange *et al.* 2022).

1.1.3 Biological functions

Ubiquitin and SUMO usually mediate their function by selective recognition of modified proteins via downstream effectors that regulate various pathways.

Ubiquitylation is largely recognized by mostly helical ubiquitin binding domains (UBD). Different classes of UBDs can be selective for monoubiquitylation but often bind to polyubiquitin chains of distinct linkages. The lysine residue forming the linkage determines the distance between the ubiquitin moieties, which is often described as open and closed conformation of ubiquitin chains (Dikic *et al.* 2009). This geometry arranges hydrophobic patches on the ubiquitin surface that are the major interaction sites with UBDs, with the I44-patch being the mostly bound one (Randles and Walters 2012). The most prominent function of ubiquitin is its role in the ubiquitin-proteasome system (UPS). By post-translational modification with K48-linked polyubiquitin chains, proteins can be targeted for

proteasomal degradation by the 26S proteasome via I44-interaction. As a result, the modified protein gets degraded by hydrolysis of the peptide bonds (Chau *et al.* 1989; Komander and Rape 2012). K63-linked polyubiquitin largely has non-degradative functions, as for example in the modification of the DNA sliding clamp PCNA, which enables error-free DNA damage bypass (Stelter and Ulrich 2003). Linear M1-linked polyubiquitin chains

In contrast, the detection of SUMOylation is mostly mediated by so called SUMO interaction motifs (SIM) that consist of short peptide stretches. A hydrophobic core forms the foundation of this interaction, while the charged flanking amino acids define the isoform selectivity (Rabiller 2007). As a result, SUMO interactions occur in a more unspecific way compared to the well-folded UBDs, which often leads to the accumulation of SUMOylated proteins in groups, such as in PML nuclear bodies (PML-NBs) as a response to oxidative stress. The sheer amount of SUMO itself, SUMOylated proteins and proteins with SIMs can form a multivalent network, leading to phase separation of the PML nuclear bodies in a droplet-like dense phase (Sahin *et al.* 2014b; Banani *et al.* 2016). Similarly, the repair of DNA double strand breaks by homologous recombination relies on the recruitment of various DNA repair factors, which undergo group-SUMOylation that holds the repair machinery together (Dou *et al.* 2010; García-Rodríguez *et al.* 2016). This stress-related conjugation is associated with SUMO2/3, while SUMO1 is mainly in a conjugated state under physiological conditions. A large portion of SUMO1 is conjugated to RanGAP1, mediating its localization to the nuclear pore complex protein RanBP2 where it mediates nuclear protein import. In contrast, SUMO2/3 is mostly unconjugated under physiological conditions. In general, SUMO has essential roles in cell cycle, cellular trafficking and genome maintenance (Mahajan *et al.* 1997; Mohanty *et al.* 2022; Gutierrez-Morton and Wang 2024).

An example of a complex intersection between the ubiquitin and SUMO systems are SUMO-targeted ubiquitin ligases (STUbLs). RNF111/Arkadia is a STUbL that uniquely recognizes SUMO2 chains capped with SUMO1 by specific tandem SIMs. In turn, RNF111/Arkadia has RING finger E3 ligase activity, which enables polyubiquitylation of the bound substrate and thus targeting it for proteasomal degradation (Erker *et al.* 2013; Sriramachandran *et al.* 2019). Ubiquitin and SUMO can also compete for the same attachment site, as has been shown for the NF-κB-inhibitor IκBα. The ubiquitin-mediated proteasomal degradation of IκBα can be inhibited if SUMO1 is conjugated to the respective ubiquitylation-site. Yet, the modification with SUMO2/3 even enhances ubiquitylation and degradation of IκBα (Desterro *et al.* 1998; Aillet *et al.* 2012).

In summary, the complexity of this system is a consequence of the interplay between ubiquitin and other UbLs, highly specific binding domains and less specific interaction motifs in a spatiotemporal manner. The overall highly dynamic nature of these processes enables the tight regulation of countless cellular processes.

1.2 Biomolecular condensates form by phase separation

Spatial organization in the cell is largely facilitated by the enclosure of organelles by membranes. The hydrophobicity of the lipid bilayer membrane with membrane-bound proteins of specific functions ensures a boundary that determines the biochemical reactions taking place in the organelle. Mitochondria are an example of how complex functions rely on a multi-membrane system. While the outer membrane controls the uptake of metabolites and proteins, the inner membrane contains the essential components of the electron transport chain for generating ATP and generates a compartment with a suitable environment for the citric acid cycle (Protasoni and Zeviani 2021).

In contrast, sophisticated cellular processes do not necessarily depend on membranes but can also occur in membrane-less organelles (MLOs), such as nucleoli, stress granules and Cajal bodies. Interestingly, MLOs contain a large number of molecules and yet, tightly concentrate them together in the absence of a physical boundary. In recent years, this phenomenon has been explained by the emerging concept of biomolecular condensates formed by liquid-liquid phase separation (LLPS), which has been reviewed multiple times (Hyman *et al.* 2014; Banani *et al.* 2017; Boeynaems *et al.* 2018). Based on theories derived from polymer chemistry and soft matter physics, MLOs can be described as a droplet-like dense phase within the cell. As a result, these droplets provide a distinct environment for biochemical reactions to take place. Due to the liquid-like nature of these droplets, MLOs can be highly dynamic and flexible. LLPS is mainly driven by networks of multivalent interactions, as further explained on stress granules (SGs): G3BP1 is a protein with internally disordered regions (IDRs) that provide multiple interaction sites for RNA under cellular stress, leading to the formation of an MLO. As a consequence, RNA-binding proteins (RBPs) are recruited, enriching the MLO in proteins and nucleic acids (Yang *et al.* 2020; Guillén-Boixet *et al.* 2020). This temporarily protects all components from damaging conditions in a spatiotemporal manner, making SG formation a reversible and dynamic process (Sidibé *et al.* 2021).

The local accumulation of biological macromolecules at high concentration carries the risk of phase transition into a solid-like irreversible condensate, often considered as aggregation. This is suggested to be related to the development of diseases, as protein

aggregation can disrupt major cellular functions. Especially in the context of neurodegenerative diseases, solidification of liquid-like droplets into fibrillar structures has been proposed as a significant factor of pathogenicity (Peskett *et al.* 2018; Morris *et al.* 2024). The origin of neurotoxic aggregation often lies in mutations and aberrant post-translational modification of so-called hallmark proteins as TDP-43, FUS or Huntingtin (Alberti and Dormann 2019).

1.2.1 Material states of biomolecular condensates

Biomolecular condensates can occur in multiple states, ranging from solid-like aggregates to liquid-like droplets. Their nature can be described by applying basic principles of the physical states of matter.

Solids rely on permanent positional arrangements of molecules, which results in a defined shape. Elasticity is a key feature of solid objects, which enables a return to the original shape after deformation. If the molecular interactions cannot compensate for the deformation, the shape can either permanently change or the object can break (Kittel 2005). An example of a solid-like condensate are the neurotoxic beta-amyloid plaques, which are formed by highly stable amyloid fibrils. The tight interaction of this structure makes the formation of this condensate irreversible, which is often the case for solid-like condensates (Chen *et al.* 2017).

In contrast, molecules in liquid objects are not arranged in a higher order, giving them a flexible shape at a defined volume. As a result, this enables a rapid exchange of components within the liquid, and droplets can undergo fusion or fission. The key factor defining the behavior of a liquid is its viscosity. Liquids tend to minimize their boundaries to a minimum, which is why they can appear as spherical droplets (Hamley 2007). An example of an early identified cellular liquid-like condensate are P granules in that dynamically form in germlines of *Caenorhabditis elegans* and consist of multivalent interactions between proteins and RNA (Brangwynne *et al.* 2009; Smith *et al.* 2016).

Gelation is an intermediate state between solid-like and liquid-like behavior. A gel in a biological context relies on the formation of an interaction network that is mainly formed by weak forces. Thus, gel-like condensates display a higher order than liquid-like droplets, but are yet more dynamic than solid-like aggregates. The nature of a gel is defined by its viscoelastic properties (Lieleg and Ribbeck 2011). An isolated FG-repeat domain derived from the nuclear pore complex (NPC) was able to form a hydrogel *in vitro* that resembled the properties of NPCs (Frey and Görlich 2007). Another example for a gel-like condensate

is the maturation of fused in sarcoma (FUS) droplets into a hydrogel, which is held together by cross-β interactions (Kato and McKnight 2021).

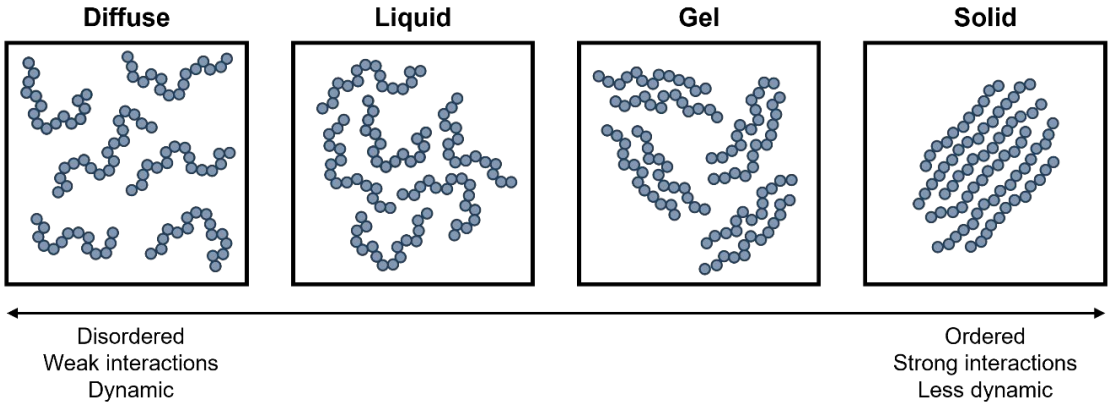

Figure 4: Different material states of biomolecular condensates. Proteins are represented as strings of beads, showing theoretical arrangements for each distinct condensate form. This figure was adapted from (Boeynaems *et al.* 2018)

Biomolecular condensates can often not be exclusively assigned to one particular state. They furthermore can transition from one state into another and change their dynamics, either in a reversible or permanent manner. All aspects of these states must be considered for understanding and describing phase separation in biological systems.

1.2.2 Molecular driving forces of phase separation

All systems tend to minimize their free energy. This must not necessarily result in the complete solution of a molecule in a solvent. Instead, molecules can prefer self-interaction over solvent-interaction if this state is thermodynamically more favorable. This largely occurs when a certain threshold is exceeded, the so-called saturation concentration C_{sat} (Mittag and Pappu 2022). Transferring this concept into a cellular environment, it can be described as the formation of a dense phase enriched in macromolecules, and a dilute phase that would be represented by the cytoplasm. The dense phase can thus be considered as a biomolecular condensate formed by phase separation (Banani *et al.* 2017; Martin and Mittag 2018).

A key requirement for this process is multivalency of the condensate components. Multivalency is based on intra- and intermolecular interactions that drive self-assembly (**Figure 5** A). Concepts derived from polymer chemistry elucidated that multivalent molecules self-assemble into large oligomers while decreasing their solubility (Xu *et al.* 2023). Multivalency can be enabled by folded interaction domains (Banani *et al.* 2016).

For example, RNA-recognition motifs (RRMs) in TDP-43 enhance phase separation by mediating multivalent interactions between RNA and TDP-43 (Grese *et al.* 2021). Self-assembly can also be promoted by internal oligomerization domains, as it is the case for the ribosome biogenesis protein Nucleophosmin1 (Mitrea *et al.* 2018). Furthermore, binding domains for post-translational modifications can also enhance phase separation. A prominent mechanism is the ubiquitylation of histones, leading to the recruitment of ubiquitin-binding proteins that enhance phase separation by forming multivalent networks (Vaughan *et al.* 2021). Finally, isolated secondary structural elements can provide contact sites for self-assembly such as helix-helix interactions or the formation of amyloid-like structures by β-sheets (Conicella *et al.* 2016; Riek 2017).

On the other hand, multivalency can be provided by IDRs that consist of multiple weakly interacting sequence elements. IDRs are especially associated with phase separation, since their conformational flexibility enables promiscuous interactions within biomolecular condensate. In some cases, IDRs can also transiently adopt secondary structures that form or stabilize upon self-interaction. Several IDRs undergoing phase separation have been classified as low-complexity domains (LCDs), which have a limited amino acid residue diversity (Kumari *et al.* 2015). A subclass of LCDs are prion-like domains (PRDs) that are usually rich in polar amino acids and secondary structure breakers like glycine and proline (Alberti *et al.* 2009; Farag *et al.* 2022). LCDs are often composed of repetitive patterns, enabling multivalency by connecting amino acids with reactive side chains (stickers) with flexible amino acids (spacers). The principle of stickers and spacers is also transferrable to multi-domain proteins, as described above. In this case, folded interaction units (sticker) can be connected by unfolded linkers (spacer), enabling flexibility for multivalent interactions (Choi *et al.* 2020).

The type of multivalent interactions of proteins undergoing phase separation relies on their molecular grammar (**Figure 5** B). The presence of uncharged polar amino acids enables weak dipole-dipole interactions between polar regions, or the formation of hydrogen bonds on specific sites. Some PRDs and LCDs contain tyrosine in their sticky motifs, which facilitate π-stacking of the aromatic rings by their delocalized electrons. Aromatic amino acids can further interact with cationic residues of positively charged amino acids. Electrostatic interactions between positively and negatively charged amino acids can promote self-assembly via specific interaction sites, while positively charged side chains can also promote binding to nucleic acids. Finally, hydrophobic contacts reduce the exposure to the solvent and in turn promote phase separation by a reduced solubility (Wang *et al.* 2018b; Murthy *et al.* 2019; Dignon *et al.* 2020; Krainer *et al.* 2021; Farag *et al.* 2023; Holehouse and Alberti 2025).

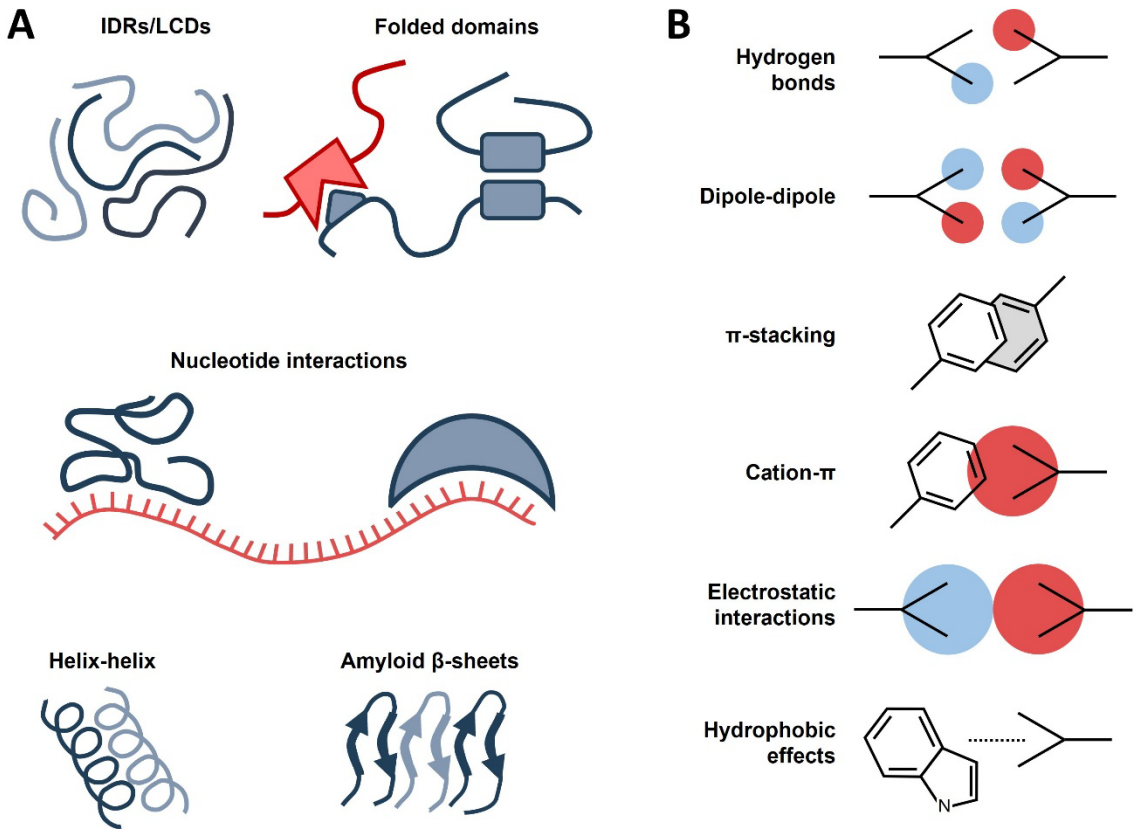

Figure 5: Molecular driving forces of phase separation. (**A**) Motif-driven multivalent interactions. Hetero- and homotypic self-assembly of unfolded IDRs or folded domain proteins (top). Exemplary interaction of sticky IDR or folded RRM with RNA (middle). Interactions of secondary structure elements (bottom). (**B**) Non-covalent interactions driving phase separation. Electron donor side chains are colored in blue, electron acceptor side chains are colored in red. Figure adapted from (Boeynaems *et al.* 2018; Nedelsky and Taylor 2019).

In summary, the diversity of multivalent interactions is very high and enables complex compositions of biomolecular condensates. As a consequence, phase separation can occur due to very distinct causes but also emerge in an unspecific manner.

1.2.3 Regulation of phase separation by environmental factors

Apart from the saturation concentration threshold mentioned above, biomolecular condensates are usually susceptible to temperature changes, due to the critical solution temperature of the scaffold proteins. A large portion of polar and aromatic amino leads to upper critical solution temperature (UCST) behavior, meaning that a protein undergoes phase transition below a certain temperature. Lower critical solution temperature (LCST) phase transition is more associated with proteins containing more hydrophobic amino acids, leading to the formation of a dense phase at higher temperatures. As a consequence, cellular mechanisms emerged that lead to the compartmentalization of

macromolecules upon temperature-related stress into protective granules (Riback *et al.* 2017; Dignon *et al.* 2020).

Especially acidic and basic amino acid residues alter their charge in a pH-dependent manner. Cellular stress, for instance hypoxia, can change cellular pH by the production of lactate. In this case, the decreasing pH neutralizes the charge of acidic amino acids, which would prevent the formation of electrostatic interactions required for phase separation. Even though pH 7.4 is considered as a physiological value, different cellular organelles have distinct pH values, ranging between pH 4.7 in lysosomes and pH 8 in mitochondria. Thus, translocation can severely alter the propensity of a protein to coacervate (Theillet *et al.* 2014; Adame-Arana *et al.* 2020).

Phase separation is highly sensitive to the presence of salt as it determines the ionic strength of a buffer system. Salt-ions are generally classified into salting-in and salting-out effects by the Hofmeister series but the definitive effect on phase separation is determined by the amino acid sequence composition (Baldwin 1996). Salt ions can have concentration-dependent effects on the propensity to promote salting-in and salting-out effects (Duan and Wang 2024). Overall, the impact of salt on phase separation is a complex issue that is not yet fully elucidated. Cells challenge salt perturbations upon osmotic stress, which can not only induce condensate formation but also transition into higher ordered aggregate states (Nott *et al.* 2015; Krainer *et al.* 2021; Grizel *et al.* 2024).

In summary, temperature, pH-value and salt concentrations are important factors that regulate phase separation, which can be perturbed by events of cellular stress.

1.2.4 Cellular organization of biomolecular condensates

Spatiotemporal regulation of phase separation can be controlled by several cellular processes. If a certain event triggers self-assembly of proteins, this eventually leads to the enrichment of macromolecules in a condensate.

Condensates can be composed out of complex networks between scaffold proteins that drive phase separation and client molecules that are recruited into the condensates. Scaffolds are the key components of condensates, which can undergo phase separation if the protein concentration exceeds a certain threshold (**Figure 6** A). Clients can be nucleic acids that interact with specific binding domains of the scaffold, but also other proteins with a limited valency that are less prone to undergo phase separation on their own (Banani *et al.* 2016). For example, the RNA-protective role of stress granules (SG) emerges from the cooperative self-assembly of G3BP with mRNA upon cellular stress, forming the scaffold

components of SGs. Additionally, several ribonucleoproteins (RNPs) are enriched in SGs as clients, while their phase separation largely relies on recruitment into the condensate (Guillén-Boixet *et al.* 2020; Yang *et al.* 2020).

Condensates can occur in heterogenous states resulting in the formation of multiple phases. For example, a solid-like core can maintain condensate stability, while a liquid-like shell provides an environment where the high concentration of macromolecules enables biochemical reactions to take place efficiently (**Figure 6** B). This can also be exemplified with SGs, where RNPs like G3BP and PABP1 together with RNA form a dense core of low dynamics, which stabilizes the condensate and enables specificity of client recruitment. In contrast, the shell is of highly dynamic nature, which facilitates the rapid exchange of components between SGs and cytoplasm (Jain *et al.* 2016; Wheeler *et al.* 2016). Another example for a multiphase condensate is the nucleolus, which is made up of a fibrillar center, a dense fibrillar component and granular component that have been show to be immiscible (Lamaye *et al.* 2011; Feric *et al.* 2016).

As several cellular processes rely on the consumption of energy, ATP is a key regulator of phase separation (Snead and Gladfelter 2019). The depletion of ATP from cells increases the viscosity of both SGs and nucleoli, which relies on the energy-dependent maintenance of condensate dynamics (Brangwynne *et al.* 2011; Jain *et al.* 2016). Furthermore, ATP itself has been described to act as a biological hydrotrope, promoting the solubilization of proteins. The cytoplasm itself is densely packed with proteins up to a concentration of 100 mg/ml. It has been hypothesized that the comparably high concentration of 5 mM cytoplasmic ATP contributes to the maintenance of protein solubility (Patel *et al.* 2017).

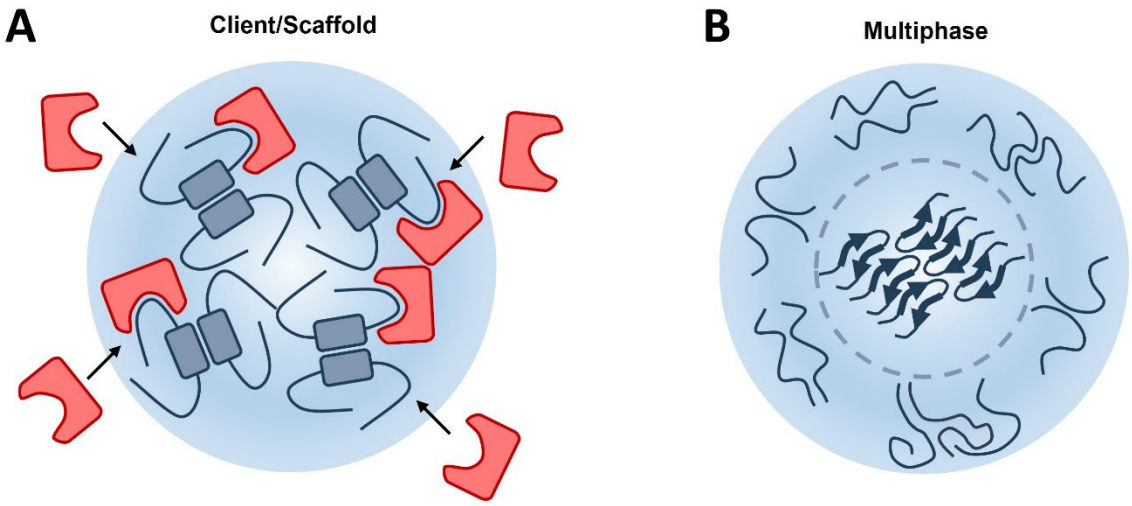

Figure 6: Cellular organization of biomolecular condensates. (**A**) Scheme of a condensate based on self-assembly of a scaffold protein (blue), which leads to the recruitment of clients (red). (**B**) Multiphase condensate with a solid-like core with protein interactions of high order (dashed line) and a liquid-like shell with protein interactions of low order. (**C**) Different theories of PTMs (red) regulating self-assembly. Promotion by specific binding domains, inhibition by blocking interaction sites, addition of multivalent interaction site, alteration of fold integrity. Figure adapted from Banani *et al.*, 2017 and Alberti and Hyman, 2021.

1.2.5 Regulation of phase separation by post-translational modifications

PTMs are versatile regulators of cellular processes and their impact on modulating phase separation is diverse. As described in **chapter 1.1**, the attachment and removal of PTMs is dynamic and can occur in a highly specific manner.

Small PTMs like phosphorylation, acetylation and methylation can alter interactions between amino acids of phase separating proteins. The attachment of a phosphate-group ($-PO_4^{2-}$) adds a significant negative charge to the modification site, which can both promote or inhibit electrostatic interactions. It was furthermore demonstrated, that phosphorylation can reduce TDP-43 self-interaction by promoting protein-solvent interactions, leading to a reduced localization in SGs (Gruijs da Silva *et al.* 2022). Acetylation ($-COCH_3$) of lysine neutralizes the positive charge of its guanidinium group (Ali *et al.* 2018). This can especially disrupt RNA-dependent phase separation, such as in acetylation of the RRM in FUS (Arenas *et al.* 2020). Methylation ($-CH_3$) alters charge distributions and bulkiness leading to a reduced propensity to form hydrogen bonds (Fuhrmann *et al.* 2015). It has been shown, that the self-assembly mechanism of FUS is perturbed upon methylation of arginine in the C-terminus, which reduces the strength of cation-π interactions with N-terminal tyrosines, resulting in a decreased accumulation of FUS in SGs (Hofweber *et al.* 2018; Qamar *et al.* 2018).

While the impact of small PTMs on biomolecular condensate regulation can often be explained by the chemical nature of the modification, protein-based PTMs such as ubiquitin and SUMO can affect phase separation in a more complex manner. The primary mode of action of both modifiers is the regulation of protein-protein interactions (**chapter 1.1.3**). It is thus not surprising, that ubiquitin binding can promote phase separation by mediating self-assembly of scaffold proteins through specific UBDs (Waite *et al.* 2024). In case of the NF-κB modulator NEMO, binding of M1-linked ubiquitin chains induces phase separation of NEMO, which is required for its kinase-activating function (Du *et al.* 2022; Goel *et al.* 2023). Ubiquitin binding can also have the opposite effect by blocking self-assembly sites. The protein quality control shuttle protein UBQLN2 self-interacts across various domains, including an UBA domain. If this UBA domain is occupied by ubiquitin, phase separation of UBQLN2 is disrupted via a reduction of multivalency (Dao *et al.* 2018). Interestingly, polyubiquitin chain binding alters UBQLN2 phase separation depending on chain geometry and the resulted exposure of the hydrophobic I44-patch. Closed conformation K48- and K11-linked chains inhibit UBQLN2 phase separation, while open conformation K63- and M1-linked chains act as enhancers, suggesting that ubiquitin chains can follow self-assembly behavior of polymers, as described in **chapter 1.2.2** (Dao *et al.* 2022).

SUMO can regulate phase separation similarly like ubiquitin, as it can be illustrated on PML-NBs. PML is the scaffold protein of PML-NB condensates and self-assembles by the formation of disulfide-bonds upon oxidative stress (Zhang *et al.* 2010). This triggers the recruitment of the SUMO-E2 Ubc9, resulting in SUMOylation of PML and a subsequent enrichment of SIM-harboring proteins in the NBs, following the client-scaffold principles. On the other side, PML itself harbors internal SIMs, leading to the sequestration of more SUMOylated proteins (Sahin *et al.* 2014a). Upon this positive feedback loop, PML-NB condensate size increases by excessive SUMOylation (Hirano and Udagawa 2022). The STUbL RNF4 targets SUMOylated NB-components for proteasomal degradation, which resolves the condensates. (Keiten-Schmitz *et al.* 2021).

These complex networks rely on multiple specific binding domains and motifs and can be considered as the classical effect of how ubiquitin and SUMO regulate condensate formation by mediating protein-protein interactions. However, several publications suggest that ubiquitin and SUMO might regulate phase separation of conjugated substrates by directly affecting their biophysical properties, which can be referred to as the intrinsic effect. As described in **chapter 1.1.1**, both ubiquitin and SUMO are considered highly soluble and stable. Experimental *in vitro* studies demonstrated that it requires high protein concentrations of ~1 mM and the presence of molecular crowding agents (10% (w/v) PEG-

8000) for ubiquitin to undergo phase separation, which seem to mainly rely on hydrogen bonds and van der Waals interactions (Poudyal *et al.* 2023). SUMO1 has been shown to phase separate at 120 µM in the presence of 15% (w/v) PEG-20000 (Arora *et al.* 2023). These studies suggest both ubiquitin and SUMO have potential self-interaction sites under certain conditions.

The stable fold of ubiquitin has been described to decrease upon chain formation with increasing length, enabling the formation of amyloid-like fibrils after heat- or shear-stress (Morimoto *et al.* 2015). The attachment of ubiquitin can even destabilize the fold of conjugated substrates close to the attachment site. The capability of unfolding depends on the type of secondary structure, while the strongest impact was observed when ubiquitin was attached to a β-sheet (Morimoto *et al.* 2016). SUMO-conjugation has been shown to induce a conformational change of the human thymine-DNA glycosylase (TDG) controlling dissociation of abasic sites at damaged DNA. Although conjugation occurred at the TDG C-terminus, SUMO mediates a *cis*-interaction with the N-terminal domain (Steinacher and Schär 2005).

In summary, ubiquitin and SUMO can regulate phase separation beyond the promotion of protein-protein interactions. Several studies suggest the relevance of an intrinsic effect on the formation of biomolecular condensates that relies on PTM-induced fold alteration of scaffold proteins and internal self-assembly sites within the PTM. A theoretical overview of simplified models is provided in **Figure 7**. However, the actual impact of this intrinsic effect on phase separation needs yet to be revealed.

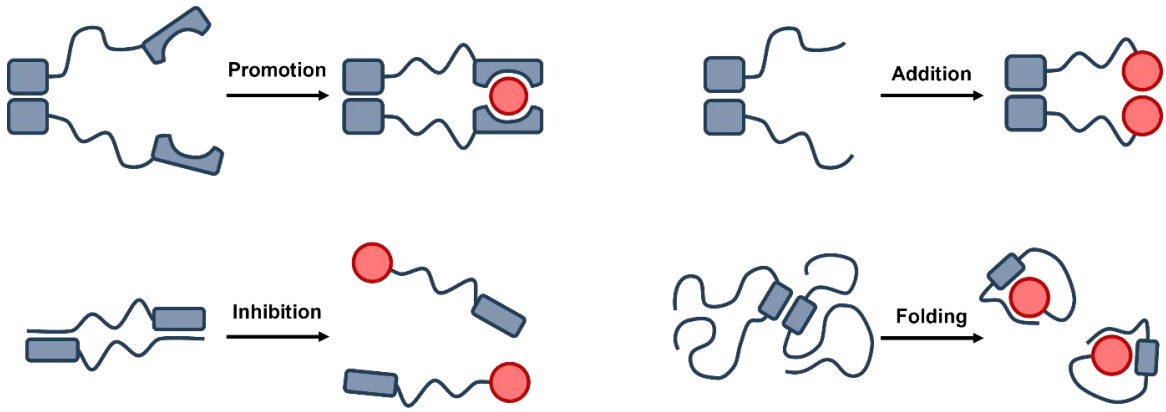

Figure 7: Regulation of self-assembly by PTMs. Different theories of PTMs regulating self-assembly. Promotion by specific binding domains, inhibition by blocking interaction sites, addition of multivalent interaction site, alteration of fold integrity. Self-assembly domains are generically indicated as rectangles. PTMs are represented as red cirlces.

1.2.6 Aberrant phase transition

Local accumulation of proteins through LLPS can promote the formation of aggregates, which is a hallmark of several neurodegenerative diseases (Zbinden *et al.* 2020; Wu *et al.* 2024). As described in **chapter 1.2.1**, aggregates possess solid-like properties and display both low dynamics and a highly ordered stable conformation. Neurotoxic solidification can occur spontaneously or due to genetically inherited mutations in disease-related proteins (Masrori and Van Damme 2020). These mutations can affect their multivalency and result in altered mechanisms of self-assembly, increasing the propensity to undergo solidification. Mutations in nuclear localization sequences (NLS) can induce cytoplasmic accumulation. The resulting formation of mislocalized condensates can severely affect the recruitment of macromolecules following the client-scaffold principle. Finally, mutations in PTM conjugation sites and PTM binding domains can alter interactions with binding partners or change the biophysical properties of biomolecular condensate components. All these mechanisms can increase the propensity of self-assembling proteins to act as a seed for aggregation through nucleation (Johnson *et al.* 2009; Suk and Rousseaux 2020; Gupta *et al.* 2021).

While liquid-like condensates often display a certain dynamic that enables a specific function, solidification can be associated with a toxic loss-of-function, but also gain-of-function if perturbing factors are recruited (Hayes and Kalab 2022). Aggregation can manifest by the irreversible formation of highly ordered structures, the entanglement of disordered proteins or transient vitrification, forming highly viscous condensates. In any case, solidification severely slows down or inhibits biological processes, which explains why aggregates are mostly considered as cytotoxic (Watanabe 1999; Halfmann 2016; Peskett *et al.* 2018).

1.2.7 Pathological relevance

Neurodegenerative diseases are classified by a progressive loss of neurons, leading to a severe impairment of memory, cognition and motion (Gorman 2008). Each disease can be associated with particular hallmark proteins, which often aggregate and mislocalization into the cytoplasm, leading to the formation of neurotoxic inclusions (Liu *et al.* 2021; Wu *et al.* 2024). How these hallmark proteins exert their toxicity is described using TDP-43, FUS and Huntingtin and their associated diseases as examples. An overview of their domain-organizations is shown in **Figure 8**, highlighting important disease-related mutations and PTM-sites of ubiquitin and SUMO.

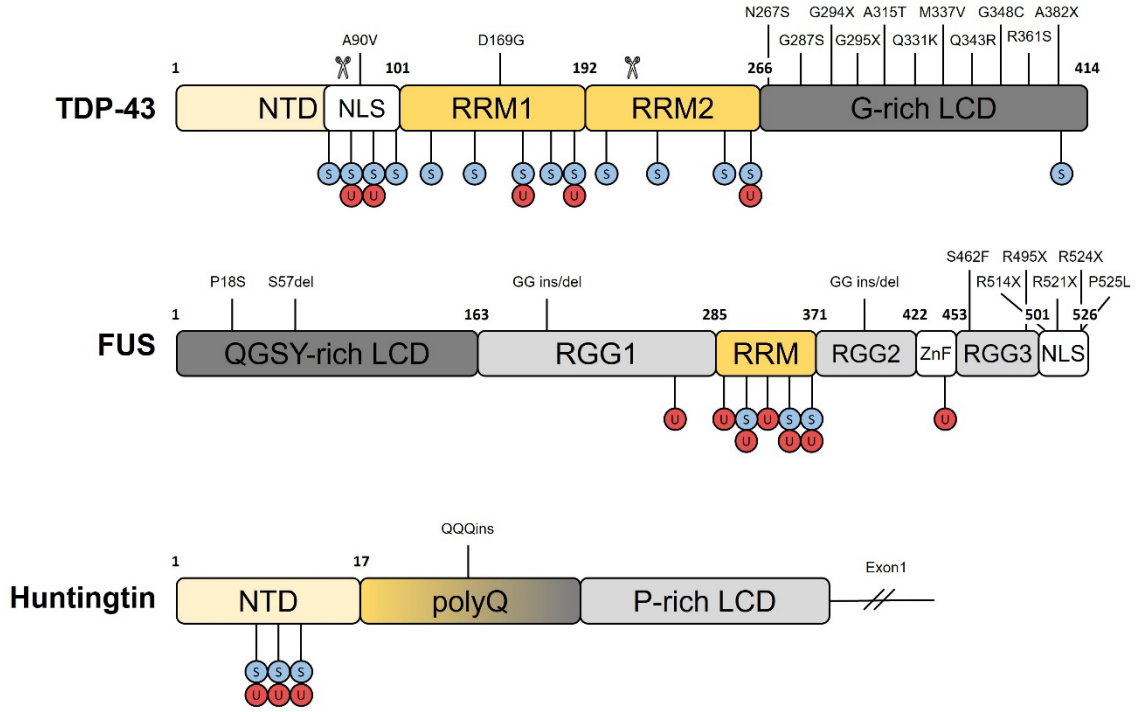

Figure 8: Hallmark proteins of neurodegenerative diseases. Domain organization of TDP-43, FUS and Htt-Ex1. Folded domains are colored in yellow, unstructured domains are colored in grey. Approximate ubiquitylation and SUMOylation sites are implicated by red and blue circles. A set of important disease-related mutation sites is implicated above each domain (X=≥2 substitutions). Arrangement, mutations and PTM-sites are adapted from current publications and phosphosite.org (Dormann and Haass 2013; Hornbeck *et al.* 2015; Jo *et al.* 2020; Elena-Real *et al.* 2023). Caspase-cleavage sites are indicated by a scissor (Zhang *et al.* 2009).

1.2.7.1 TDP-43

Amyotrophic lateral sclerosis (ALS) is a fatal disease that results in the degeneration of upper and lower motor neurons, which control voluntary muscle movements. With the disease progression, patients face muscle weakening, paralysis and eventually respiratory failure. ALS mostly occurs sporadically, while less than 10% can be related to familial inheritance. Cytoplasmic aggregation of the TAR DNA-binding protein 43 (TDP-43) is a key hallmark in ~97% of patients, suggesting a crucial role of this protein in the development of ALS (Masrori and Van Damme 2020; Mead *et al.* 2023). TDP-43 also has pathological roles in Frontotemporal dementia (FTD), which is discussed in the next **chapter 1.2.7.2**

TDP-43 is a primarily nuclear multi-domain protein that has various functions in RNA metabolism and undergoes phase separation under physiological conditions. As a splicing factor, it can regulate exon skipping and inclusion of pre-mRNA (Cheng *et al.* 2024). Its shuttling function allows the transport and stabilization of mRNA in the cytoplasm (Ratti

and Buratti 2016; Maraschi *et al.* 2021). Several studies further implicate that TDP-43 maintains neuronal physiology by transporting mRNA across axons, or regulating branching of dendrites (Alami *et al.* 2014; Herzog *et al.* 2017).

TDP-43 is largely disordered, while some domains have distinct structures. The N-terminal domain (NTD) is partially folded into an ubiquitin-like β-grasp arrangement, which induces oligomerization and is essential for the splicing activity of TDP-43 (Mompeán *et al.* 2016; Jiang *et al.* 2017). A disordered linker harbors a bipartite classical NLS that is recognized by importin (Doll *et al.* 2022). This region also harbors a caspase cleavage-site, which can generate an aggregation-prone TDP-35 C-terminal fragment (CTF-35) (Zhang *et al.* 2009). Two conserved RRMs are connected by a flexible linker and display a typical RRM-fold, consisting out of a five-stranded antiparallel β-sheet stacked on two α-helices. Interactions between both RRMs arrange both domains in a specific conformation that results in a preference for binding TG-/UG-rich nucleic acids. Another caspase cleavage-site results in the generation of a TDP-25 CTF (CTF-25) (Lukavsky *et al.* 2013; Li *et al.* 2015; Furukawa *et al.* 2016). The C-terminal LCD is a disordered region that is rich in glycine and polar uncharged amino acids. A transient helical region forms the major self-assembly site, which is further supported by a few aromatic amino acids distributed across the domain. (Conicella *et al.* 2016; Li *et al.* 2018). Furthermore, the LCD is a major protein-protein interactions site and can undergo aggregation by forming amyloid fibrils on its own (Babinchak *et al.* 2019; François-Moutal *et al.* 2019).

The exact mechanism of how aberrant TDP-43 promotes neuronal pathogenicity in ALS patients remains elusive but is considered to occur due to severely impaired protein homeostasis and RNA metabolism as key malfunctions in neurons. Yet, it is broadly suggested that neurotoxic inclusions of TDP-43 arise from its cytoplasmic mislocalization and aggregation (Tziortzouda *et al.* 2021). A theory of cytoplasmic enrichment is based on the recruitment of TDP-43 into SGs upon cellular stress, resulting in a nuclear depletion of TDP-43. Prolonged stress can impair SG resolution, leading to a transition of liquid-like TDP-43 condensates into solid-like aggregates. Trapping of TDP-43 in these inclusions inhibits its nuclear functions in RNA processing (Khalfallah *et al.* 2018; Ratti *et al.* 2020). Cytoplasmic enrichment is also promoted by the caspase-mediated cleavage of TDP-43 into CTFs, as both CTF-35 and CTF-25 lack the NLS. *In vitro* studies showed that CTFs are highly susceptible to undergo aggregation (Igaz *et al.* 2009; Kitamura *et al.* 2016). Several mutations have been found in familial ALS patients and can alter self-assembly, mislocalization and cleavage. In particular, mutations in the LCD have been described to enhance aggregation and toxicity in yeast and neurons (Johnson *et al.* 2009; Guo *et al.* 2011).

Aberrant post-translational modification of TDP-43 is a key signature of ALS, as hyperphosphorylation and polyubiquitylation was detected early in post-mortem brain cells of patients (Neumann *et al.* 2006; Neumann *et al.* 2009a). Phosphorylation occurs mainly in the LCD and relies on multiple kinases. It is suggested to directly regulate both aggregation and cytoplasmic mislocalization of TDP-43, while the distinct impact is still debated (Hans *et al.* 2020; Gruijs da Silva *et al.* 2022). Also, Neuronal inclusions have been found to be enriched in M1-, K48- and K63-linked ubiquitin chains (Nakayama *et al.* 2020). Interestingly, ubiquitylation is suggested to affect TDP-43 beyond proteasomal degradation. A direct interaction between the E2-conjugating enzyme UBE2E3 and TDP-43 reduces its solubility (Hans *et al.* 2014). The E3-ligating enzyme Parkin forms K48- and K63-linked chains on TDP-43, which promotes cytoplasmic mislocalization in a non-degradative manner (Hebron *et al.* 2013). In addition, the role of SUMOylation in TDP-43 pathogenicity has recently emerging. *In vitro* experiments showed that global inhibition of SUMOylation reduces the abundancy of TDP-43 aggregates and mutation of K136 in the RRM1 shifts TDP-43 aggregates from the cytoplasm to the nucleus. Interestingly, a SUMOylation site at K408 is embedded between two phosphorylation sites and has been shown to facilitate the cellular stress response (Maurel *et al.* 2020; Suk *et al.* 2024).

1.2.7.2 FUS

Frontotemporal dementia (FTD) is the second most common form of dementia after Alzheimer's disease and is defined by frontotemporal lobar degeneration (FTLD) as a key hallmark. Major symptoms are behavioral changes and language difficulties, progressing into severe cognitive impairments that eventually result in the patient's death (Rademakers *et al.* 2012; Antonioni *et al.* 2023). Several genetic and clinical overlaps have been shown for ALS and FTD, and patients can be affected from both diseases. Indeed, ~45% of neuronal inclusions in FTD patients are enriched in TDP-43. Moreover, the DNA/RNA-binding protein fused in sarcoma (FUS), has a rather pivotal role in ALS but is detected in ~9% of inclusions in FTD patients, caused by a related phenotype of cytoplasmic aggregation (Ling *et al.* 2013).

Similar like TDP-43, FUS has various roles in RNA metabolism but also participates in DNA repair (Zhou *et al.* 2014). FUS is largely disordered and consists of multiple domains. The N-terminal QGSY-rich domain has PRD characteristics and mediates FUS phase separation without forming transient secondary structures as observed in case of the LCD of TDP-43 (Murthy *et al.* 2019). Two RGG-rich domains, a zinc finger (ZnF) and an RRM are majorly involved in nucleic acid binding and another RGG-rich domain forms a non-

classical NLS together with a C-terminal PY-rich domain (Dormann *et al.* 2012; Loughlin *et al.* 2019).

How FUS accomplishes its neuropathogenicity is still not entirely revealed. Several mutations in the NLS have been identified to induce cytoplasmic mislocalization by disrupting the interaction between FUS and the nuclear import receptor Kapβ2. Mutations are rather associated with ALS and have only rarely been observed in *post mortem* tissue of FTD patients (Dormann *et al.* 2010; Rademakers *et al.* 2012; Nolan *et al.* 2016). In FTD patients, RGG-domains occur unmethylated, which also increases the interaction with Kapβ2 and moreover enhances phase separation of FUS (Dormann *et al.* 2012; Hofweber *et al.* 2018). FUS-positive inclusions from FTD patients have been shown to be enriched with ubiquitin. Several ubiquitylation and SUMOylation sites have been identified mostly in the RRM but the impact of both modifiers on FUS pathology remains to be elucidated (Neumann *et al.* 2009b; Mertins *et al.* 2013; Lumpkin *et al.* 2017).

1.2.7.3 Huntingtin

Huntington's disease (HD) is a genetically inherited disorder that mainly affects basal ganglia and causes deterioration of motoric and cognitive functions, as well as personality changes. It originates from a CAG expansion in the *HTT* gene, leading to abnormally long polyQ-stretches in the disease's hallmark protein huntingtin. The resulting aggregation of huntingtin promotes cell death (MacDonald *et al.* 1993; Scherzinger *et al.* 1999).

Huntingtin is a highly conserved and ubiquitously expressed protein, which has a broad range of functions primarily in neurons. As a shuttle protein, it participates in transcription but also in vesicle trafficking across axons and dendrites (Truant *et al.* 2007; Marques Sousa and Humbert 2013; Saudou and Humbert 2016). Pathological inclusions in HD patients are enriched in huntingtin-exon1 (Htt-Ex1), which originates from incomplete splicing of *HTT* or caspase-cleavage of full-length huntingtin (Graham *et al.* 2006; Neueder *et al.* 2017). Htt-Ex1 forms liquid-like condensates by phase separation that can act as seeds for aggregation. Aggregation propensity increases with polyQ-stretch length above Q36, while Q40 is the critical threshold that evidently result in the development of HD (Bates *et al.* 2015; Peskett *et al.* 2018).

Htt-Ex1 is composed of an NTD, a polyQ-stretch and a C-terminal proline-rich region. The helical NTD contributes to both LLPS and fibril formation. The polyQ-stretch is conformationally flexible but mostly helical, while the helical content is enhanced with increasing length. The resulting helix-helix interactions are the key driver of Htt-Ex1 aggregation. The proline-rich C-terminal region only occurs in mammals and has both

helix-unwinding and fibril-destabilizing effects (Tartari *et al.* 2008; Shen *et al.* 2016; Posey *et al.* 2018; Elena-Real *et al.* 2023).

Three lysine residues in the NTD can be modified with ubiquitin or SUMO. SUMO1-conjugation reduces aggregation of Htt-Ex1 in cell culture experiments but leads to enhanced neurodegeneration in a *Drosophila* disease model. Ubiquitin competes for the same conjugation sites and has been shown to enhance aggregation while abrogating neurodegeneration (Steffan *et al.* 2004). Interestingly, a lack of ubiquitylation reduces the size of Htt-Ex1 aggregates, which are more toxic for the cell. Overall, the mutation of the respective lysines K6, K9 and K15 resulted in reduced pathogenicity of Htt-Ex1 (Hakim-Eshed *et al.* 2020). It has been shown that PIAS1 is the key E3 for the modification of Htt-Ex1 not only with SUMO1 but also with SUMO2. When the authors looked into larger Htt-fragments, they found that the overexpression of SUMO2 resulted in the accumulation of aggregated Htt with elongated polyQ-stretches (O'Rourke *et al.* 2013). This draws a complicates picture of the interplay between ubiquitin and different SUMO isoforms regulating the toxicity of Htt, which seem to rely on the polyQ-stretch length.

1.3 Aims of this work

Ubiquitin and SUMO are versatile post-translational modifiers that are involved in countless cellular processes. Hence, it is not surprising that diseases can develop when the enzymatic machinery of the ubiquitin and SUMO systems is dysregulated. Ubiquitin has early been detected to be enriched in neuronal cytoplasmic inclusions, which occur in cells of neurodegenerative disease patients (Manetto *et al.* 1988). Moreover, aggregated TDP-43 as a hallmark protein in ALS and FTLD has been described to be both ubiquitylated and SUMOylated (Neumann *et al.* 2006; Wood *et al.* 2021).

Several hallmark proteins of neurodegenerative diseases form biomolecular condensates by phase separation, while this can be a precursor step into neurotoxic aggregation (Peskett *et al.* 2018; Ray *et al.* 2020). Ubiquitin and SUMO can regulate phase separation by mediating protein-protein interactions (classical effect), but it has also been shown that they can directly alter the biophysical properties of their conjugated target protein (intrinsic effect) (Morimoto *et al.* 2016; Dao *et al.* 2018).

The aim of this work is to explore and define the intrinsic effect of ubiquitin and SUMO on phase separation, which is only marginally studied to this point. Therefore, a set of IDRs derived from pathologically relevant disease hallmark proteins will be modified with either ubiquitin, SUMO1 and SUMO2 and analyzed for their propensity to form condensates in an *in vitro* screening approach. TDP-43(LCD) will be further used as a model protein to reveal the molecular mechanisms of how SUMO1 and SUMO2 regulate phase separation. Finally, the functional consequences of post-translationally modified full-length TDP-43 will be studied in a physiological context using cell-based assays. The results aim to contribute to a better understanding how TDP-43 undergoes aberrant phase separation as a hallmark of neurodegenerative diseases. A key issue to be revealed is if aberrant phenotypes are a result of the post-translational modification, or if PTMs are conjugated to regulate the pathogenicity.

2 Material and Methods

2.1 Reagents

2.1.1 Chemicals

Unless otherwise stated, all chemicals and kits used in this work were purcharsed from Carl Roth, Sigma-Aldrich or Thermo Fisher Scientific. Chemical purchases from other suppliers are listed below:

Atto-TEC	Atto594-maleimide, Atto647-maleimide
BioRad	20x Trans-Blot Turbo buffer
BioTrend	IPTG
Biozol	Thioflavin T
Cell signaling	DRAQ5
Enzo Life Science	MG-132
Fluoroprobes	AzDye488-maleimide
Life Technologies	SYBR Safe DNA stain
MedChemExpress	TAK-243
Macherey-Nagel	Nucleo Bond Xtra Midi Plus
New England Biolabs	10x CutSmart, DNA ladders, dNTPs
Qiagen	RNeasy Mini Kit, RNase-free DNNase Set, NiNTA agarose
Promega	FuGene HD transfection reagent
Roche	cOmplete Protease Inhibitor Cocktail

2.1.2 Proteins and peptides

Table 1: Commercial proteins used in this work

Protein	Supplier
Bovine serum albumin (BSA)	Sigma-Aldrich
DNA Ligation Kit	Takara
DpnI	CF15 - IMB
FastAP Alkaline Poshpatase	Thermo Fisher Scientific
Gibson assembly mix	CF15 - IMB
Herculase II DNA-polymerase	Agilent
HF DNA-polymerase	CF15 - IMB
His-3C protease	CF15 – IMB
His-TEV protease	CF15 – IMB
Lysozym	Merck
PfuUltra DNA-polymerase	Agilent
Quick blunting kit	New England Biolabs
Restriction endonucleases	New England Biolabs
Sm Nuclease	CF15 - IMB
T4 Polynucleotide Kinase	New England Biolabs
Taq DNA-polymerase	CF15 - IMB

Table 2: Peptides used in this work

Peptide	Sequence	Supplier
SUMO1-Nt	MSDQEAKPSTEDLGDKKEG	ProteGenix
SUMO1-β_2	EIHFKVK	ProteGenix

2.1.3 Antibodies

Table 3: Primary antibodies used in this work

ID	Name	Species	Source	Dilution
24	mCherry	Mouse	Abcam	1:2500
49	GFP	Mouse	Roche	1:1000
51	GFP	Rabbit	Invitrogen	1:1000
223	SUMO2	Mouse	Frauke Melchior, ZMBH	1:20
442	Ubiquitin	Rabbit	Bio-Techne	1:1000
463	TDP-43	Rabbit	Proteintech	1:1000
471	SUMO1	Rabbit	St. Johns Laboratory	1:1000

Table 4: Secondary antibodies used in this work

ID	Name	Species	Source	Dilution
91	Mouse 680LT	Donkey	Licor	1:10000
92	Mouse 800CW	Donkey	Licor	1:10000
96	Mouse HRP	Goat	Sigma	1:10000
154	Rabbit 680LT	Donkey	Licor	1:10000
155	Rabbit 800CW	Goat	Licor	1:10000
156	Rabbit HRP	Goat	Pierce	1:10000

2.2 Media and solutions

2.2.1 Media for cultivation of *E. coli*

E. coli strains for isolation of Plasmid DNA were grown on Luria Broth (LB) agar plates or in liquid LB medium. For protein expression, *E. coli* strains were either grown in LB media or Terrific Broth (TB) medium, depending on the availability. Appropriate antibiotics for selection were added in concentrations as stated in the following table.

Table 5: List of antibiotics used for the cultivation of *E. coli*.

Antibiotic	Final concentration [µg/ml]	Supplier
Ampicillin	100	CF06 - IMB
Chloramphenicol	34	CF06 - IMB
Kanamycin	30	CF06 - IMB

2.2.2 Media for cultivation of mammalian cells

Mammalian cells were cultivated in Dulbecco's Modified Eagle Medium (DMEM) supplemented with 10% (v/v) fetal bovine serum (FBS), 2 mM L-glutamine, 100 U/ml penicillin and 100 µg/ml streptomycin. Additional antibiotics for selection and maintenance of integrated plasmids are stated in the following table.

Table 6: List of antibiotics used for the cultivation of mammalian cells.

Antibiotic	Final concentration [µg/ml]	Supplier
Blasticidin	15	InvivoGen
Hygromycin	150	InvivoGen
Zeocin	100	InvivoGen

2.2.3 Buffers and solutions

General solutions were prepared by the media lab of IMB (CF06) following standard recipes: 0.5 M EDTA, 1 M KCl, 2 M $MgCl_2$, 5 M NaCl, 5x PBS, 10x TBE, 1 M Tris-HCl pH 7.5. All recipes listed below were prepared in H_2O_{dd} if not otherwise stated.

Anion exchange buffer A: 50 mM Tris pH 7.4, 50 mM NaCl

Anion exchange buffer B: 50 mM Tris pH 7.4, 1 M NaCl

Blocking solution: 5% (w/v) skim milk powder in PBS-T

Cation exchange buffer A: 25 mM Sodium acetate pH 4.5, 50 mM NaCl

Cation exchange buffer B: 25 mM Sodium acetate pH 4.5, 1 M NaCl

Denaturing pulldown buffer 1: 6 M Gua-HCl, 50 mM NaH_2PO_4, 50 mM Na_2HPO_4, 10 mM Tris-HCl pH 8, 0.1% (v/v) Tween20

Denaturing pulldown buffer 2: 8 M Urea, 80 mM NaH_2PO_4, 20 mM Na_2HPO_4, 10 mM Tris-HCl pH 6.3, 0.1% (v/v) Tween20

IMAC A buffer: 30 mM Tris-HCl pH 8, 300 mM NaCl, 15 mM imidazole

IMAC B buffer: 30 mM Tris-HCl pH 8, 300 mM NaCl, 500 mM imidazole

MES buffer: 50 mM MES, 50 mM Tris base pH 7.3, 0.1% (w/v) SDS, 1 mM EDTA

MOPS buffer: 50 mM MOPS, 50 mM Tris base pH 7.7, 0.1% (w/v) SDS, 1 mM EDTA

PBS-T: 0.1% (v/v) Tween20 in PBS

Ponceau S solution: 0.1% (w/v) Ponceau S in 5% (v/v) acetic acid

RIPA buffer: HEPES pH 7.4, 100 mM NaCl, 2.5 mM MgCl2, 0.1% (w/v) SDS, 0.5% (w/v) Sodium deoxycholate, 1% (w/v) NP-40

Simple stain: 67 ml Ethanol (99%), 52 ml phosphoric acid (85%), 115 mg Coomassie Blue G-250, up to 1 l H_2O_{dd}

Storage buffer: 20 mM HEPES pH 7.4, 150 mM NaCl, 10% (v/v) glycerol, 1 mM DTT

Storage buffer 2: 20 mM HEPES pH 7.4, 150 mM NaCl, 1 mM DTT

Storage buffer 3: 20 mM HEPES pH 7.4, 1 mM DTT

Trans-Blot Turbo buffer: 1x Trans-Blot Turbo buffer, 20% (v/v) Ethanol

2.3 Organisms

Table 7: *E. coli* strains used in this work

ID	Strain	Genotype	Purpose	Source
5	Codon+	B F– ompT hsdSB(rB-mB-) dcm+ Tetr gal l(DE3) endA Hte [argU ileY leuW Camr]	Protein expression	Stratagene
27	LOBSTR	B F– ompT hsdSB(rB-mB-) dcm+ Tetr gal l(DE3) endA Hte ArnaD SlyD [argU ileY leuW Camr]	Protein expression	Kerafast
25	Rosetta™ 2 (DE3) pLysS	F- ompT hsdSB(rB- mB-) gal dcm (DE3) pLysSRARE2 (CamR)	Protein expression	Novagen
14	Top10	F–mcrA Δ(mrr-hsdRMSmcrBC) φ80lacZΔM15 ΔlacX74 recA1 araD139 Δ(ara-leu)7697 galU galK λ– rpsL(StrR) endA1 nupG	Cloning	Invitrogen

Table 8: Mammalian cell lines used in this work

ID	Cell line	Selection	Source
26	HeLa	-	CR-UK Cell Services
408	HeLa FlpIn T-REx	Blasticidin, Zeocin	Dorothee Dormann lab
415	HeLa Flp-In T-REx mCherry-G3BP1	Blasticidin, Hygromycin	This work
445	HeLa Flp-In T-REx His-TDP-43-EGFP	Blasticidin, Hygromycin	This work
456	HeLa Flp-In T-REx His-TDP-43(CTF)-EGFP	Blasticidin, Hygromycin	This work
452	HeLa Flp-In T-REx His-TDP-43(LCD)-EGFP	Blasticidin, Hygromycin	This work

2.4 Oligonucleotides

Table 9: DNA-oligonucleotides used in this work. All DNA-oligonucleotides were purchased from Integrated DNA technology or Sigma-Aldrich. IDs of oligos created by other lab members are indicated with an asterisk.

ID	Name	Sequence
o701*	T7 seq rev	GCTAGTTATTGCTCAGCGG

o2346*	T7 seq fwd	TAATACGACTCACTATAGGG
o4835*	FKBP seq fwd	GGAGTGCAGGTGGAAACCATC
o5388	Random SUMO2 rev	AGGTTGATGTGATCGTTGTTCTCAGT
o5389	Random SUMO2 fwd	ACTGAGAACAACGATCACATCAACCT
o5649	TDP-43(LCD) rev XhoI	ATATAATATTTCTCCTCGAGCATGCCCCAACCGGA
o5878	G275C SDM fwd	CCAACTGGAACGTTCCTGTCGTTTCGGTGGTAATC CGGGT
o5879	G275C SDM rev	ACCCGGATTACCACCGAAACGACAGGAACGTTCCA GTTGG
o5882	His-FKBP rev	TTCCAGTTTTAGAAGCTCCACA
o5883	3C-L20 fwd	CTGGAAGTTCTGTTCCAGGGG
o5884	L20-FKBP fwd	ATGTGGAGCTTCTAAAACTGGAAGCTTCTGGTGCT GGCGGTTCTGAA
o5894	L20-3C rev	CCCCTGGAACAGAACTTCCAGTGTAGCGCCAGATG TGCCACCTTCAG
o5945	TDP-43(LCD) seq rev	TGGTTATTGCCCAAGC
o6003	SUMO2 Δ1-10 fwd	TGTTTTCCAACAGCAGACGGGAGTTAAGACTGAGA ACAACGATCACATCA
o6005	SUMO2-SUMO2 rev	TGATGTGATCGTTGTTCTCAGTCTTAACTCCCGTCT GCTGTTGGAAAACA
o6020	Amp rev	CAATGCTTAATCAGTGAGGCAC
o6021	Amp fwd	GTGCCTCACTGATTAAGCATTG
o6138	TDP-43(LCD)-SUMO2 SacI fwd	GAGCTCCGGTTGGGGCATGAAGACTGAGAACAAC GATCAC
o6139	SUMO2 XhoI rev	ATATATATCTCGAGACCTCCCGTCTGCTG
o6215	L20-3C-FUS(QGSY) fwd	CTGGAAGTTCTGTTCCAGGGGCCCACTAGTATGGC CTCAAACGATTATACCC
o6216	FUS(QGSY)-TEV rev	CCTGAAAGTACAGGTTCTCCTCGAGGCTGTTGTAC TGGTTCTGCT
o6217	His-FKBP L20-3C backbone fwd	CTCGAGGAGAACCTGTACTTT
o6218	His-FKBP L20-3C backbone rev	ACTAGTGGGCCCCTGGAACAGAACTTCCAG
o6225	Ub SpeI fwd	ATATATACTAGTATGCAGATTTTCGTCAAGACT
o6226	Ub SpeI rev	ATATATACTAGTAACACCTCTTAGCCTTAGCA
o6227	SUMO1 SpeI fwd	ATATATACTAGTATGTCTGACCAGGAGGC
o6228	SUMO1 SpeI rev	ATATATACTAGTAACCCCCGTTTGTTCCT
o6229	SUMO2 SpeI fwd	ATATATACTAGTATGGCCGACGAAAAGC
o6230	SUMO2 SpeI rev	ATATATACTAGTAACTCCCGTCTGCTGT
o6260	TEV-MBP fwd	CTCGAGGAGAACCTGTACTTTCAGG
o6308	FUS(RGG) fwd	ATATATACTAGTAGCAGTGGTGGTGGAGGTGGAG
o6309	FUS(RGG) revv	CTCGAGGAGAACGTTGTTGTCTGAATTATCCTGT

o6398	Htt-Ex1 SpeI fwd	ATATATACTAGTATGGCGACCCTGGAAAA
o6399	Htt-Ex1 XhoI rev	ATATATCTCGAGTGGTCGGTGCAGCGGCTCCTC
o6417	SUMO1(G97V) BamHI rev	ATATATGGATCCAACCCCCGTTTGTTCC
o6419	SUMO2(G93V) BamHI rev	ATATATGGATCCAACTCCCGTCTGCTGT
o6437	MBP seq rev	AACCTGTGGGAATTTCT
o6535	EGFP -Met GA fwd	GTGAGCAAGGGCGAGG
o6543	Ub(G75V)-TDP-43(LCD) rev	GGTTGCTGGATCCAACAACTCTTAGCCTTAGCAC
o6613	His8-MCS-TDP-43(LCD) fwd	CATCACCATCACCATCACGATATCGGATCCAGCAACCGCCAACTG
o6614	CMV-Met-His8-MCS rev	GGATCCGATATCGTGATGGTGATGGTGATGGTGATGCATGGTGGCGACCGG
o6615	Ub -Met fwd	ATATATGATATCCAGATTTTCGTCAAGACTTTGACCGGT
o6616	SUMO1 -Met fwd	ATATATGATATCTCTGACCAGGAGGCCAAACCT
o6617	SUMO2 -Met fwd	ATATATGATATCGCCGACGAAAAGCCCAAGG
o6673	His8-HindIII fwd	TAAGCTTCCACCATGCATCACCATC
o6674	EGFP_NotI rev	ATATATGCGGCCGCTTACTTGTACAGCTCGTCCATG
o6714	3xNLS blunt fwd	GACCCTAAGAAGAAGAGAAAGGTCGATCCTAAAAAGAAACGCAAAGTGGACCCCAAGAAAAAACGAAAAGTC
o6715	3xNLS blunt rev	GACTTTTCGTTTTTTCTTGGGGTCCACTTTGCGTTTCTTTTTAGGATCGACCTTTCTCTTCTTCTTAGGGTC
o6718	3xNES blunt fwd	CTGCCTCCCCTGGAGCGCCTGACCCTGCTGCCTCCCCTGGAGCGCCTGACCCTGCTGCCTCCCCTGGAGCGCCTGACCCTG
o6719	3xNES blunt rev	CAGGGTCAGGCGCTCCAGGGGAGGCAGCAGGGTCAGGCGCTCCAGGGGAGGCAGCAGGGTCAGGCGCTCCAGGGGAGGCAG
o6711	SUMO3 -Met fwd	ATATATGATATCTCCGAGGAGAAGCCCAAG
o6797	SUMO3(G92V) BamHI rev	ATATATGGATCCAACTCCCGTCTGCTGC
o6895	TDP-43(1) pCMV-His-overhang GA fwd	CATCACCATCACGATATCGGATCCAGCGAGTATATTCGTGTTACCG
o6896	TDP-43(414) EGFP-overhang rev	GAACAGCTCCTCGCCCTTGCTCACACTAGTCATGCCCCAACCGGAG
o6904	TDP-43(267) SpeI fwd	ATATATACTAGTAGCAACCGCCAACTG
o6907	EGFP seq rev	GTCAGCTTGCCGTA
o6926	TDP-43(G335A, G338A) fwd	CTAGCTGGGCTATGATGGCCATGCTGGCGAGCCAGCAGAA
o6927	TDP-43(G335A, G338A) rev	GCCAGCATGGCCATCATAGCCCAGCTAGACTGCAGCGCCG

o6928	TDP-43(A326P) fwd	GGCAATGATGGCGGCTCCACAAGCGGCGCTGCAGT
o6929	TDP-43(A326P) rev	ACTGCAGCGCCGCTTGTGGAGCCGCCATCATTGCC
o6930	TDP-43(W334G) fwd	CGGCGCTGCAGTCTAGCGGGGGTATGATGGGCATGC
o6931	TDP-43(W334G) rev	GCATGCCCATCATACCCCCGCTAGACTGCAGCGCCG
o6932	TDP-43(W385G) fwd	CGGTGCGGCAATCGGCGGGGGTAGCGCAAGCAATGC
o6933	TDP-43(W385G) rev	GCATTGCTTGCGCTACCCCCGCCGATTGCCGCACCG
o6990	SKAR fwd	CCTTCATAAACCCACCCATTGGGACAG
o6991	SKAR rev	GTGGTGGAGAAAGCCGCCTGAG
o6992	BIM fwd	TCTGAGTGTGACCGAGAAGG
o6993	BIM rev	TCTTGGGCGATCCATATCTC
o7260	TDP-43 siRNA-resistant fwd	ATATATGGATCCATGTCTGAATATATTCGGGTAACCGAA
o7261	TDP-43 siRNA-resistant rev	ATATATACTAGTCATTCCCCAGCCAGAAGAC
o7412	SUMO1 Cys-N fwd	AGTTCTGTTCCAGGGGCCCTGCATGTCTGACCAGGAGGCCAAAC
o7413	SUMO1 Cys-N rev	TTGGCCTCCTGGTCAGACATGCAGGGCCCCTGGAACAGAACTTC
o7414	TDP-43(LCD) Cys-C fwd	AAGAGCTCCGGTTGGGGCATGTGCCTCGAGGAGAACCTGTACTTTCAGGG
o7415	TDP-43(LCD) Cys-C rev	TTGGCCTCCTGGTCAGACATGCAGGGCCCCTGGAACAGAACTTC
o7563	TDP-43(220) fwd	TCACCATCACGATATCGGATCCGTTTTCATCCCGAAACCTTTCC
o7564	TDP-43(220) rev	GGAAAGGTTTCGGGATGAAAACGGATCCGATATCGTGATGGTGA
o7582	SUMO2(Δ1-6) fwd	CTGGAAGTTCTGTTCCAGGGGCCCAAGGAAGGAGTTAAGACTGAGAAC
o7583	SUMO2(Δ1-6) rev	GTTCTCAGTCTTAACTCCTTCCTTGGGCCCCTGGAACAG
o7584	SUMO2(Δ1-11) fwd	AAGTTCTGTTCCAGGGGCCCACTGAGAACAACGATCACATCA
o7585	SUMO2(Δ1-11) rev	TGATGTGATCGTTGTTCTCAGTGGGCCCCTGGAACAG
o7588	SUMO2(K42P, A46P) fwd	CTTAGCCCCCTGATGAAGCCCTATTGTGAGCGTCAGGGTT
o7589	SUMO2(K42P, A46P) rev	ACAATAGGGCTTCATCAGGGGGCTAAGCGGTGTATGTCGC
o7590	SUMO2(t4-neutral) fwd	CAGATGCAGAATCAGAATACAATTGATGTTTTCCAACAGC

o7591	SUMO2(t4-neutral) rev	CAACTGTGCGGGCGTATTTGTTTCATTGATTGGCTGCC
o7594	SUMO2(t4-ΔH-bonds) fwd	AAGCAGATACACCCGCAGTTTTGGAGATGGAGGACGAAG
o7595	SUMO2(t4-ΔH-bonds) rev	AAAACTGCGGGTGTATCTGCTTCATTGATTGGCTGCCCAT
o7600	SUMO2(D63R) fwd	AGATTCGATTCCGGTTTCGAGGGCAGCCAATCAATGAAAC
o7601	SUMO2(D63R) rev	TCATTGATTGGCTGCCCTCGAAACCGGAATCGAATCTGTCT

Table 10: RNA-oligonucleotides used in this work. Sense strand (5'-3') sequences are listed below. All siRNAs were purchased as duplex from Sigma-Aldrich.

ID	Target	Sequence
25	TDP-43	CACUACAAUUGAUAUCAAAtt
27	SUMO1	CCUUCAUAUUACCCUCUCCUUtt
31	SUMO2/3	GUCAAUGAGGCAGAUCAGAtt

2.5 Plasmids

Table 11: Plasmids for expression in *E. coli*. Plasmids constructed by someone else are marked with an asterisk. If a restriction step occurred, plasmids were conventionally ligated. Gibson assembly = GA, Site-directed mutagenesis = SDM.

ID	Name	Construction	Selection
p678*	pET3a-Ub	-	Amp
p4905*	pJ4M-TDP-43-TEV-MBP	-	Kan
p5868	pET23a-SUMO1	PCR: p2695 + o5388/5389 Restriction: NdeI/XhoI in p1237	Amp
p5869	pET23a-SUMO2	PCR: p4453 + o5390/5391 Restriction: NdeI/XhoI in p1237	Amp
p5134	pET15-His-FKBP-3C-2xSUMO2-TDP-43(LCD)-TEV-MBP	PCR: p5100 + o6020/6003 and p5100 + o6021/6005 → GA	Amp
p5232	pET15-His-FKBP-L20-3C-Ub-TDP-43(LCD)-TEV-MBP	PCR: p3969 + o5884/5894 and p5098 + o5882/5883	Amp
p5277	pET15-His-FKBP-3C-TDP-43(LCD, G275C)-TEV-MBP	SDM: p5163 + o5878/o5879	Amp
p5377	pET15-His-FKBP-3C-4xSUMO2-TDP-43(LCD)-TEV-MBP	PCR: p5376 + o6070/6071 Screened 4xSUMO2 by cPCR	Amp

p5378	pET15-His-FKBP-3C-6xSUMO2-TDP-43(LCD)-TEV-MBP	PCR: p5376 + o6070/6071 Screened 6xSUMO2 by cPCR	Amp
p5406	pET15-His-FKBP-3C-SUMO2-TDP-43(LCD)-SUMO2(Δ1-10)-TEV-MBP	PCR: p4453 + o6138/6139 Restriction: SacI/XhoI in p5100	Amp
p5419	pET15-His-FKBP-L20-3C-FUS(QGSY)-TEV-MBP	PCR: p4906 + o6215/6216 and p5232 + o6217/6218 → GA	Amp
p5472	pET15-His-FKBP-L20-3C-Ub-FUS(QGSY)-TEV-MBP	PCR: p5098 + o6225/6226 Restriction: SacI in p5419	Amp
p5473	pET15-His-FKBP-L20-3C-SUMO1-FUS(QGSY)-TEV-MBP	PCR: p5099 + o6227/6228 Restriction: SacI in p5419	Amp
p5474	pET15-His-FKBP-L20-3C-SUMO2-FUS(QGSY)-TEV-MBP	PCR: p5100 + o6229/6230 Restriction: SacI in p5419	Amp
p5513	pET15-His-FKBP-L20-3C-FUS(RGG)-TEV- MBP	PCR: p4906 + o6308/6309 Restriction: SpeI/XhoI in p5419	Amp
p5514	pET15-His-FKBP-L20-3C-Ub-FUS(RGG)-TEV- MBP	PCR: p5098 + o6225/6226 Restriction: SacI in p5513	Amp
p5515	pET15-His-FKBP-L20-3C-SUMO1-FUS(RGG)-TEV- MBP	PCR: p5099 + o6227/6228 Restriction: SacI in p5513	Amp
p5516	pET15-His-FKBP-L20-3C-SUMO2-FUS(RGG)-TEV- MBP	PCR: p5100 + o6229/6230 Restriction: SacI in p5513	Amp
p5517	pET15-His-FKBP-L20-3C-SUMO1-TDP-43(LCD)-TEV-MBP	PCR: p3969 + o5884/5894 and p5099 + o5882/5883 → GA	Amp
p5518	pET15-His-FKBP-L20-3C-SUMO2-TDP-43(LCD)-TEV-MBP	PCR: p3969 + o5884/5894 and p5100 + o5882/5883 → GA	Amp
p5582	pET15-His-FKBP-L20-3C-Htt-Ex1-Q23-TEV- MBP	PCR: p5566 + o6398/6399 Restriction: SpeI/XhoI in p5472	Amp
p5635	pET15-His-FKBP-L20-3C-Ub-Htt-Ex1-Q23-TEV- MBP	Restriction: p5582 and p5514 with SpeI	Amp
p5636	pET15-His-FKBP-L20-3C-SUMO1-Htt-Ex1-Q23-TEV-MBP	Restriction: p5582 and p5515 with SpeI	Amp
p5637	pET15-His-FKBP-L20-3C-SUMO2-Htt-Ex1-Q23-TEV-MBP	Restriction: p5582 and p5516 with SpeI	Amp
p5723	pET15-His-FKBP-L20-3C-Ub-TDP-43(LCD, G275C)-TEV-MBP	SDM: p5232 + o5878/5879	Amp
p5724	pET15-His-FKBP-L20-3C-SUMO1-TDP-43(LCD, G275C)-TEV- MBP	SDM: p5517 + o5878/5879	Amp

p5725	pET15-His-FKBP-L20-3C-SUMO2-TDP-43(LCD, G275C)-TEV- MBP	SDM: p5518 + o5878/5879	Amp
p5845	pET15-His-FKBP-3C-TDP-43(LCD)-Ub-TEV- MBP	PCR: p5163 + o6260/6797 and p5232 + o6798/6799 → GA	Amp
p5846	pET15-His-FKBP-3C-TDP-43(LCD)-SUMO1-TEV- MBP	PCR: p5163 + o6260/6797 and p5517 + o6800/6801 → GA	Amp
p5847	pET15-His-FKBP-3C-TDP-43(LCD)-SUMO2-TEV- MBP	PCR: p5163 + o6260/6797 and p5518 + o6802/6803 → GA	Amp
p5959	pET15-His-FKBP-L20-3C-TDP-43(LCD)-TEV- MBP	PCR: p5163 + o5649/6904 Restriction: Spe/XhoI in p5631	Amp
p5982	pET15-His-FKBP-L20-3C-SUMO1(SUMO2(1-15))-TDP-43(LCD)-TEV- MBP	PCR: p5895 + o6228/6229 Restriction: SpeI in p5959	Amp
p5985	pET15-His-FKBP-L20-3C-SUMO2(SUMO1(1-19))-TDP-43(LCD)-TEV- MBP	PCR: p5897 + o6226/6230 Restriction: SpeI in p5959	Amp
p6072	pET15-His-FKBP-L20-3C-SUMO1(SUMO2(29-35)-TDP-43(LCD)-TEV- MBP	PCR: p6056 + o6227/6228 Restriction: SpeI in p5959	Amp
p6073	pET15-His-FKBP-L20-3C-SUMO1(SUMO2(1-15, 29-35))-TDP-43(LCD)-TEV- MBP	PCR: p6057 + o6228/6229 Restriction: SpeI in p5959	Amp
p6074	pET15-His-FKBP-L20-3C-SUMO2(SUMO1(33-39))-TDP-43(LCD)-TEV- MBP	PCR: p6058 + o6229/6230 Restriction: SpeI in p5959	Amp
p6075	pET15-His-FKBP-L20-3C-SUMO2(SUMO1(1-19, 33-39))-TDP-43(LCD)-TEV- MBP	PCR: p6059 + o6226/6230 Restriction: SpeI in p5959	Amp
p6298	pET15-His-FKBP-L20-3C-Cys-SUMO1-TDP-43(LCD)-TEV-MBP	SDM: p5517 + o7412/7413	Amp
p6299	pET15-His-FKBP-L20-3C-SUMO1-TDP-43(LCD)-Cys-TEV- MBP	SDM: p5517 + o7414/7415	Amp
p6399	pET15-His-FKBP-L20-3C-SUMO2(Δ1-6)-TDP-43(LCD)-TEV-MBP	PCR: p5518 + o7582/6020 or o7583/6021 → GA	Amp
p6400	pET15-His-FKBP-L20-3C-SUMO2(Δ1-11)-TDP-43(LCD)-TEV-MBP	PCR: p5518 + o7584/6020 or o7585/6021 → GA	Amp
p6402	pET15-His-FKBP-L20-3C-SUMO2(K42P, A46P)-TDP-43(LCD)-TEV-MBP	PCR: p5518 + o7588/6020 or o7589/6021 → GA	Amp

p6403	pET15-His-FKBP-L20-3C-SUMO2(D63R)-TDP-43(LCD)-TEV-MBP	PCR: p5518 + o7600/6020 or o7601/6021 → GA	Amp
p6505	pET15-His-FKBP-L20-3C-SUMO2(t4-neutral)-TDP-43(LCD)-TEV-MBP	PCR: p5518 + o7590/7591 → phosphorylation	Amp
p6407	pET15-His-FKBP-L20-3C-SUMO2(ΔH-bonds)-TDP-43(LCD)-TEV-MBP	PCR: p5518 + o7594/7595 → GA	Amp

Table 12: Plasmids for expression in mammalian cells

ID	Name	Construction	Selection
p5685	pCMV-His8-TDP-43(LCD)-EGFP	Restriction: p5670 with BamHI/ BglII, PCR: o6613/6614 → GA	Kan
p5687	pCMV-His8-Ub-TDP-43(LCD)-EGFP	PCR: p5667 + o6615/6543 Restr: BamHI/EcoRV in p5685	Kan
p5688	pCMV-His8-SUMO1-TDP-43(LCD)-EGFP	PCR: p5646 + o6616/6417 Restr: BamHI/EcoRV in p5685	Kan
p5689	pCMV-His8-SUMO2-TDP-43(LCD)-EGFP	PCR: p5647 + o6617/6419 Restr: BamHI/EcoRV in p5685	Kan
p5719	pcDNA5/FRT/TO-His8-TDP-43(LCD)-EGFP	PCR: p5685 + o6673/6674 Restriction: HindIII/NotI in p5668	Amp
p5773	pCMV-His8-SUMO3-TDP-43(LCD)-EGFP	PCR: p2703 + o6718/6719 Restr: BamHI/EcoRV in p5685	Kan
p5774	pCMV-His8-3xNLS-TDP-43(LCD)-EGFP	Oligo annealing: o6714/6715 Restriction: p5685 with EcoRV	Kan
p5775	pCMV-His8-3xNLS-Ub- TDP-43(LCD)-EGFP	Oligo annealing: o6714/6715 Restriction: p5687 with EcoRV	Kan
p5776	pCMV-His8-3xNLS-SUMO1-TDP-43(LCD)-EGFP	Oligo annealing: o6714/6715 Restriction: p5688 with EcoRV	Kan
p5777	pCMV-His8-3xNES-SUMO2-TDP-43(LCD)-EGFP	Oligo annealing: o6716/6717 Restriction: p5689 with EcoRV	Kan
p5895	pCMV-His8-SUMO1(SUMO2(1-15))-TDP-43(LCD)-EGFP	gBlock: SUMO1(S2(1-15)) PCR: gBlock + o6617/6417 Restr: BamHI/EcoRV in p5685	Kan
p5897	pCMV-His8-SUMO2(SUMO1(1-19))-TDP-43(LCD)-EGFP	gBlock: SUMO2(S1(1-19)) PCR: gBlock + o6617/6419 Restr: BamHI/EcoRV in p5685	Kan
p5933	pCMV-His8-TDP-43(LCD)-Ub-EGFP	Restriction: p5932 and p5514 with SpeI	Kan
p5934	pCMV-His8-TDP-43(LCD)-SUMO1-EGFP	Restriction: p5932 and p5515 with SpeI	Kan

p5935	pCMV-His8-TDP-43(LCD)-SUMO2-EGFP	Restriction: p5932 and p5516 with SpeI	Kan
p5936	pCMV-His8-TDP-43-EGFP	PCR: p4905 + o6895/6896 and p5685 + o6535/6711 → GA	Kan
p5937	pCMV-His8-Ub-TDP-43-EGFP	Restriction: p5936 and p5687 with BamHI/EcoRV	Kan
p5938	pCMV-His8-SUMO1-TDP-43-EGFP	Restriction: p5936 and p5688 with BamHI/EcoRV	Kan
p5639	pCMV-His8-SUMO2-TDP-43-EGFP	Restriction: p5936 and p5689 with BamHI/EcoRV	Kan
p5940	pCMV-His8-TDP-43-Ub-EGFP	Restriction: p5936 and p5514 with SpeI	Kan
p5941	pCMV-His8-TDP-43-SUMO1-EGFP	Restriction: p5936 and p5515 with SpeI	Kan
p5942	pCMV-His8-TDP-43-SUMO2-EGFP	Restriction: p5936 and p5516 with SpeI	Kan
p5988	pCMV-His8-TDP-43(LCD, G335A, G338A)-EGFP	SDM: p5685 + o6926/6927	Kan
p5989	pCMV-His8-SUMO1-TDP-43(LCD, G335A, G338A)-EGFP	SDM: p5688 + o6926/6927	Kan
p5990	pCMV-His8-TDP-43(LCD, A326P)-EGFP	SDM: p5685 + o6928/6929	Kan
p5991	pCMV-His8-SUMO2-TDP-43(LCD, A326P)-EGFP	SDM: p5689 + o6928/6929	Kan
p5992	pCMV-His8-TDP-43(LCD, Δ2W)-EGFP	SDM: p5685 + o6930/6931, then + o6932/6933	Kan
p5993	pCMV-His8-SUMO2-TDP-43(LCD, Δ2W)-EGFP	SDM: p5689 + o6930/6931, then + o6932/6933	Kan
p6019	pCMV-His8-Ub-TDP-43(LCD, G335A, G338A)-EGFP	SDM: p5687 + o6926/6927	Kan
p6020	pCMV-His8-Ub-TDP-43(LCD, A326P)-EGFP	SDM: p5687 + o6928/6929	Kan
p6021	pCMV-His8-Ub-TDP-43(LCD, Δ2W)-EGFP	SDM: p5687 + o6930/6931, then + o6932/6933	Kan
p6022	pCMV-His8-SUMO2-TDP-43(LCD G335A, G338A)-EGFP	SDM: p5689 + o6926/6927	Kan
p6056	pCMV-His8-SUMO1(SUMO2(29-35))-TDP-43(LCD)-EGFP	gBlock: SUMO1(S2(29-35)) PCR: gBlock + o6616/6417 Restr: BamHI/EcoRV in p5685	Kan
p6057	pCMV-His8-SUMO1(SUMO2(1-15, 29-35))-TDP-43(LCD)-EGFP	gBlock: SUMO1(S2(1-15, 29-35)), PCR: gBlock + o6617/6417 Restr: BamHI/EcoRV in p5685	Kan
p6058	pCMV-His8-SUMO2(SUMO1(33-39))-TDP-43(LCD)-EGFP	gBlock: SUMO2(S2(33-39)) PCR: gBlock + o6617/6419	Kan

		Restr: BamHI/EcoRV in p5685	
p6059	pCMV-His8-SUMO2(SUMO1(1-19, 33-39))-TDP-43(LCD)-EGFP	gBlock: SUMO2(S2(1-19, 33-39)), PCR: gBlock + o6617/6417 Restr: BamHI/EcoRV in p5685	Kan
p6097	pcDNA5/FRT/TO-His8-TDP-43-EGFP	PCR: p5936 + o6673/6674 Restriction: HindIII/NotI in p5719	Amp
p6148	pcDNA5/FRT/TO-mCherry-G3BP1	Restriction: p4636 with HindIII/ blunting/NotI, p6023 with NheI/blunting/NotI	Amp
p6157	pCMV-His8-TDP-43(ΔNLS)-EGFP	PCR: p6156 + o7260/7261 Restr: BamHI/SpeI in p5936	Kan
p6158	pCMV-His8-Ub-TDP-43(ΔNLS)-EGFP	PCR: p6156 + o7260/7261 Restr: BamHI/SpeI in p5937	Kan
p6159	pCMV-His8-SUMO1-TDP-43(ΔNLS)-EGFP	PCR: p6156 + o7260/7261 Restr: BamHI/SpeI in p5938	Kan
p6160	pCMV-His8-SUMO2-TDP-43(ΔNLS)-EGFP	PCR: p6156 + o7260/7261 Restr: BamHI/SpeI in p5939	Kan
p6295	pCMV-His8-TDP-43(G335A, G338A)-EGFP	SDM: p5936 + o6926/6927	Kan
p6296	pCMV-His8-TDP-43(A326P)-EGFP	SDM: p5936 + o6928/6929	Kan
p6311	pCMV-His-TDP-43(6M)-EGFP	gBlock: TDP-43(6M) PCR: gBlock + o6895/6896 Restr: BamHI/SpeI in p5936	Kan
p6312	pCMV-His8-TDP-43(W334G, W385G)-EGFP	SDM: p5936 + o6930/6931, then + o6932/6933	Kan
p6371	pcDNA5/FRT/TO-His8-TDP25-EGFP	PCR: p6097 with o7563/7564 Restriction: BamHI	Amp

2.6 Methods for *E. coli*

2.6.1 Cultivation

For plasmid isolation, *E. coli* strains were grown in Luria Broth (LB) medium. BL21-derived strains for protein purification were grown in Terrific Broth (TB) medium. M9 minimal medium supplemented with ^{15}N ammonium chloride was used for heavy isotope labeling. Appropriate antibiotics were added depending on the used plasmid. In general, *E. coli* was cultivated at 37 °C and 200 rpm.

2.6.2 Transformation

Chemically competent *E. coli* strains were thawed on ice. 100-200 ng plasmid DNA was added, and cells were incubated for 15 min on ice. Transformation was carried out at 42 °C for 1 min followed by a brief incubation on ice. In case of Ampicillin resistance, cells were immediately plated on LB-Amp agar plates. For Kanamycin resistance, cells were grown at 37 °C for 1 h before plating them on LB-Kan agar plates.

2.6.3 Isolation of plasmid DNA

For preparation of small amounts of DNA, one single colony was picked to inoculate 3 ml LB medium and grown overnight as described above. Cells were harvested the next day and plasmid DNA was isolated using GeneJET Plasmid Miniprep Kit. For preparation of large amounts of DNA, one single colony was picked to inoculate 3 ml LB medium and grown throughout the day. In the evening, the culture was diluted

2.6.4 Large-scale expression for protein purification

A few colonies were picked to inoculate 25-50 ml LB or TB medium and grown overnight as described above. The pre-culture was diluted to a final OD600 of 0.1 in 1 l TB medium, which was then grown to an OD600 of 0.6-0.8. Expression was induced with IPTG, while the exact conditions are listed in **Table 13**.

2.7 Methods for mammalian cells

2.7.1 Thawing and freezing

Frozen cells were usually stored at -150 °C and thawed by briefly incubating them in a water bath at 37 °C. The cell suspension was then transferred onto a 10 cm cell culture dish containing Dulbecco's Modified Eagle Medium (DMEM) (Gibco). Cells were at least grown for two days before splitting or seeding them for subsequent experiments.

For freezing, cells were washed with Dulbecco's Phosphate-buffered Saline (DPBS) (Gibco) and detached by using Trypsin-EDTA-phenol red (Gibco) as described in **section 2.7.2**. Cells were collected and Trypsin was neutralized. After centrifugation for 3 min at 300 x g, cells were resuspended in DMEM + 10% DMSO. Approximately 1x10^6 cells were distributed per cryovial, added into a cell freezing container and stored at -20 °C. After two days, cells were transferred to a -150 °C for long-term storage.

2.7.2 Cultivation

Cells were grown in DMEM using an incubator providing constant conditions of 37 °C, 5% CO2 and 85% relative humidity. Upon reaching 90-100% confluency, cells were washed with DPBS and Trypsin was added. Cells were incubated for 7 min at 37 °C and trypsinization was quenched by the addition of a 5-fold volume DMEM. The cell suspension was then redistributed to cell cultures dishes containing fresh medium.

2.7.3 Cell counting

After trypsinization, resuspended cells were mixed 1:1 with an Erythrosin-B cell staining solution and 10 µl were transferred into a cell counting slide. Cell number was determined using a TC20 Automated Cell Counter (BioRad).

2.7.4 Harvesting

To generate cell lysate for protein level analysis, cells were washed with DPBS and collected in 0.5-1 ml cold DPBS into a 1.5 ml reaction tube. After centrifugation for 3 min at 300 x g, all liquid was removed and cells were stored at -80 °C for further processing.

2.7.5 Preparation of cell lysate

Cell pellets were thawed on ice and resuspended with an appropriate amount of RIPA buffer supplemented with 1x protease inhibitor cocktail (Roche) and SM nuclease (125 cU/ml). After incubation for 15 min, protein concentration was determined by BCA assay (Thermo Fisher Scientific) and samples were normalized. Further processing was carried out as described in 2.9.2.

2.7.6 Preparation of cells for microscopy

Cells were seeded on 96-well PhenoPlate (Revvity) to reach a confluency of approximately 70% on the day of imaging. For imaging of living cells, DRAQ5 (Invitrogen) was added to a final concentration of 5 µM for staining of nucleus and cytoplasm. After an incubation of 15 min, cells were ready for imaging.

2.7.7 Transient transfection of DNA

Transient overexpression of plasmid DNA was executed by using FuGENE HD (Promega) according to manufacturer's protocol. Cells were seeded to achieve an approximate confluence of 80% on the day of transfection. For transfection of a 10 cm dish, 3 µg of plasmid DNA were diluted in 500 µl of OptiMEM (Gibco), which was warmed up to RT before. 9 µl of FuGENE HD reagent were added and the reaction was incubated for 10 min at RT. The transfection mix was subsequently added to cells, which were at least grown for 24 h before further processing. Reactions were appropriately scaled down for transfecting smaller cell culture plates.

2.7.8 Transient transfection of siRNA

siRNA-based knockdowns was carried out using RNAiMAX (Thermo Fisher Scientific) according to manufacturer's instructions. Cells were seeded similarly as for transient overexpression of plasmid DNA. For transfection of a 6-well cell culture plate, siRNA was diluted in 500 µl OptiMEM to achieve a final concentration of 20 nM in 2.5 ml medium. 6 µl of RNAiMAX reagent was added and the reaction mix was incubated for 15 min at RT. In the meantime, cells were washed with DPBS and 2 ml OptiMEM was added. After addition of the transfection mix, cells were grown for 4-6 h, before medium cells were washed again and medium was replaced with DMEM. Cells were further processed earliest after 48 h.

2.7.9 Generation of stable cell lines

Stable cell lines were generated using the Flp-In T-REx system. Transfection mixes were equally prepared as described in **section 2.7.7**, while using 2.7 µg Flp-recombinase plasmid and 0.3 µg pcDNA5/FRT/TO plasmid. Medium was changed after 24 h and appropriate antibiotics were added after 48 h. Cells were exposed to selection medium until visible bulk cell death occurred. The remaining colonies were considered as positively integrated and allowed to recover until reaching confluence again. Gene expression was induced by the addition of Doxycycline to a final concentration of 2 ng/ml and cells were grown for at least 24 h before further processing.

2.8 Methods for manipulation and analysis of DNA

2.8.1 Determination of DNA concentration

Concentration of plasmids, DNA or RNA fragments was determined using a DeNovix DS-11 spectrophotometer.

2.8.2 Agarose gel electrophoresis

1% agarose (w/v) was dissolved in TBE and boiled. SYBR Safe DNA stain was added to a final concentration of 1:1000. DNA was mixed with 6x DNA loading dye and loaded onto the solidified gel. 1 kb or 100 bp DNA ladder were used for size determination. Gels were run at 100 V until appropriate separation of DNA fragments of interest occurred. A Fusion FX system (Vilber Lourmat) was used to visualize DNA. In the case of preparative agarose gel electrophoresis, DNA fragments of interest were cut out using a scalpel and DNA was extracted using a GeneJET Gel Extraction Kit.

2.8.3 DNA sequencing

For Sanger sequencing, 300-700 ng DNA was dissolved in 6 µl H_2O_{dd}. DNA Oligonucleotides were chosen to bind upstream of the DNA region of interest and added to a final amount of 10 pM. Sanger sequencing was carried out by StarSEQ GmbH. For whole plasmid sequencing, DNA was dissolved to a final concentration of 30 ng/ul in a total volume of 20 µl $H_2O_{dd.}$ Whole plasmid sequencing was performed by Eurofins Genomics GmbH.

2.8.4 PCR

HF polymerase (CF15) was used to amplify DNA by polymerase chain reaction (PCR) according to manufacturer's instructions. DNA oligonucleotides were designed to flank DNA regions of interest and generate overhangs with restriction sites, if necessary. Either the reaction was loaded on an agarose gel or DNA was directly purified using GeneJET PCR Purification Kit for further processing. Colony PCR was performed by using Taq polymerase (CF15) according to manufacturer's instructions. PCR products were analyzed by agarose gel electrophoresis.

2.8.5 Site-directed mutagenesis

Point mutations in plasmid DNA were inserted by generating DNA oligonucleotides containing the mutation of interest. HF polymerase (CF15) was used similarly as described above with the following modifications to allow annealing in the regions to be mutated: 10 cycles were run with an annealing temperature of 42 °C, followed by 20 cycles with an annealing temperature corresponding to the melting temperature of the whole oligonucleotide. Template DNA was digested in the PCR reaction tube by adding 1 µl DpnI (CF15) according to manufacturer's instructions. DNA was purified using GeneJET PCR Purification Kit and transformed into *E. coli* Top10.

2.8.6 Restriction cloning

1-5 µg Plasmid DNA or purified PCR products were digested with commonly used DNA restriction enzymes according to manufacturer's instructions. Reactions were loaded on agarose gels and DNA fragments of interest were prepared as described above. If necessary, fragments were blunted using NEB Quick Blunting Kit according to manufcaturer's protocol. Ligation of fragments was performed by using TaKaRa DNA Ligation Kit. Usually, insert and backbone were mixed in a molar ratio of 3:1 at a total DNA amount of 100-150 ng and mixed 1:1 with the kit solution. After incubation at 16 °C for 1 h, the whole ligation mix was transformed into competent *E. coli* Top10.

2.8.7 Gibson assembly

Scar-free ligation of DNA fragments was carried out by using a homemade Gibson assembly mix (CF15). Fragments were generated by PCR using oligonucleotides generating overhangs homologous to adjacent fragments. 100 ng of total DNA was mixed in 10 µl H_2O_{dd} with molar ratios of 1:1 between the fragments. 10 µl of Gibson assembly mix were added. The reaction was incubated at 50 °C for 1 h and subsequently transformed into competent *E. coli* Top10.

2.8.8 cDNA synthesis

Complementary DNA was synthesized from RNA using a homemade reverse transcription protocol containing M-MLV RT. 1 µg RNA was mixed with 1 µl random hexamer oligonucleotides (100 µM stock) and 1 ml dNTPs (10 mM stock) in a final volume of 12 µl H_2O_{dd}. The reaction was incubated at 65 °C for 5 min and briefly chilled on ice. 4 µl of 5x first strand buffer and 2 µl DTT (1 M stock) were added and the reaction was incubated for 2 min at 25 °C. After adding 1 µl of RT, the reaction was incubated for 10 min at 25 °C, 50 min at 42 °C and 15 min at 70 °C.

2.9 Methods for detection and analysis of proteins

2.9.1 Determination of protein concentration

Protein concentrations were determined by using a DeNovix DS-11 spectrophotometer, considering specific values for molecular weight and extinction coefficients of the corresponding protein.

2.9.2 SDS-PAGE

Sodium dodecyl sulfate-polyacrylamide gel electrophoresis was used to separate a protein mixture by size differences. Protein samples were mixed with 4x NuPAGE LDS sample buffer and incubated at 95 °C for 5 min. Crude *E. coli* cell lysate was boiled for 30 min. Samples were loaded on mPAGE® 4-12% Bis-Tris precast gels. A homemade protein ladder (CF15) was used for size determination. Gels were run in MOPS or MES buffer at 180 V for 40 min.

2.9.3 Coomassie-staining

For visualization of total protein, gels were incubated in Simple Stain solution (CF6) for 1 h or overnight at room temperature. Staining solution was discarded and gels were washed with water until removal of background signal.

2.9.4 Detection of fluorescently labeled proteins

For detection of fluorescently-labeled proteins, gels were scanned using a Typhoon FLA9500 scanner, using appropriate filter cassettes corresponding to the used dye.

2.9.5 Western blotting

For probing the presence of a specific protein, semi-dry western blotting using a Trans-Blot Turbo Transfer System (Bio-Rad) was performed. Filter paper and nitrocellulose membrane were soaked in the supplemented buffer and the transferring stack was assembled in a cassette as followed: anode (bottom) – filter paper – nitrocellulose membrane – filter paper – cathode (top). Proteins were transferred on the membrane by applying 20 V to the cassette for 12 min. The membrane was covered with PBS-T with 5% (w/v) milk and incubated at slight agitation for 30 min at room temperature. Primary antibodies were diluted in PBS-T and incubated with the membrane for either 1 h at room

temperature or overnight at 4 °C. The membrane was washed three times for 5 min with PBS-T and subsequently incubated with secondary antibodies. A Fusion FX system (Vilber Lourmat) was used to detect HRP-tagged secondary antibodies. Secondary antibodies conjugated to a fluorescent dye were detected using an Odyssey fluorescence scanner (LI-COR).

2.10 Protein purification

2.10.1 Lysis

E. coli pellets were resuspended in 30 ml lysis buffer per 5 mg bacterial cell pellet. Composition of lysis buffers were selected depending on protein characteristics and purification procedures. Usually, lysis buffer was supplemented with Protease Inhibitor Cocktail (Roche), 5 mM MgCl2, 1:1000 Benzonase (CF15) and 1 mM DTT prior to lysis. Cells were either lysed by sonication or by passing the suspension twice through a high-pressure cell homogenizer (Constant Systems) at 1.9 kb. The lysate was centrifuged at 50,000 x g and 4 °C for 30 min. The supernatant was stored on ice for further processing.

2.10.2 IMAC

Immobilized metal affinity chromatography (IMAC) was used to purify proteins harboring a polyhistidine-tag. For batch purifications, NiNTA agarose beads were equilibrated with IMAC A buffer. The cleared supernatant was added to the beads and incubated for 1 h at 4 °C at slight agitation. Beads were washed thrice with IMAC A and either kept for proceeding with on-column cleavage or elution. Elution was carried out by incubating beads with 5 ml IMAC B per 1 ml of bead slurry at 4 °C and slight agitation for 5 min. Elution was analyzed by SDS PAGE and Coomassie-staining. For liquid chromatography assisted purification, an NGC system (Bio-Rad) was used. Sample pump and system pump A were flushed in IMAC A and system pump B was flushed in IMAC B. 5 ml HisTrap HP columns (Cytiva) were equilibrated in IMAC A. Cleared and filtered protein lysate was applied via the sample pump. The column was washed with IMAC A until the UV baseline was reached. Protein was eluted by applying a linear gradient of IMAC B over 10 column volumes. Fraction with a size of 1-2 ml were collected and analyzed by SDS PAGE and Coomassie-staining.

2.10.3 On-column cleavage

Washed beads were resuspended in 20 ml IMAC A per 5 ml bead slurry, supplemented with 1 mM DTT and 1 mg His-3C protease (CF15). The reaction was incubated 1 h at room temperature. A polypropylene column was used to separate supernatant from bead slurry. Cleavage efficiency was analyzed by SDS PAGE and Coomassie-staining.

2.10.4 Ion exchange chromatography

Cation or anion exchange were chosen depending on the isoelectric point of the protein of interest. Briefly, lysis was performed in salt-free buffer as described above and the cleared lysate was loaded on an NGC system (Bio-Rad). 5 ml HiTrapSP and HiTrapQ HP columns were used for cation or anion exchange chromatography, respectively. The column was washed until the UV baseline was reached. Protein was eluted by applying a linear gradient of high salt buffer (anion/cation exchange buffer B) over 10-20 column volumes. Fraction with a size of 1-2 ml were collected and analyzed by SDS PAGE and Coomassie-staining.

2.10.5 Size exclusion chromatography

Size exclusion chromatography (SEC) was used for polishing, buffer exchange or removal of excess dye. The sample was concentrated to < 5 ml using concentrators (NeoLab or Amicon) with molecular weight cutoffs according to the size of the protein of interest. Superdex75 or 200 columns (Cytiva) with bed volumes of either 10x300 mm or 16x600 mm were equilibrated in a suitable protein storage buffer on an NGC system (Bio-Rad) or Äkta Go system (Cytiva). The sample was injected on the column using a 5 ml loop and eluted using one column volume of storage buffer. Fraction with a size of 0.3-2 ml were collected and analyzed by SDS PAGE and Coomassie-staining. Purified protein was concentrated, flash-frozen in liquid nitrogen and stored at -70°C.

2.10.6 Protein labeling

Fluorescent dyes conjugated with maleimide were used for labeling of proteins with single cysteines. The reaction was prepared in DTT-free buffer at a protein concentration of 100 µM with a 2-fold excess of dye. Labeling was carried out for 2 h at room temperature and slight agitation. After quenching the reaction by adding 2 mM DTT excess dye was removed by using SEC. Labeling efficiency was determined as described in **section 2.9.4**.

Table 13: Purification scheme for proteins used in this work. Purification support for several TDP-43(LCD) variants was generously given by IMB's core facility for protein production.

Protein	Plasmid	Expression	Purification	Source
Ubiquitin	p678	Rosetta™ 2(DE3)pLysS 1 mM IPTG, 16°C, o/n	1. Lysis at pH 4.5 2. Heat-shock: 65 °C 3. HiTrap SP HP 5 ml 4. Superdex75 16/600	This work
SUMO1 SUMO2	p5868 p5869	Rosetta™ 2(DE3)pLysS 1 mM IPTG 37°C, 4 h	1. Lysis at pH 7.4 2. HiTrap Q HP 5 ml 3. Superdex75 16/600	This work
TDP-43	p4905	Codon+ 1 mM IPTG 16 °C, o/n	1. HisTrap 5 ml 2. Superdex200 16/600	This work
TDP-43(LCD) variants	All remaining plasmids from **Table 11**	Codon+ 1 mM IPTG 16 °C, o/n	1. IMAC: batch 2. On-column cleavage 3. Superdex200 16/600	This work + CF15
Labeled TDP-43(LCD) variants	p5277 p5723 p5724 p5725 p6298 p6299	Codon+ 1 mM IPTG 16 °C, o/n	1. IMAC: batch 2. On-column cleavage 3. Superdex200 16/600 4. Maleimide-labeling 5. Superdex200 16/600	This work
FUS(QGSY) variants	p5419 p5472 p5473 p5474	Codon+ 1 mM IPTG 16 °C, o/n	1. IMAC: batch 2. On-column cleavage 3. Superdex200 16/600	This work
FUS(RGG) variants	p5513 p5514 p5515 p5516	Codon+ 1 mM IPTG 16 °C, o/n	1. IMAC: batch 2. On-column cleavage 3. Superdex200 16/600	This work
Ht-Ex1(Q23) variants	p5582 p5635 p5636 p5637	Codon+ 1 mM IPTG 16 °C, o/n	1. IMAC: batch 2. On-column cleavage 3. Superdex200 16/600	This work

2.11 Phase separation assays

2.11.1 Turbidity assay

Measuring turbidity can provide information on how proteins phase separation occurs *in situ*. IDRs of interest were diluted to 10-50 µM in an appropriate phase separation buffer to reach a final volume of 20 µl. Reaction mixes were transferred into black polystyrene clear bottom 384-well microplates (Corning). Phase separation was induced by the addition of 0.1 mg/ml TEV-protease for 50 µM IDR. For lower IDR concentrations, TEV amounts were appropriately scaled. Control reactions in the absence of TEV-protease were also performed. Plates were sealed with PCR foil to avoid evaporation. Turbidity was assessed by measuring OD_{395} using a Spark M20 microplate reader (Tecan) at 25 °C for 1-3 h. Z-position was determined directly from a reference well.

2.11.2 Droplet formation assay

IDRs of interest were diluted to 10-50 µM in an appropriate phase separation buffer to reach a final volume of 50 µl. The reaction mix was transferred into 18-well µ-Slide with glass bottom (Ibidi) and phase separation was induced by adding TEV-protease. Droplets were imaged using an AF7000 widefield microscope (Leica) using differential interference contrast microscopy (DIC) for unlabeled protein. Fluorescently labeled proteins were imaged using appropriate filter cubes for the corresponding fluorophore. All images were recorded at RT.

2.11.3 FRAP

Fluorescence recovery after photobleaching was performed using a Stellaris 8 FALCON laser scanning confocal microscope (Leica) with the integrated FRAP module. Samples were similarly prepared as described in the previous **section 2.11.2**. A 63x oil immersion objective was used. Images were recorded at resolution of 256x256 pixels at a scanning rate of 600 Hz and pinhole size of 1 AU. A white light laser set to 480 nm at 0.4% power was used for imaging and a 488 nm laser at 10% power was used for photobleaching. Bleaching regions were selected to cover approximately 50% of a droplet. Images were recorded every 0.5 s, with three images pre-bleaching, ten images bleaching and 240 images post-bleaching. Additional ROIs were selected after imaging to cover the whole droplet region and the background. Raw data were analyzed using EasyFRAP (Koulouras *et al.* 2018) and visualized with GraphPad Prism 8.

2.11.4 FRET-AB

Förster resonance energy transfer acceptor bleaching (FRET-AB) was performed using a Stellaris 8 FALCON laser scanning confocal microscope (Leica) with the integrated FRET-AB module. AzDye488- and ATTO594-labeled proteins were mixed in varying ratios to a final concentration of 50 µM in storage buffer 2. Phase-separation was induced by the addition of 0.1 mg/ml TEV-protease. A 63x oil immersion objective was used. Images were recorded at resolution of 128x128 pixels at a scanning rate of 400 Hz and pinhole size of 1 AU. Both dyes were imaged using a white light laser set to 480 nm or 590 nm at 0.2% power. Acceptor bleaching was executed using a white light laser set to 590 nm at 100% power for 3 frames. Bleaching regions were selected to cover approximately 50% of a droplet. Raw fluorescence intensity values of ROIs (Donor pre, donor post, acceptor pre, acceptor post) were directly converted into FRET efficiency using the built-in evaluation tool.

2.11.5 Droplets in cells

Droplets were imaged after preparing transfected cells as described in **section 2.7.6** using an Opera Phenix High-Content Screening System (Perkin Elmer). A 40x water objective with autofocus in confocal mode was used. EGFP signal was imaged with 100% laser power for 40, mCherry signal with 100% laser power for 500 ms and DRAQ5 with 100% laser power for 100 ms. For each well, 30 positions were imaged with 5-7 planes at 0.7 µm spacing. Droplets were quantified with an automated pipeline using the built-in evaluation software. Cell regions (membrane, nuclei, cytoplasm) were detected using DRAQ5 signal. EGFP intensity was calculated, and positively transfected cells were selected if the median intensity value was above 150. Spots were separately detected in nuclei and cytoplasm. The number of cells harboring more than 5 droplets were divided by the total number of transfected cells as a measure of phase separation.

2.12 Determination of protein-protein and protein-peptide interactions

2.12.1 Denaturing Ni-NTA pulldown

Cell pellets from 10 cm cell culture dishes were thawed on ice and resuspended in 1 ml Gua-HCl-buffer (denaturing pulldown buffer A) supplemented with 15 mM Imidazole. Lysis was carried out by sonication with 10 pulses, 40% duty cycle and output 1. 70 µl NiNTA agarose beads (Qiagen) per sample were washed with Gua-HCl-buffer and mixed with the

lysate. After 1 h incubation at RT at gentle rotation, beads were washed 3x with 1 ml Gua-HCl-buffer, followed by 3x 1 ml Urea-buffer (denaturing pulldown buffer B). Protein was eluted by boiling the beads for 5 min at 95 °C in 100 µl 1x LDS supplemented with 20 mM DTT and 200 mM Imidazole. Samples were briefly centrifuged, and the supernatant was separated from beads for further analysis by western blotting.

2.12.2 Fluorescence polarization

Fluorescence polarization (FP) was used to quantify protein-peptide interactions. FITC-labeled peptides were pre-ordered (ProteoGenix) and resuspended in storage buffer 2. Interaction partners were prepared in serial dilutions covering a range between 400 µM and 2 µM in a volume of 19 µl. Peptides were added to reach a final concentration of 5 nM. FP was measured using a Spark M20 microplate reader (Tecan) at 25 °C. Excitation wavelength was set to 485 nM and emission wavelength was set to 520 nm. Gain was set to 100 and Z-position was determined from a reference well.

2.13 Spectroscopic methods

2.13.1 CD spectroscopy

Circular dichroism (CD) spectra were recorded using a J-1500 CD spectrophotometer (Jasco). Samples were prepared in 10 mM Na-phosphate buffer pH 7 in the absence of salt and at final protein concentrations below 0.1 mg/ml. CD was recorded over a wavelength from 260-190 nm at 25 °C. Voltage threshold was set to 600 V. Data were analyzed with the integrated software and further processed using GraphPad Prism 8.

2.13.2 ThT fluorescence

Thioflavin-T (ThT) fluorescence was measured to determine protein aggregation. Samples were prepared similarly as described in **section 2.11.1**, but in the presence of 20 µM ThT. After the addition of TEV protease, ThT fluorescence was measured using a Spark M20 microplate reader (Tecan) with a monochromator. Excitation wavelength was set to 440 nm and emission wavelength was measured between 465-600 nm from the bottom of the plate with 30 flashes per reading. Bottom Z-position is fixed at 30000 µm and gain was set to 50 manually. ThT fluorescence was measured daily for 20 days. Raw data were processed using GraphPad Prism 8.

2.14 Mass spectrometry

2.14.1 HDX-MS

Hydrogen-Deuterium Exchange Mass Spectrometry (HDX-MS) was used for the detection of structural changes upon SUMO1 fusion to TDP-43(LCD) in comparison to SUMO1 mixed with TDP-43(LCD). HDX-MS is based on the exchange of protons at backbone amides. The exposure to deuterium serves as a label for the identification of conformational changes upon a certain event, because the uptake depends on the accessibility of the respective amide. The conformation could for instance be altered by the binding of a ligand, the introduction of a mutation, or the conjugation to another protein. Quantification of deuterated regions is enabled by HPLC-coupled mass spectrometry, where deuterium-exposed peptides can be subsequently compared to non-deuterated control peptides derived from a protein that does not harbor the respective conformational change (James *et al.* 2022).

This experiment was performed and analyzed by Joshua Vollrath in Julian Langer's lab at the Max Planck Institute of Biophysics using an automated HDX-2 system (Waters). In brief, deuterium uptake was compared between two conditions harboring either 15 µM of SUMO1-TDP-43(LCD) or 15 µM SUMO1 mixed with 15 µM TDP-43(LCD). Each condition was exposed to deuterated and non-deuterated storage buffer 2 for multiple time points (0, 30, 120, 600 and 2100 s). D_2O uptake was quenched by the addition of equal volumes of ice cold 150 mM potassium phosphate pH 2.2 for 30 s. Samples were injected into a chromatography system and digested using a nepenthesi-2/pepsin column. Afterwards, peptides were separated using a C18 reversed-phase column by elution with a linear acetonitrile gradient. All chromatography steps were carried out at 0 °C to minimize deuterium back exchange. Peptides were analyzed using a Synapt G2-Si mass spectrometer (Waters) based on retention time, mass-to-charge ratio and precursor ion mobility.

Peptides were assigned using the ProteinLynx Global Server 3.0.3 (Waters) and relative D_2O uptake was calculated using HDExaminer (Sierra Analytics) comparing deuterated and non-deuterated peptides. Relative D_2O uptake was visualized on AlphaFold2-predicted structures of TDP-43 (AF-Q13148) and SUMO1 (AF-P63165).

2.14.2 Crosslinking-MS

Crosslinking mass spectrometry (Crosslinking-MS) was used for the identification of SUMO2-TDP-43(LCD) interaction sites. This experiment was performed in collaboration with Jiaxuan Chen at the core facility for proteomics at the IMB Mainz. The experimental layout is based on the usage of Sulfo-SDA (Thermo Fisher Scientific) with a 3.9 Å spacer arm for capturing close interactions and heavy-isotope labeling to distinguish between intra- and intermolecular interactions. SUMO2-TDP-43(LCD) was mixed with ^{15}N-SUMO2-TDP-43(LCD) at equimolar ratio to reach a final protein concentration of 50 µM in storage buffer 2. Sulfo-SDA was prepared in serial dilutions to cover molar crosslinker:protein ratios between 50:1 and 1:1 in storage buffer 2, as well. Protein and crosslinker solutions were mixed and incubated at RT for 1 h to allow reaction of the NHS-warhead. Without further quenching, 0.1 mg/ml TEV-protease was added and the reaction was further incubated for 1 h. The Diazirine-warhead was activated by exposing the reaction mixes to 5000 mJ/cm^2 UV-A. The samples were subsequently mixed with 4xLDS and loaded onto SDS-PAGE. After Coomassie- staining, bands of interest were cut out and submitted to the core facility for proteomics.

In brief, gel pieces were destained in 25 mM ammonium bicarbonate and 50% ethanol (v/v) followed by protein reduction in 10 mM DTT at 56 °C and alkylation in 50 mM iodoacetamide at RT in the dark. Proteins were digested by trypsin in 50 mM ammonium bicarbonate at 37 °C o/n. Peptides were extracted using acetonitrile and acidified by the addition of formic acid. An EASY-nLC 1200 UHPLC system (Thermo Fisher Scientific) equipped with a C18 reversed-phase column was used to separate peptides by an acetonitrile gradient. Peptides were analyzed by an Orbitrap Exploris 480 mass spectrometer based on mass-to-charge ratios and precursor ion mobility. Raw data were processed using ProteWizard (Chambers *et al.* 2012) and peak lists were searched using the SIM-XL software (Lima *et al.* 2018). Intra- and intermolecular crosslinks were visualized using xiNET (Combe *et al.* 2015).

2.15 Computational methods

2.15.1 Disorder prediction

For prediction of protein disorder and secondary structural elements, IUPred2A was used (Mészáros *et al.* 2018). Protein sequences of IDRs were submitted to the IUPred2A server. Disorder score values were extracted from the raw data and plotted with GraphPad Prism.

2.15.2 Structure prediction and analysis

AlphaFold2 and AlphaFold3 were used for predictions of protein structures (Abramson *et al.* 2024). Protein sequences were submitted to the AlphaFold server with an automatically selected number of seeds per prediction. CIF files were converted into PDB files for further analysis. PDB files were loaded into PyMOL 3, and protein structures were manually adjusted and colorized. The integrated measurement wizard was used for calculating molecular distances.

3 Results

3.1 Effects of ubiquitin and SUMO on IDRs

Several neurodegenerative disease-associated proteins harboring internally disordered regions (IDR) are reported to be modified with ubiquitin, SUMO1 or SUMO2, while their physiological and pathological functions often remain unclear (**chapter 1.2.7**). Ubiquitin and SUMO have been shown to regulate phase separation by their classical effect, while the intrinsic effect through PTM-conjugation on the modified protein is only poorly studied (**chapter 1.2.5**). In this chapter, I wanted to establish a platform for generating ubiquitylated and SUMOylated IDRs of different properties. Comparing their phase separation behavior with unmodified IDRs mixed with ubiquitin in SUMO allows me to draw conclusions of this intrinsic effect and highlight differences between the modifiers.

3.1.1 Selection of suitable IDRs

The amino acid composition of IDRs defines which molecular interactions contribute to self-assembly and thus defines the mechanisms of self-assembly (**chapter 1.2.2**). It can be assumed that ubiquitin and SUMO are highly sensitive to particular sequence elements (**chapter 1.1.1**), so I wanted to cover a set of IDRs with different characteristics that has a high relevance in the context of neurodegenerative diseases. Hence, I used IDRs from hallmark proteins of ALS, FTD and HD (**chapter 1.2.7**): TDP-43(LCD), Htt-Ex1(Q23), FUS(QGSY) and FUS(RGG). Disorder scores were calculated using IUPred2A and potential structural elements were predicted using AlphaFold2 (**Figure 9** A and B).

The LCD of TDP-43 is G-rich and forms a transient α-helix from residue 321 to 340, which is considered as the main self-assembly side (Conicella *et al.* 2016). It is largely polar and contains several aromatic amino acid residues that further contribute to self-assembly. Both disorder prediction and AlphaFold2 suggest that TDP-43(LCD) is largely unstructured, showing a helical region in agreement with literature (Conicella *et al.* 2020).

Htt-Ex1 harbors a poly-Q stretch that is abnormally extended in Huntington's disease patients (Yang and Yang 2020). IUPred2A predicts disorder throughout the whole IDR, while AlphaFold2 shows an α-helix from residue 1-40 that is subsequently broken by a P-stretch, which has recently been confirmed by NMR (Elena-Real *et al.* 2023). The overall complexity of this IDR is fairly low, with glutamine and proline making up more than 60% of all amino acids. I used a stretch length of 23 glutamines, which is below the critical

aggregation threshold for the development of HD but has been shown to undergo LLPS (Scherzinger *et al.* 1999; Peskett *et al.* 2018).

FUS harbors IDRs of different characteristics, so I made use of the N-terminal QGSY-domain and one of the three RGG-domains FUS(QGSY) harbors typical features of a prion-like domain being enriched in polar amino acids. Similar to Htt-Ex1, the high number of 37 glutamines makes this domain in particular sensitive to the formation of amyloid fibrils. 15% of the amino acids are tyrosines with the potential of π-stacking. The formation of secondary structures has not been reported so far and were also not shown by computational methods in this study (Chen *et al.* 2019; Murthy *et al.* 2019).

FUS(RGG) is an LCD consisting out of 47% Glycine with several RGG-repeats. This tripeptide is especially susceptible to the binding of nucleic acids but can also promote weak multivalent interactions leading to self-assembly, following the sticker/spacer principle (**chapter 1.2.2**). Similar to FUS(QGSY), FUS(RGG) is most likely not forming secondary structure elements (Murthy *et al.* 2019; Loughlin *et al.* 2019).

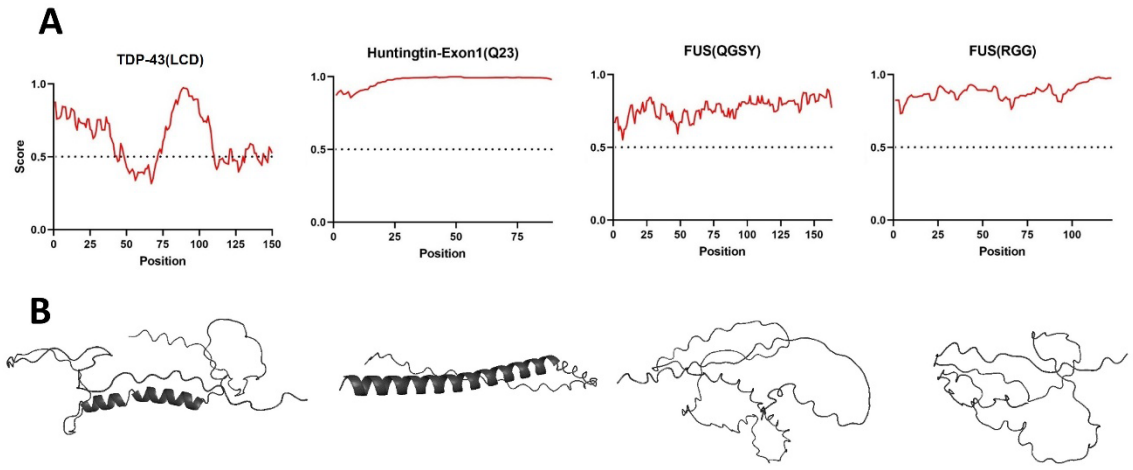

Figure 9: Disorder and structure prediction of TDP-43(LCD), Htt-Ex1(Q23), FUS(QGSY) and FUS(RGG). (A) Amino acid sequences were submitted to IUPred2A for prediction of disorder. A score above 0.5 indicates intrinsically disordered regions. **(B)** AlphaFold2 was used to determine potential secondary structure elements. IDRs are shown in the carton representation.

Taken together, the selected set of IDRs covers various properties. Both α-helices and repeat motifs provide binding sites for potential protein-protein interactions in an intra- and intermolecular manner. The combination of the broad variety between the IDRs amino acid composition allows the detection of generic effects of each modifier in regard to phase separation.

3.1.2 Construct design

Post-translational modifiers (PTMs) can modulate phase separation by promoting protein-protein interaction (classical effect) or by directly altering the biophysical properties of their conjugation target (intrinsic effect), as described in **section 1.2.5**. I designed an expression system for the production of ubiquitylated or SUMOylated IDRs in *E. coli*, which wdas optimized for high protein yields and convenient accessibility for modulations. The construct arrangement is shown in **Figure 10**.

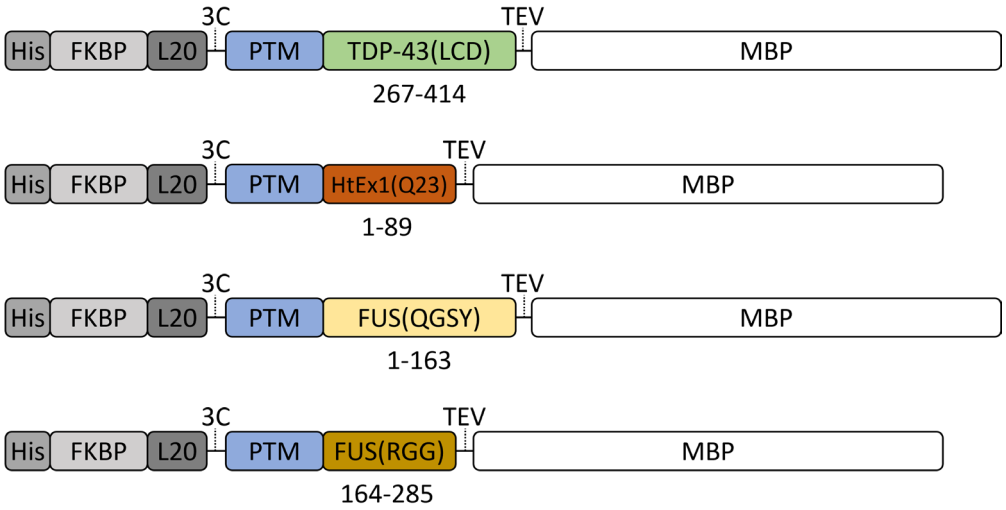

Figure 10: Expression constructs of IDRs for protein production. IDR sequences were derived from pathologically relevant proteins. Numbers below indicate positions within the original protein sequence. Solubility is boosted with N-terminal FKBP and C-terminal MBP, which are cleavable by either 3C-protease or TEV-protease, respectively.

I decided to mimic PTM conjugation by generating N-terminal fusions with each IDR. Native conjugation sites can be hard to determine and furthermore, respective combinations of conjugation enzymes are often unknown. Even in cases of known E2/E3 pairs, enzymatic turnover is barely complete, while chemical linkage approaches face different issues. Furthermore, linear fusions with PTMs have been shown to properly mimic biological functions in several systems, as substrate recognition by “readers” not only relies on UBDs and SIMs but also on substrate-specific binding domains (Asimaki *et al.* 2022). In each modifier, the C-terminal glycine was mutated to valine to increase protein stability and protection of the covalent bond against protease cleavage (**chapter 1.1.2**).

IDRs are often prone to phase separate or aggregate, so they need to be either purified under denaturing conditions or attached to a solubility tag. As fused ubiquitin or SUMO might cause problems due to defective refolding when using chaotropic agents, I decided to use a TEV-cleavable MBP-tag at the C-terminus of each IDR and purify under native

conditions, which has been shown to enable purification of full-length TDP-43 and FUS (Hofweber *et al.* 2018; Gruijs da Silva *et al.* 2022). Overall solubility was furthermore increased by the addition of an N-terminal His-FKBP-tag, which can be removed by the addition of 3C-protease. This has two major benefits for the purification procedure and future applications. First, proteins can be coupled to NiNTA agarose beads during IMAC purification and Ub/SUMO-TDP-43-MBP can be released without elution procedure in high imidazole buffer, leaving only a GP-remnant at the PTM's N-terminus. Second, The FKBP can serve as a dimerization site for the recruitment of various factors, such as ubiquitylation or SUMOylation enzymes. Proper accessibility of the 3C-site and sufficient flexibility of the FKBP-tag was assured by introducing a 20 amino acid long flexible linker. Additional constructs with swapped 3C-/TEV-sites did result in lower protein expression (data not shown).

Taken together, this procedure resulted in an average yield of 5-10 mg protein per liter of bacterial expression culture with high purity. An exemplary Coomassie-stained SDS-PAGE monitoring the purification procedure is shown in the following **Figure 11**.

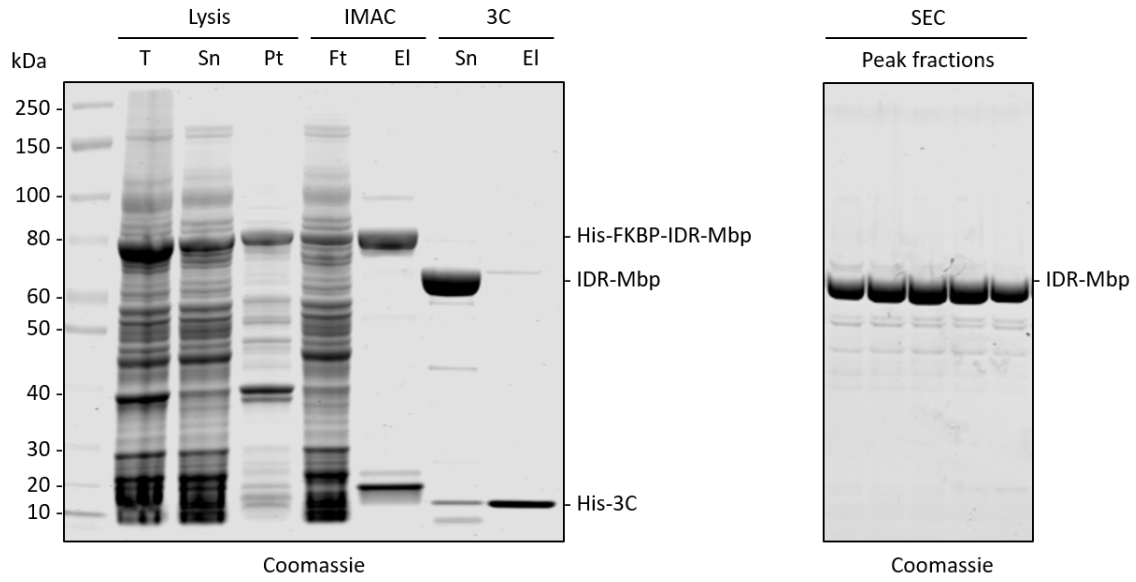

Figure 11: Exemplary three-step IDR purification. IMAC and SEC purification steps were monitored by SDS-PAGE and Coomassie-staining. (T) Total, (Sn) supernatant, (Pt) pellet, (Ft) dlow-through, (El) elution.

3.1.3 Interaction of IDRs with non-conjugated post-translational modifiers

The distinction between the classical and the intrinsic effects of ubiquitin and SUMO was assessed by probing for consequences on phase separation of each IDR in the presence

of the non-conjugated, free modifiers. If the IDRs do not contain binding sites, no effect on phase separation by the presence of ubiquitin or SUMO should be detectable. I screened for salt and molecular crowding conditions where each unmodified IDR would undergo phase separation. TDP-43(LCD) phase-separated at a concentration of 10 µM in the presence of 150 mM NaCl and 5% (w/v) PEG-8000 in a HEPES-based buffer. Droplets were detected after less than 1 h. HttEx1(Q23) required the absence of salt and 10% (w/v) PEG-8000 to undergo phase separation at 20 µM. Furthermore, droplets were best detectable after 12 h. Both FUS(QGSY) and FUS(RGG) phase separated at a protein concentration of 10 µM in the presence of 10% (w/v) PEG-8000 and formed droplets after 1 h. However, FUS(QGSY) required a slightly lower salt concentration of 25 mM NaCl in comparison to 50 mM NaCl for FUS(RGG) (screening data not shown).

In the final experiment, I mixed each IDR with equimolar concentrations of either ubiquitin, SUMO1 or SUMO2. Phase separation was then assessed by measuring turbidity and imaging droplets after TEV-induced removal of MBP. Indeed, TDP-43(LCD), Htt-Ex1(Q23), FUS(QGSY) and FUS(RGG) show equal turbidity kinetics and total absorbance values in the absence and presence of ubiquitin, SUMO1 or SUMO2 (**Figure 12** A). Droplets had comparable morphologies for each set of IDRs, supporting the turbidity assay data (**Figure 12** B). The completeness of the cleavage reaction was monitored for each sample by SDS-PAGE and Coomassie-staining (**Appendix 1**).

In conclusion, no PTM assessed in this experiment affected the propensity of the tested IDRs to undergo phase separation. This makes TDP-43(LCD), Htt-Ex1(Q23), FUS(QGSY) and FUS(RGG) suitable candidates to investigate the effect of conjugation of ubiquitin, SUMO1 and SUMO2 on the intrinsic effect on phase separation.

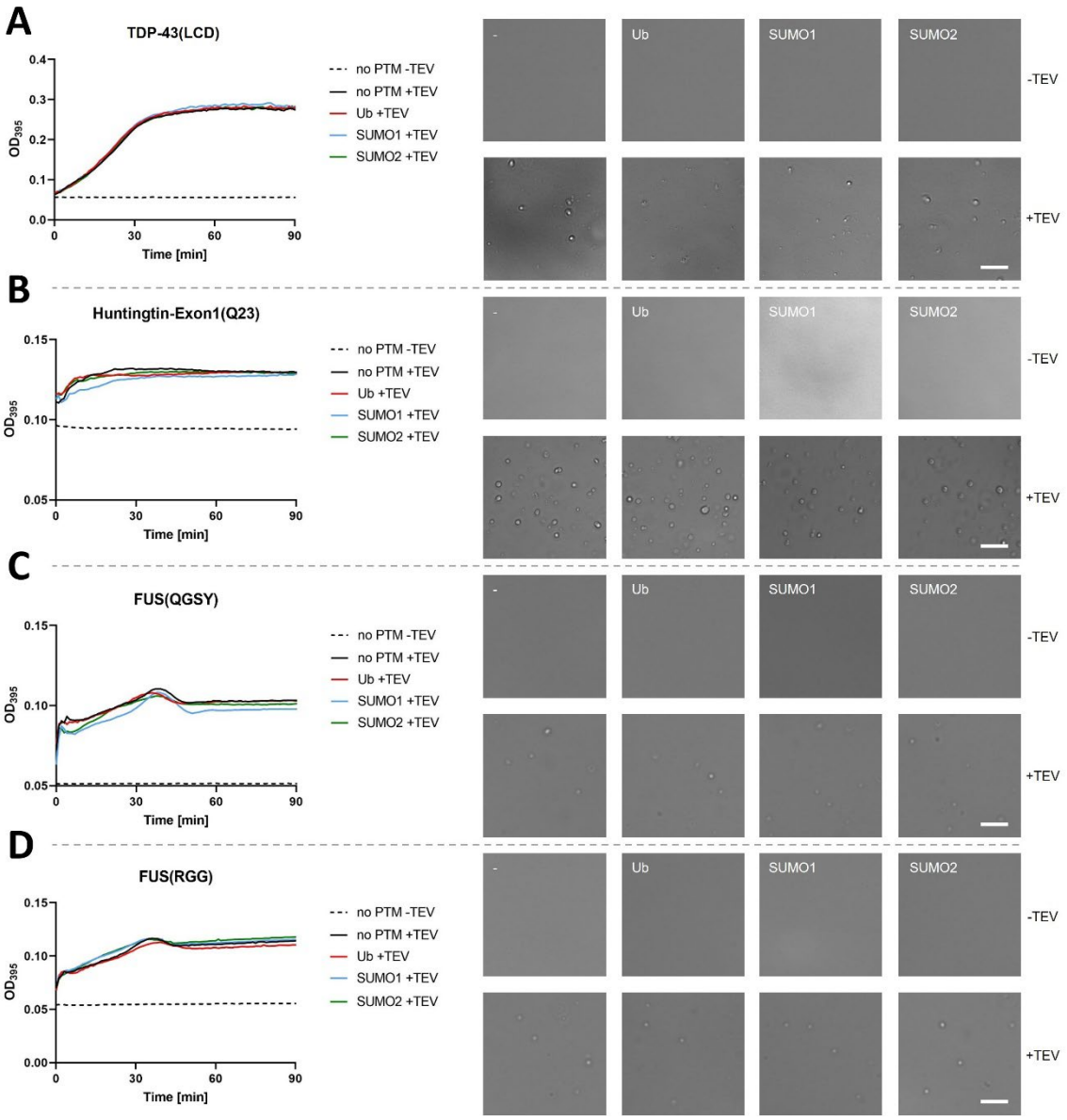

Figure 12: Interactions of IDRs with unconjugated post-translational modifiers. Purified (**A**) TDP-43(LCD), (**B**) Htt-Ex1(Q23), (**C**) FUS(QGSY) and (**D**) FUS(RGG) were mixed with equimolar concentrations of ubiquitin, SUMO1 or SUMO2. Phase separation was induced by the addition of TEV protease for removal of MBP-tag. Turbidity was measured *in situ* by using a plate reader. Error bars are not displayed for better visibility. Representative DIC images of droplet formation after 1 h. Scale bar: 10 µm

3.1.4 Intrinsic effect of fusing post-translational modifiers on IDRs

Linear fusion of a post-translational modifier to a protein of interest can be used as a strategy to mimic conjugation (Asimaki *et al.* 2022). As described in **section 3.1.2**, either ubiquitin, SUMO1 or SUMO2 were genetically fused to the N-terminus of TDP-43(LCD), Htt-Ex1(Q23), FUS(QGSY) or FUS(RGG) and purified from *E. coli*. Each IDR was assessed for phase separation with the same conditions as used in **section 3.1.3**.

Interestingly, the fusion of ubiquitin and SUMO resulted in strong differences within each set of IDRs, as monitored by turbidity and droplet formation (**Figure 13** A and B). Cleavage reactions were monitored by SDS-PAGE and Coomassie-staining (**Appendix 2**).

For TDP-43(LCD), fusion of ubiquitin and SUMO2 strongly enhanced phase separation, while SUMO1-fusion behaves almost as the unmodified control protein. Ubiquitin-fusion droplets appeared slightly amorphous. Ub-TDP-43(LCD) also showed slight phase separation without TEV-induced removal of MBP, as indicated by a slight increase in turbidity and the detection of a few droplets.

The striking difference between the two SUMO isoforms was also observed for Htt-Ex1(Q23), where SUMO1-fusion even completely abrogated phase separation, demonstrated by low turbidity values and the complete absence of droplets. SUMO2-fusion droplets were larger in size, compared to all other conditions.

For both FUS IDRs, ubiquitin-fusion slightly increased phase separation, whereas SUMO1- and SUMO2-fusions further enhanced turbidity to a similar extent. In addition, SUMO1- and SUMO2-FUS(IDR) droplets appeared larger compared to ubiquitin fusions and the unmodified control proteins. All PTM fusions to FUS(RGG) led to the formation of condensates in the absence of TEV protease, while SUMO2-FUS(RGG)-MBP phase separated the earliest and Ub-FUS(RGG)-MBP the latest.

While TDP-43(LCD), FUS(QGSY) and FUS(RGG) phase plateaued after less than 2 h upon TEV-cleavage, Htt-Ex1(Q23) fusion proteins required at least 10 h to reach saturation.

Taken together, all modifiers have diverse effects on the respective IDRs, which is not surprising due to their structural and compositional differences (**chapter 3.1.1**). Yet, SUMO2-fusions are most prone to enhance phase separation. SUMO1-fusions either behave comparable like SUMO2-fusions, or they reduce LLPS. Ubiquitin-fusion always enhanced LLPS but to different extents. The usage of PEG-8000 as a crowding agent creates an unnatural environment that does not accurately mimic cellular conditions. Countless proteins have been reported to undergo phase separation in the presence of PEG-8000, while even Ubiquitin formed condensates at concentrations of almost 1 mM in 10% PEG-8000 (Poudyal *et al.* 2023). A more favorable environment to study the intrinsic effect of PTMs would thus require buffer conditions in the absence of molecular crowding agents.

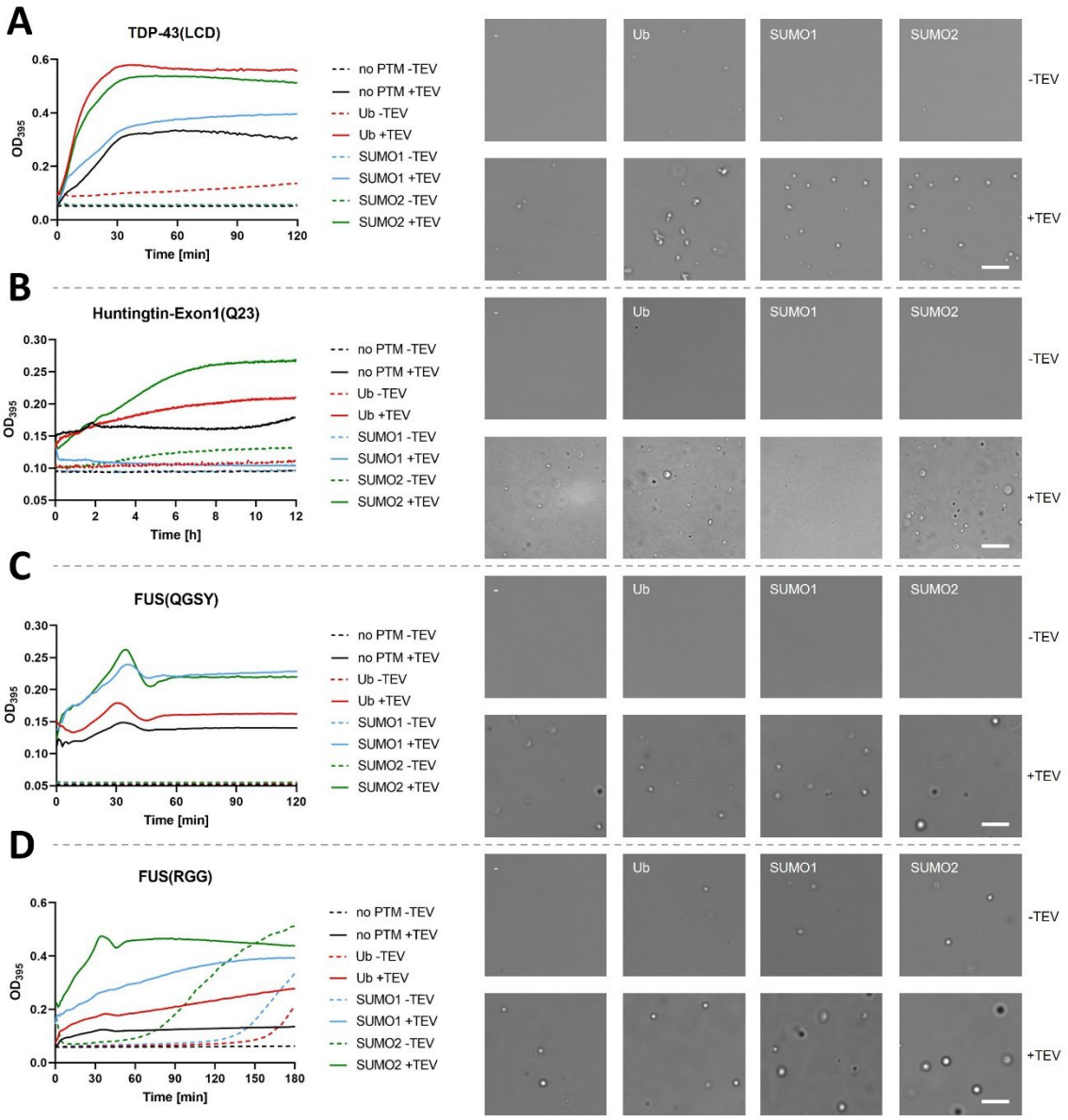

Figure 13: Intrinsic effect of fused post-translational modifiers on phase separation of different IDRs. Purified fusions of (**A**) TDP-43(LCD), (**B**) Htt-Ex1(Q23), (**C**) FUS(QGSY) and (**D**) FUS(RGG) with ubiquitin, SUMO1 or SUMO2 were diluted in PEG-containing buffer. Phase separation was induced by the addition of TEV protease for removal of MBP-tag. Turbidity was measured *in situ* by using a plate reader showing the mean of three technical replicates. Error bars are not displayed for better visibility. Representative DIC images of droplet formation were taken after 2 h for TDP-43(LCD), FUS(QGSY) and FUS(RGG), and after 10 h for Htt-Ex1(Q23). Scale bar: 10 µm

3.2 Characterization of Ub-/SUMO-TDP-43(LCD)

In this chapter, I further investigated the impact of ubiquitin- and SUMO-fusions using TDP-43(LCD) as a model protein. TDP-43 is a highly significant protein in current neurodegenerative research because of its major roles in the development of ALS and FTD (**chapter 1.2.7.1**). The LCD itself is an interesting model protein for the purpose of this work because of it sophisticated multivalent self-assembly mechanism and modification sites for ubiquitylation and SUMOylation at the N- and C-termini (François-Moutal *et al.* 2019). TDP-43(LCD) has been reported to phase separate in the absence of molecular crowding agents at physiological pH with increasing NaCl concentrations, showing UCST behavior (Babinchak *et al.* 2019). In this chapter, I wanted to analyze the impact of ubiquitin- and SUMO-fusions on TDP-43(LCD) in a minimal system and further characterize the biophysical properties of the condensate. Furthermore, I investigated phase separation of TDP-43(LCD) in a cellular environment by using mammalian cells as an expression platform.

3.2.1 TDP-43(LCD) phase separates in the absence of crowding agents

First, I assessed how TDP-43(LCD) and the respective fusion proteins with ubiquitin, SUMO1 and SUMO2 behave in a minimal system. I used protein concentrations of 50 µM in HEPES buffer with a physiological salt concentration of 150 mM NaCl and measured turbidity *in situ* at 25 °C (**Figure 14** A) and imaged potential condensates by DIC microscopy after 1 h (**Figure 14** B). In contrast to the presence of PEG-8000 (**chapter 3.1.4**), unmodified TDP-43(LCD) displayed the highest turbidity values. Small condensates appeared at a high number and at an irregular shape, indicating a phase separation state that can rather be associated with a gel-like state (**chapter 1.2.1**). For both ubiquitin- and SUMO2-TDP-43(LCD), turbidity values were reduced but condensate size was drastically increased, and their shape furthermore appeared round and regular. This suggests that the fusion of ubiquitin and SUMO2 enhances the liquid properties of TDP-43(LCD) condensates. Strikingly, SUMO1-TDP-43(LCD) did not undergo measurable phase separation, indicating that SUMO1 inhibits the phase separation mechanism of TDP-43(LCD).

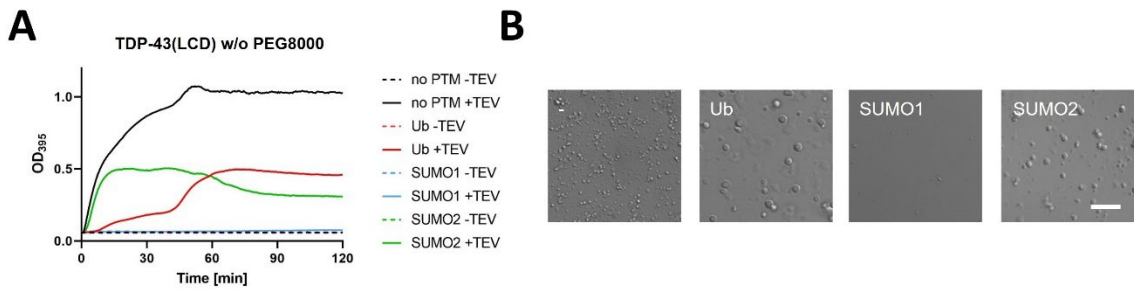

Figure 14: TDP-43(LCD) phase separation in the absence of molecular crowding agents. Phase separation of Ub-, SUMO1- and SUMO2-fusions to TDP-43(LCD) was analyzed by adding 0.1 mg/ml TEV-protease to 50 µM protein in the absence of molecular crowding agents. **(A)** Turbidity was measured *in situ* by using a plate reader. Error bars are not displayed for better visibility. **(B)** Representative DIC images of droplet formation were taken after 2 h. Scale bar: 10 µm

To gain further into droplet morphology, I used fluorescently labeled TDP-43(LCD). Introduction of a single cysteine at position G275 in the IDR does not interfere with phase separation and enables labeling using maleimide chemistry (Babinchak *et al.* 2019). I generated protein mixtures with 5% AzDye488-labeled protein and monitored phase separation under the same conditions as stated above at different time intervals during 3 h (**Figure 15**).

Fluorescence microscopy revealed several novel aspects of the previously detected droplets. First, TDP-43(LCD) droplets aged throughout the time course and ultimately appeared to show delicate fibril-like structures after 3h.

Second, both Ub- and SUMO2-TDP-43(LCD) droplets started to settle to the bottom of the microscopy slide after roughly 1 h, exhibiting a wetting-effect of the surface that further increased over the time. This effect is considered as an enhancement of liquid-like phase separation, as gravity and capillary effects drives spreading of the droplets on the surface (Chao *et al.* 2022). As a consequence, turbidity decreases due to the altered light scattering by a reduced number of particles compared to TDP-43(LCD) without a PTM (**Figure 14** A). It can thus be concluded that ubiquitin and SUMO2 both act as enhancers of TDP-43(LCD) phase separation. As unmodified TDP-43(LCD) eventually seems to undergo a liquid-solid phase transition, Ub- and SUMO2-TDP-43(LCD) remain liquid-like for a longer time.

Third, SUMO1-TDP-43(LCD) showed very few irregular spots after 2-3 h. Even at concentrations up to 400 µM, no distinct phase separation of SUMO1-TDP-43(LCD) was observed (**Appendix 4**). I conclude that the fusion of SUMO1 acts as a strong inhibitor of

TDP-43(LCD) phase separation in a minimal system, containing only the protein of interest and TEV-protease under physiological conditions.

Taken together, the tendencies between the modifiers are the same as observed in molecular crowding agent (**chapter 3.1.4**), but each effect is enhanced in the absence of: both ubiquitin- and SUMO2-fusion enhance TDP-43(LCD) phase separation, while the fusion of SUMO1 acts as an inhibitor. These observed phenotypes serve as the foundation of this thesis. The drastic effects of all three modifiers themselves on TDP-43(LCD) are already notable, but the striking differences between SUMO1 and SUMO2 suggest unique mechanisms for how phase separation of a largely unstructured protein can be modulated by the conjugation of highly similar post-translational modifiers.

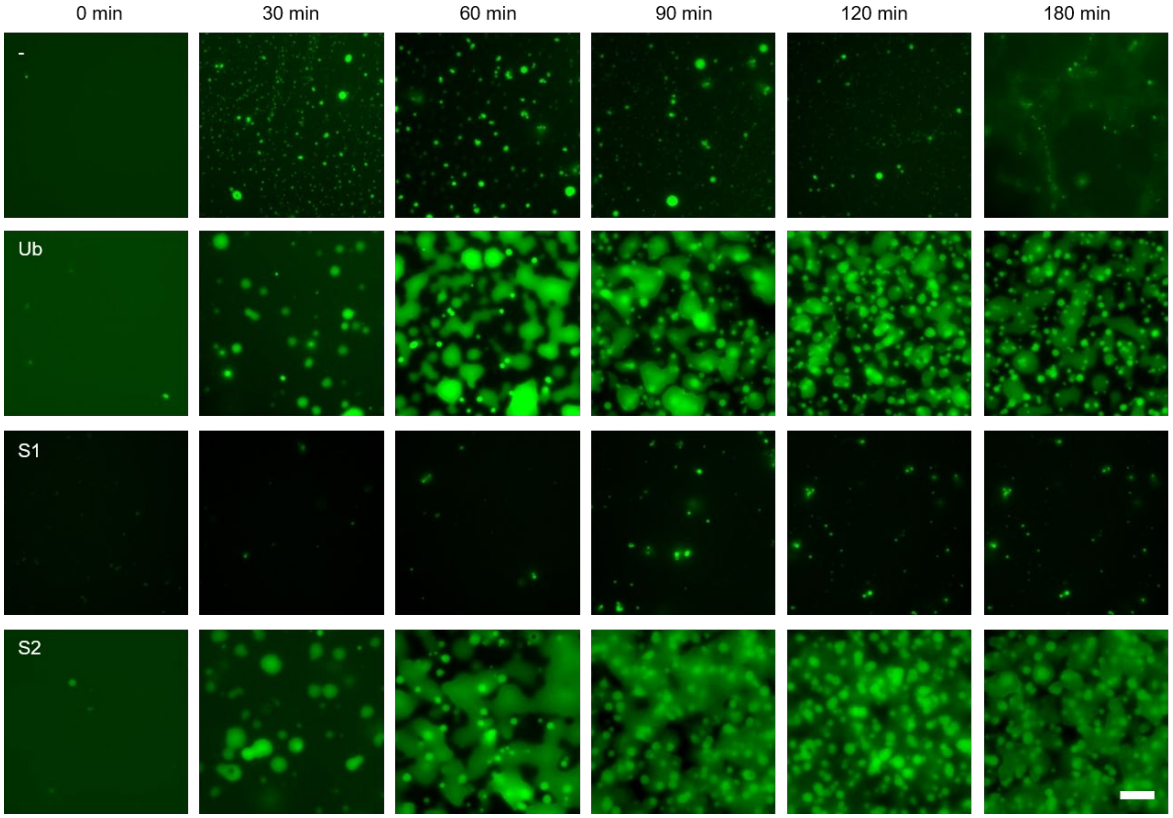

Figure 15: Analysis of fluorescently labeled TDP-43(LCD) droplet formation *in situ*. Phase separation of AzDye488-labeled Ub-, SUMO1- and SUMO2-TDP-43(LCD) was induced as described before. Droplet formation was monitored using fluorescence microscopy over a time course of 3 h. Scale bar: 10 µm.

3.2.2 Mixed droplets of modified and unmodified TDP-43(LCD)

Protein modification with PTMs can occur at varying stoichiometries that is often highly sensitive to spatiotemporal events in the cell (Prus *et al.* 2019). To mimic partial post-translation modification of TDP-43(LCD) and therefore the situation inside the cell, I

generated mixtures with distinct proportions of unmodified to modified TDP-43(LCD). I made use of the AzDye488-labeled fusion proteins shown in the previous section, but additionally generated Atto647-labeled TDP-43(LCD) to distinguish between modified and unmodified proteins by fluorescence microscopy. Each reaction mix contained 50 µM of total protein, while either 100%, 95% (47.5 µM), 90 (45 µM), 50% (25 µM) or 0% AzDye488-TDP-43(LCD) was modified with Ub, SUMO1 or SUMO2, and the remaining protein was filled up with Atto647-TDP-43(LCD). Phase separation was induced as described previously and droplets were imaged after 1 h.

Ub-TDP-43(LCD) phase separated in huge settling droplets, which were observed slightly later in the previous section (**Figure 15**). These small variances are a result of different batches of protein, as each fusion protein was purified multiple times. At only 5% TDP-43(LCD), smaller droplets appeared and the fraction of settled structured was reduced. In the presence of 10% TDP-43(LCD), a diffuse haze appeared around the droplets, similarly as for aged TDP-43(LCD) in **Figure 15**. At an equimolar ratio, droplet size drastically decreased, and condensates appeared comparable as in sole TDP-43(LCD) reactions. Interestingly, Ub-TDP-43(LCD) co-localized with TDP-43(LCD) at all tested concentrations, as indicated by white signal in the merged images

As SUMO1-TDP-43(LCD) did not form droplets in the previous experiment, it was interesting to observe how this trend further proceeded in a population with a decreasing degree of modification. Small portions of TDP-43(LCD) already induced the formation of a fibril-like structure, which merged together with SUMO1-TDP-43(LCD). Again, equimolar ratios resulted in a comparable phenotype to purely unmodified TDP-43(LCD) and the formation of small droplets in addition to the above-mentioned smear.

SUMO2-TDP-43(LCD) behaved fairly similar to Ub-TDP-43(LCD), which is not surprising due to the comparable phenotypes observed before. However, SUMO2 had a less dominant effect than Ub-TDP-43(LCD), resulting in the appearance of aggregates as described above. At equimolar concentrations of modified and unmodified TDP-43(LCD), the phenotype induced by SUMO2-fusion was not observable anymore. Once more, both proteins co-localized at all tested ratios, clearly indicated by white signal in the merged image.

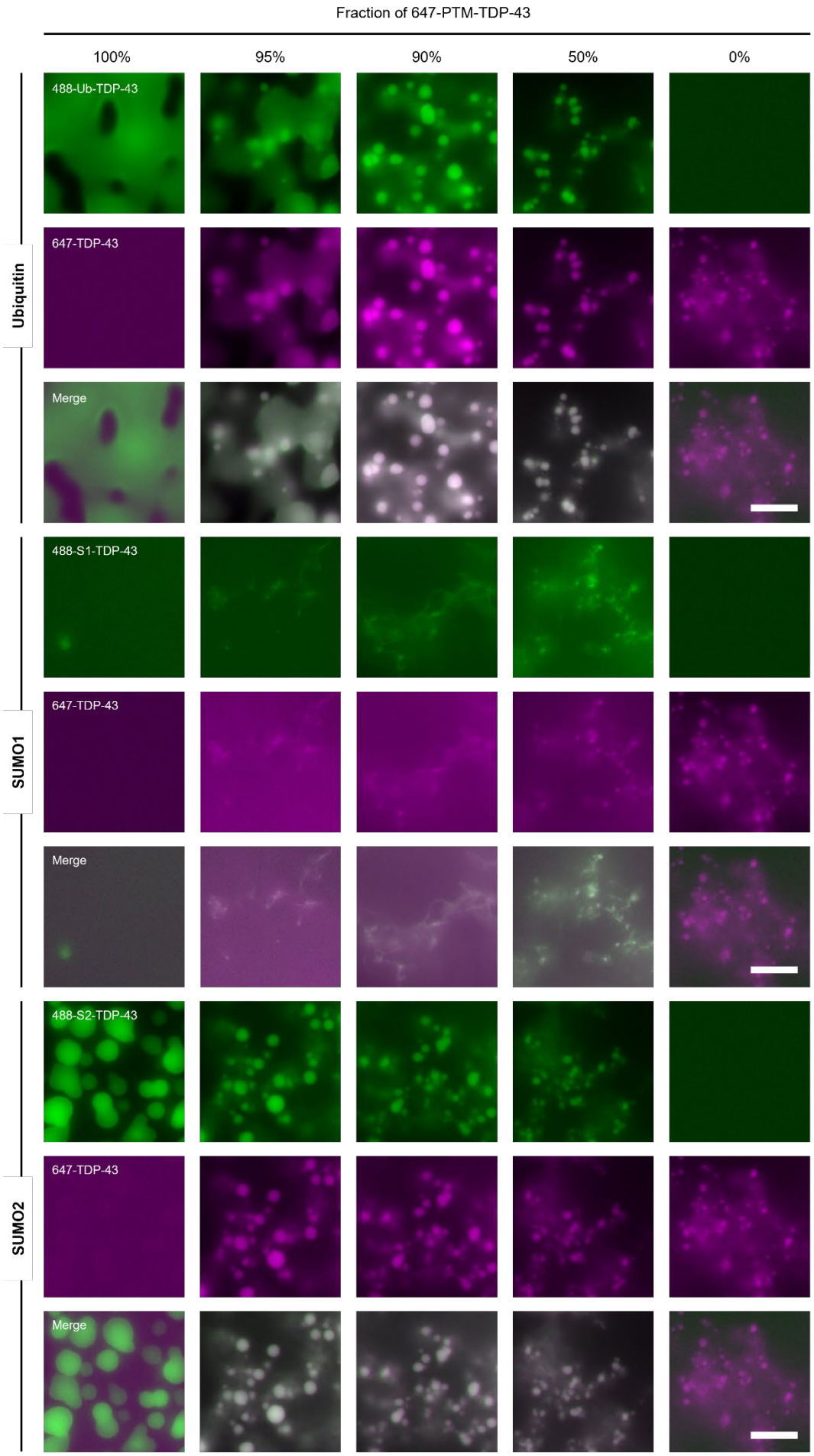
Fraction of 647-PTM-TDP-43
100%
95%
90%
50%
0%
Ubiquitin
488-Ub-TDP-43
647-TDP-43
Merge
SUMO1
488-S1-TDP-43
647-TDP-43
Merge
SUMO2
488-S2-TDP-43
647-TDP-43
Merge

Figure 16: Mixed condensates of modified and unmodified TDP-43(LCD). AzDye488-labeled Ub-, SUMO1, or SUMO2-TDP-43(LCD) (green) were mixed with Atto647-labeled TDP-43(LCD) (purple) at different molar ratios at a total concentration of 50 µM. Phase separation was induced as described before and droplet formation was monitored after 1 h by fluorescence microscopy, probing for the respective wavelengths. White signal indicates merging. Scale bar: 10 µm.

In conclusion, TDP-43(LCD) has a dominant phenotype that is only suppressed at a high degree of ubiquitylated or SUMOylated protein. Yet, the effect of modified and unmodified TDP-43(LCD) merging in all conditions was quite intriguing. This suggests a common mechanism of TDP-43(LCD) self-assembly that is either supported by ubiquitin and SUMO2 or inhibited by SUMO1. It can be assumed that a molecule of unmodified TDP-43(LCD) can interact with a Ub-/SUMO-fusion protein to form condensates.

It is not surprising that a low concentration of unmodified TDP-43(LCD) is sufficient to promote an aggregation-like phenotype *in vitro*, since fibril formation is usually initiated by nucleation. This means that a small proportion of aggregated protein can act as a seed in this process. However, the situation might differ in a cellular context, as this effect is mostly studied in artificial environments (Kumar *et al.* 2023).

3.2.3 Biophysical characterization of TDP-43(LCD) condensates

The following section will provide a detailed biophysical characterization of TDP-43(LCD) phase separation dependence on ubiquitin, SUMO1 and SUMO2. This helps understanding the nature of the condensates and gives insights in the mechanism of self-assembly. I investigated droplet mobility, as well as molecular driving forces of condensate assembly, and tried to obtain insight into potential secondary structure formations of ubiquitin- and SUMO-fused TDP-43(LCD).

3.2.3.1 Liquid properties

Fluorescence recovery after photobleaching (FRAP) is a commonly used method to obtain insights into the liquidness of condensates (Taylor *et al.* 2019). I used the same experimental setup as described in **section 3.2.1** for the fluorescence microscopy time course. SUMO1-TDP-43(LCD) was not analyzed, as this construct did not form any droplets. Droplets from each construct were bleached after either 30 min or 2 h after TEV-cleavage and fluorescence recovery was measured every sec for 2 min. Comparing the fluorescence recovery after a shorter and a longer time point allows to draw conclusions about aging of the condensates. The more liquid a droplet is, the higher its mobility is. With

a progressive aging of the condensates, mobility should decrease as the condensates are expected to eventually solidify. Data were analyzed by easyFRAP and a double term exponential equation was used to determine mobile fractions (Koulouras *et al.* 2018).

After 30 min (**Figure 17** A), untagged TDP-43(LCD) recovered up to 50%, while both Ub-TDP-43(LCD) and SUMO2-TDP-43(LCD) showed a very similar recovery around 75%. This indicates that Ub and SUMO2 boost the liquidity of TDP-43(LCD) droplets. The mobile fraction of aged TDP-43(LCD) droplets almost halved after 2 h in comparison to 30 min (**Figure 17** B). Also, Ub- and SUMO2-TDP-43(LCD) droplets became less liquid, while the aging effect was less pronounced, resulting in a reduction of the mobile phase by roughly 25-30%. In conclusion, the data suggest that fusion of Ub or SUMO2 shifts the phase separation of TDP-43(LCD) in a more liquid-like manner.

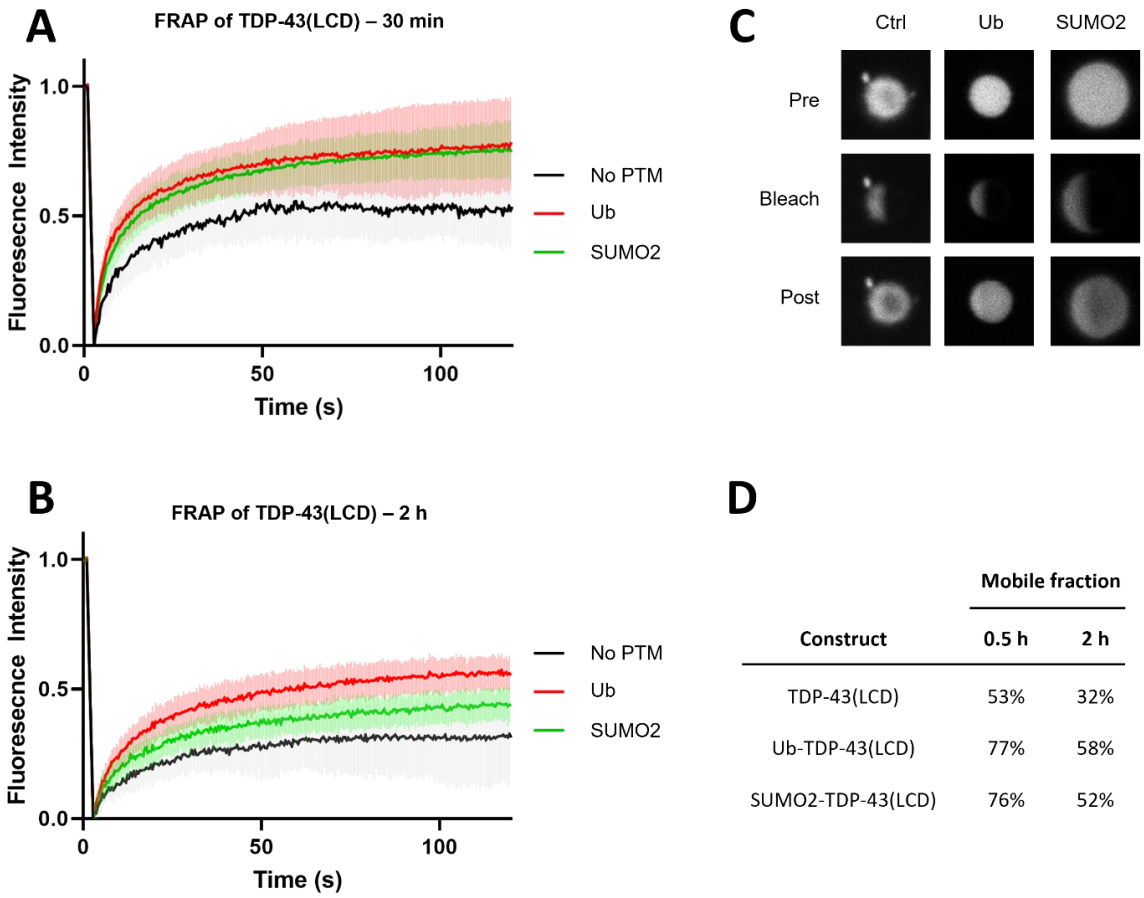

Construct	Mobile fraction 0.5 h	2 h
TDP-43(LCD)	53%	32%
Ub-TDP-43(LCD)	77%	58%
SUMO2-TDP-43(LCD)	76%	52%

Figure 17: FRAP of TDP-43(LCD). Phase separation of AzDye488-labeled Ub-, and SUMO2-TDP-43(LCD) was induced as described before. Droplets were bleached after 0.5 h (**a**) and 2 h (**b**). Fluorescence recovery was monitored for 2 min (n=10 per construct). (**C**) Exemplary images pre bleaching, directly after bleaching and 2 min post bleaching. (**D**) Data were analyzed using easyFRAP for determination of mobile fraction.

3.2.3.2 Dependance on hydrophobic interactions

1,6-hexanediol is an aliphatic alcohol that is commonly used to disrupt phase separation as it inhibits weak hydrophobic interaction, which are main drivers of self-assembly (Kroschwald *et al.* 2017). I monitored phase separation by turbidity assays (**Figure 18** A) and fluorescence microscopy (**Figure 18** B) in the absence or presence of 1% or 2% 1,6-hexanediol. At 1% 1,6-hexanediol, turbidity of Ub- and SUMO2-TDP-43(LCD) was reduced by approximately 50%, while TDP-43(LCD) turbidity was barely affected. Fluorescence microscopy revealed that the wetting effect of Ub-TDP-43(LCD) slightly decreased but was nearly not observable for SUMO2-TDP-43(LCD). At 2% 1,6-hexanediol, turbidity of TDP-43(LCD) values also decreased by approximately 50%. Ub- and SUMO2-TDP-43(LCD) turbidity was almost similar as the control reaction without TEV-protease. Interestingly, Ub- and SUMO2-TDP-43(LCD) droplets adopt a similar shape like the TDP-43(LCD) control protein.

In conclusion, the data suggest that weak hydrophobic interactions might be a crucial driver for the enhancement of phase separation by fusing ubiquitin or SUMO2 to TDP-43(LCD).

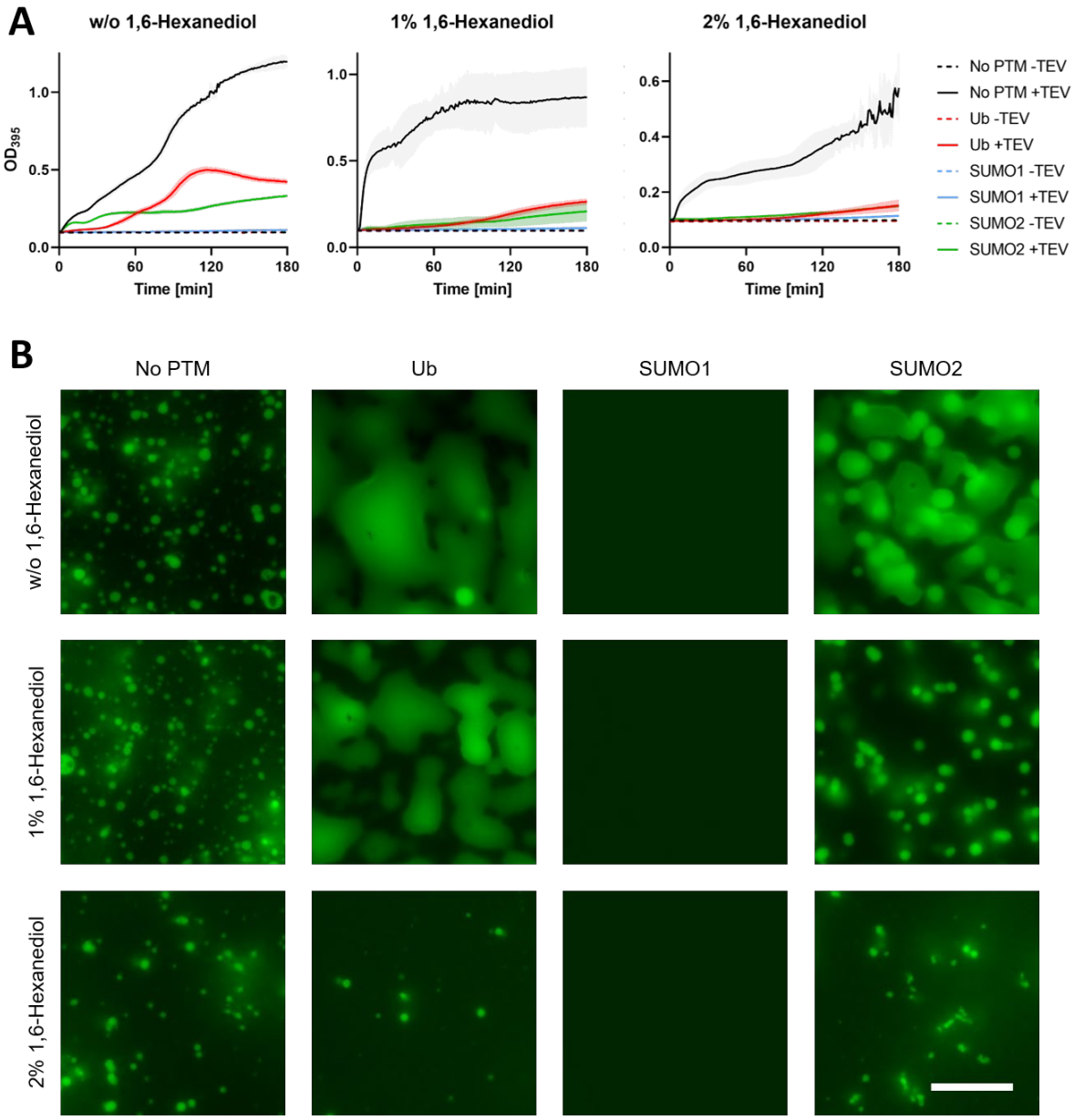

Figure 18: TDP-43(LCD) condensates are sensitive to 1,6-Hexanediol. Phase separation of unlabeled or AzDye488-labeled Ub-, SUMO1- and SUMO2-TDP-43(LCD) was induced as described before in the absence or presence of 1% or 2% 1,6-Hexanediol. **(A)** Turbidity was measured *in situ* in a plate reader. **(B)** Representative fluorescence microscopy images of droplet formation were taken after 2 h. Scale bar: 10 µm

3.2.3.3 Dependance on electrostatic interactions

Electrostatic interactions can be interrupted by high salt concentrations (Nott *et al.* 2015). Therefore, I analyzed phase separation in the absence or presence of NaCl up to concentrations of 600 mM. I slightly changed the experimental setup, as TEV-protease strongly loses activity at salt concentrations higher than 200 mM (Nallamsetty *et al.* 2004). Phase separation was induced in a 1.5 ml reaction tube by the addition of 0.1 mg/ml TEV

protease at RT and the reaction was subsequently distributed into microscopy slides. Respective salt concentrations were achieved by the addition of NaCl from a 5 M stock solution. Droplets need at least 10 min to settle to the bottom of the microscopy slide and it was expected that the droplet shape might change due to sensitivity to pipetting. Indeed, the untagged control protein TDP-43(LCD) adopted a clumped conformation, and I barely observed any surface wetting by Ub- and SUMO2-TDP-43(LCD) in comparison to **chapter 3.2.1** (**Figure 15**). Yet, phase separation of all four constructs was clearly reduced with increasing salt concentrations. Even SUMO1-TDP-43(LCD) formed a diffuse amorphous haze in the absence of salt. Ub- and SUMO2-TDP-43(LCD) condensates appeared at a size up to 10 µm and gradually shrunk with increasing salt concentration up to 300 mM. A further increase to 600 mM did not have any effect. TDP-43(LCD) condensates were resistant to all tested NaCl concentrations.

Altogether, phase separation of Ub- and SUMO2-TDP-43(LCD) seems to rely on electrostatic interactions. Hence, it is difficult to conclude if the sole Ub- and SUMO2-fusion mediates the effect, since the untagged control construct clumps together due to the experimental procedure. Yet, this experiment once again shows evidence that ubiquitin and SUMO2 promote condensate liquidity.

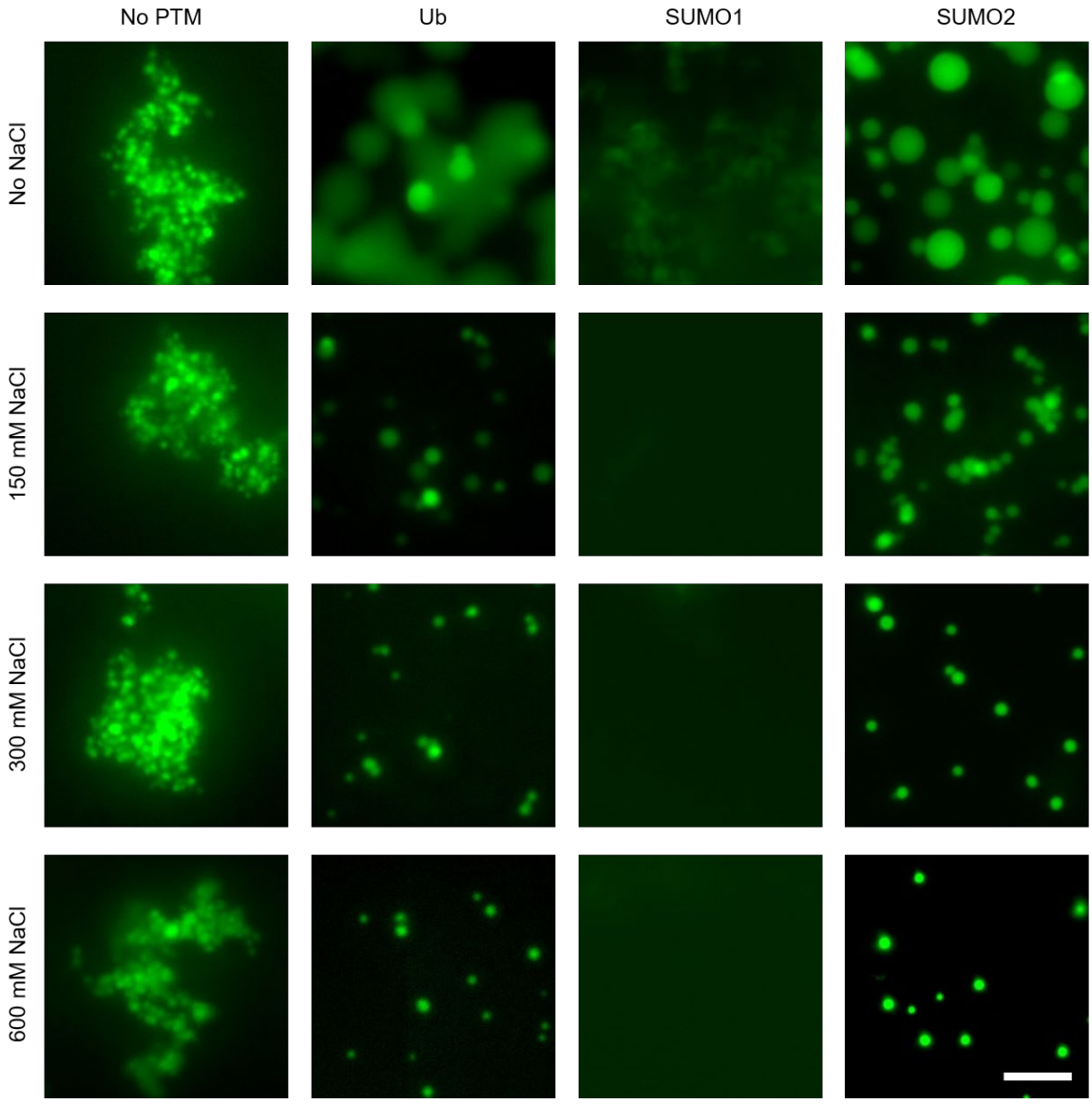

Figure 19: TDP-43(LCD) condensates are sensitive to salt. Phase separation of AzDye488-labeled Ub-, SUMO1- and SUMO2-TDP-43(LCD) was induced as described before in the presence of various NaCl concentrations. Droplet formation was monitored using fluorescence microscopy after 2 h. Scale bar: 10 µm.

3.2.3.4 Aggregation properties

Thioflavin-T (ThT) is a fluorescent dye that is widely used to characterize solid-like protein aggregation. Bound to amyloid fibrils, free rotation of the benzothiazole group and the benzylamine group is prevented, which leads to inhibition of quenching after excitation (Xue *et al.* 2017). I used Thioflavin-T to gain insight on the aggregation behavior of Ub-/SUMO-TDP-43(LCD) by mixing 50 µM protein with 25 µM Thioflavin-T and monitoring aggregation over time. The fluorescence spectra displayed characteristic peaks at 480 nm after excitation at 450 nm, with SUMO2-TDP-43(LCD) having the strongest signal, TDP-

43(LCD) and SUMO1-TDP-43(LCD) behaving similarly and Ub-TDP-43(LCD) having the weakest signal (**Figure 20** A). However, no characteristic sigmoidal curve could be observed even after 20 days (**Figure 20** C), which raises doubts that the method could be executed properly. One would expect an exponential increase of fluorescence intensity, as protein fibril formation is usually driven by nucleation (Chatani and Yamamoto 2018). The lack of a control protein that undergoes aggregation and technical difficulties with the plate reader did not allow me to draw conclusions on TDP-43(LCD) aggregation upon fusion of ubiquitin or SUMO.

Nevertheless, this experiment requires optimization to explore the effect of ubiquitin and SUMO on different phase transition mechanisms of TDP-43(LCD). The phenotype of untagged TDP-43(LCD) forming irregularly shaped condensates (**Figure 15**) strongly suggests that the droplets become less dynamic and most likely undergo a solidification. It might be interesting to establish appropriate experiments to distinguish between gel-like and solid-like condensation.

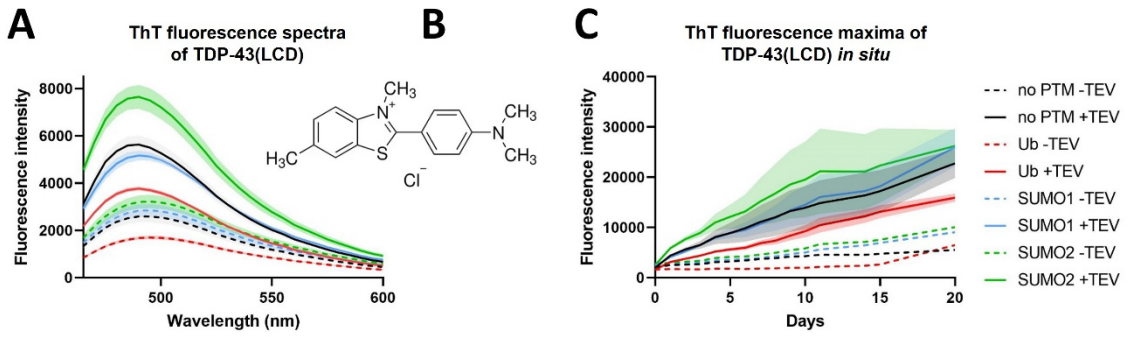

Figure 20: Aggregation of TDP-43(LCD). (**A**) Phase separation of Ub-, SUMO1- and SUMO2-TDP-43(LCD) was induced as described before in the presence of Thioflavin-T (**B**) and fluorescence spectra were recorded after excitation at 450 nm. The plot shows representative spectra after 5 d. (**C**) Aggregation was monitored *in situ* for 20 d.

3.2.3.5 Changes in secondary structure

Ubiquitylation has been shown to directly affect the protein fold of its conjugation partner (Morimoto *et al.* 2016). The drastic phenotype differences between ubiquitin, SUMO1 and SUMO2 on TDP-43(LCD) suggested fold changes that should be detectable by comparing PTM fusions with PTM mixtures as shown in **chapter 3.1.3**. The molecular weight of up to 67 kDa makes TDP-43(LCD) fusion proteins not applicable to NMR spectroscopy. I used far-UV CD spectroscopy to detect global fold changes in the secondary structure of the fusion proteins. Therefore, I prepared mixtures of either 10 µM Ub-/SUMO-TDP-43(LCD) or 10 µM untagged TDP-43(LCD) with the respective free, non-conjugated modifier and

induced phase separation as described before. However, the voltage was too high to obtain meaningful spectra, most likely due to excessive absorption of the turbid solution. Therefore, I only analyzed the spectra of Ub-/SUMO-TDP-43(LCD) in the absence of TEV-protease (**Figure 21**). The general spectra indicate a strong presence of α-helices, which is explainable due to the presence of MBP in the reaction mix. Yet, fusion of each modifier enhanced the signal in the range between 210-225 nm, compared to TDP-43(LCD) mixed with the respective modifier. This result must be taken with caution, as removal of MBP was not possible to achieve for me.

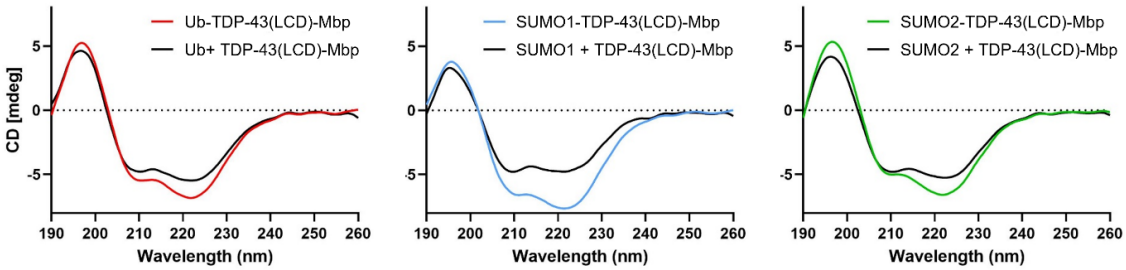

Figure 21: Far-UV spectra of TDP-43(LCD) mixed or fused with ubiquitin, SUMO1 or SUMO2. CD spectra were recorded for either 10 µM Ub-/SUMO-TDP-43(LCD) or 10 µM Ub/SUMO and 10 µM TDP-43(LCD) in the absence of salt at 25 °C.

In summary, I showed by various methods that Ub- and SUMO2-fusion enhance liquid-liquid phase separation of TDP-43(LCD). This phenotype most likely relies on multiple molecular interactions that most likely include hydrophobic and electrostatic interactions. The involvement of hydrogen-bonds can further be investigated by using low concentrations of Urea (Poudyal *et al.* 2023). The formation of secondary structural elements induced by PTM-fusions could not reliably be determined and potential liquid-to-solid transitions of TDP-43(LCD) need to be further investigated.

3.2.4 Analysis of TDP-43(LCD) in a cellular context

The cytotoxic CTF-25 and CTF-35 fragments of TDP-43 mainly rely on self-assembly mechanisms of the LCD of TDP-43 and accumulate in the cytoplasm (**chapter 1.2.7.1**). Hence, it is interesting to study how ubiquitin- and SUMO-fusions affect TDP-43(LCD) in a cellular context.

Therefore, I modified a pEGFP-C1 to clone His-tagged TDP-43(LCD)-EGFP. EGFP was fused to the C-terminus of TDP-43(LCD) to keep a similar construct arrangement as in the *in vitro* assays and not having a bulky protein at the flexible N-termini of SUMO1 and

SUMO2. These constructs were transiently transfected into HeLa cells, which were subsequently imaged by live cell high-throughput confocal fluorescence microscopy and an automated analysis pipeline that quantifies transfected cells forming droplets. This enables the screening of a high number of different constructs with relatively low effort compared to testing purified proteins *in vitro*, since it only requires a transfection step, and imaging can be executed without the need of cell fixation and antibody-related staining methods.

In this section, I investigated how altering the cellular localization of TDP-43(LCD) or the fusion-position of the PTM change condensate formation. Furthermore, I tested how a set of multivalency-mutations in TDP-43(LCD) affect phase separation in dependance of ubiquitin- and SUMO-fusions.

3.2.4.1 Effects of PTM-fusions on TDP-43(LCD)

First, I wanted to assess the general phenotype of N-terminal ubiquitin- and SUMO-fusions on TDP-43(LCD) to see if it reflects the observations that I made *in vitro* (**Figure 22** A, upper lane). The expression of TDP-43(LCD)-EGFP resulted in a largely cytoplasmic expression, while only roughly 20% of positively transfected cells showed condensates. Upon fusion with ubiquitin and SUMO2, the number of transfected cells with droplets drastically increased up to almost 40% and 50%, respectively. While both constructs have the same phenotype *in vitro*, condensate shape varies in the cellular system. Ub-TDP-43(LCD) forms amorphous condensates that are unevenly distributed through the cell. In comparison, SUMO2-TDP-43(LCD) is clearly forming two different populations of round droplets, residing both in the cytoplasm and in the nucleus. Strikingly, fusion of SUMO1 almost abolished condensate formation of TDP-43(LCD) (<5%).

Next, I wanted to determine if the observed phenotypes rely on the cellular localization mediated by the fusion of the modifier, so I generated plasmids that force TDP-43(LCD) either in the nucleus or into the cytoplasm. For TDP-43(LCD), Ub-TDP-43(LCD) and SUMO1-TDP-43(LCD), I fused a 3xNLS to the N-terminus and transfected cells as described above. Protein localization of the 3xNLS-fusions was indeed pronounced in the nucleus (**Figure 22** A, middle lane), but surprisingly all constructs showed a similar effect with approximately 70% of transfected cells forming droplets, which is a strong increase (**Figure 22** B). The 3xNLS itself has a molecular weight of almost 3 kDa and can be considered as a considerable addition that might block the flexible N-terminus of SUMO1.

Since SUMO2-TDP-43(LCD) formed prominent droplets in the cytoplasm, I used a 3xNES to deplete the protein from the nucleus. No droplets were detectable in the nucleus, while

droplet formation in the cytoplasm appeared similar as in the construct without a localization signal (**Figure 22** A, middle lane). Indeed, the overall propensity of approximately 50% transfected cells forming condensates was not affected (**Figure 22** B), shown by a similar number of transfected cells with droplets.

Last, I rearranged the expression constructs, by positioning Ub or SUMO at the C-terminus of TDP-43(LCD), N-terminally of EGFP. Ubiquitin and ubiquitin-like modifiers are usually conjugated to target proteins by their C-terminal di-Glycine motif, which makes this a highly artificial system. Yet, it might enable insights into how the position of the PTM is relevant for TDP-43(LCD) phase separation. A similar setup failed in an *in vitro* setup due to proteins being unstable throughout the purification procedure and the subsequent phase separation assays (**Appendix 3**). In mammalian cells, reasonable expression was achieved for TDP-43(LCD)-SUMO1 and TDP-43(LCD)-SUMO2 compared to the N-terminally tagged constructs. Expression of ubiquitin-tagged constructs was weaker, especially for the C-terminal fusion (**Figure 22** E). Condensate formation propensity was overall reduced in this experimental series, which is most likely the result of variances in the transfection reagent batch. However, the basic phenotypes induced by ubiquitin, SUMO1 or SUMO2 fusions remained comparable (**Figure 22** D). TDP-43(LCD)-Ub barely formed condensates, but this result has to be considered with caution due to a very low expression level.

In comparison, changing the position of SUMO allowed to draw conclusions due to equal expression levels as shown by western blot (**Figure 22** E). Fusing SUMO1 to the C-terminus of TDP-43(LCD) induced phase separation to a comparable extent as untagged TDP-43(LCD), and droplets appeared mainly in the nucleus (**Figure 22** A, lower lane). As TDP-43(LCD)-SUMO1 expression is reduced compared to untagged TDP-43(LCD) but still forms condensates, this strongly suggests that C-terminal fusion of SUMO1 abolishes the inhibitory effect on TDP-43(LCD) phase. Positioning of SUMO2 at the C-terminus of TDP-43(LCD) did not affect the phenotype and phase separation was similarly enhanced as with an N-terminal fusion, showing approximately 20% transfected cells with droplet formation (**Figure 22** E). Therefore, I am assuming that the sheer presence of SUMO2 as a conjugated protein is sufficient to enhance condensation, regardless of the attachment site.

Altogether, these results suggest that SUMO1 accomplishes its inhibitory effect via its flexible N-terminus, while SUMO2 might act as an enhancer of phase separation by a more general mechanism.

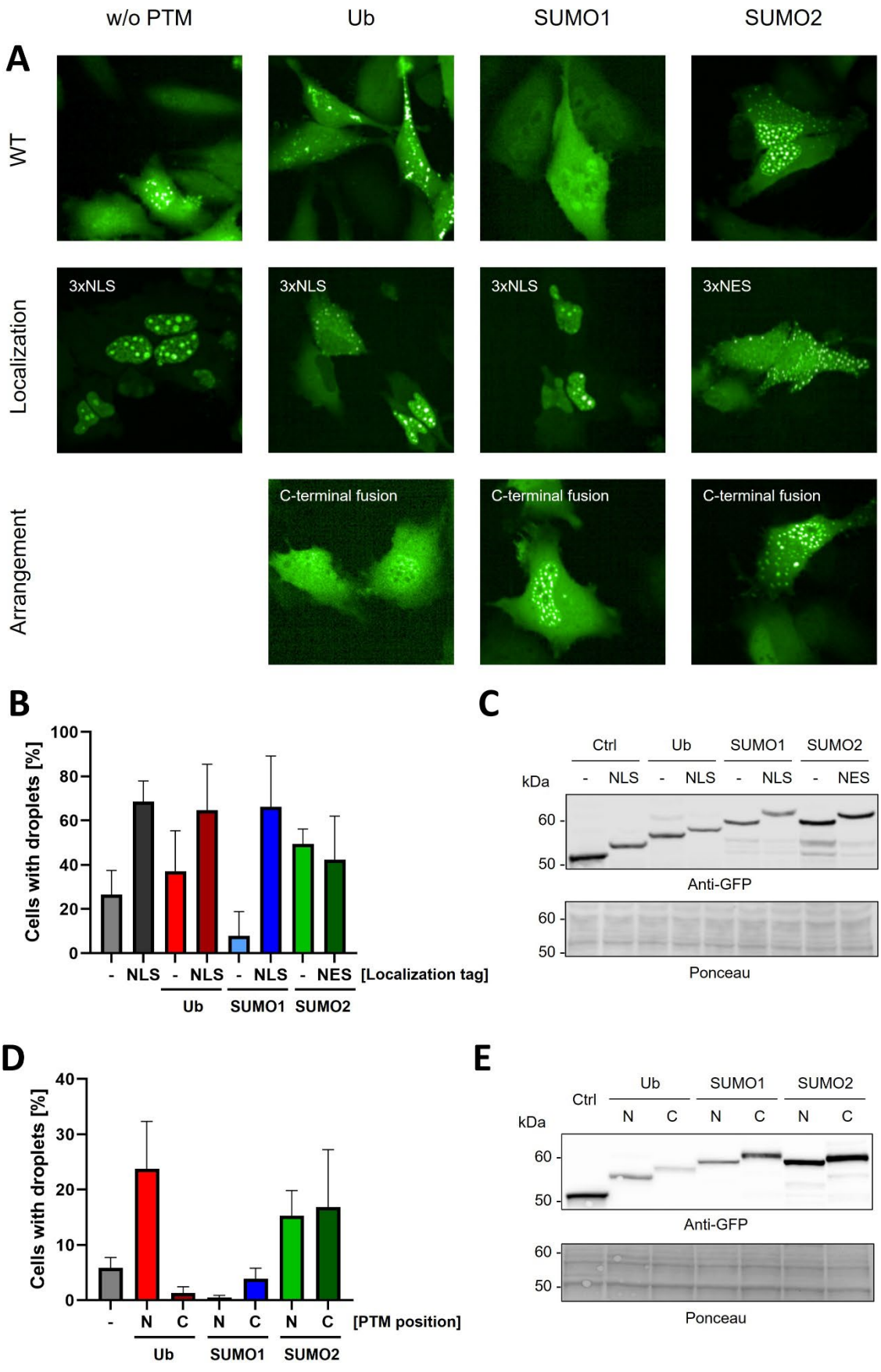
w/o PTM
Ub
SUMO1
SUMO2
A
WT
Localization
Arrangement
3xNLS
3xNLS
3xNLS
3xNES
C-terminal fusion
C-terminal fusion
C-terminal fusion
B
Cells with droplets [%]
100
80
60
40
20
0
- NLS - NLS - NLS - NES [Localization tag]
Ub
SUMO1
SUMO2
C
Ctrl
Ub
SUMO1
SUMO2
kDa
- NLS - NLS - NLS - NES
60
50
Anti-GFP
60
50
Ponceau
D
Cells with droplets [%]
40
30
20
10
0
- N C N C N C [PTM position]
Ub
SUMO1
SUMO2
E
Ctrl
Ub
SUMO1
SUMO2
kDa
N C N C N C
60
50
Anti-GFP
60
50
Ponceau

Figure 22: Characterization of TDP-43(LCD) in mammalian cells. (**A**) EGFP-tagged TDP-43(LCD) was transiently overexpressed in HeLa cells with the indicated modifiers. Phase separation behavior of NLS- or NES-tagged constructs were compared with untagged fusion proteins by fluorescence microscopy (**A**, middle lane) and (**B**) fractions of transfected cells with droplets were quantified (n=3). (**C**) Protein expression was analyzed by western blot using an antibody against GFP. Constructs harboring Ub or SUMO at then- or C-terminus of TDP-43(LCD) were expressed in HeLa cells and analyzed by fluorescence microscopy (**A**, lower lane). (**D**) Fractions of transfected cells with droplets were quantified (n=3). (**E**) Protein expression was analyzed by western blot using an antibody against GFP.

3.2.4.2 Interplay between PTMs and TDP-43(LCD) phase separation mutations

The mechanism of TDP-43(LCD) self-assembly has largely been resolved. In brief, a conserved transient α-helix spanning residues 321-340 induces self-assembly together with a few distributed aromatic amino acids (**chapter 1.2.7.1**). I wanted to investigate how ubiquitin and SUMO interfere with TDP-43(LCD) mutants that are described to alter phase separation. Since the α-helix is the main self-assembly site, I generated the mutant A326P, which has been shown to disrupt helicity (Conicella *et al.* 2016). The transient nature of this α-helix moreover offered the opportunity to stabilize the secondary structure by introducing the mutations G335A and G338A, which were described to enhance helicity and thus also phase separation (Conicella *et al.* 2020). It has also been showed that W334 and W385 have the strongest impact on inducing self-assembly, so I generated a double mutant where both tryptophans were mutated to glycine (Li *et al.* 2018). The modified protein sequences were submitted to AlphaFold, and a simulation of the conserved helical region is shown in **Figure 23** A. All phase separation mutants were cloned into the TDP-43(LCD) sequence as C-terminal fusions to ubiquitin, SUMO1, or SUMO2 to generate EGFP-tagged mammalian expression vectors as described in the previous section. As SUMO1-TDP-43(LCD) did not form any droplets, there was no need in generating plasmids harboring phase separation reducing mutants A326P and W334G/W385G.

Plasmids were transfected as described before and phase separation was quantified in live cells. Expression of constructs harboring G335A/G338A strongly enhanced droplet formation compared to WT TDP-43(LCD) (**Figure 23** B). Up to 80% of cells transfected with either TDP-43(LCD), Ub-TDP-43(LCD) or SUMO2-TDP-43(LCD) contained droplets (**Figure 23** C), while the overall effect of enhanced phase separation was most pronounced in case of SUMO2-TDP-43(LCD). Strikingly, this strong phenotype induced by enhanced helicity could not be observed in the case of SUMO1-TDP-43(LCD), which was still largely soluble and unable to form droplets. This indicates an interaction between SUMO1 and the α-helix in TDP-43(LCD). As the sheer presence of SUMO1 in a reaction mix with TDP-43(LCD) does not have any effect (**section 3.1.3**), the phenotype of inhibited

phase separation by SUMO1-fusion is most likely based on very weak intramolecular interactions.

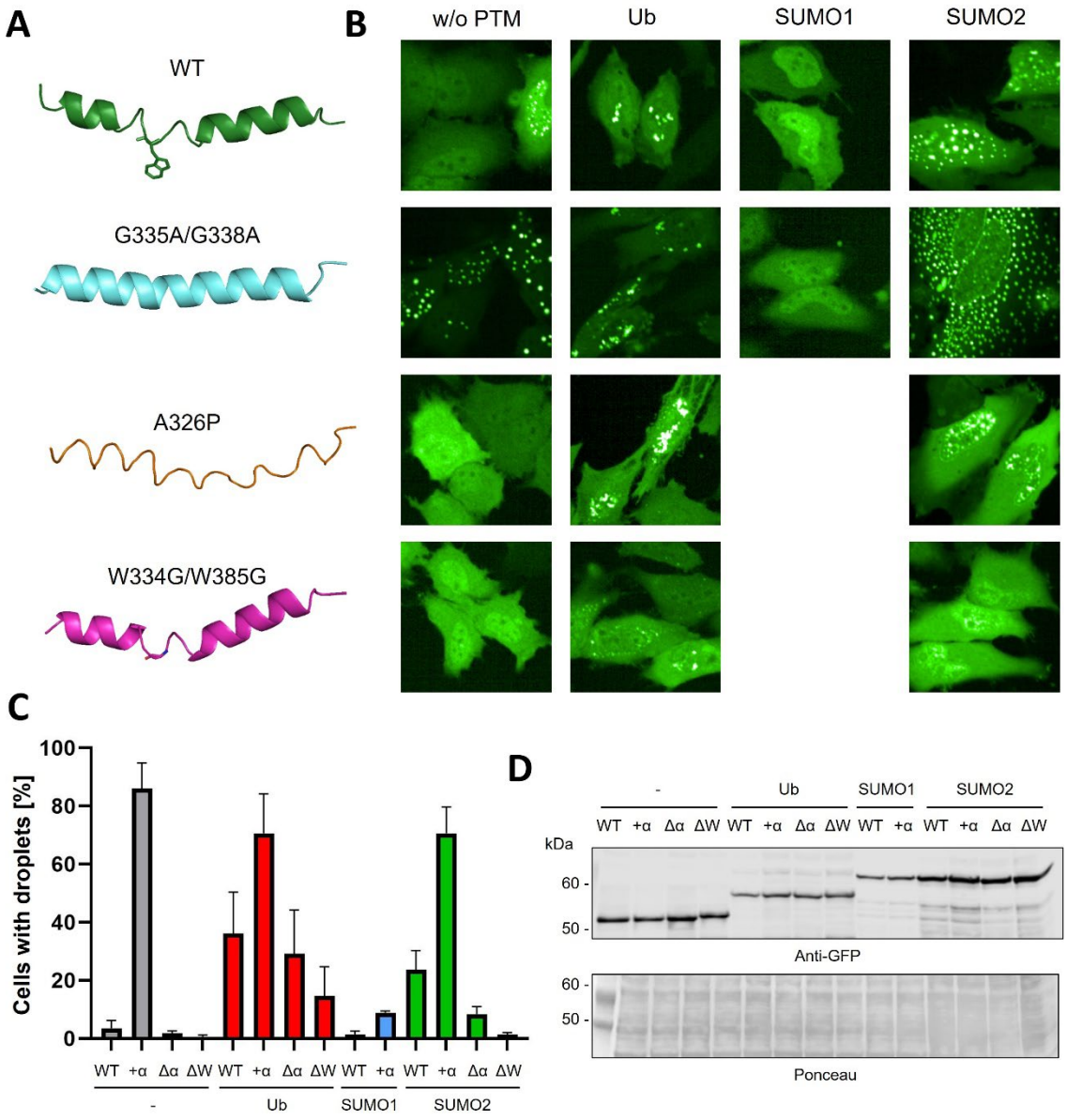

Figure 23: Effects of Ubiquitin and SUMO on phase separation mutants of TDP-43(LCD). (**A**) TDP-43(LCD) mutations were subjected to AlphaFold2 and representative models are shown as cartoons. WT in green displays W334 as stick. Enhanced helicity mutant (+α) G335A/G338A in cyan. Reduced helicity mutant (Δα) A326P in orange. Reduced multivalency mutant (ΔW) W334G/W385G in pink with W334G mutation showed as stick. (**B**) EGFP-tagged TDP-43(LCD) harboring respective mutations were transiently overexpressed in HeLa cells. (**C**) Fractions of transfected cells with droplets were quantified (n=3). (**D**) Protein expression was analyzed by western blot an antibody against GFP.

Disrupting the α-helix by introducing the mutation A326P decreased droplet formation in case of Ub- and SUMO2-TDP-43(LCD), while almost no droplets were detectable for TDP-

43(LCD). Interestingly, both PTM-tagged proteins harboring A326P phase separated stronger than TDP-43(LCD) with WT sequence. Self-assembly is most likely a synergistic effect mediated by helix-helix interactions and π-stacking, so this result shows how the loss of one component can possibly be compensated by ubiquitin and SUMO2. Both modifiers might provide a specific binding site or generally enhance multivalency by their amino acid composition (**chapter 1.2.2**).

Decreasing general multivalency by mutating W334G/W385G had a similar effect but with an increased impact compared to A326P mutants. Ub-TDP-43(LCD) condensates appeared faint and small, while SUMO2-TDP-43(LCD) expression did not form condensates. This further supports the assumption of compensating losses of self-assembly sites by these modifiers as discussed before. Indeed, it raises the possibility that both ubiquitin and SUMO2 can serve as an intramolecular client, considering TDP-43(LCD) as the phase separation scaffold. Further experiments are required to identify how both PTMs enhance phase separation on a molecular level and whether they interact with themselves or with specific regions in TDP-43(LCD) in order to enhance multivalency.

Overall, this experiment provided insights into how each tested PTM exerts its respective phenotype, suggesting critical regions and potential binding sites. Most likely, SUMO1 blocks an important self-assembly site. If we consider the general enhancement of phase separation by Ubiquitin and SUMO2 observed in **section 3.1.4**, both might increase overall multivalency of the protein they are attached to in an unspecific manner. If SUMO1 has a similar ability to enhance self-assembly in the absence of a suitable binding site within a protein prone to undergo phase separation remains to be found out.

3.3 Unique mechanism of SUMO isoforms modulating phase separation

Several experiments in **chapter 3.2** showed drastic differences in the behavior of TDP-43(LCD) phase separation upon fusion with SUMO1 or SUMO2. Both modifiers share a similar fold but only 50% of their amino acid sequence is conserved. Given this fact, it is likely that regions of distinct amino acid compositions are responsible for the according phenotypes. The following section will describe how a combinational approach of mass-spectrometry and microscopy gives structural insights in the mechanisms of prevention or enhancement of liquid-liquid phase separation.

3.3.1 SUMO1-TDP-43(LCD) is enriched at SUMO2-TDP-43(LCD) droplet surface

As SUMO1 and SUMO2 provide exactly opposing effects on TDP-43(LCD) phase separation, I wanted to find out how a mixed population of both modifiers would affect phase separation. Therefore, I analyzed phase separation of different ratios of AzDye488-labeled SUMO1-TDP-43(LCD) and Atto647-labeled SUMO2-TDP-43(LCD), similarly as described in **section 3.2.2**. Each reaction would contain either 100% (50 µM), 95% (47.5 µM), 90 (45 µM), 50% (25 µM) or 0% Atto647-SUMO2-TDP-43(LCD), while the remaining protein was filled up with AzDye488-SUMO1-TDP-43(LCD) to reach a total protein concentration of 50 µM. Phase separation was induced as described previously and droplets were imaged after 1 h. As shown in **Figure 24**, SUMO2-TDP-43(LCD) forms the previously observed phenotype, with a gradual decrease in droplet size upon reduction of protein concentration. At 50% SUMO2-TDP-43(LCD), only small irregular condensates can be detected, while no condensates were observed at 10% SUMO2-TDP-43(LCD).

Small portions of SUMO1-TDP-43(LCD) in the reaction mix did not change the SUMO2-induced phenotype but led to colocalization of both protein populations. Strikingly, SUMO1-TDP-43(LCD) seems to have a strong aversion of fully entering the droplets. It rather accumulates at the droplet surface, demonstrated by the formation of a white ring in the merged images at 90% and 95% of SUMO2-TDP-43(LCD). The SUMO1-TDP-43(LCD) signal itself shows a strong decrease in fluorescence intensity in the center of each droplet. Analyzing turbidity of mixed condensates *in situ* showed similar optical density patterns if SUMO2-TDP-43(LCD) makes up 50% of the population (**Figure 25** D). No significant turbidity or condensate formation could be observed below this threshold.

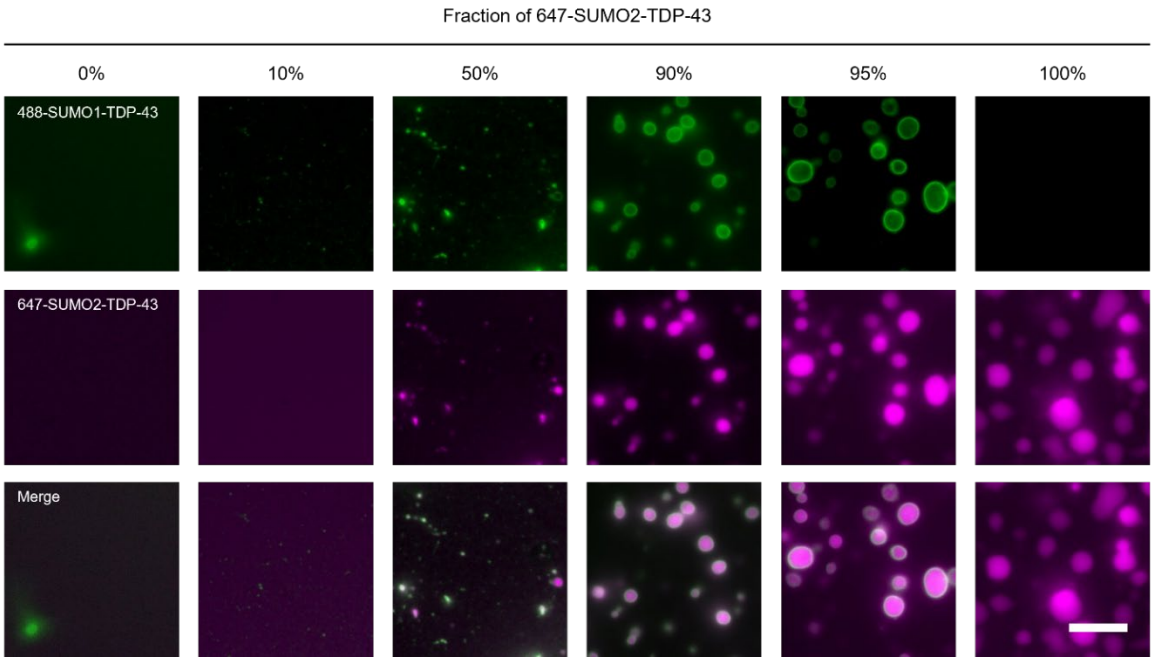

Figure 24: Mixed condensates of SUMO1-TDP-43(LCD) and SUMO2-TDP-43(LCD). AzDye488-labeled SUMO1-TDP-43(LCD) (green) were mixed with Atto647-labeled SUMO2-TDP-43(LCD) (purple) at different molar ratios at a total concentration of 50 µM. Phase separation was induced as described before and droplet formation was monitored after 1 h, probing for the respective wavelengths. White signal indicates merging. Scale bar: 20 µm.

The origin of the reluctant mixing of both protein populations must lie in the specific effect of SUMO1 on TDP-43(LCD) phase separation. Thus, I hypothesize that within a SUMO1-TDP-43(LCD) molecule, the LCD unit might enter the droplet by interacting with another LCD fused to SUMO2, while SUMO1 stays in the soluble surrounding of the droplet. To analyze this, I used site-specific labeling fluorescent labeling of SUMO1-TDP-43(LCD) and Förster resonance energy transfer acceptor bleaching (FRET-AB), as described by Joshi et al., 2023. Additionally, to the SUMO1-TDP-43(LCD) construct harboring the mutation G275C in the LCD (referred to as “center”), I also generated plasmids where a single cysteine was either incorporated at the N- or the C-terminus of the whole protein. I purified and labeled all three variants with AzDye488 and additionally labeled SUMO2-TDP-43(LCD) at G275C with Atto594 to allow efficient FRET, as Atto647 was not a suitable dye. A proposed model based on SUMO1 staying outside of the droplet is shown in **Figure 25** A. Since the donor dye fluorescence is quenched if the acceptor dye is in close proximity, the distinct dye positions on SUMO1-TDP-43(LCD) could serve as a measure how close different regions localize into SUMO2-induced droplets. Bleaching of the acceptor dye would thus lead to an increase in the fluorescence intensity of the donor dye

when FRET is occurring. The relative FRET efficiency E is calculated as follows, where I is the fluorescence intensity of the donor.

$$E = \frac{I_{488(post-bleach)} - I_{488(pre-bleach)}}{I_{488(post-bleach)}}$$

A higher FRET efficiency would thus indicate a closer proximity between both molecules. Exemplary micrographs of 2.5 µM Azdye488-labeled SUMO1-TDP-43(LCD) variants and 47.5 µM Atto594-labeled SUMO2-TDP-43(LCD) before and after photobleaching of the acceptor are shown in **Figure 25** B. For each dye position, 20 droplets were bleached as described in **section 2.11.4** and FRET efficiency was calculated with the equation shown above (**Figure 25** C). Exemplary fluorescence microscopy images for assessing more droplets are shown in **Appendix 5**.

Positioning of the donor dye at the C-terminus of SUMO1-TDP-43(LCD) resulted in the highest FRET efficiency of around 30%. In comparison, proteins labeled at the N-terminus, or the center of the protein showed a lower FRET efficiency with a mean of 15%. If SUMO1 would be equally enriched in the droplet, no differences in FRET efficiency would be observed. It can thus be concluded that the LCD is present within the droplet, while SUMO1 has a preference to stay outside of the droplet. The similar values observed for labeling at the N-terminus and center are most likely due to the labeling position “center” at G275C. This residue is close to the C-terminus of SUMO1 but far away from the main self-assembly site of TDP-43(LCD), starting with the helical region at position 320-343 and including crucial tryptophanes W334, W385 and W412 (Conicella *et al.* 2020). As a result, the LCD of a SUMO1-tagged molecule can most likely interact with SUMO2-TDP-43(LCD) to a certain extent.

In conclusion, a mix of SUMO1- and SUMO2-TDP-43(LCD) can undergo phase separation, but SUMO1 has a strong preference for staying outside of the droplet. As an equimolar mix of SUMO1- and SUMO2-TDP-43 leads to mixed phenotype, both inhibitory and enhancing mechanisms of the respective modifier might rely on interactions of comparable strengths. The following sections will elucidate these mechanisms in detail.

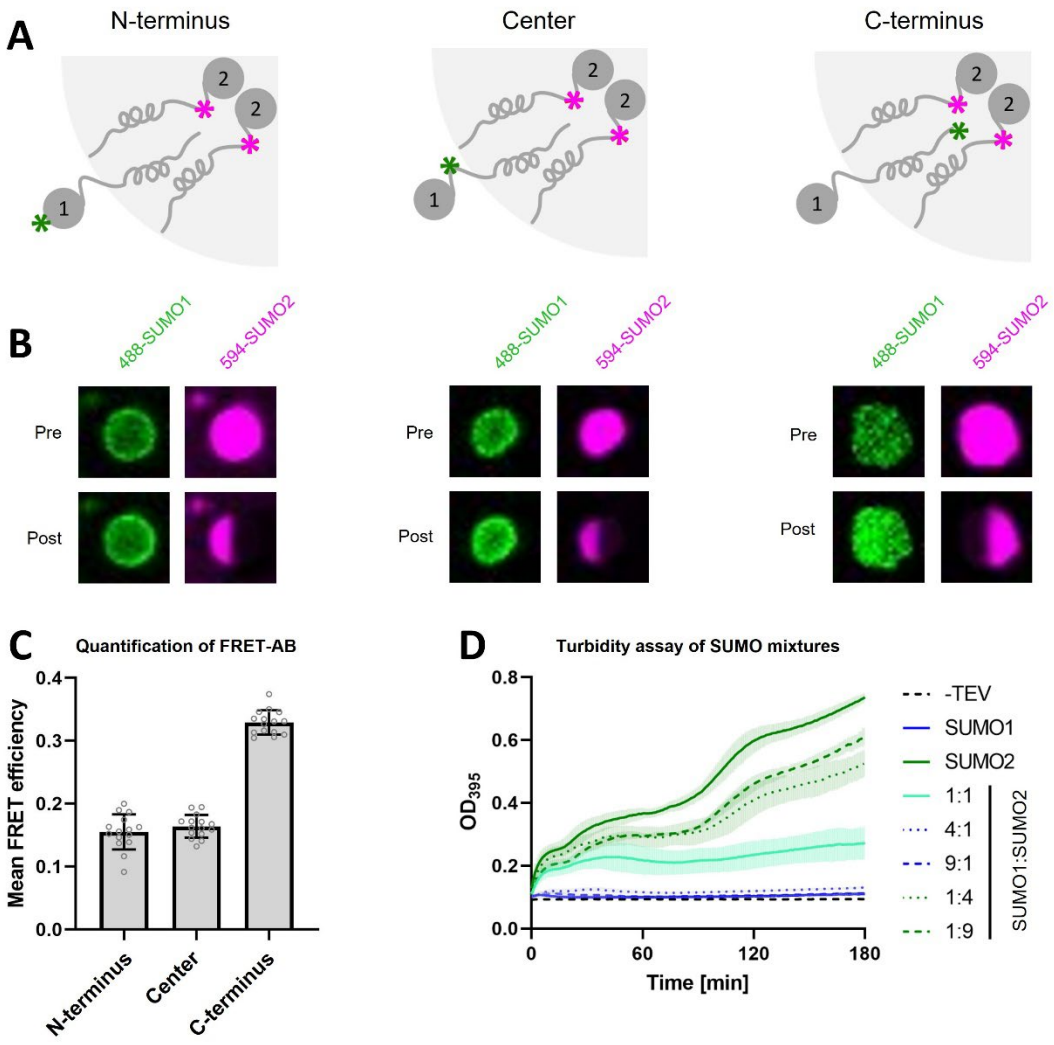

Figure 25: Estimation of molecular distances in mixed SUMO1- SUMO2-TDP-43(LCD) droplets. (**A**) Site-specific incorporation of single cysteine residues in SUMO1-TDP-43(LCD) enabled labeling with Atto594 at different positions. (**B**) Exemplary images of pre-bleaching and post-bleaching of SUMO1-TDP-43(LCD)/SUMO2-TDP-43(LCD) mixtures. (**C**) Quantification of FRET-AB by measurement of mean FRET efficiency (n=20 droplets per construct). (**D**) Turbidity measurement *in situ* of different stoichiometric ratios of SUMO1- and SUMO2-TDP-43(LCD).

3.3.2 SUMO1 blocks the major self-assembly site of TDP-43(LCD)

The sheer presence of SUMO1 in a reaction mix together with TDP-43(LCD) does not show any effect at equimolar concentration, as shown in **section 3.1.3**. Therefore, it can be assumed that specific interactions between SUMO1 and TDP-43(LCD) only occur if both moieties are forced to be in close proximity as it occurs in case of a post-translational modification. Since IDRs are usually highly flexible proteins, conventional structural methods like X-ray crystallography or cryo-EM cannot be applied in case of TDP-43(LCD). Hydrogen-Deuterium Exchange Mass Spectrometry (HDX-MS) is a powerful method to

identify interaction sites of proteins in a solute state under native conditions (**chapter 2.14.1**), which we applied in a collaborative approach. Based on the identified regions of interaction between TDP-43(LCD) and SUMO1, I generated hybrid-SUMO-TDP-43(LCD), where the respective regions of interest were exchanged between SUMO1 and SUMO2. Furthermore, I tried to quantify the binding strength between the identified interacting regions.

3.3.2.1 Identification of interaction sites by HDX-MS

To perform HDX-MS experiments, we collaborated with Joshua Vollrath from Julian Langer's lab at the MPI for Biophysics (Frankfurt, Germany). We decided to compare deuterium uptake between SUMO1-TDP-43(LCD) fusion protein and a mixture of SUMO1 and TDP-43(LCD). Assuming specific interactions require a covalent linkage between both proteins, a reduced deuterium uptake at certain positions would provide information about regions where SUMO1 and TDP-43(LCD) interact with each other when they are brought in close proximity.

The HDX-MS experiments were carried out by Joshua Vollrath who prepared the samples, operated the HPLC-MS system and analyzed the data. As shown in **Figure 26** A and B, peptides were detected for the query sequences of the TDP-43(LCD) and SUMO1 query sequences. The relative deuterium uptake of the SUMO1-TDP-43(LCD) fusion protein was compared to a mixture of SUMO1 and TDP-43(LCD) and plotted on structures of TDP-43(LCD) (**Figure 26** C) and SUMO1 (**Figure 26** D). A reduced deuterium uptake of the fusion protein compared to the mixed proteins is indicated in blue coloring of the respective structural elements, while an increased uptake is respectively colored in red.

The strongest reductions in deuterium uptake on TDP-43(LCD) were detected for the C-terminus and strikingly, for the transient α-helix (**Figure 26** C) after 30 s of deuterium exposure. This clearly indicates that SUMO1 can block this important self-assembly site, which explains why TDP-43(LCD) does not undergo phase separation upon fusion with SUMO1. Interestingly, peptides harboring W412 also show a decreased deuterium uptake. As described before, this residue contributes to phase separation of the LCD, so SUMO1 potentially blocks self-assembly sites in a bivalent manner. No differences in deuterium uptake between fusion and mix were detected after 600 s and 2100 s of deuterium exposure. This observation was expected, since a deuterium back-exchange can predominate the deuterium uptake at later time points. Thus, early time points of less than 60 s deuterium exposure are considered to be most reliable.

For SUMO1, reduced deuterium uptake was detected for the flexible N-terminus and β_2-sheet (**Figure 26** D) after 30 s and 120 s. This makes it very likely that both regions can bind to the α-helix of TDP-43(LCD). Furthermore, the β_1-sheet and the α-helix of SUMO1 surrounding β_2-sheet show an increased deuterium uptake, suggesting a slight conformational opening that enhances accessibility of the β_2-sheet. Interestingly, deuterium uptake of the α-helix was reduced in the fusion protein at later time points. It can be hypothesized that this region might also act as a binding interface for TDP-43(LCD) after minor conformational changes of the overall SUMO1-fold.

Overall, the HDX-MS experiments suggest interesting interactions between two self-assembly-sites of TDP-43(LCD) with both N-terminus and β_2-sheet of SUMO1. Even though HDX-MS as a method for structural biology is limited to capture interactions on a peptide level without single amino acids resolution, we were able to propose interaction sites that might explain the SUMO1-induced phenotype of inhibiting TDP-43(LCD) phase separation. It cannot be concluded from this experiment if the interaction between TDP-43(LCD) and SUMO1 N-terminus, β_2-sheet and α-helix occurs in multiple steps. This would require advanced 2D NMR experiments. Furthermore, it can be suggested that SUMO1 might decrease the helicity of the transient TDP-43(LCD) α-helix, which also remains to be elucidated by other methods.

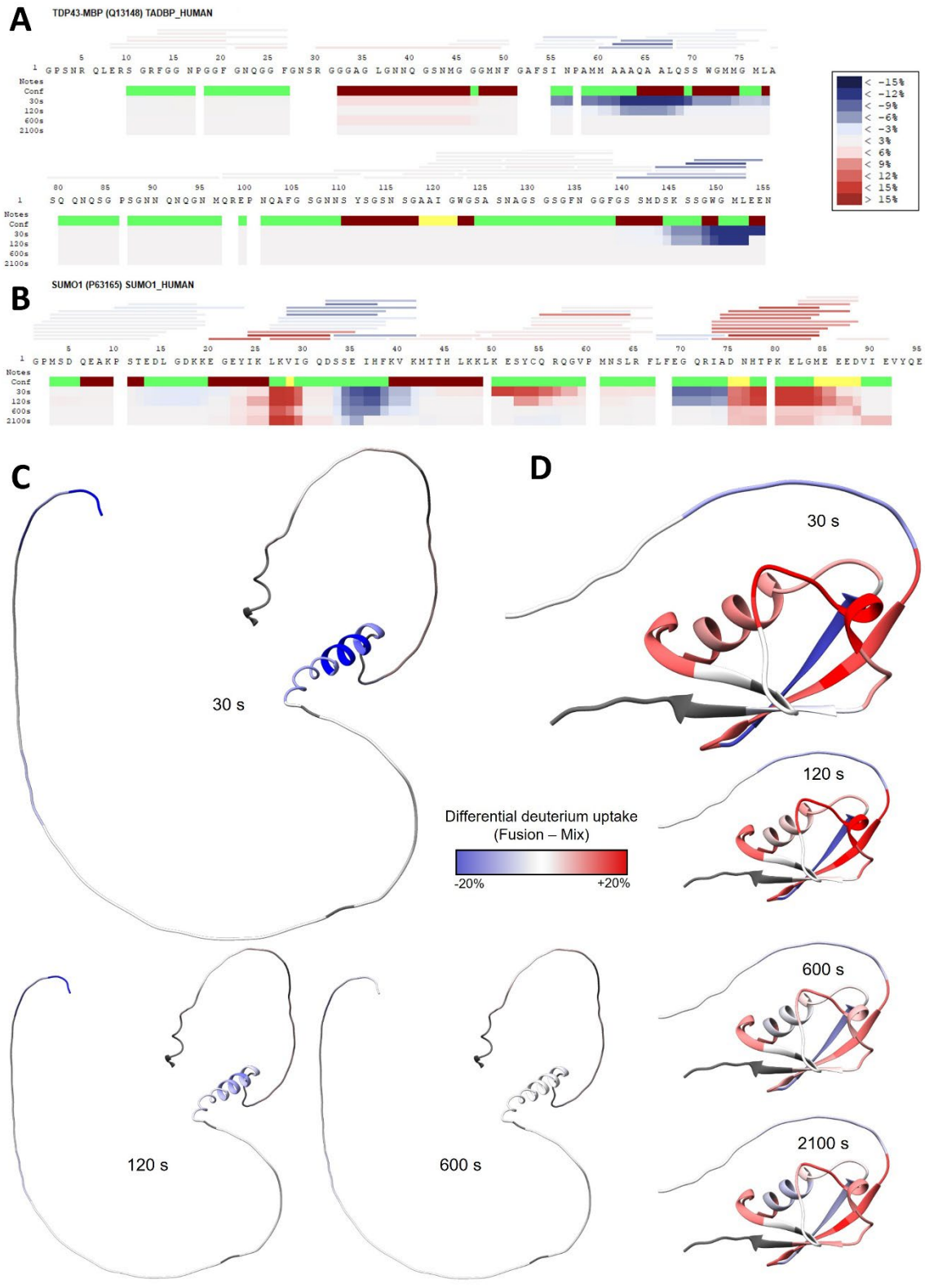

Figure 26: HDX-MS of SUMO1-TDP-43(LCD). Deuterated- and non-deuterated SUMO1-TDP-43(LCD) or SUMO1 mixed with TDP-43(LCD) were analyzed by mass spectrometry. Relative D_2O uptake was compared between both conditions for identification of interaction sites between SUMO1 and TDP-43(LCD). Assignment of identified peptides to the query sequences of (**A**) TDP-43(LCD) and (**B**) SUMO1. Relative D_2O uptake per time-point is plotted on the proteins sequences

in a color-code according to the box on the right site. Relative D_2O uptake visualized on structures of (**C**) TDP-43(LCD) (AF-Q13148) and (**D**) SUMO1 (AF-P63165) over various time points.

3.3.2.2 Experimental confirmation of interaction sites

As the HDX-MS experiment did not provide interaction data between SUMO1 and TDP-43(LCD) on a single amino acid resolution, I decided to mutate the identified regions. Mutating the TDP-43(LCD) α-helix is not a suitable approach here, since a reduction in helicity is just decreasing phase separation in general as shown in **chapter 3.2.4**. and thus, not providing a readout. It has been described before that certain elements can be exchanged between SUMO1 and SUMO2 (Zhu *et al.* 2008). Indeed, structural integrity has been confirmed for a chimeric SUMO1 protein, harboring α-helix and β_2-sheet from SUMO1. Inspired by this study, I generated SUMO1 and SUMO2 hybrid plasmids for expression in *E. coli* and in human cells, containing either the flexible N-terminus, β_2-sheet, or both elements of the respective other isoform (**Figure 27**). The mutated regions are listed in detail in the following **Table 14**.

Table 14: Hybridized regions in SUMO isoforms. Mutated regions are listed with the respective replacement region of the other isoform.

Isoform	Mutation	Region	Replacement
SUMO1	Nt	1-19	1-15
	β_2	33-39	29-35
SUMO2	Nt	1-15	1-19
	β_2	29-35	33-39

I purified the hybridized SUMO-fusion proteins on TDP-43(LCD) and analyzed *in vitro* phase separation by measuring turbidity (**Figure 27** B) and droplet formation by DIC microscopy (**Figure 27** C). Strikingly, I was able to not only reverse the phenotype of SUMO1 but also turn SUMO2 into an inhibitor of TDP-43(LCD) phase separation with the hybridization approach. In detail, SUMO1(Nt/β_2)-TDP-43 showed a significant turbidity, while the curve progression even followed a similar pattern as for SUMO2-TDP-43(LCD) at a lower overall intensity. The double mutant also led to droplet formation to an extent that is comparable with WT SUMO2-TDP-43(LCD). Conversely, inserting the N-terminus and β_2-sheet from SUMO1 into SUMO2 inhibited phase separation to a level below the detection limit of both assays, reflecting the behavior of WT SUMO1-TDP-43(LCD). Equal cleavage reactions were probed by SDS-PAGE and Coomassie-staining (**Appendix 6**).

Both assays suggest that the effect of inhibiting phase separation requires both N-terminus and β_2-sheet of SUMO1, as the single replacements had weaker effects. While SUMO1 containing N-terminus or β_2-sheet of SUMO2 showed a strong reduction in droplet formation, SUMO2 with the respective SUMO1 elements had decreased levels of phase separation. Especially SUMO2(β_2)-TDP-43(LCD) still formed round droplets that are characteristic for SUMO2, but to reduced size and number. For each isoform, the phenotype-reversing effect was more pronounced in case of mutation of the flexible N-terminus, compared to the β_2-sheet.

Analyzing the effect of SUMO hybrids on TDP-43(LCD) droplet formation in cells gave comparable results to the *in vitro* data. Almost 20% of cells expressing SUMO1(Nt/β_2)-TDP-43-EGFP formed droplets, which is a strong increase compared to the WT SUMO1-construct, where less than 5% of transfected cells showed droplet formation. Expression of SUMO2(Nt/β_2)-TDP-43(EGFP)-EGFP led to a decrease of more than 10% in droplet formation compared to WT SUMO2-TDP-43(LCD).

In summary, I was able to show that both SUMO1 N-terminus and β_2-sheet are required to inhibit phase separation of TDP-43(LCD) *in vitro* and in mammalian cells. Interestingly, this effect could be abolished when these regions in SUMO1 were substituted with the respective regions from SUMO2, leading to a hybrid SUMO1-TDP-43(LCD) that almost behaved as WT SUMO2-TDP-43(LCD). A complementary approach for hybrid SUMO2-TDP-43(LCD) with SUMO1 elements resulted in the inhibition of phase separation. Altogether, this experimental series confirmed the suggested findings of the HDX-MS experiment.

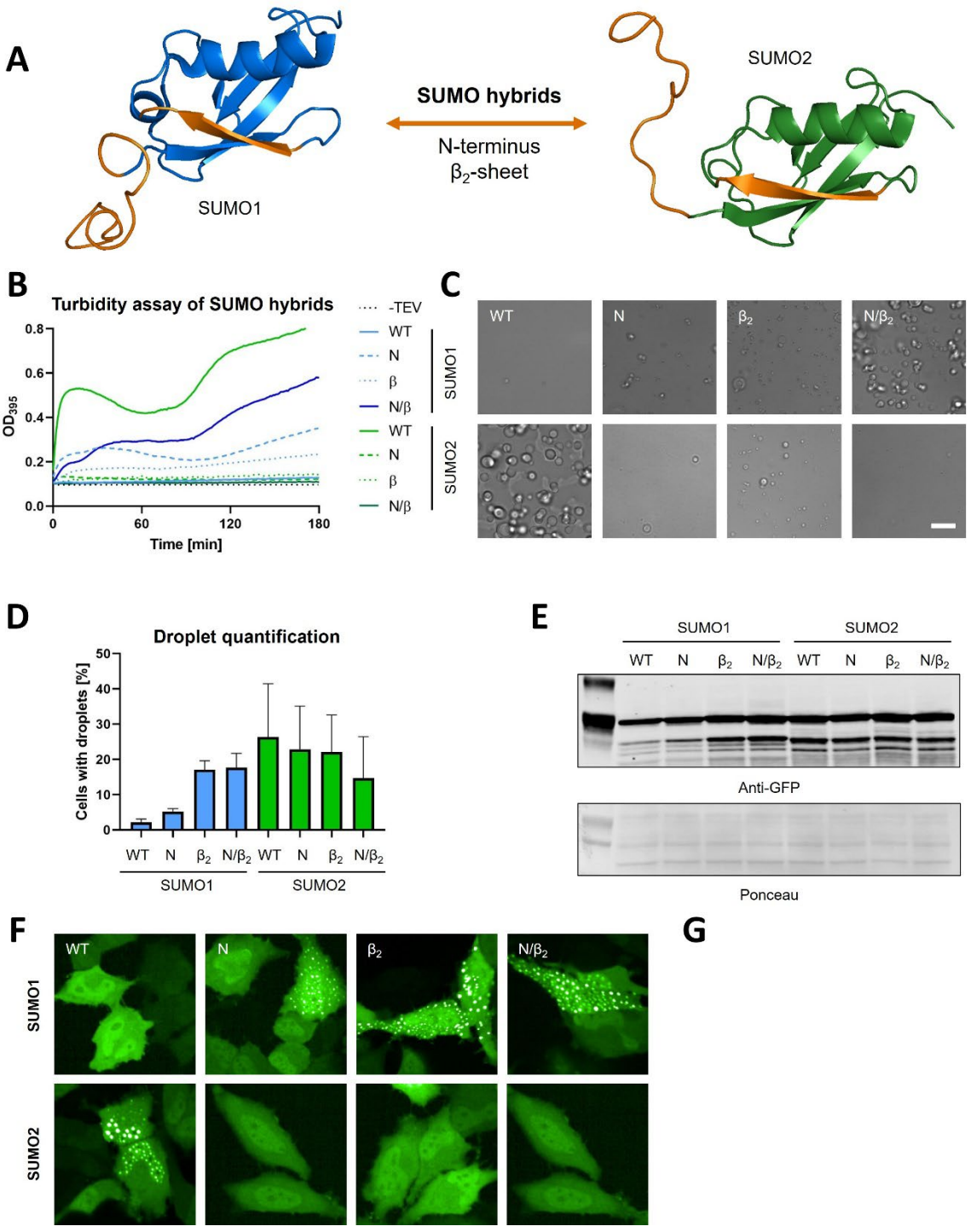

Figure 27: Confirmation of interaction sites between SUMO1 and TDP-43(LCD). (**A**) SUMO hybrid generation by exchanging N-terminus and β_2-sheet between SUMO1 (PDB:2KQS) and SUMO2 (PDB:2N1W). (**B**) Turbidity of TDDP43(LCD) tagged with SUMO hybrids was measured *in situ* by using a plate reader. (**C**) Representative DIC images of droplet formation were taken after 2 h. Scale bar = 10 µm (**D**) Quantification of droplet formation in HeLa cells transfected with TDP-43(LCD)-EGFP tagged with SUMO hybrids. (**E**) Protein expression was analyzed by western blot. (**F**) Exemplary fluorescence microscopy images.

3.3.2.3 Quantification of interaction strength between binding regions

Mixing SUMO1 and TDP-43(LCD) in a equimolar ratio did not result in any effect on phase separation (**Figure 12** in **chapter 3.1.3**). It can thus be assumed that the underlying interaction between the in the previous chapter identified regions is of a very weak nature. I approached to quantify the binding strength between both structural elements of SUMO1 and TDP-43(LCD). Therefore, I ordered peptides with the respective sequences from SUMO1, which allowed me to use higher concentrations in comparison to use full-length recombinantly produces SUMO1 (**Figure 28** A). Mixing each peptide at a 10-fold molar excess with TDP-43(LCD) did not show any significant effect on inhibiting phase separation, as probed by turbidity assay. However, a 50-fold molar excess of the N-terminal peptide inhibited phase separation to a strong extent (**Figure 28** B). I proceeded with analyzing droplet formation using DIC microscopy, which confirmed the inhibitory effect of the N-terminal peptide of SUMO1. The β_2-sheet-peptide alone inhibited phase separation only to a minor extent according to the turbidity assay, while less aggregation-prone structures could be detected compared to TDP-43(LCD) alone (**Figure 28** C).

I tried to determine K_D values starting with the N-terminal peptide using fluorescence polarization assays using FITC-labeled peptide (**Appendix 6**). Even though binding was detected starting at ~100 µM, I could not achieve sufficient concentrations of TDP-43(LCD) to achieve sigmoidal curves for calculating K_D values. Interestingly, I detected a slightly stronger interaction between the N-terminal peptide and full-length TDP-43, starting at ~15 µM. Using fluorescently labeled TDP-43(LCD) is not a suitable approach due to the reduced capacity of inhibiting tumbling by a comparably small peptide.

Taken together, this experiment supports the necessity of SUMO1 being conjugated to TDP-43(LCD), as the interaction between both binding partners is very weak. This also rules out the possibility of spontaneous binding of free SUMO1 having a sufficient effect on inhibiting TDP-43(LCD) phase separation, confirming the findings described in **chapter 3.1.3**. Further quantitative methods can enable interesting insights into the mechanism the interaction between the TDP-43(LCD) α-helix and the SUMO1 N-terminus or β_2-sheet.

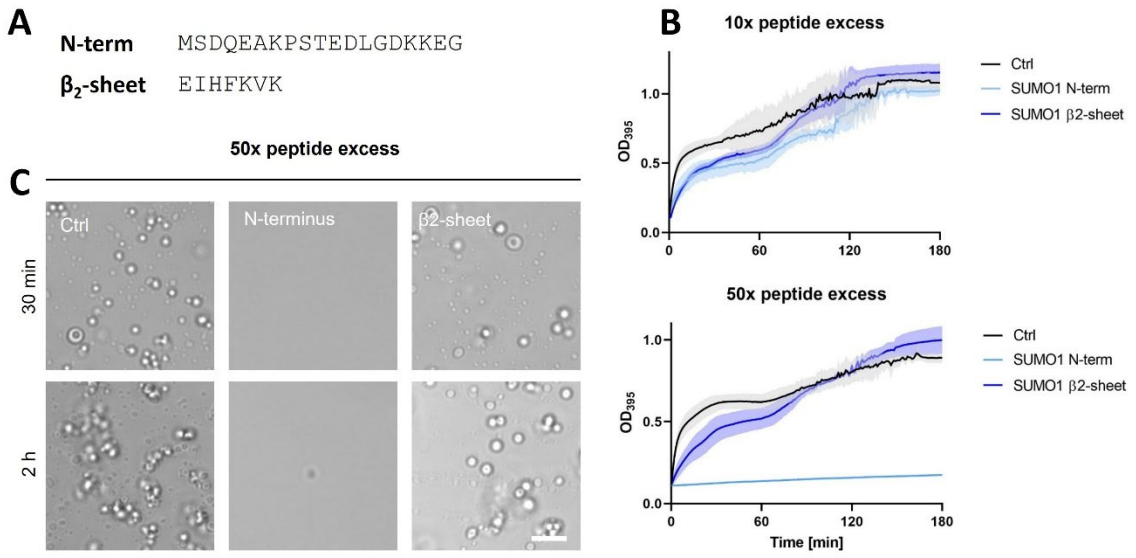

Figure 28: Quantification of interaction strength between SUMO1 peptides and TPD43(LCD). (**A**) Sequence of SUMO1 peptides. (**B**) SUMO1 peptides were mixed with 50 µM TDP-43(LCD) at different molar ratios. Turbidity was measured as described before. (**C**) Representative DIC images of TDP-43(LCD) droplet formation in the presence of SUMO1 peptides. Scale bar = 10 µm.

In conclusion, we found a unique mechanism how phase separation of TDP-43(LCD) can be inhibited by selective binding of SUMO1. Both HDX-MS data and follow-up confirmation experiments *in vitro* and in cells strongly suggest that the helical main self-assembly site of TDP-43(LCD) is blocked by a bivalent binding of the SUMO1 N-terminus and the β_2-sheet. This interaction is most likely of a weak nature, while a defined binding strength remains to be determined as shown by FP assays and an exact KD needs to be determined.

3.3.3 SUMO2 intrinsically enhances phase separation of TDP-43(LCD)

In contrast to the inhibitory effect of SUMO1 that is TDP-43-specific, SUMO2 seems to enhance phase separation of IDRs in a general manner, as I also showed for other IDRs (**chapter 3.1.4**). This raises the interesting question, if an increasing number of SUMO2-moieties will enhance this effect, since especially SUMO2 is known to form polymeric chains (**chapter 1.1.2** and **1.1.3**). I mimicked SUMO2 chains by generating linear fusions of two or four SUMO2-moieties on TDP-43(LCD) (**Figure 29** A). As SUMO2 chains are mainly linked via K11, I removed amino acids 1-10 of SUMO2 to provide the appropriate spacing between each SUMO moiety in the chain. I purified the respective fusion proteins and compared phase separation with unmodified TDP-43(LCD) and SUMO2-TDP-43(LCD) as described before. Indeed, increasing the length of SUMO2-chains enhanced

phase separation, as shown by the turbidity assays (**Figure 29** B). Interestingly, turbidity values dropped after peaking in the first 45 min. This effect also occurred for SUMO2-TDP-43(LCD), but only to a lesser extent. When analyzing droplet formation with DIC microscopy, I could observe that 2x and 4xSUMO2-TDP-43(LCD) phase separated in huge droplets that settled to the ground of the microscope slide. This is a similar wetting effect as observed for Ub- and SUMO2-TDP-43(LCD) condensates 3 h after inducing phase separation and indicates an enhancement of the liquid properties of the condensates (**Figure 15** in **chapter 3.2.1**). Equal cleavage reactions were probed by SDS-PAGE and Coomassie-staining (**Appendix 7**).

In conclusion, an increasing chain length of polySUMO2 enhances phase separation of TDP-43(LCD). It remains elusive if this effect relies on the presence of a polymeric chain or the sheer number of SUMO2 molecules. To test this, varying numbers of SUMO2 moieties could be distributed across TDP-43(LCD). An additional designed 6xSUMO2-TDP-43(LCD) was not stable during the protein purification procedure (data not shown).

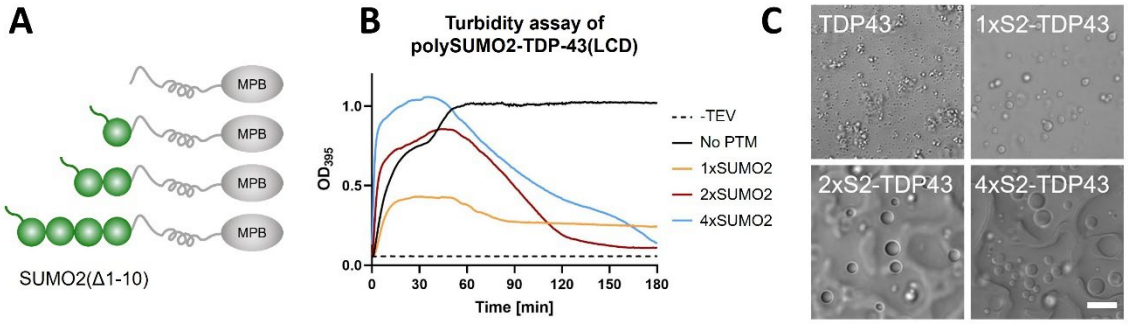

Figure 29: Mimicking polySUMO2 chains on TDP-43(LCD). (**A**) Arrangement of multiple SUMO2 moieties on TDP-43(LCD). The flexible N-termini of all proximal SUMO2 moieties has been removed to mimick spacing of native polymeric SUMO2 chains. (**B**) Turbidity assay of polySUMO2-TDP-43(LCD). (**C**) Representative DIC microscopy images. Scale bar = 10 µm.

3.3.3.1 Identification of interaction sites by XL-MS

Next, I tried to address the question, how SUMO2 enhances phase separation. As discussed in **chapter 3.3.2**, evaluating the potential of SUMO2 to affect the fold of its conjugated target is difficult due to the internally disordered state of TDP-43(LCD). Thus, I wanted to investigate if SUMO2 can interact with itself and if so, to identify the interaction regions on SUMO2. Again, together with Joshua Vollrath, we tried to use HDX-MS to compare deuterium uptake of SUMO2-TDP-43(LCD) in a soluble state with attached MBP, or in a phase-separated state after MBP is cleaved off using TEV protease. However, HDX-MS is not yet established as a method to measure relative deuterium uptake in a

phase separated state. Indeed, the uptake spectra under this condition were of low quality and we were not able to identify regions of interactions (data not shown).

Crosslinked-coupled mass spectrometry (XL-MS) can be used to capture and identify protein-protein interactions in various ways. XL-MS is usually limited to certain functional groups due to the used crosslinker, and additionally it is difficult to distinguish between intra- and intermolecular interactions. A method for the identification of homodimers has been described, using stable-isotope labeling (Lima *et al.* 2018). The usage of ^{15}N-labeled protein enables to distinguish between intramolecular *cis*-interactions and intermolecular *trans*-interactions. The proof-of-concept experiment of this study relies on controlled denaturation and an NHS-based amine-amine crosslinker, which limits the detection of interaction sites. Conventional NHS-crosslinking mainly captures the reactive sidechain of lysine and primary amines but can also capture other amino acid residues in rare events, as for example serine, threonine or tyrosine. Instead, I decided to use Sulfo-SDA (Thermo Fisher Scientific), which is a heterobifunctional crosslinker with an NHS-warhead and a photoreactive diazirine group (**Figure 30** A). The diazirine group can be activated by UV-A irradiation, leading to a nonspecific reaction with any functional group (**Figure 30** A).

Induction of phase separation by TEV-cleavage of MBP allowed me to implement a highly controllable two-step crosslinking process using Sulfo-SDA (**Figure 30** B). First, I purified ^{15}N-labeled SUMO2-TDP-43(LCD) and mixed it with (regular) ^{14}N-SUMO2-TDP-43(LCD) together with Sulfo-SDA at different ratios of crosslinker to protein. Due to the high reactivity of the NHS-group in an aqueous environment, both proteins were monolinked with Sulfo-SDA. I induced phase separation for 2 h as described before and photoactivated the diazirine group, which due to its 3.9 Å spacer arm should in theory link a ^{14}N- with a ^{15}N-labeled protein when they are in close proximity. The formation of multimers was compared with another reaction that was not treated with TEV-protease by SDS-PAGE and Coomassie- staining (**Figure 30** C and D). Comparing both conditions showed several bands that only appeared when phase separation was induced. I excised gel pieces of interest and submitted them to the IMB Core Facility for Proteomics. Further sample processing, HPLC-MS operation and data analysis was performed by Jiaxuan Chen.

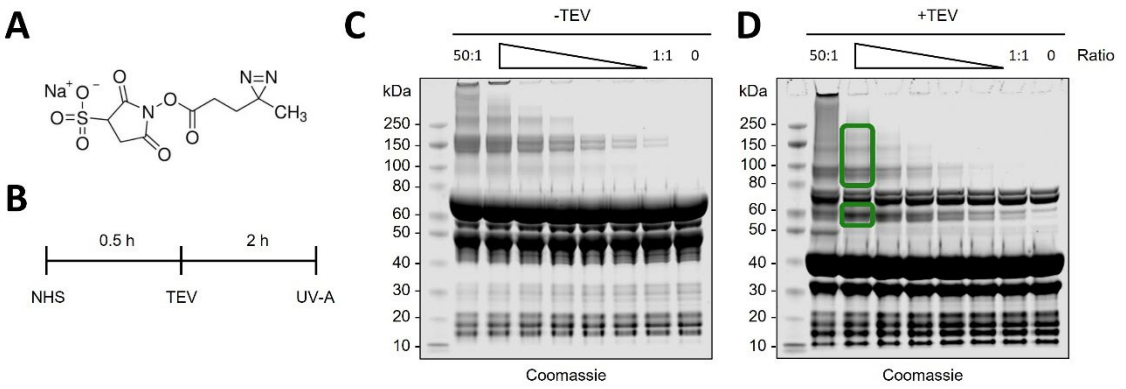

Figure 30: Crosslinking of SUMO2-TDP-43(LCD). (**A**) Structure of the Sulfo-SDA crosslinker. (**B**) Workflow for capturing interaction sites of phase separated SUMO2-TDP-43(LCD) using Sulfo-SDA. Coomassie-stained gel of crosslinked SUMO2-TDP-43(LCD) without (**C**) and with (**D**) TEV-protease using different Sulfo-SDA to protein ratios. Green boxes indicate cut out gel pieces.

The detected crosslinks were mapped on the sequence of SUMO2 (**Figure 31**). As expected, barely any crosslinks were detected on TDP-43(LCD) because it only harbors a single lysine (data not shown). In general, it should be mentioned that the peptide assignment software was not optimized to distinguish between ^{14}N- and ^{15}N-labeled peptides. Thus, one must consider the potential detection of false positive crosslinks. I highlighted crosslinking sites with peptides of a score ≥3.5 with bold lines, which can be considered as interactions of high confidence. Both inter- and intramolecular crosslinks are almost perfectly mirrored on ^{14}N- and ^{15}N-labeled protein. The most prominent intermolecular crosslinking signals on SUMO2 were detected between the N-terminus and amino acids T70-T83 of the t4-loop in *cis*. Interestingly, similar crosslinking sites were also detected in *trans*. This indicates that the N-terminus of SUMO2 has a general potential to bind to the t4-loop. Further *cis*-interactions were identified within the N-terminus of SUMO2 itself and are most likely explainable with random movements due to the flexibility of this region. Crosslinks in *cis* between β_1-sheet (H17/I18) and β_2-sheet (K33), as well as α-helix (K45) and t4-loop (N68-D71) most likely occur because of the close proximity between the respective structural elements within one molecule. Crosslinking sites of lower confidence suggest *trans*-interactions between front and rear end of the flexible N-termini of two molecules. Moreover, *trans*-crosslinks between N-terminus and the α-helix (C48/E49), as well as α-helix and t4 loop (T70, T72 or A74-D80) propose additional binding sites. Equal *cis*-crosslinks were detected between the same amino acid residues.

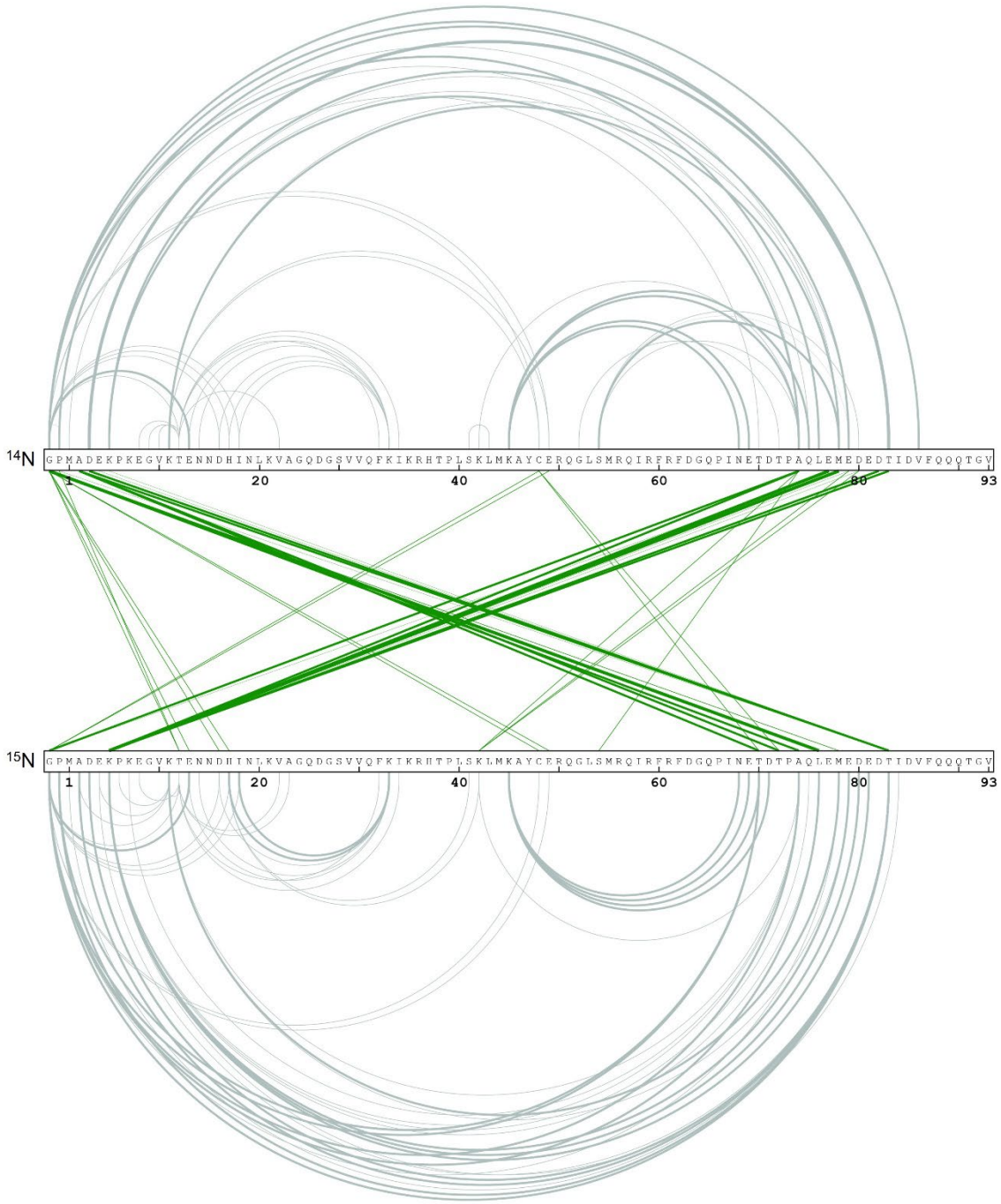

Figure 31: Crosslinking-MS of SUMO2 fused to TDP-43. Raw data visualization with xiNET. Intermolecular crosslinks (green) and intramolecular crosslinks (grey) were plotted on the amino acid sequence of SUMO2. Crosslinked peptides with a score ≥3.5 are highlighted in bold lines.

Overall, the XL-MS experiment strongly indicates that SUMO2 enhances phase separation by increasing multivalency through its ability to interact with itself. Strikingly, the proposed interactions were observed both in an intra- and intermolecular manner. This leads to the hypothesis that common intramolecular interactions within one SUMO2 molecule could

also occur on the same sites between two SUMO2 molecules in close proximity. So far, SUMO2 has not been described to self-associate. The modification of a phase separating protein like TDP-43(LCD) would thus lead to a situation where two SUMO2 molecules would be forced into close proximity, which would in turn enable the interactions described above.

3.3.3.2 Experimental confirmation of interaction sites

To prove this hypothesis, I generated SUMO2 mutants based on the identified interacting regions and analyzed their phase separation behavior *in vitro* (**Figure 32** A). If a crucial interaction is disrupted, the SUMO2-mutant attached to TPD43(LCD) should not enhance phase separation, and it can be expected that the fusion protein behaves comparable to unmodified TDP-43(LCD).

Based on the multiple interactions detected in the flexible N-terminus, I generated different truncations of this region, deleting either the first 6, 11 or 15 amino acid residues (**Figure 32** B). Removal of the entire SUMO2 N-terminus (Δ1-15) resulted in a drastic change of the liquid-like droplet phenotype. Similar to TDP-43(LCD) without a PTM, condensates appeared at a higher number and in a more irregular shape. This shows that the liquidness of SUMO2-TDP-43(LCD) is probably promoted by the interaction of the N-terminus of one SUMO2-molecule with the surface of another molecule. Interestingly, shorter truncations had the opposite effect and rather led to a phenotype that can be interpreted as an enhancement of liquid-like phase separation. SUMO2(Δ1-6) slightly enhanced droplet size and led to surface wetting, as described in **section 3.2.1**. This effect got even more pronounced when the N-terminus was further truncated (Δ1-11), resulting in large, settled condensates and droplets of an equally round shape, similar as observed above for 4xSUMO2-TDP-43(LCD). This indicates that there might be a hierarchy between *cis*- and *trans*-interactions of the SUMO2 N-terminus with the SUMO2 surface, which is further discussed in **chapter 4.2.3**.

The t4-loop has a high number of negatively charged amino acids. Neutralizing the charge might abolish binding to the flexible N-terminus containing several lysines. I generated E→Q and D→N mutations in the region 71-82, which is where we detected crosslinks of high confidence with the N-terminal region. Phase separation of this was most similar to the unmodified TDP-43(LCD) control. Condensates of the t4-mutant appeared small and with an irregular shape, barely distinguishable from the control protein (**Figure 32** B). In conclusion, the t4-loop can be considered as an interaction site for the N-terminus of SUMO2, both in *cis* and in *trans*.

A set of other mutants based on the XL-MS data yielded results that were more ambiguous. Reducing the propensity of hydrogen bond formation by mutation of polar amino acid residues in the t4 loop (T70A, T72A and Q75V) seemed to enhance liquid-like phase separation by promoting the formation of settled droplets to a weak extent. Opposing the charge of an exposed aspartate (D63R) reduced droplet number and size, but the characteristic round droplet shape was comparable with WT SUMO2. Both sites probably play an important role in SUMO2-mediated alteration of TDP-43(LCD) phase separation. As a few crosslinks were detected that originate in the α-helix, I tried to reduce helicity to investigate its role as a binding site (K42P, A46P). Inducing phase separation of this protein resulted in a pronounced aggregation-like phenotype. It is not surprising that resolution of the helix results in major misfolding as it is the central structural element of the SUMO2 fold. Thus, the misfolded SUMO2 unit could act as aggregation seed that further promotes liquid-solid phase transition of the aggregation-prone TDP-43(LCD). Unraveling the role of these three mutations requires additional experiments.

All mutants were also analyzed by turbidity assay (**Figure 32** C). The high diversity of the condensates made it difficult to interpret this result, as the turbidity assay is not suitable to distinguish between irregular solid-associated phase separation and liquid-like phase separation and surface wetting. Equal cleavage reactions were probed by SDS-PAGE and Coomassie-staining (**Appendix 7**).

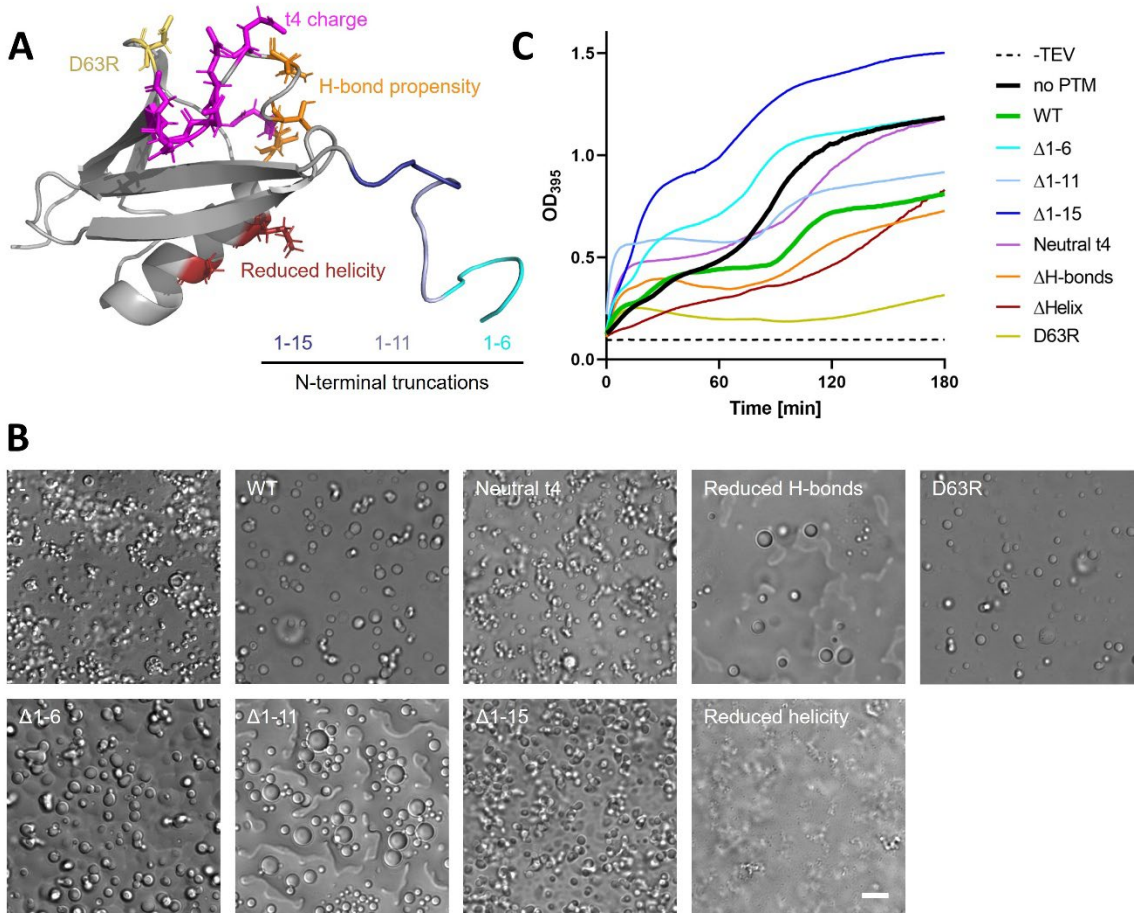

Figure 32: Validation of SUMO2 self-interaction sites. (**A**) Proposed interaction regions were mapped on the structure of SUMO2 (PDB:2n1w). Mutated amino acid residues are shown as stick representations. (**B**) Representative DIC microscopy images of SUMO2 interaction mutants. Scale bar = 10 µm. (**C**) Turbidity assay of SUMO interaction mutants.

Due to the limited resolution of HDX-MS and XL-MS, I was not able to identify key amino acids that are the drivers of the respective phenotypes of SUMO1- and SUMO2-regulated phase separation of TDP-43(LCD). Yet, the unambiguous identification of crucial regions in both SUMO isoforms suggest unique and novel mechanisms that have not been described so far.

A schematic representation of my findings is summarized in **Figure 33**. SUMO1 can act as a TDP-43(LCD)-specific inhibitor of phase separation. Here, the SUMO1 N-terminus and β_2-sheet bind to the α-helix of TDP-43(LCD), which is its major self-assembly site. In contrast, SUMO2 enhancing phase separation of TDP-43(LCD) appears to be largely substrate independent. A weak interaction between the N-terminus and the t4-loop of SUMO2 that usually occurs in *cis* can also form in *trans* when several SUMO2 molecules come into close proximity, as it is the case for a scenario where a phase separating protein

is post-translationally modified with SUMO2. Apparently, a shorter N-terminus favors the *trans* interaction over the *cis* interaction, promoting phase separation even further. Point mutations within the both SUMO regions could ultimately reveal the exact contact sites. MBP-free SUMO-TDP-43(LCD) could also be analyzed by NMR, while peak shifts could be analyzed by comparing similar conditions as used for both HDX-MS and XL-MS experiments.

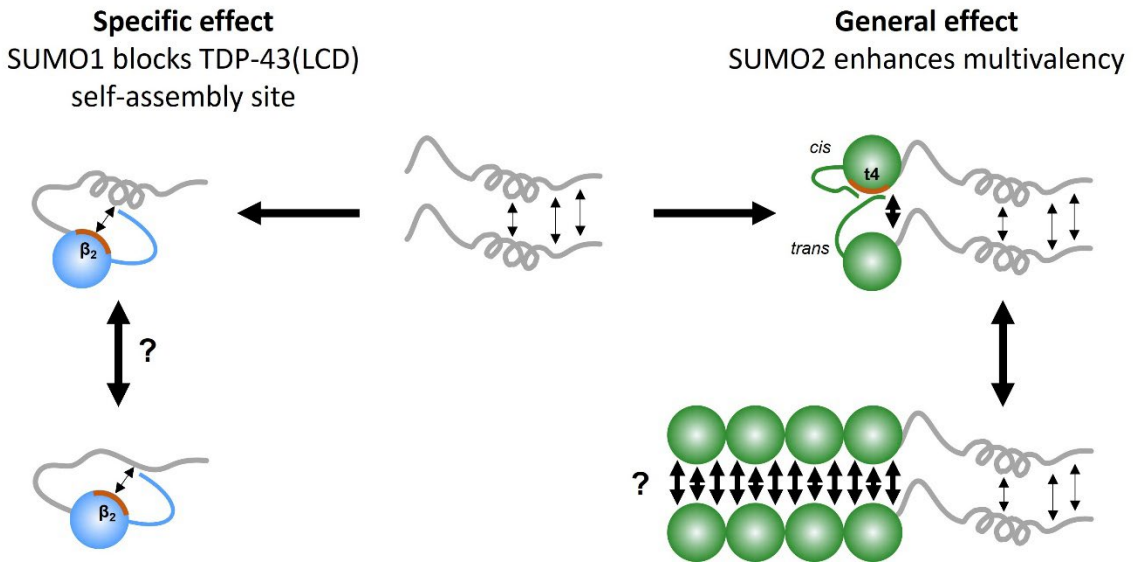

Figure 33: Novel mechanisms of how different SUMO isoforms regulate phase separation. The self-assembly site of TDP-43(LCD) can be blocked by SUMO1 (blue), which inhibits phase separation. SUMO2 (green) can enhance phase separation by increasing multivalency via a *cis/trans*-dependent interaction.

3.4 Physiological relevance of TDP-43 ubiquitylation and SUMOylation

As described in **chapter 1.2.7.1**, TDP-43 is a multidomain protein whose phase separation relies on mechanisms beyond its LCD. Especially the properly folded N-terminal domain drives dimerization of TDP-43 and thus, is a major regulator of phase separation. Both RRMs engage in polynucleotide binding, which is usually considered as a key component in the formation of multivalent interaction networks. Major cellular functions are controlled by an NLS which enables shuttling of TDP-43 between nucleus and cytoplasm. Therefore, in comparison to the isolated LCD, the phase separation mechanism of full-length TDP-43 is more complex, which makes it less suitable as a model protein to study how ubiquitin and SUMO can modulate phase separation mechanisms. However, it offers the possibility to investigate functional consequences of ubiquitylation and SUMOylation on TDP-43 function. Several studies showed that ubiquitylation and SUMOylation can have severe impacts on the function and localization of TDP-43 (Hebron *et al.* 2013; Hans *et al.* 2014; Maraschi *et al.* 2021).

3.4.1 Characterization of PTM-fusions on full-length TDP-43 in a cellular context

TDP-43 has multiple reported ubiquitylation and SUMOylation sites, which have been identified by several while the SUMO-isoform is mostly not considered (Mertins *et al.* 2013; Lumpkin *et al.* 2017; Hendriks *et al.* 2018). Interestingly, in the NTD only phosphorylation sites have been detected (Kametani *et al.* 2009). To gain first insights into the effect of conjugation of one specific modifier to TDP-43, I made use of the linear fusion system as described in **section 3.2.4**. Therefore, I arranged ubiquitin, SUMO1 or SUMO2 at either the N- or C-terminus and analyzed phase separation by quantifying transfected cells with droplets.

For visualization purposes, an EGFP-tag was fused to the C-terminus of TDP-43. Overexpression in HeLa cells resulted in nuclear droplets of small size and high number (**Figure 34** A). Transfection with unmodified TDP-43-EGFP resulted in the highest fraction of transfected cells that droplets (**Figure 34** B). Analysis of expression levels by western blot showed comparable expression levels between TDP-43-EGFP and all respective fusion proteins with ubiquitin, SUMO1 and SUMO2 (**Figure 34** C).

Strikingly, N-terminal fusion of SUMO1 to full-length TDP-43 inhibited phase separation, as shown by a reduction to less than 30% of transfected cells with droplets at comparable protein levels to unmodified TDP-43. A C-terminal fusion had no pronounced effect on reducing phase separation of TDP-43. This is in agreement to my previous findings, since

a free N-terminus of SUMO1 is required for its inhibitory effect on TDP-43 phase separation (**chapter 3.2.4.1**).

In contrast, fusions with ubiquitin and SUMO2 reduced the number of transfected cells with droplets, which first was surprising as both modifiers enhanced phase separation of TDP-43(LCD) (**Figure 22**). Yet, both modifiers altered the shape, size and localization of the condensates to a certain extent. Both N- and C-terminal fusion of ubiquitin led to an enhanced enrichment of cytoplasmic condensate formation. This is an interesting finding, because pathological aggregation of TDP-43 is not only highly associated with cytoplasmic localization but also with ubiquitylation (Tran and Lee 2022). In the case of SUMO2, both N- and C-terminal fusions appeared to increase the droplet size. Interestingly, K408 close to the C-terminal end of TDP-43 has been shown to be SUMOylated (Lumpkin *et al.* 2017). The data sets should be further analyzed for quantification of droplet size and EGFP-signal in a compartment-dependent manner to obtain more conclusions about the effect of each modifier on the phase separation phenotype.

Altogether, linear fusions of ubiquitin and SUMO to full-length TDP-43 show a similar trend as observed for TDP-43(LCD). SUMO1-fusion was proficient in the inhibition of phase separation. For SUMO2-fusions, condensates appeared at a bigger size, which might indicate an enhancement of liquidness. Ub-fusions formed regularly shaped condensates, in comparison to the irregular foci formed by Ub-TDP-43(LCD). To claim that Ub- and SUMO2-fusions enhance LLPS of TDP-43, additional experiments are needed.

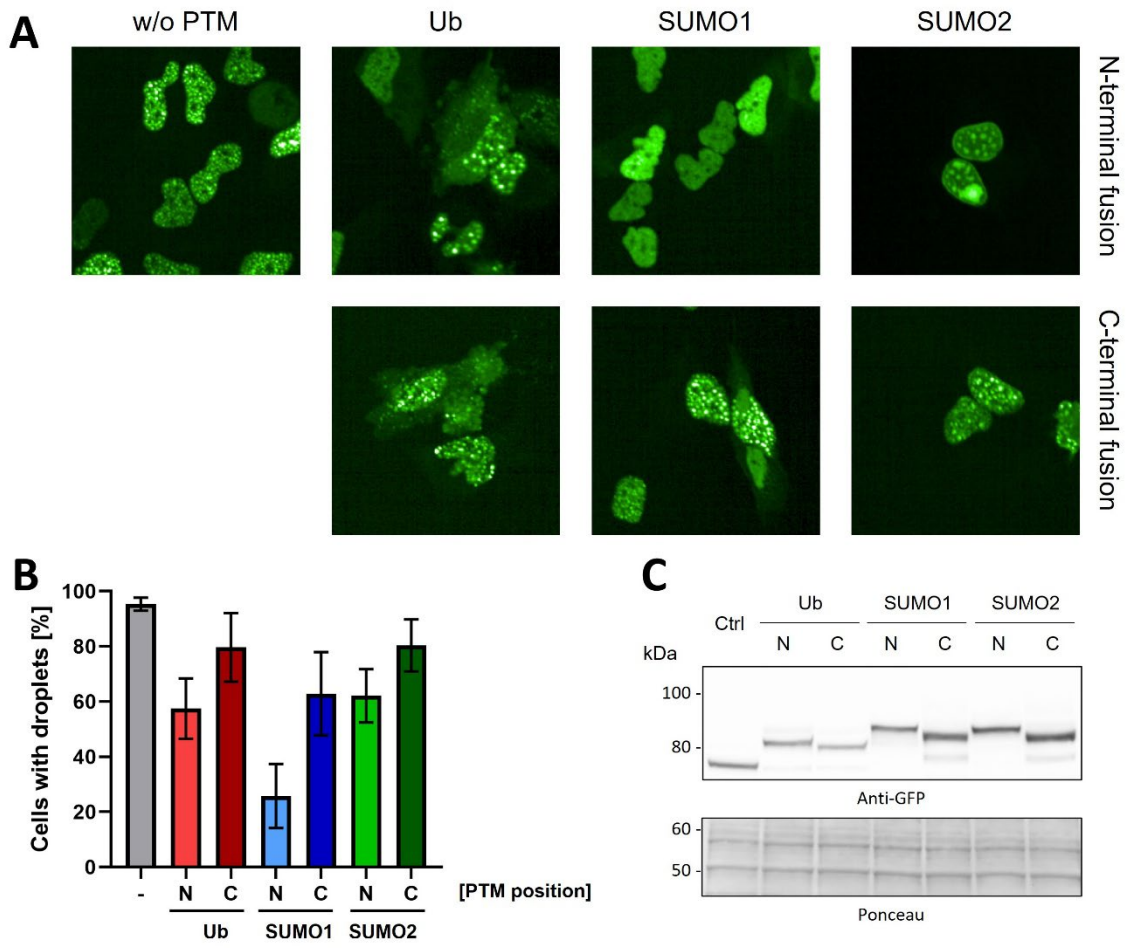

Figure 34: Linear fusions of Ub/SUMO to TDP-43 variants. (**A**) Exemplary fluorescence microscopy images of transiently overexpressed EGFP-tagged TDP-43 in HeLa cells. N- and C-terminal fusion of PTMs were compared with each other (upper and middle lane). (**B**) Quantification of transfected cells with droplets (n=3) and (**C**) analysis of expression levels by western blot.

3.4.2 The role of endogenous PTMs on phase separation of TDP-43

Since TDP-43 harbors several sites for endogenous modification with ubiquitin and SUMO, I wanted to test if I can generate conditions where overexpressed TDP-43 is mainly conjugated with one particular modifier. Due to the intriguing mechanisms described in **chapter 3.3**, I focused on the differences between the SUMO isoforms. Therefore, I made use of isoform-specific siRNA-mediated knockdowns of either SUMO1 or SUMO2/3. Subsequently, I transiently overexpressed cells with His-tagged TDP-43-EGFP. As TDP-43 is mostly modified upon cellular stress, I compared unperturbed cells with cells that were incubated at 43 °C for 2 h prior to harvesting. I separately collected samples for analyzing knockdown-efficiency and pulldown-samples for the detection of PTMs on TDP-43. An overview of the experimental workflow is shown in **Figure 35** A.

Western blot analysis of knockdown-efficiency in whole cell lysate showed a strong depletion of SUMO1 upon transfection of siRNA targeting SUMO1. The analysis of knockdown-efficiency for SUMO2 was more challenging due to the quality of the used SUMO2-antibody. However, a depletion of SUMO2 was clearly detectable, since the increase of SUMO2-levels upon heat shock was absent upon knockdown of SUMO2 (**Figure 35** B).

Pulldowns were performed under denaturing conditions to avoid cleavage of the conjugates from TDP-43 by DUBs and SENPs (**chapter 1.1.2**). The pulldown elutions were analyzed by western blotting, using antibodies for SUMO1, SUMO2 and ubiquitin. The heat shocked of cells enhanced signals for SUMO1, SUMO2 and ubiquitin after transfection with control siRNA in comparison to untreaded cells (**Figure 35** B).

Upon knockdown of SUMO1, almost no SUMO1 signal was observable after pulldown of TDP-43, while SUMO2 and ubiquitin signals were unaffected. In contrast, depletion of SUMO2/3 resulted in no detectable SUMO2/3 signal but also in a reduction in SUMO1 signal. Furthermore, an increase of ubiquitin chains was observable under stressed conditions, which was slightly decreased upon knockdown of SUMO1. Using TAK-234 as an inhibitor for ubiquitin E1 resulted in a strong reduction in ubiquitin chains on TDP-43 after 1 h of treatment, which allows to provide a situation where TDP-43 SUMOylation could be studied in the absence of ubiquitylation (**Appendix 8**). This experiment showed that very specific conditions can be generated, where distinct post-translational modification levels of TDP-43 are achieved.

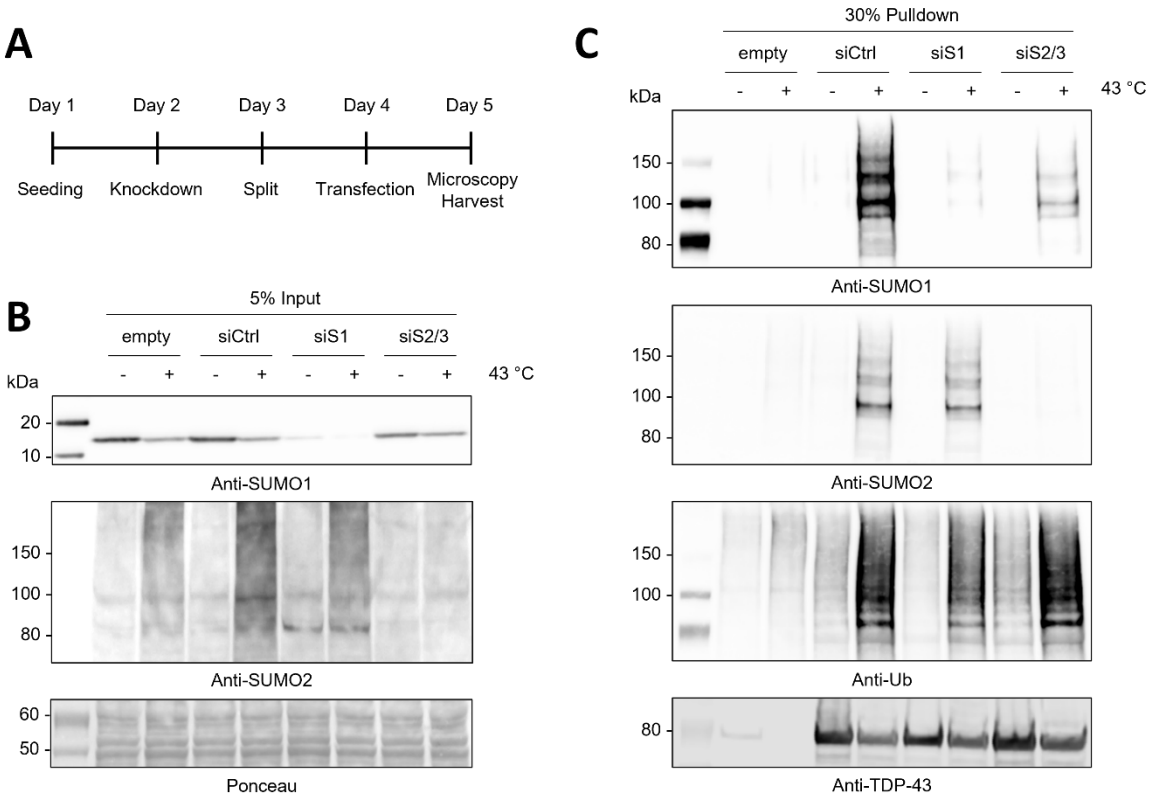

Figure 35: Detection of endogenous PTMs on TDP-43. (**A**) Experimental workflow for generating defined conditions of post-translationally modified TDP-43 in HeLa cells and subsequent analysis by pulldowns or microscopy. (**B**) Analysis of knockdown efficiency in whole cell lysate by western blotting, using antibodies against SUMO1 and SUMO2. (**C**) Ubiquitylation and SUMOylation of transiently overexpressed TDP-43 in cells depleted of SUMO1 or SUMO2/3 were analyzed by denaturing NiNTA-pulldowns and western blotting, using antibodies against SUMO1, SUMO2, ubiquitin and TDP-43.

I used this setup to screen how isoform-specific depletion of SUMO affects phase separation of different TDP-43-constructs under different cellular stress conditions. Therefore, I transfected cells depleted of either SUMO1, SUMO2/3 or all three isoforms with EGFP-tagged TDP-43, TDP-43(ΔNLS) and TDP-43(CTF-25). TDP-43(ΔNLS) has a mutated NLS which results in its accumulation in the cytoplasm. CTF-25 is a cleavage product of TDP-43, which is considered to be a pathological hallmark that promotes neurotoxic aggregation (Berning and Walker 2019). Cells were exposed to several stress factors prior to imaging. Treatment with 100 µM $NaAsO_2$ for 1 h or 1 mM H_2O_2 for 2 h were used for generating oxidative stress. Proteasomal degradation was inhibited by the addition of 30 µM MG-132 for 4 h, which induces proteotoxic stress. Exposure to 43 °C for 2 h induced a heat shock, leading to thermal stress.

Under unperturbed conditions, transient overexpression of EGFP-tagged TDP-43 resulted in the same phenotypes as observed before (**Figure 36** in **chapter 3.4.1**). In comparison, TDP-43(ΔNLS) primarily localized in the cytoplasm. The pathological mutant TDP-43(CTF-25) formed irregular cytoplasmic foci that seem to clump together, and additional small spots appeared in the nucleus (**Figure 36** A). All applied stress conditions enhanced condensate formation. For TDP-43, the number of condensates drastically increased and proteasomal inhibition (MG-132) resulted in the accumulation of cytoplasmic EGFP-signal. Both TDP-43(ΔNLS) and TDP-43(CTF-25) formed irregular foci throughout the cell.

No differences in phase separation behavior of TDP-43 were observable upon depletion of different SUMO isoforms as it was the case for experiments using linear fusions of PTMs. Yet, I quantified transfected cells with condensates as described before (**Figure 36** B). For TDP-43, sodium arsenite, proteasomal inhibition and heat stress resulted in a slightly elevated number of transfected cells with condensates upon depletion of SUMO1. Assuming that SUMO1 inhibits phase separation, this effect was expected but to a more pronounced extent. Similarly, knockdown of SUMO2/3 slightly decreased the number of transfected cells forming condensates upon sodium arsenite treatment and heat. This is also an expected effect as SUMO2 acts as an enhancer of phase separation.

Condensate formation of all other TDP-43 constructs was only screened in one single large-scale test experiment. Thus, the results need to be considered with caution. In fact, the absence of SUMO1 resulted in a reduced number of transfected cells with condensates, whereas depletion of SUMO2/3 increased the numbers. This stands in contrast to all previously collected data and opposes the suggested mechanism in **Figure 33**.

In summary, I could not show a meaningful impact of endogenous PTMs that work in the favor of the previously suggested mechanism. Furthermore, this experiment must be performed in more biological replicates to obtain statistical significance.

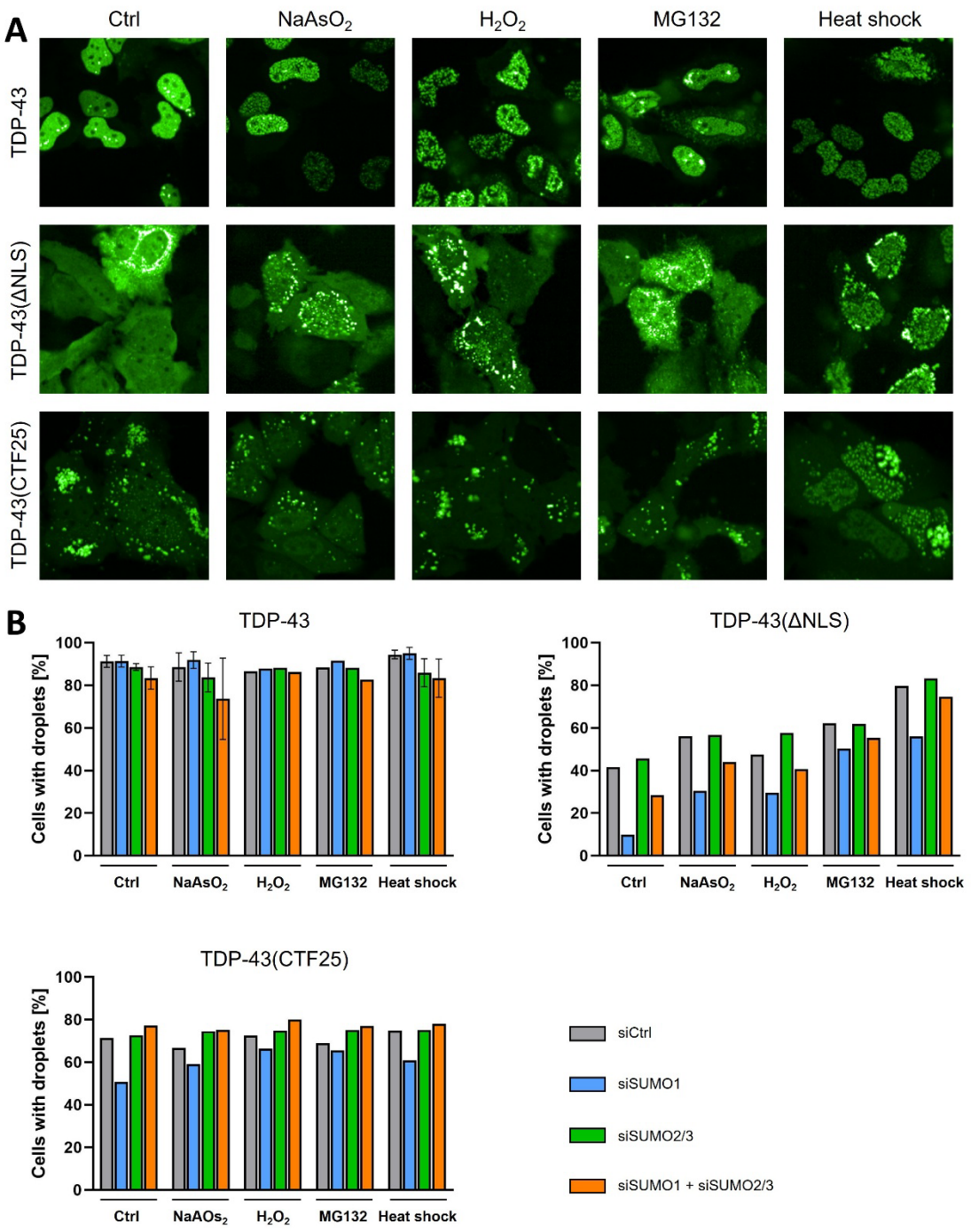

Figure 36: Phase separation of TDP-43-variants upon cellular stress. (**A**) Exemplary fluorescence microscopy images of HeLa cells depleted of SUMO that were transiently transfected with TDP-43-variants and exposed to cellular stress factors. (**B**) Quantification of transfected cells with droplets (n=3 for all experiments with error bars, n=1 for all remaining experiments).

3.4.3 Effects of impaired phase separation on modification of TDP-43 by PTMs

Since TDP-43 self-assembly is mediated by multivalent interactions where all protein domains contribute to, it is likely that disrupting these mechanisms can alter post-translational modification of TDP-43 with ubiquitin and SUMO (**chapter 1.2.5**). To address

this question, I made use of a set of mutations that I characterized before (**chapter 3.2.4**). Both A326P (1P) and W345G/W85G (2W) inhibited phase separation, while G335A/G338A (2G) strongly enhanced condensate formation of TDP-43(LCD) (**Figure 23**). I mutated the respective sites in full-length TDP-43 and also added a further N-terminal domain mutant (6M) that is described to be deficient in oligomerization and should thus not undergo phase separation (Pérez-Berlanga *et al.* 2023).

Upon transient overexpression of EGFP-tagged TDP-43 in HeLa cells, I first analyzed condensate formation by fluorescence microscopy (**Figure 37** A) and 6M indeed showed a reduction in visible droplets but an overall weaker GFP signal implying low expression. 1P and 2W were completely deficient in droplet formation for TDP-43(LCD), which was not necessarily the case for full-length TDP-43, as several cells showed prominent foci in the nucleus. However, I did not observe any cells with dense droplet pattern as it was the case for WT TDP-43. Increasing helicity by the 2G mutation clearly led to a strong enhancement of cytoplasmic GFP signal, and a fraction of cells containing large amounts of small spots, indicating a similar trend as observed for this mutation in TDP-43(LCD). I did not quantify these effects in detail but rather shifted to the impact of the respective mutants on the post-translational modifications on TDP-43.

Therefore, I performed denaturing NiNTA-pulldowns as in the previous **chapter 3.4.2** and assessed the ubiquitylation and SUMOylation pattern on TDP-43 by western blotting (**Figure 37** C). It has to be mentioned first, that the low expression of 6M observed by fluorescence microscopy was also confirmed by analyzing protein levels in the input samples (**Figure 37** B). All other mutants expressed to a similar extent. Most prominently, 2W and 1P led to a strong increase of ubiquitylation and SUMOylation with both isoforms on TDP-43. Despite the pronounced phenotype of 2G, no significant difference in post-translational modification of TDP-43 could be observed.

Altogether, this experiment suggests that post-translational modification of TDP-43 can be either a consequence of altered self-assembly mechanisms or an attempt of the cell to rescue physiological phase separation, which is further discussed **chapter 4.3.3**

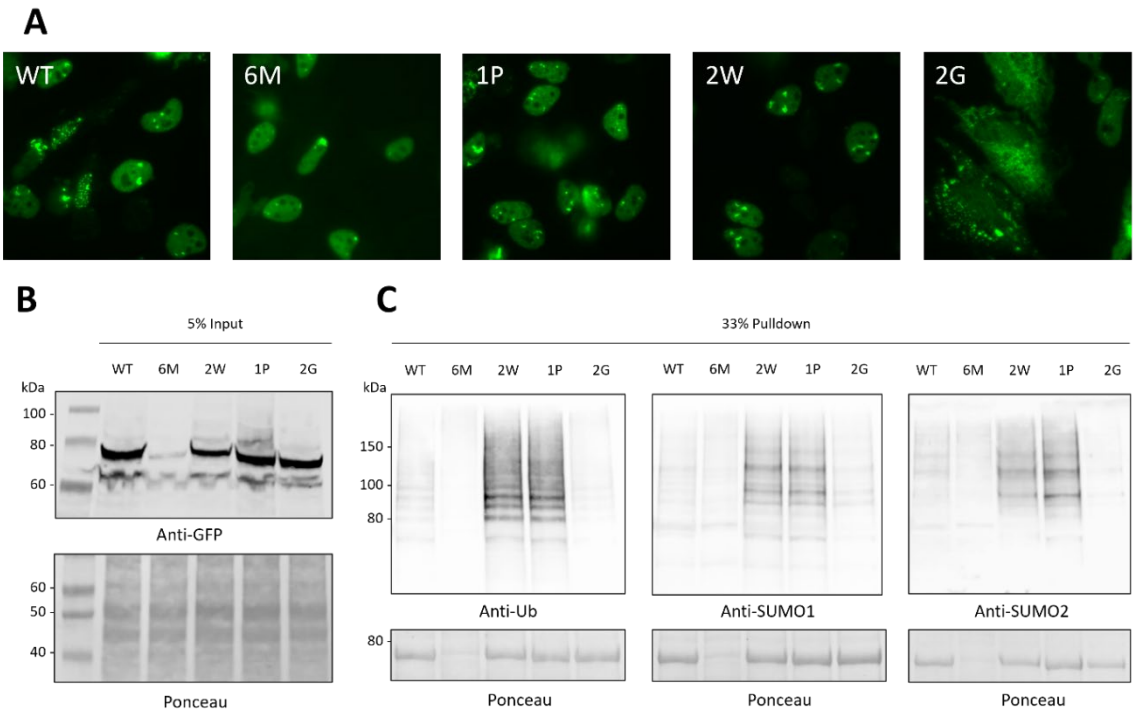

Figure 37: Post-translational modification of TDP-43 phase separation mutants. (**A**) Exemplary fluorescence microscopy images of HeLa cells transfected with EGFP-tagged TDP-43 plasmids harboring mutations that alter phase separation. (**B**) Analysis of expression levels by western blotting using an antibody against GFP. (**C**) Analysis of Ubiquitylation and SUMOylation patterns by denaturing NiNTA-pulldowns and western blotting using antibodies against ubiquitin, SUMO1 and SUMO2.

3.4.4 Impact of TDP-43 ubiquitylation and SUMOylation on RNA processing

TDP-43 has some well-described functions in the cellular metabolism (**chapter 1.2.7.1**). As a promiscuous RNA-binding protein (RBP), TDP-43 participates in RNA splicing as for example in exon skipping (Buratti *et al.* 2001). It has been shown that a phase separation-deficient TDP-43 mutant maintained overall splicing activity, showing minor deviations of exon skipping in comparison to WT TDP-43 (Schmidt *et al.* 2019). I wanted to analyze if mimicking of ubiquitylated or SUMOylated TDP-43 affects this function. Therefore, I made use of a similar experimental setup as described before (Gruijs da Silva *et al.* 2022).

After knockdown of endogenous TDP-43, I transiently overexpressed EGFP-tagged TDP-43-fusions with ubiquitin, SUMO1 or SUMO2 similarly as in **section 3.4.1** and harvested samples for protein and RNA extraction. I confirmed by western blotting that endogenous TDP-43 was depleted and the different EGFP-tagged TDP-43 variants were expressed at comparable levels (**Figure 38** A). Afterwards, I isolated total RNA and generated cDNA, which enabled me to analyze two known splicing targets of TDP-43, *SKAR* and *BIM*

(Tollervey *et al.* 2011; Fiesel *et al.* 2012). Both exons are skipped in the presence of TDP-43, which results in the appearance of shorter DNA fragments in an agarose gel upon depletion of TDP-43 (**Figure 38** B). For *SKAR*, the expression of EGFP-tagged TDP-43 partially rescued exon skipping, while the efficiency was slightly lower in case of fusions with ubiquitin and SUMO. I observed the opposite situation for *BIM*, where Ub-/SUMO-fusion proteins had a higher efficiency in restoring the splicing pattern of endogenous TDP-43. In comparison, overexpression of TDP-43 without a modifier resulted in a different ratio of splicing products and the presence of an additional signal slightly below 400 bp that was otherwise only observable upon depletion of endogenous TDP-43.

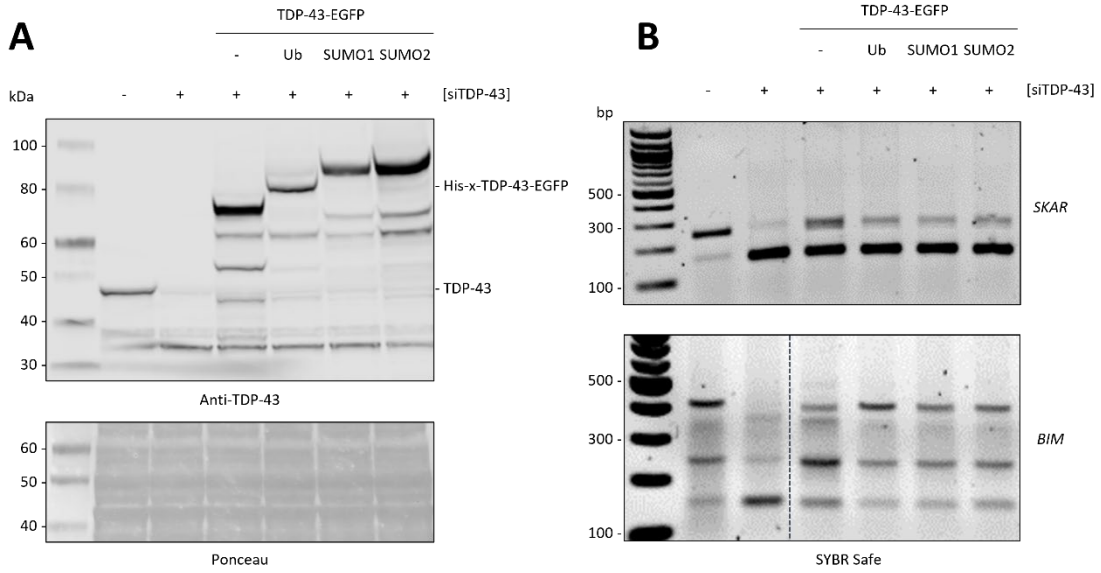

Figure 38: Impact of ubiquitin and SUMO on TDP-43 splicing activity. (**A**) Monitoring the depletion of endogenous TDP-43 and the expression of EGFP-tagged TDP-43-fusions with ubiquitin and SUMO by western blotting. (**B**) Analysis of splicing patterns by amplification of SKAR and BIM from cDNA by agarose gel electrophoresis.

This experiment showed that there are minor differences in the effects of modified and unmodified TDP-43 on exon skipping of two exemplary splicing targets. However, I did not observe contrasting impacts between the modifiers. It must also be considered that this semi-quantitative PCR only monitors the steady state of a certain splicing product and qPCR would reveal more detailed insights into the processing of these targets. For further investigation, more splicing targets could be analyzed in a different manner, also including other mechanisms like exon inclusion. A genome-wide analysis of the transcriptome by high-throughput RNA-sequencing would be a more complex approach. This could provide a global and more detailed picture of the impact of each modifier.

In summary, the role of ubiquitin and SUMO on the functionality of TDP-43 requires further investigations. The N- and C-terminal fusions of ubiquitin and SUMO to TDP-43 clearly suggest a high impact of the PTMs on phase separation of TDP-43. Depletion of endogenous SUMO is a severe intervention into the cell and did not result in conclusive results how endogenous post-translational modification of TDP-43 changes phase separation. The role of protein levels by overexpression is discussed **in chapter 4.3.2.2**. Due to the multi-domain organization of TDP-43, the attachment site for the PTM might have a bigger relevance, which is further discussed in **chapter 4.3.2.1**. Follow-up experiments to discover functions of ubiquitin and SUMO in TDP-43 phase separation are suggested in **chapter 4.4.1**.

4 Discussion

4.1 SUMO1 inhibits phase separation of TDP-43

While the role of a particular SUMO isoform on its conjugation target often remains enigmatic, I could clearly demonstrate that SUMO1-fusion has a distinct impact by inhibiting phase separation of TDP-43(LCD) (**chapter 3.2.1**). This effect relies on specific interactions between the SUMO1 N-terminus and β2-sheet with the α-helix and C-terminus of TDP-43(LCD) (**chapter 3.3.2**). In this section, I will discuss the nature of this interaction and potential mechanistic scenarios, also in the context of full-length TDP-43. I will furthermore elaborate on isoform-specificity for SUMO1 and target-specificity for different IDRs.

4.1.1 Obstruction of self-assembly sites in TDP-43(LCD)

Self-assembly via multivalent interactions are often difficult to narrow down to specific protein regions or even distinct amino acids. TDP-434(LCD) is a suitable model protein to study how a specific PTM affects phase separation as its mechanism of self-assembly is partially resolved (Li *et al.* 2018). As the α-helix is a major self-assembly site of TDP-43(LCD), it is not surprising that binding of SUMO1 to this region inhibits phase separation. The helix is of transient nature and is most likely stabilized upon self-interaction of TDP-43(LCD) (Conicella *et al.* 2016). This raises several interesting assumptions about how SUMO1 affects this region.

On the one hand, SUMO1 could simply bind to the α-helix and prevent helix-helix interactions, which is supported by the reduced deuterium uptake that was measured in the HDX-MS experiments (**Figure 26** C). On the other hand, a more sophisticated mechanism could involve the resolution of the helical structure. The addition of proline is well-established as a helix breaker due to its dihedral angle (Li *et al.* 1996; Jacob *et al.* 1999). By mutating A315P, I could show that an intact α-helix is essential for the phase separation of TDP-43(LCD) as this construct did not form condensates (**Figure 23**). Whether SUMO1 resolves the helix or the binding of SUMO1 to the helix is sufficient for the reduced self-assembly remains elusive. In fact, the mutation of G335A/G338A has been shown to enhance helicity, while decreasing condensate mobility (Conicella *et al.* 2020). When I overexpressed this TDP-43(LCD) variant in HeLa cells, I could observe a strong increase in condensate number. Yet, the fusion of SUMO1 still largely inhibited condensate formation comparable to its fusion to WT TDP-43(LCD) (**Figure 23**). If

G335A/G338A increases the surface of the self-interaction site or enhances the helix stability, SUMO1-fusion is still capable of blocking this site or resolving the helix, respectively.

The potential of a PTM to unfold a secondary structural element relies on the stability of the secondary structure, which is directly affected by the tertiary protein structure (Morimoto *et al.* 2016). It can be assumed that an α-helix that is supported by neighboring β-sheets as in the case for RRMs is less prone to be destabilized by PTM conjugation in close proximity (Lukavsky *et al.* 2013). It can be speculated that the internally disordered nature of TDP-43(LCD) most likely excludes any helix-protective mechanisms and helicity might decrease upon interaction with SUMO1.

Finally, HDX-MS data also showed a reduced deuterium uptake in a peptide that harbors W412 when comparing SUMO1 fused to TDP-43(LCD) and SUMO1 mixed with TDP-43(LCD) (**Figure 26** C). This site has been shown to contribute to self-assembly of TDP-43(LCD) amongst other aromatic amino acid residues (Li *et al.* 2018). Due to the absence of any secondary structures, this region is supposed to be highly accessible for deuterium uptake in case of soluble TDP-43(LCD) as it was the case during the HDX-MS experiments. The reduced deuterium uptake in the fusion protein compared to the protein mix persists until later time points of deuterium exposure, which suggests that this region could be stably surrounded by SUMO1.

Most of these scenarios could be elucidated by applying structural biology techniques of higher resolution than HDX-MS. The most powerful experimental approach to further reveal the interactions between TDP-43(LCD) and SUMO1 would be multi-dimensional NMR, as it could enable both identification of interaction sites on an amino acid resolution but also grants insights into the degree of helicity. In this study, I used MBP-tagged SUMO1-TDP-43(LCD) with a molecular weight of ~68 kDa, which is too large to get a sufficient peak separation in 2D-NMR experiments (Puthenveetil and Vinogradova 2019). The preparation of SUMO1-TDP-43(LCD) without MBP would result in a protein of 26.5 kDa, making it suitable for 2D-NMR. As SUMO1-TDP-43(LCD) does not phase separate after removal of MBP under various conditions (**Appendix 4**), soluble protein could be produced in *E. coli*. As an alternative approach, SUMO1-TDP-43(LCD) could be purified from inclusion bodies under denaturing conditions, as described by Babinchak *et al.*, 2019. Here, the impact of the harsh purification conditions on the protein integrity has to be carefully considered, as the protocol requires high concentrations of Urea, HPLC purification using acetonitrile and lyophilization (Babinchak *et al.* 2019).

4.1.2 Specific elements in SUMO1 that block TDP-43(LCD) self-assembly sites

SUMO1 and SUMO2 share a similar fold and have a sequence identity of less than 50% (**Figure 2** C and D). Their opposing effects on regulating phase separation of TDP-43(LCD) is thus intriguing and requires a detailed analysis of the identified elements in SUMO1 that interact with TDP-43(LCD). The HDX-MS data clearly showed how the N-terminus and β_2-sheet of SUMO1 are blocked when it is attached to TDP-43(LCD), which inhibited phase separation (**Figure 26** D). The N-terminus of SUMO1 is four amino acids longer and is more negatively charged in comparison to the N-terminus of SUMO2. The SUMO1 β_2-sheet has an exposed glutamate and histidine, where SUMO2 harbors less reactive valine and glutamine residues at the respective positions (**Figure 2**).

As the HDX-MS experiment did not provide interaction sites on an amino acid resolution, I first approached to mutate entire structural regions. An exchange of α-helix and β_2-sheet of SUMO1 with the same elements from SUMO2 has been demonstrated to assign SUMO2-specific binding capacity to a chimeric protein based on SUMO1 (Zhu *et al.* 2008). I thus assumed that a loss of β_2-sheet and N-terminus could deprive the capacity of SUMO1 to inhibit phase separation of TDP-43(LCD) when being exchanged with the respective elements of SUMO2. With this approach I was able to mutate large elements of SUMO1, without the knowledge of particular amino acid interaction sites, while maintaining structural integrity of the protein fold. Indeed, both *in vitro* experiment and mammalian cell culture models confirmed the importance of both regions for phase separation of TDP-43(LCD). This was further supported by a mutated SUMO2 protein, which harbored N-terminus and β_2-sheet of SUMO1. Insertion of these two elements almost entirely reversed the LLPS-enhancing properties of SUMO2. In conclusion, the presence of both N-terminus and β_2-sheet from SUMO1 can turn SUMO2 into a similar inhibitor of phase separation as WT SUMO1.

Interestingly, only the double mutants of both N-terminus and β_2-sheet were sufficient to entirely reverse the impacts of SUMO1 and SUMO2 on TDP-43(LCD) phase separation, while single mutants only had mild impacts (**Figure 27**). This suggests a potential binding mechanism that is based on avidity. Whether SUMO1 binds to TDP-43(LCD) in a two-step process, or if one sequence element blocks the TDP-43(LCD) α-helix and the other one binds to W412 remains elusive and requires additional experiments as suggested in the previous section.

Another important aspect of the SUMO1 N-terminus is its requirement to move freely. C-terminal fusion of SUMO1 to TDP-43 did not inhibit phase separation (**Figure 22** and **Appendix 3**). An arrangement like this is rather non-physiological as the fusion is not

based on the modifier's C-terminal GG-motif and thus orients the modifier differently towards the substrate. It also most likely prevents the ability of the SUMO1 N-terminus to move freely towards the self-assembly sites of TDP-43(LCD). Interestingly, expression of 3xNLS-SUMO1-TDP-43(LCD)-EGFP resulted in the formation of condensates in the nucleus (**Figure 22**). Three assumptions can be made based on this observation: First, forcing the protein from ubiquitous localization into a comparably smaller compartment like the nucleus can result that the C_{sat} is exceeded (**chapter 1.2.2**). Second, fusion to SUMO1 could recruit TDP-43(LCD) into nuclear biomolecular condensates following the client-scaffold principle (**chapter 1.2.4**). Lastly, the N-terminal fusion of a 3xNLS adds an element of a considerable size to the flexible N-terminus of SUMO1. Indeed, the 3xNLS has a molecular weight of ~3 kDa and AlphaFold3 simulations suggest that it can adopt a partially helical structure (**Appendix 9**). In combination with its highly positive net charge of +12 (-4 for the SUMO1 N-terminus), it is very likely that the addition of a 3xNLS severely affects the SUMO1 N-terminus and inhibits its interaction with TDP-43(LCD). Steric effects of the 3xNLS could be tested by replacing it with a 3xNES, which should have a different effect on the inhibition of TDP-43(LCD) phase separation by SUMO1-fusion.

Mixing SUMO1 and TDP-43(LCD) at equimolar concentrations had no effect on phase separation and large excess of peptides derived from SUMO1 N-terminus and β_2-sheet were required for efficient inhibition (**Figure 12** and **Figure 28**). This suggests a very weak interaction between both interaction partners, which is further supported by the performed FP experiment (**Appendix 6**). Since I was not able to add sufficiently high concentrations of TDP-43(LCD) to FITC-SUMO1-Nt peptide to reach saturation, for instance surface plasmon resonance (SPR) could be used, which enables the measurements of weaker K_D in the millimolar range (Douzi 2017).

4.1.3 Phase separation-inhibiting effects of SUMO1 beyond TDP-43(LCD)

In comparison to the isolated LCD, full-length TDP-43 phase separates by a more sophisticated mechanism of self-assembly, which further involves oligomerization of the NTD and nucleotide interactions with the RRMs (Jiang *et al.* 2017; Zacco *et al.* 2019). Strikingly, SUMO1-fusion to TDP-43 largely inhibited phase separation in mammalian cells, even though unmodified TDP-43 is highly prone to form condensates (**Figure 34**). This interesting observation still needs to be validated with purified components in *in vitro* experiments.

The multi-domain organization of TDP43 bears the potential of additional interaction sites for SUMO1. Indeed, I measured a slightly better binding of the SUMO1 N-terminal peptide

to full-length TDP-43 in comparison to TDP-43(LCD) (**Appendix 6**). It would be interesting to study if SUMO1 binds to another interface within TDP-43 by executing a comparable HDX-MS study with full-length TDP-43 as described in **chapter 3.3.2.1**. This could also provide general insights into the mechanism of TDP-43 self-assembles. If SUMO1 only blocks the α-helical region in the LCD, does the NTD still self-interact (Wang *et al.* 2018a)? Why is this not entirely sufficient to drive phase separation of TDP-43?

Screening how PTMs regulate phase separation of different IDRs also showed that SUMO1-fusion inhibits phase separation of Htt-Ex1(Q23) (**Figure 13** B). This finding is in agreement with a study showing that conjugation of Htt-Ex1 with SUMO1 results its aggregation (Steffan *et al.* 2004). FUS(QGSY) and FUS(RGG) whose phase separation is enhanced by the fusion of SUMO1 are entirely disordered while Htt-Ex1(Q23) adopts a helical confirmation (Burke *et al.* 2015; Elena-Real *et al.* 2023). This helix is of a completely different amino acid composition as the helix in TDP-43(LCD), and the exact mechanism how Htt-Ex1 self-assembles and undergoes phase transition into solid-like aggregates is not fully understood. Still, this raises the question if helicity provides an interaction site for SUMO1 on Htt-Ex1. If the same elements of SUMO1 are responsible for the inhibitory effects as for TDP-43(LCD), an exchange of SUMO1 N-terminus and β_2-sheet with SUMO2 should abolish this effect, as shown in **Figure 27**. Additionally, HDX-MS or other structural methods could reveal how SUMO1 blocks the self-assembly of Htt-Ex1, or if this effect relies on an entirely different mechanism.

In summary, SUMO1 appears to have distinct effects on regulating phase separation that depend on the attached IDR. There might be a balance between SUMO1 specifically interacting with elements of the attached protein or by generically interacting with itself in a similar manner to SUMO2 (**chapter 4.2.5**). The potential to inhibit phase separation of a substrate can thus only occur if a) SUMO1 interacts at the site of self-assembly and b) if this interaction has a higher binding strength than SUMO1 interacting with itself.

4.2 SUMO2 is a general enhancer of phase separation

In contrast to the diverse effects of SUMO1, SUMO2 had a strong propensity to enhance phase separation of all tested IDRs (**chapter 3.1.4**). This effect relies on the interaction between the SUMO2 N-terminus and t4-loop, which can occur within the same SUMO2 molecule (*cis*), but also intermolecularly when two SUMO2-molecules are in close proximity (*trans*) (**chapter 3.3.3**). This situation can occur when an IDR self-assembles

while having SUMO2 attached. In this chapter, I will discuss this generic and IDR-independent effect of SUMO2, also regarding experimental limitations of the XL-MS experiment. Furthermore, the capability of ubiquitin and SUMO1 to act similarly as enhancers of phase separation will be addressed.

4.2.1 Identification of self-interaction sites within SUMO2

Using stable-isotope labeling of SUMO2-TDP-43(LCD) and the heterobifunctional crosslinker Sulfo-SDA enabled the MS-based identification of both intramolecular *cis*-crosslinked and intermolecular *trans*-crosslinked peptides derived from SUMO2 fused to TDP-43(LCD) in a phase separated state. *Cis*-crosslinked peptides of high scores between the N-terminus and the t4-loop of SUMO2 occurred in both ^{14}N- and ^{15}N-labeled SUMO2-TDP-43(LCD) and indicate a basal affinity between these regions that goes beyond random contacts by fluctuations of the flexible N-terminus. Interestingly, this contact was also detected between the N-terminus of a ^{14}N-labeled protein and the t4-loop of a ^{15}N-labeled protein and vice versa, which clearly indicates *trans*-interactions between SUMO2-molecules upon phase separation of SUMO2-TDP-43(LCD) (**Figure 31**).

Similar as described in the previous section, MS-based structural biology approaches only reveal information on a peptide level, so the identification of interaction sites with amino acid resolution requires additional methods with NMR being the most powerful approach. The capability of Sulfo-SDA for capturing interaction sites is also mostly limited to amino acids with primary amine functional groups due to the NHS-warhead of the crosslinker. Still, the fact that several exposed lysines of SUMO2 were not detected in crosslinked peptides supports the credibility of the regions identified in this experiment.

There are currently no studies that assess the capability of free SUMO2 to undergo phase separation, but both SUMO1 and ubiquitin have been shown to require high protein concentration and the presence of molecular crowding agents to phase separate, so it can be assumed that SUMO2 might behave similarly (Arora *et al.* 2023; Poudyal *et al.* 2023). In conclusion, the enhancement of phase separation by SUMO2 must rely on self-assembly of a scaffold protein that brings several SUMO2-molecules into close proximity. In the absence of a self-assembling conjugation target, SUMO2 most likely does not phase separate under physiological conditions. Both PML-NB assembly and DNA repair foci are associated with group SUMOylation, so it can be hypothesized that the mechanism identified here could contribute to the condensate stability of these biological assemblies (Dou *et al.* 2010; Sahin *et al.* 2014b).

4.2.2 Electrostatic interactions of SUMO2 in *trans* as a driver of LLPS

The t4-loop is the longest largely unstructured region in SUMO2 with 19 amino acids (**Figure 2** D, PDB:2n1w), which is especially enriched in negatively charged amino acids and has a net charge of -7. I was able to abolish the LLPS-enhancing effect of SUMO2 on TDP-43(LCD) phase separation by neutralizing the charge of six glutamates (E→Q) and aspartates (D→N) in the SUMO2 t4-loop, which was the main contact sites with the N-terminus in *trans*. Indeed, this mutant protein behaved similarly as untagged TDP-43(LCD) in *in vitro* phase separation experiments (**Figure 32** D).

The N-terminus of SUMO2 has a slightly negative net charge of -2, which indicates that the N-terminus and the negatively charged t4-loop should repel each other, which is apparently not the case. Yet, there are a few lysines in the N-terminus that could be involved in electrostatic interactions with aspartate and glutamate in the t4-loop, which is further supported by the fact that phase separation of SUMO2-TDP-43(LCD) was strongly reduced in the presence of ionic strength. In contrast, phase separation of unmodified TDP-43(LCD) was less affected this (**Figure 19**).

Interestingly, electrostatic interactions are often linked to phase separation of proteins forming liquid-like condensates as the germ granule component Ddx4 or the Alzheimer's disease-associated protein tau (Nott *et al.* 2015; Farag *et al.* 2023). Aggregation is often associated with hydrophobic interactions (Raschke *et al.* 2001; Farag *et al.* 2023). Self-assembly of TDP-43(LCD) partially relies on helix-helix interactions, which is largely of hydrophobic nature (Conicella *et al.* 2020). The addition of electrostatic interactions between SUMO2-moieties in *trans* thus adds another self-interaction element, that could potentially shift TDP-43(LCD) condensates from gel-like to more liquid-like properties, which is also supported by an increase of droplet mobility as determined by FRAP analysis (**Figure 17**).

4.2.3 A *cis*/*trans* switch of the SUMO2-N-terminus with an unstructured loop

A gradual truncation of the SUMO2 N-terminus changed the condensate appearance drastically. While short- (Δ1-6) and mid-length (Δ1-11) truncations made the droplets more liquid-like, an entire truncation (Δ1-15) led to a gel-like condensate phenotype. This suggests some interesting assumptions on the hierarchy between *cis*- and *trans*-interaction of the N-terminus and t4-loop of SUMO2.

The SUMO2 N-terminus has the potential to transiently interact in *cis* with the t4-loop (**Figure 30**). When being conjugated to a protein that undergoes self-assembly, SUMO2-moieties come into close proximity and a competition between *cis*- and *trans*-interactions

arises. If the N-terminus is truncated, the distance between the remnant and the t4-loop on a single SUMO2 moiety increases, which lowers the chance of an efficient *cis*-interaction. However, considering the high flexibility of the internally disordered TDP-43(LCD), the same structural elements would still be able to interact in *trans*, which would further promote the LLPS-enhancing effect and could potentially explain why SUMO2(Δ1-6)-TDP-43(LCD) behaves more liquid-like in comparison to a fusion of WT SUMO2. Deletion of the first six amino acids results in the loss of two negatively charged amino acid residues. The interaction between the remaining lysines and the negatively charged t4-loop might occur more favorably than in comparison with the WT N-terminus.

How the deletion of the first eleven amino acids of SUMO2 strongly enhances LLPS of TDP-43(LCD) remains enigmatic. The remnant N-terminus only consists out of negatively charged amino acids, asparagine and threonine, whose propensity to interact with the negatively charged t4-loop is rather unlikely. It can thus be imagined that the absence of the first eleven amino acids enables interaction between the N-terminal remnant and one of the positively charged surfaces of SUMO2, as for example the t2-loop or β_2-sheet (**Figure 2** A). An XL-MS experiment with a similar setup as performed in **chapter 3.3.3.1** could provide insights into the underlying mechanism for enhancing liquidity.

A truncation of the entire N-terminus would deprive the major *trans*-interaction site with the SUMO2-surface that has been identified in this work. As a consequence, the self-assembly mechanism of TDP-43(LCD) itself would dominate the phenotype, while SUMO2 self-interaction would play a negligible role. Yet, the XL-MS experiment showed a few crosslinked peptides of SUMO2-TDP-43(LCD) with lower scores were detected that suggest additional self-interactions sites. The *trans*-interactions in SUMO2 between K42 and E79/D80 (**Figure 39** A) or C48/E49 and T70/T72 (**Figure 39** B) can most likely not occur in *cis*, due to the spatial arrangement of the atoms. In contrast, interactions between K45 and N68/E69/T70 were only detected in *cis*, which is reasonable due to the close distance of their functional groups (**Figure 39** C).

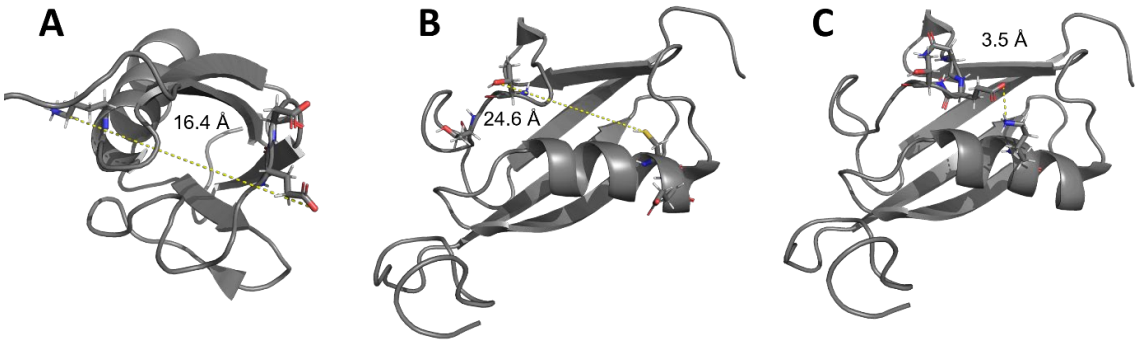

Figure 39: Exclusive *cis*- and *trans*-interactions of SUMO2. Interaction sites were mapped on the structure of SUMO2 (PDB:2n1w) based on crosslinked peptides identified in the SUMO2-TDP-43(LCD) XL-MS experiment (**Figure 31**). Exemplary molecular distances were calculated in PyMOL 3. (**A**) *Trans*-interaction between K42 and E79/D80. (B) *Trans*-interaction between C48/E49 and T70/T72. (C) *Cis*-interaction between K45 and N68/E69/T70.

It is unclear whether the detected *trans*-interactions are a cause or a consequence of SUMO2 self-interaction, as I was not able to assign distinct roles to these sites based on mutational studies. I hypothesized that T70/T72 could participate in hydrogen bonding with amino acids of the α-helix, so I mutated them to alanine. Yet, the resulting construct appeared to phase-separate in an even more liquid-like manner as WT SUMO2-TDP-43(LCD). Reducing SUMO2-helicity resulted in diffuse aggregation, which might be driven by a loss of the structural integrity of SUMO2. To confirm this, CD-spectra of the isolated SUMO2-mutant that harbors prolines as helix-breakers could be recorded and compared to WT SUMO2.

4.2.4 Polymeric SUMO2-chains enhance multivalency

The formation of polymeric SUMO2(/3) chains occurs mainly on K11 (Jansen and Vertegaal 2021, **chapter 1.1.3**). If a SUMO2 chain is considered as a polymer, each SUMO2-moiety could be represented as one bead that mediates a contact site. Thus, an increasing number of beads (or a longer SUMO2 chain respectively) would enhance multivalency, following the principles of polymer self-assembly (Mohanty *et al.* 2022; Xu *et al.* 2023). This explains while LLPS increases with the length of SUMO2 chains on TDP-43(LCD), as shown in **chapter 3.3.3**.

To mimic the natural spacing between K11-linked chains, I generated linear fusions of SUMO2(Δ1-11) that lack the majority of the flexible N-terminus. As discussed in the previous chapter, the mechanism of this truncation is unclear but seems to enhance the

liquid-like properties of TDP-43(LCD) condensates. Yet, the interaction sites identified in this work explain why an increasing number of SUMO2-moieties enhance LLPS when being fused to TDP-43(LCD). Following the principle of stickers and spacers (**chapter 1.2.2**), the remnant N-terminus and the exposed C-terminus of SUMO2 can be considered as a spacers that enable dynamic movement of the globular core elements, which represents the sticky elements that mediate self-assembly (Ginell and Holehouse 2023).

The enzymatic synthesis of polymeric SUMO2 chains on TDP-43(LCD) would allow studying the impact of the N-terminus. Purifying SUMO2 chains of different lengths might be similarly executable as described for ubiquitin chains using cation exchange chromatography (Dong *et al.* 2011). Due to the chain formation, several flexible N-termini would accumulate in close proximity. Their high internal dynamic could lead to them behaving as IDRs and potentially even promote entanglement-induced aggregation (Baiesi *et al.* 2019; Sulkowska 2020).

4.2.5 Enhancement of phase separation by SUMO1

Intriguingly, SUMO1-fusions enhanced phase separation of the completely unstructured IDRs FUS(QGSY) and FUS(RGG), while it acted as an inhibitor of phase separation in case of the partially folded TDP-43(LCD) and Htt-Ex1(Q23) (**Figure 13**). This indicates that SUMO1 has the potential to follow a similar mechanism of enhancing phase separation like SUMO2, when an attractive binding site in the conjugated protein is missing. Indeed, the N-terminus of SUMO1 has recently been reported to interact with the surface of SUMO1 on several sites (Richter *et al.* 2024). The most prominent self-interaction was proposed with the SIM-binding groove in the β2-sheet and the α-helix based on NMR data. By applying MD simulations, the same interaction was barely predicted within SUMO2, but to an even stronger extent in the *C. elegans* SUMO protein Smo-1.

Interactions between N-terminus and the t4-loop of SUMO1 were detected by NMR similarly as in our XL-MS experiment for SUMO2. Interestingly, MD simulations showed no significant difference in this interaction between SUMO1, SUMO2, Smo1 and Smt3. Yet, comparing the t4-loop sequences of SUMO1 and SUMO2 shows a drastic difference in the net charge with -3 for SUMO1 and -7 for SUMO2.

In conclusion, one can assume that the presumable *cis*-interaction between the SUMO1 N-terminus and SIM-binding groove could turn over into a *trans*-interaction when several SUMO1-moieites come into close proximity as it likely occurred in the case of the FUS-derived IDRs.

4.2.6 Enhancement of phase separation by ubiquitin

Comparing the effect of ubiquitin- and SUMO2-fusions on TDP-43(LCD) phase separation *in vitro* showed a very similar phenotype (**Figure 15**). Both modifiers enhanced the liquidity of TDP-43(LCD) as shown by FRAP analysis, with ubiquitin having an even stronger effect than SUMO2 in aged condensates (**Figure 17** B). However, ubiquitin-fused TDP-43(LCD) had a slightly higher resistance against 1,6-Hexanediol, which indicates that hydrophobic interactions contribute to less to the self-assembly mechanism than it is the case for SUMO2 (

Figure 18).

In contrast to SUMO, ubiquitin does not have a flexible N-terminus but rather immediately folds into a β-sheet (**Figure 2** D). In conclusion, the mechanism how ubiquitin enhances must rely on different structural elements. However, the Ub-TDP-43(LCD) condensates were also highly sensitive to high salt concentrations indicating an involvement of electrostatic interactions as observed for SUMO2 (**Figure 19**).

The expression of Ub-TDP-43(LCD)-EGFP in mammalian cells resulted in irregular aggregation-like foci, while SUMO2-TDP-43(LCD)-EGFP phase separated in round droplets (**Figure 22**). Ubiquitin was also more proficient than SUMO2 in rescuing condensate formation of TD43(LCD) mutants that were deficient in self-assembly (**Figure 23**). This indicates a higher self-interaction affinity for ubiquitin, which could be investigated by SPR, measuring K_D values of Ub- and SUMO2-TDP-43(LCD) to themselves.

The condensate shape might be a result of the recruitment of ubiquitin-binding proteins that could alter the condensate's properties, as the N-terminal fusion of ubiquitin can have biological consequences (Asimaki *et al.* 2022). Of course, SUMO1- and SUMO2-fusions can also recruit binding partners, but they might be of different nature, which explains the differences in the phenotypes. This experiment thus highlights the importance of analyzing phase separation in isolated systems with defined reaction conditions, while cellular expression obtains the respective biological insights.

Altogether, the SUMO2 N-terminus appears to generally interact with the SUMO2 t4-loop but can shift from a *cis*-interaction to a *trans*-interaction, when several SUMO2 molecules come into close proximity. This suggests a generic mechanism for the enhancement of phase separation that appears to be independent of the conjugated substrate and the attachment site. How SUMO1 and ubiquitin enhanced phase separation of the FUS-derived IDRs remains elusive and require additional experiments.

4.3 Biological significance of TDP-43 ubiquitylation and SUMOylation

After characterizing the inhibitory effect of SUMO1-fusions and the enhancing effect of SUMO2-fusions on phase separation of TDP-43(LCD), I was able to observe partially comparable impacts on full-length TDP-43 in mammalian cells (**Figure 34**). This was surprising, since phase separation of TDP-43 relies on more than self-assembly of the LCD but rather involves multiple domains and interactions with other macromolecules (**chapter 1.2.7.1**). Thus, this finding supports the impact of ubiquitin- and SUMO-conjugation to TDP-43 on phase separation.

TDP-43 participates in various pathways such as RNA metabolism and the cellular stress response (Ratti and Buratti 2016). This enables multiple opportunities to study the biological consequences of ubiquitylation and SUMOylation, which I will discuss in this chapter. I will furthermore elaborate the interplay between aberrant phase separation and post-translational modifications, with a particular focus on neurodegenerative diseases.

4.3.1 Comparison of TDP-43(LCD) and full-length TDP-43 phase separation

Self-assembly of TDP-43 is a complex process that is based on multivalent interactions that occur across the whole protein. Apart from the C-terminal LCD, the N-terminal NTD majorly drives self-assembly of TDP-43 by oligomerization (Conicella *et al.* 2016; Wang *et al.* 2018a; Li *et al.* 2018). Furthermore, interaction with GU-rich RNA has been identified as a key regulator of TDP-43 phase separation (Grese *et al.* 2021).

4.3.1.1 SUMO1

Due to the variety of multivalent interactions across TDP-43, it was intriguing to see that the transient overexpression of N-terminally fused SUMO1 to TDP-43 strongly inhibited condensate formation in mammalian cells at similar expression levels in comparison to unmodified TDP-43 (**Figure 34**). This supports the importance of the LCD as a self-assembly site, while multivalent interaction sites in the remaining domains were apparently not sufficient to fully maintain a phase separated state of TDP-43. Yet, a small fraction of transfected cells still formed condensates, which suggests that NTD- and RNA-driven oligomerization mediates partial or unstable self-assembly. One could furthermore speculate about an additional interaction site between SUMO1 and TDP-43 that does not affect self-assembly. Indeed, I observed a slightly higher affinity in an FP-assay for the SUMO1 N-terminus peptide to TDP-43 compared to TDP-43(LCD) (**Appendix 6**). This

hypothesis could be investigated by probing for crosslinks of SUMO1-TDP-43 in a simplified XL-MS experiment without stable-isotope labeling. In agreement with the in **chapter 3.3.2** identified mechanism, C-terminal fusion of SUMO1 was not proficient in inhibiting phase separation of TDP-43. Furthermore, nuclear localization of SUMO1-TDP-43 was not impaired (**Figure 34** A). This indicates that SUMO1 is most likely not interacting with the NLS close to the NTD, which mainly consists out of positively charged amino acids (Winton *et al.* 2008).

4.3.1.2 SUMO2

In contrast, the impact of SUMO2 fusion to TDP-43 was harder to interpret due to the limited set of performed experiments. Transfected cells expressing SUMO2-TDP-43 formed condensates at a smaller number, but larger size compared to unmodified TDP-43 (**Figure 34**). This observation is comparable to the behavior of SUMO2-TDP-43(LCD) and TD43(LCD) in *in vitro* phase separation experiments (**Figure 14** B) but different to mammalian cell culture experiments, where TDP-43(LCD) barely formed any condensates (**Figure 22** A). Confirming that SUMO2 similarly enhances liquid-like properties of full-length TDP-43 requires FRAP analysis. Yet, the mechanism identified in **chapter 3.3.3** and discussed in **chapter 4.2.2** indicates that SUMO2 should similarly add a multivalent interaction element to full-length TDP-43 as it does to TDP-43(LCD). As shown for TDP-43(LCD), the expression of TDP-43 with a C-terminal SUMO2-fusion led to an increased number of cells forming condensates (**Figure 22** B and **Figure 34** B). This is line with the fact that a large element fused to the SUMO2 N-terminus would interfere with *cis*-interactions, but not *trans*-interactions with the t4-loop (see **chapter 4.2.3**).

4.3.1.3 Ubiquitin

While the N-terminal fusion of ubiquitin to TDP-43(LCD) resulted in the formation of irregular foci, ubiquitin-fusions to full-length TDP-43 formed condensates that appeared similar as unmodified TDP-43. Strikingly, EGFP-signal also occurred in the cytoplasm (**Figure 34** A). This suggests a potential role of ubiquitin as a factor for shuttling TDP-43 from the nucleus into the cytoplasm. Attaching ubiquitin as a linear fusion might trigger the interaction with a protein harboring a UBD and a TDP-43-specific binding domain, which has the capability to alter the cellular localization of TDP-43. Exemplary, this has been shown for the UBIN-POST-complex that shuttles K48-linked polyubiquitylated proteins from the nucleus into the cytoplasm (Hirayama *et al.* 2018). A similar mechanism could

explain the cytoplasmic localization of TDP-43 but requires the identification of the responsible shuttle protein.

4.3.2 Experimental challenges in studying the impact of PTMs on TDP-43

Studying the impact of distinct ubiquitylation and SUMOylation events of any protein is challenging due to the complexity of the PTM's systems, incorporating writers, erasers and readers of each particular modifier (Komander and Rape 2012). Many proteins harbor multiple conjugation sites, the degree of modification (e.g. chain formation or fraction of modified protein) can vary, and the exact combination of E2 and E3 is often unknown (Lips *et al.* 2020; Sun and Zhang 2022).

4.3.2.1 Impact of the attachment site of PTMs on phase separation

The expression of linear PTM fusions generates permanently and entirely modified proteins of interest. N-terminal fusions are closely mimicking conjugation to a physiological site, as attachment via the C-terminal GG-motif enables conformational flexibility of the modifier (Powers *et al.* 2018). Mutation of the GG-motif to a GV-motif maintains stability of the linear fusion due to its resistance against proteases (Johnson *et al.* 1995). Furthermore, the PTM's N-terminus is available for the formation of M1-linked chains in the case of ubiquitin and for dynamic movement in case of SUMO (Nguyen *et al.* 2022; Richter *et al.* 2024).

All initial experiments for testing the impact of fused modifiers to different IDRs were performed with N-terminal fusions of the PTMs (**Figure 13**). Surprisingly, the C-terminal attachment of ubiquitin and SUMO to TDP-43 resulted in instable protein *in vitro* (**Appendix 3**) but not after expression in mammalian cells (**Figure 22** E and **Figure 34** C). C-terminal expression is a rather unphysiological approach, as it blocks the N-terminus but leaves an accessible C-terminal GG-motif and furthermore arranges the modifier in reverse orientation in respect of the target. Consequently, a different protein surface is in proximity to the attachment site at TDP-43, as in the case for N-terminal fusion.

Especially in the context of full-length TDP-43, the attachment site of ubiquitin and SUMO must be carefully considered. First, the N-terminal fusion of SUMO1 was not entirely proficient in inhibiting phase separation of TDP-43 (**Figure 34**). The origin of this incomplete effect might occur due to the long distance between the SUMO1-fusion site at the N-terminus and blocking self-assembly of the α-helix at the C-terminus. One could

speculate about a more pronounced effect when SUMO1 is attached to a lysine which is closer to the helix in the LCD of TDP-43.

Second, the fold-altering effect of ubiquitin described in **chapter 4.3.1.3** suggests that structural integrity of particular elements within TDP-43 as NLS or RRMs could be affected by the attachment site of the PTM (Morimoto *et al.* 2016). This could alter the accessibility of these elements. An exemplary mechanism has been shown for p53, which is polyubiquitylated by the RING-E3 MDM2, resulting in an exposure of the NES of p53 (Gu *et al.* 2001; Lohrum *et al.* 2001). Similarly, ubiquitylation could cover the NLS of TDP-43, which indeed has lysines that have been detected to be ubiquitylated (and SUMOylated) in proteomics screens (Hendriks *et al.* 2014; Akimov *et al.* 2018). Ubiquitylation at K48 has been shown to be important for the nuclear localization of TDP-43 (Hans *et al.* 2018)

Third, ubiquitylation and SUMOylation at specific sites can interfere with other PTM-sites. It has been shown that ubiquitylation of K408 prevents phosphorylation of neighboring serines, in case of the TDP-43-derived CTF-25, showing how ubiquitin can function as a steric obstacle. Strikingly, a loss of ubiquitylation at the distant K95 appears to have a similar effect on phosphorylation (Hans *et al.* 2018).

Fourth, the steric effect of the PTMs could also alter the caspase-mediated cleavage of TDP-43 into the neurotoxic CTF-25- and CTF-35-fragments. The major cleavage sites haven been identified after D89 and D174, respectively (Li *et al.* 2015). Both sides harbor ubiquitylation and SUMOylation sites in close proximity that might protect these sites from caspase-mediated cleavage (Hendriks *et al.* 2014; Akimov *et al.* 2018)

Attachment site-dependent effects could be investigated by applying a Sortase-mediated based approach for site-specific ubiquitylation and SUMOylation, which is both applicable for purified proteins as overexpression in mammalian cells (Fottner *et al.* 2019).

In summary, it can be postulated that sequence-depend effects of PTMs on TDP-43 as in the case of alter cellular localization by ubiquitin or inhibition of phase separation by SUMO1 depend on the conjugation site. In contrast, the generic effect of SUMO2 enhancing phase separation can probably occur largely independent of the attached position.

4.3.2.2 Artificially enhanced protein levels by transient overexpression

Phase separation of TDP-43 is highly affected by its protein concentration. It has been shown that TDP-43 binds to the 3’ UTR of its own mRNA to suppress expression by a negative feedback loop (Ayala *et al.* 2011). Elevated TDP-43 protein levels in transgenic

mice promoted an ALS-like phenotype regarding progressive muscle weakness (Yang *et al.* 2022). Transient overexpression of GFP-tagged TDP-43(ΔNLS) results in varying protein levels of different populations that each had a distinct phenotype. Cells with a low expression level of TDP-43(ΔNLS) showed a diffuse GFP-signal that only punctuated upon exposure to oxidative stress and co-localized with SGs. In cells with high expression levels, TDP-43(ΔNLS) formed SG-independent condensates that became highly immobile after stress (Yan *et al.* 2024).

These findings clearly indicate that protein levels of overexpressed TDP-43 should be considered in evaluating the findings of this work. Transient overexpression usually results in higher protein expression levels compared to endogenous expression (Schwinn *et al.* 2020). While TDP-43 was shown to undergo phase separation at endogenous protein levels, it can be assumed that overexpressed TDP-43 is more prone to form condensates due to the concentration dependence of phase separation (Gasset-Rosa *et al.* 2019). Yet, N-terminal fusion of SUMO1 was proficient in inhibiting phase separation of both full-length TDP-43 and TDP-43(LCD), which indicates that each SUMO1 moiety blocks the α-helix of the respective attached LCD even under transient overexpression conditions (**Figure 22** and **Figure 34**). Since high protein concentrations of SUMO1-TDP-43(LCD) did not yet undergo phase separation *in vitro*, it can be assumed that SUMO1 acts as an inhibitor of self-assembly largely independent of protein levels (**Appendix 4**). At comparable expression levels, Ub- and SUMO2-fusions strongly promoted condensate formation of TDP-43(LCD), while unmodified TDP-43(LCD) barely formed condensates (**Figure 22**). Studying the impact of ubiquitin and SUMO2 modification in this context is challenging and requires considering additional factors such as the attachment site and the degree of modification to evaluate if both modifiers have a critical impact on enhancing phase separation of TDP-43 at physiological protein concentrations.

4.3.3 Interplay of aberrant phase separation and PTMs

Ubiquitylation and SUMOylation is strongly associated with mislocalized and aggregated TDP-43 in ALS and FTD patients (Neumann *et al.* 2006; Arai *et al.* 2006; Maurel *et al.* 2020). The dependency between ubiquitylation and SUMOylation and neurotoxic aggregation of TDP-43 is still debated and yet, it is questionable if the post-translational modification is a cause or a consequence of cytoplasmic inclusions (Sternburg *et al.* 2022).

I probed endogenous post-translational modification of full-length TDP-43-mutants deficient in LCD self-assembly by interfering with its main self-assembly sites which are the transient α-helix (A326P) and a few tryptophanes (W334G/W385G) (Conicella *et al.*

2016; Li *et al.* 2018). These mutants showed enhanced levels of ubiquitylation and SUMOylation compared to WT TDP-43 but also formed condensates to a minor extent (**Figure 37** C). This raises the question whether the remaining multivalent elements in NTD and RRMs are sufficient to drive condensate formation or if the hyper-modification with ubiquitin, SUMO1 and SUMO2 is necessary for this. As ubiquitin and SUMO2 appear to be general enhancers of phase separation, it could be hypothesized that their conjugation is an attempt to maintain phase separation of TDP-43 (**Figure 13**). Furthermore, the enhanced levels of ubiquitin and SUMO conjugated to TDP-43 could be interpreted as a response of the UPS for clearance of the aberrantly phase separating protein (Wang and Matunis 2023; Müller and Hoppe 2024). Identification and subsequent deletion of modification sites would allow to test how TDP-43 would form condensates when the LCD is deficient in self-assembly.

In previous experiments with the same mutations in TDP-43(LCD) constructs, I showed that both mutants almost completely inhibited phase separation (**Figure 23**). Analysis of expression levels in the whole cell lysate by western blotting using a GFP antibody does not allow clear conclusions about the type of PTM. Yet, fusion of ubiquitin and SUMO induced strongly pronounced ladders in case of all three tested LLPS mutants compared to the respective modifier fused to WT TDP-43(LCD), which can be associated with the formation of ubiquitin and SUMO2 chains respectively (**Appendix 10**). Fusion of N-terminal modifiers can act as a chain initiator, but it remains unclear what causes the enhanced PTM levels in mutant TDP-43(LCD) (Johnson *et al.* 1995). An interesting experiment would be the MS-based analysis of these polymeric chains in terms of linkage and composition. Interestingly, fusions of ubiquitin and SUMO2 only partially rescued phase separation of TDP-43(LCD) mutants deficient in self-assembly, with ubiquitin being slightly more proficient (**Figure 23** C). This strengthens the hypothesis that both modifiers can only exert their role as enhancers of phase separation if the attached substrate is capable to self-assemble (**chapter 4.2.1**).

Both full-length TDP-43-variants with mutated α-helix or tryptophanes in the LCD formed only a few irregular spots per cell, while WT TDP-43 condensates appeared at smaller size but far higher numbers. FRAP analysis would allow conclusions if the condensates were rather liquid-like or solid-like. This would be of particular interest, since ubiquitin chains have been shown to drive aggregation of their attached substrate (Morimoto *et al.* 2015). A novel pathological mechanism could hyper-modify TDP-43, which in turn became more prone to aggregate. Examples would be stress-induced ubiquitylation and SUMOylation or the dysregulation of a TDP-43-specific E2/E3 pair as it is associated with cancer (Enserink 2015; Sampson *et al.* 2023; Sheng *et al.* 2024).

Lastly, sequestration of ubiquitin into cytoplasmic inclusions has been suggested to exert its neurotoxicity by depleting the cellular pool of free ubiquitin, which leads to a dysfunction of the UPS (Farrawell *et al.* 2020). As a consequence, less ubiquitin would be available for exertion of its cellular functions (**chapter 1.1.3**). This could be tested by providing a larger pool of free ubiquitin to the cell by transient overexpression.

In summary, the conjugation of ubiquitin and SUMO can have widespread consequences on TDP-43 in several manners: the propensity to undergo phase separation, initiation of aggregation, protein fold integrity, processing into smaller fragments, altering cellular localization and even competition with PTMs of other classes as phosphorylation. Elucidation of distinct effects by each ubiquitin, SUMO1 and SUMO2 on TDP-43 would require a comprehensive analysis where each potentially modified lysine residue is systematically studied.

4.4 Future perspectives

4.4.1 Further insight into the biological role of Ub/SUMO on TDP-43

This work provided structural insights into two opposing mechanisms on modulating phase separation of the LCD of TDP-43 by SUMO1 as an inhibitor and SUMO2 as an enhancer, which could be similarly obtained for ubiquitin by applying structural MS-based methods as HDX-MS and XL-MS. However, further work is required to understand the significance and the biological consequences of these modifications on full-length TDP-43.

While preliminary experiments of expressing N-terminal fusions of PTMs to TDP-43 in mammalian cells suggested similar effects as observed for TDP-43(LCD), *in vitro* experiments are required to test if TDP-43 phase separation is inhibited or enhanced by the respective modifiers. Sortase-mediated conjugation of the modifiers at distinct positions could be performed for assessing the role of the attachment site, which is a complex experiment that requires optimized cell lines for genetic code expansion (Fottner *et al.* 2019). Additionally, an interaction between TDP-43 and free, unconjugated modifiers was not tested in this work. This has to be carefully assessed, as the full-length protein harbors additional domains that could play a role as potential binding sites for the modifiers. Furthermore, the transition of TDP-43 from liquid-like droplets into solid-like condensates should be analyzed for both LCD and full-length protein in regards of the attached modifier.

Another interesting aspect is to investigate condensates of TDP-43 in mammalian cells with a particular focus on assessing the mobility of the different fusion proteins. FRAP analysis would enable to assess the material properties of the condensates formed by each modifier. This would allow conclusions whether ubiquitin and SUMO2 have similar LLPS-enhancing effects on TDP-43, as I observed for TDP-43(LCD).

Therefore, different material types promoted by the respective modifiers would determine how TDP-43 migrates through the cell. As TDP-43 can accumulate in SGs, liquid-like modified TDP-43 might be recruited more efficiently into SGs (Khalfallah *et al.* 2018). SUMO1-mediated solubilization might prevent this sequestration, while ubiquitin-induced nuclear export could facilitate the recruitment of TDP-43 into SGs (**chapter 4.3.1.3**). Recently, the recruitment of TDP-43 into SG has been shown as a trigger of TDP-43 aggregation by a demixing process (Yan *et al.* 2024). It would thus be interesting to assess if the modifiers can protect TDP-43 from aggregation in this context.

Lastly, TDP-43 contributes to the maintenance of genome stability and has been shown to participate in the nonhomologous end joining-mediated repair of DNA double-strand breaks. The recruitment of TDP-43 to these sites of DNA damage has been shown by laser micro-irradiation in the nucleus (Mitra *et al.* 2019; Fang *et al.* 2023). Depending on the effect of each modifier on condensate mobility, it should be investigated how each PTM has the potential to facilitate or impede DNA repair by TDP-43.

4.4.2 Polymeric functions of SUMO and ubiquitin chains

Considering SUMO and ubiquitin chains as polymers opens up novel perspectives to study their impact on regulating phase separation. As discussed in **chapter 4.2.4**, the propensity of a SUMO2 chain to self-assemble grows with an increasing chain length as each SUMO2 moiety would add up a multivalent element. Given the relevance of the flexible N-terminus, enzymatically synthesized SUMO2 chains on TDP-43(LCD) or another suitable IDR should be compared with linear fusions as used in **chapter 3.3.3**. There is little evidence for the existence and relevance of SUMO1 chains in a cellular environment (Yang *et al.* 2006; Celen and Sahin 2020). Yet, it would be interesting to study if a recombinant SUMO1 chain made up from linear fusions of SUMO1-moieties would behave similarly as SUMO2 chain. This should be first tested on FUS(QGSY) and FUS(RGG), since SUMO1 enhanced phase separation of both IDRs. For TDP-43(LCD), it could be assumed that an increasing number of SUMO1-moieties could compete with the LCD-specific inhibition of phase separation. SUMO1 has been shown to also interact with itself, and there might be a balance of SUMO1/LCD interactions and SUMO1/SUMO1 interactions that will shift

towards enhancing self-assembly if a certain threshold of SUMO1-moeties is exceeded (Richter *et al.* 2024). The impact of an absence of SUMO2/3 chains conjugated to TDP-43 in mammalian cells could be studied by siRNA-mediated depletion of SENP6 and SENP7, which are the main depolymerizing enzymes for SUMO chains. Since both enzymes process a variety of targets, major cellular perturbations might be considered that could also affect phase separation of TDP-43 (Hickey *et al.* 2012; Jansen and Vertegaal 2021).

While SUMO2/3 chains are mainly linked via K11, ubiquitin harbors seven internal lysines and the N-terminal methionine that all participate in chain formation (Matic *et al.* 2008; Ikeda and Dikic 2008). While I did not investigate the mechanism how the fusion of ubiquitin enhanced phase separation of all tested IDR (**Figure 13**), ubiquitin chains could be similarly considered as a chain of sticky elements, where each moiety would provide one or multiple self-assembly sites. Considering that ubiquitin chains adopt certain geometries dependent on their linkage site, it would be interesting to study how the exposure of certain motifs would affect phase separation (Ye *et al.* 2012). Chains of preferably closed conformations as for example K48-linked chains are mainly involving interactions between I44-patches, resulting in the assembly of tightly packed tetraubiquitin elements (Varadan *et al.* 2002). As a consequence, these chain types have a reduced exposure of overall ubiquitin surface to the solvent in comparison to chains with an open confirmation, as for example K63-linked chains (Tenno *et al.* 2004).

Since the molecular interactions that form the foundation of the phase separation enhancing effect of ubiquitin are unknown, it is hard to estimate which chain conformation would be more proficient in enhancing phase separation. To investigate this, one could make use of a set of tailor-made E3s to generate ubiquitin chains of distinct linkages (Wegmann *et al.* 2022). The attachment to a phase separating IDR can be performed based on implementing this system together with chemically-induced dimerization for the recruitment of linkage-selective enzymes to a substrate of choice (Renz *et al.* 2024). Based on these studies, I initialized a workflow to elongate K48- and K63-linked chains on Ub-TDP-43(LCD) with populations of different chain lengths *in vitro* (data not shown). By using K48R and K63R ubiquitin mutants, diubiquitylated TDP-43(LCD) could be generated. Given the fact that ATP acts as a hydrotrope and could inhibit phase separation, reactions need to be carefully purified from ATP and enzymes of the ubiquitylation cascade (Patel *et al.* 2017). The subsequent analysis of phase separation would then allow to obtain insights into polymeric functions of ubiquitin chains of different length and linkage.

5 References

Abramson J, Adler J, Dunger J, Evans R, Green T, Pritzel A, Ronneberger O, Willmore L, Ballard AJ, Bambrick J, Bodenstein SW, Evans DA, Hung C-C, O'Neill M, Reiman D, Tunyasuvunakool K, Wu Z, Žemgulytė A, Arvaniti E, Beattie C, Bertolli O, Bridgland A, Cherepanov A, Congreve M, Cowen-Rivers AI, Cowie A, Figurnov M, Fuchs FB, Gladman H, Jain R, Khan YA, Low CMR, Perlin K, Potapenko A, Savy P, Singh S, Stecula A, Thillaisundaram A, Tong C, Yakneen S, Zhong ED, Zielinski M, Žídek A, Bapst V, Kohli P, Jaderberg M, Hassabis D, Jumper JM (2024). Accurate structure prediction of biomolecular interactions with AlphaFold 3. *Nature* **630**, 493–500. doi:10.1038/s41586-024-07487-w

Adame-Arana O, Weber CA, Zaburdaev V, Prost J, Jülicher F (2020). Liquid Phase Separation Controlled by pH. *Biophysical Journal* **119**, 1590–1605. doi:10.1016/j.bpj.2020.07.044

Aillet F, Lopitz-Otsoa F, Egaña I, Hjerpe R, Fraser P, Hay RT, Rodriguez MS, Lang V (2012). Heterologous SUMO-2/3-Ubiquitin Chains Optimize IκBα Degradation and NF-κB Activity. *PLoS ONE* **7**, e51672. doi:10.1371/journal.pone.0051672

Akimov V, Barrio-Hernandez I, Hansen SVF, Hallenborg P, Pedersen A-K, Bekker-Jensen DB, Puglia M, Christensen SDK, Vanselow JT, Nielsen MM, Kratchmarova I, Kelstrup CD, Olsen JV, Blagoev B (2018). UbiSite approach for comprehensive mapping of lysine and N-terminal ubiquitination sites. *Nature Structural & Molecular Biology* **25**, 631–640. doi:10.1038/s41594-018-0084-y

Akutsu M, Dikic I, Bremm A (2016). Ubiquitin chain diversity at a glance. *Journal of Cell Science* **129**, 875–880. doi:10.1242/jcs.183954

Alami NH, Smith RB, Carrasco MA, Williams LA, Winborn CS, Han SSW, Kiskinis E, Winborn B, Freibaum BD, Kanagaraj A, Clare AJ, Badders NM, Bilican B, Chaum E, Chandran S, Shaw CE, Eggan KC, Maniatis T, Taylor JP (2014). Axonal Transport of TDP-43 mRNA Granules Is Impaired by ALS-Causing Mutations. *Neuron* **81**, 536–543. doi:10.1016/j.neuron.2013.12.018

Alberti S, Dormann D (2019). Liquid–Liquid Phase Separation in Disease. *Annual Review of Genetics* **53**, 171–194. doi:10.1146/annurev-genet-112618-043527

Alberti S, Halfmann R, King O, Kapila A, Lindquist S (2009). A systematic survey identifies prions and illuminates sequence features of prionogenic proteins. *Cell* **137**, 146–158. doi:10.1016/j.cell.2009.02.044

Alberti S, Hyman AA (2021). Biomolecular condensates at the nexus of cellular stress, protein aggregation disease and ageing. *Nature Reviews Molecular Cell Biology* **22**, 196–213. doi:10.1038/s41580-020-00326-6

Ali I, Conrad RJ, Verdin E, Ott M (2018). Lysine Acetylation Goes Global: From Epigenetics to Metabolism and Therapeutics. *Chemical reviews* **118**, 1216–1252. doi:10.1021/acs.chemrev.7b00181

Antonioni A, Raho EM, Lopriore P, Pace AP, Latino RR, Assogna M, Mancuso M, Gragnaniello D, Granieri E, Pugliatti M, Di Lorenzo F, Koch G (2023).

Frontotemporal Dementia, Where Do We Stand? A Narrative Review. *International Journal of Molecular Sciences* **24**, 11732. doi:10.3390/ijms241411732

Arai T, Hasegawa M, Akiyama H, Ikeda K, Nonaka T, Mori H, Mann D, Tsuchiya K, Yoshida M, Hashizume Y, Oda T (2006). TDP-43 is a component of ubiquitin-positive tau-negative inclusions in frontotemporal lobar degeneration and amyotrophic lateral sclerosis. *Biochemical and Biophysical Research Communications* **351**, 602–611. doi:10.1016/j.bbrc.2006.10.093

Arenas A, Chen J, Kuang L, Barnett KR, Kasarskis EJ, Gal J, Zhu H (2020). Lysine acetylation regulates the RNA binding, subcellular localization and inclusion formation of FUS. *Human Molecular Genetics* **29**, 2684–2697. doi:10.1093/hmg/ddaa159

Arora S, Roy DS, Maiti S, Ainavarapu SRK (2023). Phase Separation and Aggregation of a Globular Folded Protein Small Ubiquitin-like Modifier 1 (SUMO1). *The Journal of Physical Chemistry Letters* **14**, 9060–9068. doi:10.1021/acs.jpclett.3c02092

Asimaki E, Petriukov K, Renz C, Meister C, Ulrich HD (2022). Fast friends – Ubiquitin-like modifiers as engineered fusion partners. *Seminars in Cell & Developmental Biology* **132**, 132–145. doi:10.1016/j.semcdb.2021.11.013

Ayala YM, De Conti L, Avendaño-Vázquez SE, Dhir A, Romano M, D'Ambrogio A, Tollervey J, Ule J, Baralle M, Buratti E, Baralle FE (2011). TDP-43 regulates its mRNA levels through a negative feedback loop. *The EMBO journal* **30**, 277–288. doi:10.1038/emboj.2010.310

Babinchak WM, Haider R, Dumm BK, Sarkar P, Surewicz K, Choi J-K, Surewicz WK (2019). The role of liquid–liquid phase separation in aggregation of the TDP-43 low-complexity domain. *Journal of Biological Chemistry* **294**, 6306–6317. doi:10.1074/jbc.RA118.007222

Baiesi M, Orlandini E, Seno F, Trovato A (2019). Sequence and structural patterns detected in entangled proteins reveal the importance of co-translational folding. *Scientific Reports* **9**, 8426. doi:10.1038/s41598-019-44928-3

Baldwin RL (1996). How Hofmeister ion interactions affect protein stability. *Biophysical Journal* **71**, 2056–2063.

Banani SF, Lee HO, Hyman AA, Rosen MK (2017). Biomolecular condensates: organizers of cellular biochemistry. *Nature Reviews Molecular Cell Biology* **18**, 285–298. doi:10.1038/nrm.2017.7

Banani SF, Rice AM, Peeples WB, Lin Y, Jain S, Parker R, Rosen MK (2016). Compositional Control of Phase-Separated Cellular Bodies. *Cell* **166**, 651–663. doi:10.1016/j.cell.2016.06.010

Bates GP, Dorsey R, Gusella JF, Hayden MR, Kay C, Leavitt BR, Nance M, Ross CA, Scahill RI, Wetzel R, Wild EJ, Tabrizi SJ (2015). Huntington disease. *Nature Reviews Disease Primers* **1**, 1–21. doi:10.1038/nrdp.2015.5

Bernier-Villamor V, Sampson DA, Matunis MJ, Lima CD (2002). Structural Basis for E2-Mediated SUMO Conjugation Revealed by a Complex between Ubiquitin-Conjugating Enzyme Ubc9 and RanGAP1. *Cell* **108**, 345–356. doi:10.1016/S0092-8674(02)00630-X

Berning BA, Walker AK (2019). The Pathobiology of TDP-43 C-Terminal Fragments in ALS and FTLD. *Frontiers in Neuroscience* **13**. doi:10.3389/fnins.2019.00335

Boeynaems S, Alberti S, Fawzi NL, Mittag T, Polymenidou M, Rousseau F, Schymkowitz J, Shorter J, Wolozin B, Van Den Bosch L, Tompa P, Fuxreiter M (2018). Protein Phase Separation: A New Phase in Cell Biology. *Trends in Cell Biology* **28**, 420–435. doi:10.1016/j.tcb.2018.02.004

Brangwynne CP, Eckmann CR, Courson DS, Rybarska A, Hoege C, Gharakhani J, Jülicher F, Hyman AA (2009). Germline P Granules Are Liquid Droplets That Localize by Controlled Dissolution/Condensation. *Science* **324**, 1729–1732. doi:10.1126/science.1172046

Brangwynne CP, Mitchison TJ, Hyman AA (2011). Active liquid-like behavior of nucleoli determines their size and shape in Xenopus laevis oocytes. *Proceedings of the National Academy of Sciences* **108**, 4334–4339. doi:10.1073/pnas.1017150108

Buratti E, Dörk T, Zuccato E, Pagani F, Romano M, Baralle FE (2001). Nuclear factor TDP-43 and SR proteins promote in vitro and in vivo CFTR exon 9 skipping. *The EMBO Journal* **20**, 1774–1784. doi:10.1093/emboj/20.7.1774

Burke KA, Janke AM, Rhine CL, Fawzi NL (2015). Residue-by-Residue View of In Vitro FUS Granules that Bind the C-Terminal Domain of RNA Polymerase II. *Molecular Cell* **60**, 231–241. doi:10.1016/j.molcel.2015.09.006

Butt TR, Edavettal SC, Hall JP, Mattern MR (2005). SUMO fusion technology for difficult-to-express proteins. *Protein Expression and Purification* **43**, 1–9. doi:10.1016/j.pep.2005.03.016

Cappadocia L, Lima CD (2018). Ubiquitin-like Protein Conjugation: Structures, Chemistry, and Mechanism. *Chemical Reviews* **118**, 889–918. doi:10.1021/acs.chemrev.6b00737

Celen AB, Sahin U (2020). Sumoylation on its 25th anniversary: mechanisms, pathology, and emerging concepts. *The FEBS Journal* **287**, 3110–3140. doi:10.1111/febs.15319

Chambers MC, Maclean B, Burke R, Amodei D, Ruderman DL, Neumann S, Gatto L, Fischer B, Pratt B, Egertson J, Hoff K, Kessner D, Tasman N, Shulman N, Frewen B, Baker TA, Brusniak M-Y, Paulse C, Creasy D, Flashner L, Kani K, Moulding C, Seymour SL, Nuwaysir LM, Lefebvre B, Kuhlmann F, Roark J, Rainer P, Detlev S, Hemenway T, Huhmer A, Langridge J, Connolly B, Chadick T, Holly K, Eckels J, Deutsch EW, Moritz RL, Katz JE, Agus DB, MacCoss M, Tabb DL, Mallick P (2012). A cross-platform toolkit for mass spectrometry and proteomics. *Nature Biotechnology* **30**, 918–920. doi:10.1038/nbt.2377

Chao Y, Ramírez-Soto O, Bahr C, Karpitschka S (2022). How liquid–liquid phase separation induces active spreading. *Proceedings of the National Academy of Sciences* **119**, e2203510119. doi:10.1073/pnas.2203510119

Chatani E, Yamamoto N (2018). Recent progress on understanding the mechanisms of amyloid nucleation. *Biophysical Reviews* **10**, 527–534. doi:10.1007/s12551-017-0353-8

Chau V, Tobias JW, Bachmair A, Marriott D, Ecker DJ, Gonda DK, Varshavsky A (1989). A multiubiquitin chain is confined to specific lysine in a targeted short-lived protein. *Science (New York, N.Y.)* **243**, 1576–1583. doi:10.1126/science.2538923

Chen C, Ding X, Akram N, Xue S, Luo S-Z (2019). Fused in Sarcoma: Properties, Self-Assembly and Correlation with Neurodegenerative Diseases. *Molecules* **24**, 1622. doi:10.3390/molecules24081622

Chen G, Xu T, Yan Y, Zhou Y, Jiang Y, Melcher K, Xu HE (2017). Amyloid beta: structure, biology and structure-based therapeutic development. *Acta Pharmacologica Sinica* **38**, 1205–1235. doi:10.1038/aps.2017.28

Cheng F, Chapman T, Zhang S, Morsch M, Chung R, Lee A, Rayner SL (2024). Understanding age-related pathologic changes in TDP-43 functions and the consequence on RNA splicing and signalling in health and disease. *Ageing Research Reviews* **96**, 102246. doi:10.1016/j.arr.2024.102246

Choi J-M, Holehouse AS, Pappu RV (2020). Physical Principles Underlying the Complex Biology of Intracellular Phase Transitions. *Annual review of biophysics* **49**, 107–133. doi:10.1146/annurev-biophys-121219-081629

Clague MJ, Urbé S, Komander D (2019). Breaking the chains: deubiquitylating enzyme specificity begets function. *Nature Reviews Molecular Cell Biology* **20**, 338–352. doi:10.1038/s41580-019-0099-1

Combe CW, Fischer L, Rappsilber J (2015). xiNET: Cross-link Network Maps With Residue Resolution*. *Molecular & Cellular Proteomics* **14**, 1137–1147. doi:10.1074/mcp.O114.042259

Conicella AE, Dignon GL, Zerze GH, Schmidt HB, D'Ordine AM, Kim YC, Rohatgi R, Ayala YM, Mittal J, Fawzi NL (2020). TDP-43 α-helical structure tunes liquid–liquid phase separation and function. *Proceedings of the National Academy of Sciences* **117**, 5883–5894. doi:10.1073/pnas.1912055117

Conicella AE, Zerze GH, Mittal J, Fawzi NL (2016). ALS Mutations Disrupt Phase Separation Mediated by α-Helical Structure in the TDP-43 Low-Complexity C-Terminal Domain. *Structure* **24**, 1537–1549. doi:10.1016/j.str.2016.07.007

Damgaard RB (2021). The ubiquitin system: from cell signalling to disease biology and new therapeutic opportunities. *Cell Death & Differentiation* **28**, 423–426. doi:10.1038/s41418-020-00703-w

Dao TP, Kolaitis R-M, Joo Kim H, O'Donovan K, Martyniak B, Colicino E, Hehnly H, Taylor JP, Castañeda CA (2018). Ubiquitin modulates liquid-liquid phase separation of UBQLN2 via disruption of multivalent interactions. *Molecular cell* **69**, 965-978.e6. doi:10.1016/j.molcel.2018.02.004

Dao TP, Yang Y, Presti MF, Cosgrove MS, Hopkins JB, Ma W, Loh SN, Castañeda CA (2022). Mechanistic insights into enhancement or inhibition of phase separation by different polyubiquitin chains. *EMBO reports* **23**, e55056. doi:10.15252/embr.202255056

Desterro JMP, Rodriguez MS, Hay RT (1998). SUMO-1 Modification of IκBα Inhibits NF-κB Activation. *Molecular Cell* **2**, 233–239. doi:10.1016/S1097-2765(00)80133-1

Dignon GL, Best RB, Mittal J (2020). Biomolecular Phase Separation: From Molecular Driving Forces to Macroscopic Properties. *Annual Review of Physical Chemistry* **71**, 53–75. doi:10.1146/annurev-physchem-071819-113553

Dikic I, Schulman BA (2023). An expanded lexicon for the ubiquitin code. *Nature Reviews Molecular Cell Biology* **24**, 273–287. doi:10.1038/s41580-022-00543-1

Dikic I, Wakatsuki S, Walters KJ (2009). Ubiquitin-binding domains — from structures to functions. *Nature Reviews Molecular Cell Biology* **10**, 659–671. doi:10.1038/nrm2767

Doll SG, Meshkin H, Bryer AJ, Li F, Ko Y-H, Lokareddy RK, Gillilan RE, Gupta K, Perilla JR, Cingolani G (2022). Recognition of the TDP-43 nuclear localization signal by importin α1/β. *Cell reports* **39**, 111007. doi:10.1016/j.celrep.2022.111007

Dong KC, Helgason E, Yu C, Phu L, Arnott DP, Bosanac I, Compaan DM, Huang OW, Fedorova AV, Kirkpatrick DS, Hymowitz SG, Dueber EC (2011). Preparation of Distinct Ubiquitin Chain Reagents of High Purity and Yield. *Structure* **19**, 1053–1063. doi:10.1016/j.str.2011.06.010

Dormann D, Haass C (2013). Fused in sarcoma (FUS): An oncogene goes awry in neurodegeneration. *Molecular and Cellular Neuroscience* **56**, 475–486. doi:10.1016/j.mcn.2013.03.006

Dormann D, Madl T, Valori CF, Bentmann E, Tahirovic S, Abou-Ajram C, Kremmer E, Ansorge O, Mackenzie IRA, Neumann M, Haass C (2012). Arginine methylation next to the PY-NLS modulates Transportin binding and nuclear import of FUS. *The EMBO Journal* **31**, 4258–4275. doi:10.1038/emboj.2012.261

Dormann D, Rodde R, Edbauer D, Bentmann E, Fischer I, Hruscha A, Than ME, Mackenzie IRA, Capell A, Schmid B, Neumann M, Haass C (2010). ALS-associated fused in sarcoma (FUS) mutations disrupt Transportin-mediated nuclear import. *The EMBO Journal* **29**, 2841–2857. doi:10.1038/emboj.2010.143

Dou H, Huang C, Singh M, Carpenter PB, Yeh ETH (2010). Regulation of DNA repair through deSUMOylation and SUMOylation of replication protein A complex. *Molecular Cell* **39**, 333–345. doi:10.1016/j.molcel.2010.07.021

Douzi B (2017). Protein–Protein Interactions: Surface Plasmon Resonance. In 'Bacterial Protein Secretion Systems: Methods and Protocols'. (Eds L Journet, E Cascales.) pp. 257–275. (Springer: New York, NY) doi:10.1007/978-1-4939-7033-9_21

Du M, Ea C-K, Fang Y, Chen ZJ (2022). Liquid phase separation of NEMO induced by polyubiquitin chains activates NF-κB. *Molecular Cell* **82**, 2415-2426.e5. doi:10.1016/j.molcel.2022.03.037

Duan C, Wang R (2024). A Unified Description of Salt Effects on the Liquid–Liquid Phase Separation of Proteins. *ACS Central Science* **10**, 460–468. doi:10.1021/acscentsci.3c01372

Elena-Real CA, Sagar A, Urbanek A, Popovic M, Morató A, Estaña A, Fournet A, Doucet C, Lund XL, Shi Z-D, Costa L, Thureau A, Allemand F, Swenson RE, Milhiet P-E, Crehuet R, Barducci A, Cortés J, Sinnaeve D, Sibille N, Bernadó P (2023). The structure of pathogenic huntingtin exon 1 defines the bases of its aggregation

propensity. *Nature Structural & Molecular Biology* **30**, 309–320. doi:10.1038/s41594-023-00920-0

Enserink JM (2015). Sumo and the cellular stress response. *Cell Division* **10**, 4. doi:10.1186/s13008-015-0010-1

Erker Y, Neyret-Kahn H, Seeler JS, Dejean A, Atfi A, Levy L (2013). Arkadia, a novel SUMO-targeted ubiquitin ligase involved in PML degradation. *Molecular and Cellular Biology* **33**, 2163–2177. doi:10.1128/MCB.01019-12

Fang M, Deibler SK, Nana AL, Vatsavayai SC, Banday S, Zhou Y, Almeida S, Weiss A, Brown RH, Seeley WW, Gao F-B, Green MR (2023). Loss of TDP-43 function contributes to genomic instability in amyotrophic lateral sclerosis. *Frontiers in Neuroscience* **17**. doi:10.3389/fnins.2023.1251228

Farag M, Borcherds WM, Bremer A, Mittag T, Pappu RV (2023). Phase separation of protein mixtures is driven by the interplay of homotypic and heterotypic interactions. *Nature Communications* **14**, 5527. doi:10.1038/s41467-023-41274-x

Farag M, Cohen SR, Borcherds WM, Bremer A, Mittag T, Pappu RV (2022). Condensates formed by prion-like low-complexity domains have small-world network structures and interfaces defined by expanded conformations. *Nature Communications* **13**, 7722. doi:10.1038/s41467-022-35370-7

Farrawell NE, McAlary L, Lum JS, Chisholm CG, Warraich ST, Blair IP, Vine KL, Saunders DN, Yerbury JJ (2020). Ubiquitin Homeostasis Is Disrupted in TDP-43 and FUS Cell Models of ALS. *iScience* **23**, 101700. doi:10.1016/j.isci.2020.101700

Feric M, Vaidya N, Harmon TS, Mitrea DM, Zhu L, Richardson TM, Kriwacki RW, Pappu RV, Brangwynne CP (2016). Coexisting liquid phases underlie nucleolar sub-compartments. *Cell* **165**, 1686–1697. doi:10.1016/j.cell.2016.04.047

Fiesel FC, Weber SS, Supper J, Zell A, Kahle PJ (2012). TDP-43 regulates global translational yield by splicing of exon junction complex component SKAR. *Nucleic Acids Research* **40**, 2668–2682. doi:10.1093/nar/gkr1082

Finley D, Bartel B, Varshavsky A (1989). The tails of ubiquitin precursors are ribosomal proteins whose fusion to ubiquitin facilitates ribosome biogenesis. *Nature* **338**, 394–401. doi:10.1038/338394a0

Flotho A, Melchior F (2013). Sumoylation: a regulatory protein modification in health and disease. *Annual Review of Biochemistry* **82**, 357–385. doi:10.1146/annurev-biochem-061909-093311

Fottner M, Brunner A-D, Bittl V, Horn-Ghetko D, Jussupow A, Kaila VRI, Bremm A, Lang K (2019). Site-specific ubiquitylation and SUMOylation using genetic-code expansion and sortase. *Nature Chemical Biology* **15**, 276–284. doi:10.1038/s41589-019-0227-4

François-Moutal L, Perez-Miller S, Scott DD, Miranda VG, Mollasalehi N, Khanna M (2019). Structural Insights Into TDP-43 and Effects of Post-translational Modifications. *Frontiers in Molecular Neuroscience* **12**. doi:10.3389/fnmol.2019.00301

Frey S, Görlich D (2007). A Saturated FG-Repeat Hydrogel Can Reproduce the Permeability Properties of Nuclear Pore Complexes. *Cell* **130**, 512–523. doi:10.1016/j.cell.2007.06.024

Fuhrmann J, Clancy KW, Thompson PR (2015). Chemical Biology of Protein Arginine Modifications in Epigenetic Regulation. *Chemical Reviews* **115**, 5413–5461. doi:10.1021/acs.chemrev.5b00003

Furukawa Y, Suzuki Y, Fukuoka M, Nagasawa K, Nakagome K, Shimizu H, Mukaiyama A, Akiyama S (2016). A molecular mechanism realizing sequence-specific recognition of nucleic acids by TDP-43. *Scientific Reports* **6**, 20576. doi:10.1038/srep20576

Fushman D, Walker O (2010). Exploring the Linkage Dependence of Polyubiquitin Conformations Using Molecular Modeling. *Journal of Molecular Biology* **395**, 803–814. doi:10.1016/j.jmb.2009.10.039

García-Rodríguez N, Wong RP, Ulrich HD (2016). Functions of Ubiquitin and SUMO in DNA Replication and Replication Stress. *Frontiers in Genetics* **7**. doi:10.3389/fgene.2016.00087

Gasset-Rosa F, Lu S, Yu H, Chen C, Melamed Z, Guo L, Shorter J, Da Cruz S, Cleveland DW (2019). Cytoplasmic TDP-43 De-mixing Independent of Stress Granules Drives Inhibition of Nuclear Import, Loss of Nuclear TDP-43, and Cell Death. *Neuron* **102**, 339-357.e7. doi:10.1016/j.neuron.2019.02.038

Gasteiger E, Hoogland C, Gattiker A, Duvaud S, Wilkins MR, Appel RD, Bairoch A (2005). Protein Identification and Analysis Tools on the ExPASy Server. In 'The Proteomics Protocols Handbook'. (Ed JM Walker.) pp. 571–607. (Humana Press: Totowa, NJ) doi:10.1385/1-59259-890-0:571

Ginell GM, Holehouse AS (2023). An Introduction to the Stickers-and-Spacers Framework as Applied to Biomolecular Condensates. *Methods in Molecular Biology (Clifton, N.J.)* **2563**, 95–116. doi:10.1007/978-1-0716-2663-4_4

Goel S, Oliva R, Jeganathan S, Bader V, Krause LJ, Kriegler S, Stender ID, Christine CW, Nakamura K, Hoffmann J-E, Winter R, Tatzelt J, Winklhofer KF (2023). Linear ubiquitination induces NEMO phase separation to activate NF-κB signaling. *Life Science Alliance* **6**. doi:10.26508/lsa.202201607

Goldstein G, Scheid M, Hammerling U, Schlesinger DH, Niall HD, Boyse EA (1975). Isolation of a polypeptide that has lymphocyte-differentiating properties and is probably represented universally in living cells. *Proceedings of the National Academy of Sciences* **72**, 11–15. doi:10.1073/pnas.72.1.11

Gorman AM (2008). Neuronal cell death in neurodegenerative diseases: recurring themes around protein handling. *Journal of Cellular and Molecular Medicine* **12**, 2263. doi:10.1111/j.1582-4934.2008.00402.x

Graham RK, Deng Y, Slow EJ, Haigh B, Bissada N, Lu G, Pearson J, Shehadeh J, Bertram L, Murphy Z, Warby SC, Doty CN, Roy S, Wellington CL, Leavitt BR, Raymond LA, Nicholson DW, Hayden MR (2006). Cleavage at the Caspase-6 Site Is Required for Neuronal Dysfunction and Degeneration Due to Mutant Huntingtin. *Cell* **125**, 1179–1191. doi:10.1016/j.cell.2006.04.026

Grese ZR, Bastos AC, Mamede LD, French RL, Miller TM, Ayala YM (2021). Specific RNA interactions promote TDP-43 multivalent phase separation and maintain liquid properties. *EMBO reports* **22**, e53632. doi:10.15252/embr.202153632

Grizel AV, Gorsheneva NA, Stevenson JB, Pflaum J, Wilfling F, Rubel AA, Chernoff YO (2024). Osmotic stress induces formation of both liquid condensates and amyloids by a yeast prion domain. *Journal of Biological Chemistry* **300**. doi:10.1016/j.jbc.2024.107766

Gruijs da Silva LA, Simonetti F, Hutten S, Riemenschneider H, Sternburg EL, Pietrek LM, Gebel J, Dötsch V, Edbauer D, Hummer G, Stelzl LS, Dormann D (2022). Disease-linked TDP-43 hyperphosphorylation suppresses TDP-43 condensation and aggregation. *The EMBO Journal* **41**, e108443. doi:10.15252/embj.2021108443

Gu J, Nie L, Wiederschain D, Yuan ZM (2001). Identification of p53 sequence elements that are required for MDM2-mediated nuclear export. *Molecular and Cellular Biology* **21**, 8533–8546. doi:10.1128/MCB.21.24.8533-8546.2001

Guillén-Boixet J, Kopach A, Holehouse AS, Wittmann S, Jahnel M, Schlüßler R, Kim K, Trussina IREA, Wang J, Mateju D, Poser I, Maharana S, Ruer-Gruß M, Richter D, Zhang X, Chang Y-T, Guck J, Honigmann A, Mahamid J, Hyman AA, Pappu RV, Alberti S, Franzmann TM (2020). RNA-Induced Conformational Switching and Clustering of G3BP Drive Stress Granule Assembly by Condensation. *Cell* **181**, 346-361.e17. doi:10.1016/j.cell.2020.03.049

Guo W, Chen Y, Zhou X, Kar A, Ray P, Chen X, Rao EJ, Yang M, Ye H, Zhu L, Liu J, Xu M, Yang Y, Wang C, Zhang D, Bigio EH, Mesulam M, Shen Y, Xu Q, Fushimi K, Wu JY (2011). An ALS-associated mutation affecting TDP-43 enhances protein aggregation, fibril formation and neurotoxicity. *Nature Structural & Molecular Biology* **18**, 822–830. doi:10.1038/nsmb.2053

Gupta R, Sahu M, Srivastava D, Tiwari S, Ambasta RK, Kumar P (2021). Post-translational modifications: Regulators of neurodegenerative proteinopathies. *Ageing Research Reviews* **68**, 101336. doi:10.1016/j.arr.2021.101336

Gutierrez-Morton E, Wang Y (2024). The role of SUMOylation in biomolecular condensate dynamics and protein localization. *Cell Insight* **3**, 100199. doi:10.1016/j.cellin.2024.100199

Hakim-Eshed V, Boulos A, Cohen-Rosenzweig C, Yu-Taeger L, Ziv T, Kwon YT, Riess O, Phuc Nguyen HH, Ziv NE, Ciechanover A (2020). Site-specific ubiquitination of pathogenic huntingtin attenuates its deleterious effects. *Proceedings of the National Academy of Sciences* **117**, 18661–18669. doi:10.1073/pnas.2007667117

Halfmann R (2016). A glass menagerie of low complexity sequences. *Current Opinion in Structural Biology* **38**, 18–25. doi:10.1016/j.sbi.2016.05.002

Hamley IW (2007). 'Introduction to Soft Matter– Revised Edition'. (John Wiley & Sons, Ltd: Chichester, UK) doi:10.1002/9780470517338

Hans F, Eckert M, Zweydorf F von, Gloeckner CJ, Kahle PJ (2018). Identification and characterization of ubiquitinylation sites in TAR DNA-binding protein of 43 kDa (TDP-43). *The Journal of Biological Chemistry* **293**, 16083. doi:10.1074/jbc.RA118.003440

Hans F, Fiesel FC, Strong JC, Jäckel S, Rasse TM, Geisler S, Springer W, Schulz JB, Voigt A, Kahle PJ (2014). UBE2E Ubiquitin-conjugating Enzymes and Ubiquitin Isopeptidase Y Regulate TDP-43 Protein Ubiquitination. *The Journal of Biological Chemistry* **289**, 19164–19179. doi:10.1074/jbc.M114.561704

Hans F, Glasebach H, Kahle PJ (2020). Multiple distinct pathways lead to hyperubiquitylated insoluble TDP-43 protein independent of its translocation into stress granules. *Journal of Biological Chemistry* **295**, 673–689. doi:10.1016/S0021-9258(17)49926-1

Hayes LR, Kalab P (2022). Emerging Therapies and Novel Targets for TDP-43 Proteinopathy in ALS/FTD. *Neurotherapeutics: The Journal of the American Society for Experimental NeuroTherapeutics* **19**, 1061–1084. doi:10.1007/s13311-022-01260-5

Hebron ML, Lonskaya I, Sharpe K, Weerasinghe PPK, Algarzae NK, Shekoyan AR, Moussa CE-H (2013). Parkin ubiquitinates Tar-DNA binding protein-43 (TDP-43) and promotes its cytosolic accumulation via interaction with histone deacetylase 6 (HDAC6). *The Journal of Biological Chemistry* **288**, 4103–4115. doi:10.1074/jbc.M112.419945

Hendriks IA, D'Souza RCJ, Yang B, Verlaan-de Vries M, Mann M, Vertegaal ACO (2014). Uncovering global SUMOylation signaling networks in a site-specific manner. *Nature Structural & Molecular Biology* **21**, 927–936. doi:10.1038/nsmb.2890

Hendriks IA, Lyon D, Su D, Skotte NH, Daniel JA, Jensen LJ, Nielsen ML (2018). Site-specific characterization of endogenous SUMOylation across species and organs. *Nature Communications* **9**, 2456. doi:10.1038/s41467-018-04957-4

Herzog JJ, Deshpande M, Shapiro L, Rodal AA, Paradis S (2017). TDP-43 misexpression causes defects in dendritic growth. *Scientific Reports* **7**, 15656. doi:10.1038/s41598-017-15914-4

Hickey CM, Wilson NR, Hochstrasser M (2012). Function and regulation of SUMO proteases. *Nature Reviews Molecular Cell Biology* **13**, 755–766. doi:10.1038/nrm3478

Hirano S, Udagawa O (2022). SUMOylation regulates the number and size of promyelocytic leukemia-nuclear bodies (PML-NBs) and arsenic perturbs SUMO dynamics on PML by insolubilizing PML in THP-1 cells. *Archives of Toxicology* **96**, 545–558. doi:10.1007/s00204-021-03195-w

Hirayama S, Sugihara M, Morito D, Iemura S, Natsume T, Murata S, Nagata K (2018). Nuclear export of ubiquitinated proteins via the UBIN-POST system. *Proceedings of the National Academy of Sciences of the United States of America* **115**, E4199–E4208. doi:10.1073/pnas.1711017115

Hofweber M, Hutten S, Bourgeois B, Spreitzer E, Niedner-Boblenz A, Schifferer M, Ruepp M-D, Simons M, Niessing D, Madl T, Dormann D (2018). Phase Separation of FUS Is Suppressed by Its Nuclear Import Receptor and Arginine Methylation. *Cell* **173**, 706-719.e13. doi:10.1016/j.cell.2018.03.004

Holehouse AS, Alberti S (2025). Molecular determinants of condensate composition. *Molecular Cell* **85**, 290–308. doi:10.1016/j.molcel.2024.12.021

Hornbeck PV, Zhang B, Murray B, Kornhauser JM, Latham V, Skrzypek E (2015). PhosphoSitePlus, 2014: mutations, PTMs and recalibrations. *Nucleic Acids Research* **43**, D512-520. doi:10.1093/nar/gku1267

Hyman AA, Weber CA, Jülicher F (2014). Liquid-Liquid Phase Separation in Biology. *Annual Review of Cell and Developmental Biology* **30**, 39–58. doi:10.1146/annurev-cellbio-100913-013325

Igaz LM, Kwong LK, Chen-Plotkin A, Winton MJ, Unger TL, Xu Y, Neumann M, Trojanowski JQ, Lee VM-Y (2009). Expression of TDP-43 C-terminal Fragments in Vitro Recapitulates Pathological Features of TDP-43 Proteinopathies. *The Journal of Biological Chemistry* **284**, 8516–8524. doi:10.1074/jbc.M809462200

Ikeda F, Dikic I (2008). Atypical ubiquitin chains: new molecular signals. *EMBO reports* **9**, 536–542. doi:10.1038/embor.2008.93

Ivanova KA, Belogurov AA, Kudriaeva AA (2024). Architectonics of Ubiquitin Chains (A Review). *Russian Journal of Bioorganic Chemistry* **50**, 1182–1201. doi:10.1134/S106816202404006X

Jacob J, Duclohier H, Cafiso DS (1999). The Role of Proline and Glycine in Determining the Backbone Flexibility of a Channel-Forming Peptide. *Biophysical Journal* **76**, 1367–1376. doi:10.1016/S0006-3495(99)77298-X

Jain S, Wheeler JR, Walters RW, Agrawal A, Barsic A, Parker R (2016). ATPase modulated stress granules contain a diverse proteome and substructure. *Cell* **164**, 487–498. doi:10.1016/j.cell.2015.12.038

James EI, Murphree TA, Vorauer C, Engen JR, Guttman M (2022). Advances in Hydrogen/Deuterium Exchange Mass Spectrometry and the Pursuit of Challenging Biological Systems. *Chemical Reviews* **122**, 7562–7623. doi:10.1021/acs.chemrev.1c00279

Jansen NS, Vertegaal ACO (2021). A Chain of Events: Regulating Target Proteins by SUMO Polymers. *Trends in Biochemical Sciences* **46**, 113–123. doi:10.1016/j.tibs.2020.09.002

Jiang L-L, Xue W, Hong J-Y, Zhang J-T, Li M-J, Yu S-N, He J-H, Hu H-Y (2017). The N-terminal dimerization is required for TDP-43 splicing activity. *Scientific Reports* **7**, 6196. doi:10.1038/s41598-017-06263-3

Jo M, Lee S, Jeon Y-M, Kim S, Kwon Y, Kim H-J (2020). The role of TDP-43 propagation in neurodegenerative diseases: integrating insights from clinical and experimental studies. *Experimental & Molecular Medicine* **52**, 1652–1662. doi:10.1038/s12276-020-00513-7

Johnson BS, Snead D, Lee JJ, McCaffery JM, Shorter J, Gitler AD (2009). TDP-43 Is Intrinsically Aggregation-prone, and Amyotrophic Lateral Sclerosis-linked Mutations Accelerate Aggregation and Increase Toxicity*. *Journal of Biological Chemistry* **284**, 20329–20339. doi:10.1074/jbc.M109.010264

Johnson ES, Ma PCM, Ota IM, Varshavsky A (1995). A Proteolytic Pathway That Recognizes Ubiquitin as a Degradation Signal *. *Journal of Biological Chemistry* **270**, 17442–17456. doi:10.1074/jbc.270.29.17442

Joshi A, Walimbe A, Avni A, Rai SK, Arora L, Sarkar S, Mukhopadhyay S (2023). Single-molecule FRET unmasks structural subpopulations and crucial molecular events during FUS low-complexity domain phase separation. *Nature Communications* **14**, 7331. doi:10.1038/s41467-023-43225-y

Kametani F, Nonaka T, Suzuki T, Arai T, Dohmae N, Akiyama H, Hasegawa M (2009). Identification of casein kinase-1 phosphorylation sites on TDP-43. *Biochemical and Biophysical Research Communications* **382**, 405–409. doi:10.1016/j.bbrc.2009.03.038

Kato M, McKnight SL (2021). The low-complexity domain of the FUS RNA binding protein self-assembles via the mutually exclusive use of two distinct cross-β cores. *Proceedings of the National Academy of Sciences* **118**, e2114412118. doi:10.1073/pnas.2114412118

Keiten-Schmitz J, Röder L, Hornstein E, Müller-McNicoll M, Müller S (2021). SUMO: Glue or Solvent for Phase-Separated Ribonucleoprotein Complexes and Molecular Condensates? *Frontiers in Molecular Biosciences* **8**. doi:10.3389/fmolb.2021.673038

Khalfallah Y, Kuta R, Grasmuck C, Prat A, Durham HD, Vande Velde C (2018). TDP-43 regulation of stress granule dynamics in neurodegenerative disease-relevant cell types. *Scientific Reports* **8**, 7551. doi:10.1038/s41598-018-25767-0

Kitamura A, Nakayama Y, Shibasaki A, Taki A, Yuno S, Takeda K, Yahara M, Tanabe N, Kinjo M (2016). Interaction of RNA with a C-terminal fragment of the amyotrophic lateral sclerosis-associated TDP43 reduces cytotoxicity. *Scientific Reports* **6**, 19230. doi:10.1038/srep19230

Kittel C (2005). 'Introduction to Solid State Physics' 8th Edition. (John Wiley & Sons, Inc) Available at: http://metal.elte.hu/~groma/Anyagtudomany/kittel.pdf [accessed 13 December 2024]

Komander D, Rape M (2012). The ubiquitin code. *Annual Review of Biochemistry* **81**, 203–229. doi:10.1146/annurev-biochem-060310-170328

Koulouras G, Panagopoulos A, Rapsomaniki MA, Giakoumakis NN, Taraviras S, Lygerou Z (2018). EasyFRAP-web: a web-based tool for the analysis of fluorescence recovery after photobleaching data. *Nucleic Acids Research* **46**, W467–W472. doi:10.1093/nar/gky508

Krainer G, Welsh TJ, Joseph JA, Espinosa JR, Wittmann S, de Csilléry E, Sridhar A, Toprakcioglu Z, Gudiškytė G, Czekalska MA, Arter WE, Guillén-Boixet J, Franzmann TM, Qamar S, George-Hyslop PS, Hyman AA, Collepardo-Guevara R, Alberti S, Knowles TPJ (2021). Reentrant liquid condensate phase of proteins is stabilized by hydrophobic and non-ionic interactions. *Nature Communications* **12**, 1085. doi:10.1038/s41467-021-21181-9

Kroschwald S, Maharana S, Alberti S (2017). Hexanediol: a chemical probe to investigate the material properties of membrane-less compartments. *Matters*. doi:10.19185/matters.201702000010

Kumar ST, Nazarov S, Porta S, Maharjan N, Cendrowska U, Kabani M, Finamore F, Xu Y, Lee VM-Y, Lashuel HA (2023). Seeding the aggregation of TDP-43 requires

post-fibrillization proteolytic cleavage. *Nature Neuroscience* **26**, 983–996. doi:10.1038/s41593-023-01341-4

Kumari B, Kumar R, Kumar M (2015). Low complexity and disordered regions of proteins have different structural and amino acid preferences. *Molecular BioSystems* **11**, 585–594. doi:10.1039/C4MB00425F

Lamaye F, Galliot S, Alibardi L, Lafontaine DLJ, Thiry M (2011). Nucleolar structure across evolution: The transition between bi- and tricompartmentalized nucleoli lies within the class Reptilia. *Journal of Structural Biology* **174**, 352–359. doi:10.1016/j.jsb.2011.02.003

Lange SM, Armstrong LA, Kulathu Y (2022). Deubiquitinases: From mechanisms to their inhibition by small molecules. *Molecular Cell* **82**, 15–29. doi:10.1016/j.molcel.2021.10.027

Li H-R, Chiang W-C, Chou P-C, Wang W-J, Huang J (2018). TAR DNA-binding protein 43 (TDP-43) liquid–liquid phase separation is mediated by just a few aromatic residues. *Journal of Biological Chemistry* **293**, 6090–6098. doi:10.1074/jbc.AC117.001037

Li Q, Yokoshi M, Okada H, Kawahara Y (2015). The cleavage pattern of TDP-43 determines its rate of clearance and cytotoxicity. *Nature Communications* **6**, 6183. doi:10.1038/ncomms7183

Li SC, Goto NK, Williams KA, Deber CM (1996). Alpha-helical, but not beta-sheet, propensity of proline is determined by peptide environment. *Proceedings of the National Academy of Sciences of the United States of America* **93**, 6676–6681.

Li W, Ye Y (2008). Polyubiquitin chains: functions, structures, and mechanisms. *Cellular and Molecular Life Sciences: CMLS* **65**, 2397–2406. doi:10.1007/s00018-008-8090-6

Licchesi JDF, Laman H, Ikeda F, Bolanos-Garcia VM (2020). Editorial: E3 Ubiquitin Ligases: From Structure to Physiology. *Frontiers in Physiology* **11**. doi:10.3389/fphys.2020.621053

Lieleg O, Ribbeck K (2011). Biological Hydrogels as Selective Diffusion Barriers. *Trends in cell biology* **21**, 543–551. doi:10.1016/j.tcb.2011.06.002

Lima DB, Melchior JT, Morris J, Barbosa VC, Chamot-Rooke J, Fioramonte M, Souza TACB, Fischer JSG, Gozzo FC, Carvalho PC, Davidson WS (2018). Characterization of homodimer interfaces with cross-linking mass spectrometry and isotopically labeled proteins. *Nature Protocols* **13**, 431–458. doi:10.1038/nprot.2017.113

Ling S-C, Polymenidou M, Cleveland DW (2013). Converging mechanisms in ALS and FTD: Disrupted RNA and protein homeostasis. *Neuron* **79**, 416–438. doi:10.1016/j.neuron.2013.07.033

Lips C, Ritterhoff T, Weber A, Janowska MK, Mustroph M, Sommer T, Klevit RE (2020). Who with whom: functional coordination of E2 enzymes by RING E3 ligases during poly-ubiquitylation. *The EMBO Journal* **39**, e104863. doi:10.15252/embj.2020104863

Liu Y-J, Kuo H-C, Chern Y (2021). A system-wide mislocalization of RNA-binding proteins in motor neurons is a new feature of ALS. *Neurobiology of Disease* **160**, 105531. doi:10.1016/j.nbd.2021.105531

Lohrum MA, Woods DB, Ludwig RL, Bálint E, Vousden KH (2001). C-terminal ubiquitination of p53 contributes to nuclear export. *Molecular and Cellular Biology* **21**, 8521–8532. doi:10.1128/MCB.21.24.8521-8532.2001

Lois LM, Lima CD (2005). Structures of the SUMO E1 provide mechanistic insights into SUMO activation and E2 recruitment to E1. *The EMBO Journal* **24**, 439–451. doi:10.1038/sj.emboj.7600552

Loughlin FE, Lukavsky PJ, Kazeeva T, Reber S, Hock E-M, Colombo M, Von Schroetter C, Pauli P, Cléry A, Mühlemann O, Polymenidou M, Ruepp M-D, Allain FH-T (2019). The Solution Structure of FUS Bound to RNA Reveals a Bipartite Mode of RNA Recognition with Both Sequence and Shape Specificity. *Molecular Cell* **73**, 490-504.e6. doi:10.1016/j.molcel.2018.11.012

Lukavsky PJ, Daujotyte D, Tollervey JR, Ule J, Stuani C, Buratti E, Baralle FE, Damberger FF, Allain FH-T (2013). Molecular basis of UG-rich RNA recognition by the human splicing factor TDP-43. *Nature Structural & Molecular Biology* **20**, 1443–1449. doi:10.1038/nsmb.2698

Lumpkin RJ, Gu H, Zhu Y, Leonard M, Ahmad AS, Clauser KR, Meyer JG, Bennett EJ, Komives EA (2017). Site-specific identification and quantitation of endogenous SUMO modifications under native conditions. *Nature Communications* **8**, 1171. doi:10.1038/s41467-017-01271-3

MacDonald ME, Ambrose CM, Duyao MP, Myers RH, Lin C, Srinidhi L, Barnes G, Taylor SA, James M, Groot N, MacFarlane H, Jenkins B, Anderson MA, Wexler NS, Gusella JF, Bates GP, Baxendale S, Hummerich H, Kirby S, North M, Youngman S, Mott R, Zehetner G, Sedlacek Z, Poustka A, Frischauf A-M, Lehrach H, Buckler AJ, Church D, Doucette-Stamm L, O'Donovan MC, Riba-Ramirez L, Shah M, Stanton VP, Strobel SA, Draths KM, Wales JL, Dervan P, Housman DE, Altherr M, Shiang R, Thompson L, Fielder T, Wasmuth JJ, Tagle D, Valdes J, Elmer L, Allard M, Castilla L, Swaroop M, Blanchard K, Collins FS, Snell R, Holloway T, Gillespie K, Datson N, Shaw D, Harper PS (1993). A novel gene containing a trinucleotide repeat that is expanded and unstable on Huntington's disease chromosomes. *Cell* **72**, 971–983. doi:10.1016/0092-8674(93)90585-E

Mahajan R, Delphin C, Guan T, Gerace L, Melchior F (1997). A Small Ubiquitin-Related Polypeptide Involved in Targeting RanGAP1 to Nuclear Pore Complex Protein RanBP2. *Cell* **88**, 97–107. doi:10.1016/S0092-8674(00)81862-0

Manetto V, Perry G, Tabaton M, Mulvihill P, Fried VA, Smith HT, Gambetti P, Autilio-Gambetti L (1988). Ubiquitin is associated with abnormal cytoplasmic filaments characteristic of neurodegenerative diseases. *Proceedings of the National Academy of Sciences of the United States of America* **85**, 4501–4505. doi:10.1073/pnas.85.12.4501

Maraschi A, Gumina V, Dragotto J, Colombrita C, Mompeán M, Buratti E, Silani V, Feligioni M, Ratti A (2021). SUMOylation Regulates TDP-43 Splicing Activity and Nucleocytoplasmic Distribution. *Molecular Neurobiology* **58**, 5682–5702. doi:10.1007/s12035-021-02505-8

Marques Sousa C, Humbert S (2013). Huntingtin: Here, There, Everywhere! *Journal of Huntington's Disease* **2**, 395–403. doi:10.3233/JHD-130082

Martin EW, Mittag T (2018). The relationship of sequence and phase separation in protein low-complexity regions. *Biochemistry* **57**, 2478–2487. doi:10.1021/acs.biochem.8b00008

Masrori P, Van Damme P (2020). Amyotrophic lateral sclerosis: a clinical review. *European Journal of Neurology* **27**, 1918–1929. doi:10.1111/ene.14393

Matic I, van Hagen M, Schimmel J, Macek B, Ogg SC, Tatham MH, Hay RT, Lamond AI, Mann M, Vertegaal ACO (2008). *In Vivo* Identification of Human Small Ubiquitin-like Modifier Polymerization Sites by High Accuracy Mass Spectrometry and an *in Vitro* to *in Vivo* Strategy*. *Molecular & Cellular Proteomics* **7**, 132–144. doi:10.1074/mcp.M700173-MCP200

Maurel C, Chami AA, Thépault R-A, Marouillat S, Blasco H, Corcia P, Andres CR, Vourc'h P (2020). A role for SUMOylation in the Formation and Cellular Localization of TDP-43 Aggregates in Amyotrophic Lateral Sclerosis. *Molecular Neurobiology* **57**, 1361–1373. doi:10.1007/s12035-019-01810-7

Mead RJ, Shan N, Reiser HJ, Marshall F, Shaw PJ (2023). Amyotrophic lateral sclerosis: a neurodegenerative disorder poised for successful therapeutic translation. *Nature Reviews Drug Discovery* **22**, 185–212. doi:10.1038/s41573-022-00612-2

Mertins P, Qiao JW, Patel J, Udeshi ND, Clauser KR, Mani DR, Burgess MW, Gillette MA, Jaffe JD, Carr SA (2013). Integrated proteomic analysis of post-translational modifications by serial enrichment. *Nature Methods* **10**, 634–637. doi:10.1038/nmeth.2518

Mészáros B, Erdős G, Dosztányi Z (2018). IUPred2A: context-dependent prediction of protein disorder as a function of redox state and protein binding. *Nucleic Acids Research* **46**, W329–W337. doi:10.1093/nar/gky384

Mitra J, Guerrero EN, Hegde PM, Liachko NF, Wang H, Vasquez V, Gao J, Pandey A, Taylor JP, Kraemer BC, Wu P, Boldogh I, Garruto RM, Mitra S, Rao KS, Hegde ML (2019). Motor neuron disease-associated loss of nuclear TDP-43 is linked to DNA double-strand break repair defects. *Proceedings of the National Academy of Sciences of the United States of America* **116**, 4696–4705. doi:10.1073/pnas.1818415116

Mitrea DM, Cika JA, Stanley CB, Nourse A, Onuchic PL, Banerjee PR, Phillips AH, Park C-G, Deniz AA, Kriwacki RW (2018). Self-interaction of NPM1 modulates multiple mechanisms of liquid–liquid phase separation. *Nature Communications* **9**, 842. doi:10.1038/s41467-018-03255-3

Mittag T, Pappu RV (2022). A conceptual framework for understanding phase separation and addressing open questions and challenges. *Molecular Cell* **82**, 2201–2214. doi:10.1016/j.molcel.2022.05.018

Mohanty P, Kapoor U, Sundaravadivelu Devarajan D, Phan TM, Rizuan A, Mittal J (2022). Principles Governing the Phase Separation of Multidomain Proteins. *Biochemistry* **61**, 2443–2455. doi:10.1021/acs.biochem.2c00210

Mompeán M, Romano V, Pantoja-Uceda D, Stuani C, Baralle FE, Buratti E, Laurents DV (2016). The TDP-43 N-terminal domain structure at high resolution. *The FEBS Journal* **283**, 1242–1260. doi:10.1111/febs.13651

Morimoto D, Walinda E, Fukada H, Sou Y-S, Kageyama S, Hoshino M, Fujii T, Tsuchiya H, Saeki Y, Arita K, Ariyoshi M, Tochio H, Iwai K, Namba K, Komatsu M, Tanaka K, Shirakawa M (2015). The unexpected role of polyubiquitin chains in the formation of fibrillar aggregates. *Nature Communications* **6**, 6116. doi:10.1038/ncomms7116

Morimoto D, Walinda E, Fukada H, Sugase K, Shirakawa M (2016). Ubiquitylation Directly Induces Fold Destabilization of Proteins. *Scientific Reports* **6**, 39453. doi:10.1038/srep39453

Morrell R, Sadanandom A (2019). Dealing With Stress: A Review of Plant SUMO Proteases. *Frontiers in Plant Science* **10**. doi:10.3389/fpls.2019.01122

Morris OM, Toprakcioglu Z, Röntgen A, Cali M, Knowles TPJ, Vendruscolo M (2024). Aggregation of the amyloid-β peptide (Aβ40) within condensates generated through liquid-liquid phase separation. *Scientific Reports* **14**, 22633. doi:10.1038/s41598-024-72265-7

Müller L, Hoppe T (2024). UPS-dependent strategies of protein quality control degradation. *Trends in Biochemical Sciences* **49**, 859–874. doi:10.1016/j.tibs.2024.06.006

Murthy AC, Dignon GL, Kan Y, Zerze GH, Parekh SH, Mittal J, Fawzi NL (2019). Molecular interactions underlying liquid−liquid phase separation of the FUS low-complexity domain. *Nature Structural & Molecular Biology* **26**, 637–648. doi:10.1038/s41594-019-0250-x

Nakayama Y, Tsuji K, Ayaki T, Mori M, Tokunaga F, Ito H (2020). Linear Polyubiquitin Chain Modification of TDP-43-Positive Neuronal Cytoplasmic Inclusions in Amyotrophic Lateral Sclerosis. *Journal of Neuropathology and Experimental Neurology* **79**, 256–265. doi:10.1093/jnen/nlz135

Nallamsetty S, Kapust RB, Tözsér J, Cherry S, Tropea JE, Copeland TD, Waugh DS (2004). Efficient site-specific processing of fusion proteins by tobacco vein mottling virus protease in vivo and in vitro. *Protein Expression and Purification* **38**, 108–115. doi:10.1016/j.pep.2004.08.016

Nedelsky NB, Taylor JP (2019). Bridging biophysics and neurology: aberrant phase transitions in neurodegenerative disease. *Nature Reviews Neurology* **15**, 272–286. doi:10.1038/s41582-019-0157-5

Neueder A, Landles C, Ghosh R, Howland D, Myers RH, Faull RLM, Tabrizi SJ, Bates GP (2017). The pathogenic exon 1 HTT protein is produced by incomplete splicing in Huntington's disease patients. *Scientific Reports* **7**, 1307. doi:10.1038/s41598-017-01510-z

Neumann M, Kwong LK, Lee EB, Kremmer E, Flatley A, Xu Y, Forman MS, Troost D, Kretzschmar HA, Trojanowski JQ, Lee VM-Y (2009a). Phosphorylation of S409/410 of TDP-43 is a consistent feature in all sporadic and familial forms of TDP-43 proteinopathies. *Acta Neuropathologica* **117**, 137–149. doi:10.1007/s00401-008-0477-9

Neumann M, Rademakers R, Roeber S, Baker M, Kretzschmar HA, Mackenzie IRA (2009b). A new subtype of frontotemporal lobar degeneration with FUS pathology. *Brain* **132**, 2922–2931. doi:10.1093/brain/awp214

Neumann M, Sampathu DM, Kwong LK, Truax AC, Micsenyi MC, Chou TT, Bruce J, Schuck T, Grossman M, Clark CM, McCluskey LF, Miller BL, Masliah E, Mackenzie IR, Feldman H, Feiden W, Kretzschmar HA, Trojanowski JQ, Lee VM-Y (2006). Ubiquitinated TDP-43 in Frontotemporal Lobar Degeneration and Amyotrophic Lateral Sclerosis. *Science* **314**, 130–133. doi:10.1126/science.1134108

Nguyen KT, Ju S, Kim S-Y, Lee C-S, Lee C, Hwang C-S (2022). N-Terminal Modifications of Ubiquitin via Methionine Excision, Deamination, and Arginylation Expand the Ubiquitin Code. *Molecules and Cells* **45**, 158–167. doi:10.14348/molcells.2022.2027

Nolan M, Talbot K, Ansorge O (2016). Pathogenesis of FUS-associated ALS and FTD: insights from rodent models. *Acta Neuropathologica Communications* **4**, 99. doi:10.1186/s40478-016-0358-8

Nott TJ, Petsalaki E, Farber P, Jervis D, Fussner E, Plochowietz A, Craggs TD, Bazett-Jones DP, Pawson T, Forman-Kay JD, Baldwin AJ (2015). Phase Transition of a Disordered Nuage Protein Generates Environmentally Responsive Membraneless Organelles. *Molecular Cell* **57**, 936–947. doi:10.1016/j.molcel.2015.01.013

O'Rourke JG, Gareau JR, Ochaba J, Song W, Raskó T, Reverter D, Lee J, Monteys AM, Pallos J, Mee L, Vashishtha M, Apostol BL, Nicholson TP, Illes K, Zhu Y-Z, Dasso M, Bates GP, Difiglia M, Davidson B, Wanker EE, Marsh JL, Lima CD, Steffan JS, Thompson LM (2013). SUMO-2 and PIAS1 Modulate Insoluble Mutant Huntingtin Protein Accumulation. *Cell reports* **4**, 362–375. doi:10.1016/j.celrep.2013.06.034

Panavas T, Sanders C, Butt TR (2009). SUMO Fusion Technology for Enhanced Protein Production in Prokaryotic and Eukaryotic Expression Systems. In 'SUMO Protocols'. (Ed HD Ulrich.) pp. 303–317. (Humana Press: Totowa, NJ) doi:10.1007/978-1-59745-566-4_20

Patel A, Malinovska L, Saha S, Wang J, Alberti S, Krishnan Y, Hyman AA (2017). ATP as a biological hydrotrope. *Science* **356**, 753–756. doi:10.1126/science.aaf6846

Pérez-Berlanga M, Wiersma VI, Zbinden A, De Vos L, Wagner U, Foglieni C, Mallona I, Betz KM, Cléry A, Weber J, Guo Z, Rigort R, de Rossi P, Manglunia R, Tantardini E, Sahadevan S, Stach O, Hruska-Plochan M, Allain FH, Paganetti P, Polymenidou M (2023). Loss of TDP-43 oligomerization or RNA binding elicits distinct aggregation patterns. *The EMBO Journal* **42**, e111719. doi:10.15252/embj.2022111719

Perry JJP, Tainer JA, Boddy MN (2008). A SIM-ultaneous role for SUMO and ubiquitin. *Trends in Biochemical Sciences* **33**, 201–208. doi:10.1016/j.tibs.2008.02.001

Peskett TR, Rau F, O'Driscoll J, Patani R, Lowe AR, Saibil HR (2018). A Liquid to Solid Phase Transition Underlying Pathological Huntingtin Exon1 Aggregation. *Molecular Cell* **70**, 588-601.e6. doi:10.1016/j.molcel.2018.04.007

Pichler A, Fatouros C, Lee H, Eisenhardt N (2017). SUMO conjugation – a mechanistic view. *Biomolecular Concepts* **8**, 13–36. doi:10.1515/bmc-2016-0030

Plechanovová A, Jaffray EG, Tatham MH, Naismith JH, Hay RT (2012). Structure of a RING E3 ligase and ubiquitin-loaded E2 primed for catalysis. *Nature* **489**, 115–120. doi:10.1038/nature11376

Posey AE, Ruff KM, Harmon TS, Crick SL, Li A, Diamond MI, Pappu RV (2018). Profilin reduces aggregation and phase separation of huntingtin N-terminal fragments by preferentially binding to soluble monomers and oligomers. *Journal of Biological Chemistry* **293**, 3734–3746. doi:10.1074/jbc.RA117.000357

Poudyal M, Patel K, Gadhe L, Sawner AS, Kadu P, Datta D, Mukherjee S, Ray S, Navalkar A, Maiti S, Chatterjee D, Devi J, Bera R, Gahlot N, Joseph J, Padinhateeri R, Maji SK (2023). Intermolecular interactions underlie protein/peptide phase separation irrespective of sequence and structure at crowded milieu. *Nature Communications* **14**, 6199. doi:10.1038/s41467-023-41864-9

Powers KT, Lavering ED, Washington MT (2018). Conformational Flexibility of Ubiquitin-Modified and SUMO-Modified PCNA Shown by Full-Ensemble Hybrid Methods. *Journal of Molecular Biology* **430**, 5294–5303. doi:10.1016/j.jmb.2018.10.017

Protasoni M, Zeviani M (2021). Mitochondrial Structure and Bioenergetics in Normal and Disease Conditions. *International Journal of Molecular Sciences* **22**, 586. doi:10.3390/ijms22020586

Prus G, Hoegl A, Weinert BT, Choudhary C (2019). Analysis and Interpretation of Protein Post-Translational Modification Site Stoichiometry. *Trends in Biochemical Sciences* **44**, 943–960. doi:10.1016/j.tibs.2019.06.003

Puthenveetil R, Vinogradova O (2019). Solution NMR: A powerful tool for structural and functional studies of membrane proteins in reconstituted environments. *The Journal of Biological Chemistry* **294**, 15914–15931. doi:10.1074/jbc.REV119.009178

Qamar S, Wang G, Randle SJ, Ruggeri FS, Varela JA, Lin JQ, Phillips EC, Miyashita A, Williams D, Ströhl F, Meadows W, Ferry R, Dardov VJ, Tartaglia GG, Farrer LA, Schierle GSK, Kaminski CF, Holt CE, Fraser PE, Schmitt-Ulms G, Klenerman D, Knowles T, Vendruscolo M, George-Hyslop PS (2018). FUS Phase Separation Is Modulated by a Molecular Chaperone and Methylation of Arginine Cation-π Interactions. *Cell* **173**, 720-734.e15. doi:10.1016/j.cell.2018.03.056

Rabiller M (2007). Interactions of SUMO proteins. Available at: https://duepublico2.uni-due.de/receive/duepublico_mods_00013565 [accessed 27 November 2024]

Rademakers R, Neumann M, Mackenzie IRA (2012). Recent advances in the molecular basis of frontotemporal dementia. *Nature reviews. Neurology* **8**, 423–434. doi:10.1038/nrneurol.2012.117

Randles L, Walters KJ (2012). Ubiquitin and its binding domains. *Frontiers in bioscience (Landmark edition)* **17**, 2140–2157.

Raschke TM, Tsai J, Levitt M (2001). Quantification of the hydrophobic interaction by simulations of the aggregation of small hydrophobic solutes in water. *Proceedings of the National Academy of Sciences* **98**, 5965–5969. doi:10.1073/pnas.111158498

Ratti A, Buratti E (2016). Physiological functions and pathobiology of TDP-43 and FUS/TLS proteins. *Journal of Neurochemistry* **138**, 95–111. doi:10.1111/jnc.13625

Ratti A, Gumina V, Lenzi P, Bossolasco P, Fulceri F, Volpe C, Bardelli D, Pregnolato F, Maraschi A, Fornai F, Silani V, Colombrita C (2020). Chronic stress induces formation of stress granules and pathological TDP-43 aggregates in human ALS fibroblasts and iPSC-motoneurons. *Neurobiology of Disease* **145**, 105051. doi:10.1016/j.nbd.2020.105051

Ray S, Singh N, Kumar R, Patel K, Pandey S, Datta D, Mahato J, Panigrahi R, Navalkar A, Mehra S, Gadhe L, Chatterjee D, Sawner AS, Maiti S, Bhatia S, Gerez JA, Chowdhury A, Kumar A, Padinhateeri R, Riek R, Krishnamoorthy G, Maji SK (2020). α-Synuclein aggregation nucleates through liquid–liquid phase separation. *Nature Chemistry* **12**, 705–716. doi:10.1038/s41557-020-0465-9

Renz C, Asimaki E, Meister C, Albanèse V, Petriukov K, Krapoth NC, Wegmann S, Wollscheid H-P, Wong RP, Fulzele A, Chen J-X, Léon S, Ulrich HD (2024). Ubiquiton-An inducible, linkage-specific polyubiquitylation tool. *Molecular Cell* **84**, 386-400.e11. doi:10.1016/j.molcel.2023.11.016

Riback JA, Katanski CD, Kear-Scott JL, Pilipenko EV, Rojek AE, Sosnick TR, Drummond DA (2017). Stress-Triggered Phase Separation Is an Adaptive, Evolutionarily Tuned Response. *Cell* **168**, 1028-1040.e19. doi:10.1016/j.cell.2017.02.027

Richter SM, Jin F, Ritterhoff T, Fergin A, Maurer E, Frank A, Hajnal A, Klevit R, Gräter F, Flotho A, Melchior F (2024). SUMO's intrinsically disordered N-terminus is an intramolecular inhibitor of SUMO - SIM interactions. *eLife* **13**. doi:10.7554/eLife.95313.1

Riek R (2017). The Three-Dimensional Structures of Amyloids. *Cold Spring Harbor Perspectives in Biology* **9**, a023572. doi:10.1101/cshperspect.a023572

Sahin U, Ferhi O, Jeanne M, Benhenda S, Berthier C, Jollivet F, Niwa-Kawakita M, Faklaris O, Setterblad N, de Thé H, Lallemand-Breitenbach V (2014a). Oxidative stress–induced assembly of PML nuclear bodies controls sumoylation of partner proteins. *Journal of Cell Biology* **204**, 931–945. doi:10.1083/jcb.201305148

Sahin U, de Thé H, Lallemand-Breitenbach V (2014b). PML nuclear bodies: Assembly and oxidative stress-sensitive sumoylation. *Nucleus* **5**, 499–507. doi:10.4161/19491034.2014.970104

Sampson C, Wang Q, Otkur W, Zhao H, Lu Y, Liu X, Piao H-L (2023). The roles of E3 ubiquitin ligases in cancer progression and targeted therapy. *Clinical and Translational Medicine* **13**, e1204. doi:10.1002/ctm2.1204

Saudou F, Humbert S (2016). The Biology of Huntingtin. *Neuron* **89**, 910–926. doi:10.1016/j.neuron.2016.02.003

Scherzinger E, Sittler A, Schweiger K, Heiser V, Lurz R, Hasenbank R, Bates GP, Lehrach H, Wanker EE (1999). Self-assembly of polyglutamine-containing huntingtin fragments into amyloid-like fibrils: Implications for Huntington's disease pathology. *Proceedings of the National Academy of Sciences* **96**, 4604–4609. doi:10.1073/pnas.96.8.4604

Schmidt HB, Barreau A, Rohatgi R (2019). Phase separation-deficient TDP43 remains functional in splicing. *Nature Communications* **10**, 4890. doi:10.1038/s41467-019-12740-2

Schrödinger L, DeLano W (2020). PyMOL. Available at: http://www.pymol.org/pymol

Schulman BA, Harper JW (2009). Ubiquitin-like protein activation by E1 enzymes: the apex for downstream signalling pathways. *Nature Reviews Molecular Cell Biology* **10**, 319–331. doi:10.1038/nrm2673

Schwinn MK, Steffen LS, Zimmerman K, Wood KV, Machleidt T (2020). A Simple and Scalable Strategy for Analysis of Endogenous Protein Dynamics. *Scientific Reports* **10**, 8953. doi:10.1038/s41598-020-65832-1

Shen K, Calamini B, Fauerbach JA, Ma B, Shahmoradian SH, Serrano Lachapel IL, Chiu W, Lo DC, Frydman J (2016). Control of the structural landscape and neuronal proteotoxicity of mutant Huntingtin by domains flanking the polyQ tract Ed JW Kelly. *eLife* **5**, e18065. doi:10.7554/eLife.18065

Sheng X, Xia Z, Yang H, Hu R (2024). The ubiquitin codes in cellular stress responses. *Protein & Cell* **15**, 157–190. doi:10.1093/procel/pwad045

Sidibé H, Dubinski A, Vande Velde C (2021). The multi-functional RNA-binding protein G3BP1 and its potential implication in neurodegenerative disease. *Journal of Neurochemistry* **157**, 944–962. doi:10.1111/jnc.15280

Smith J, Calidas D, Schmidt H, Lu T, Rasoloson D, Seydoux G (2016). Spatial patterning of P granules by RNA-induced phase separation of the intrinsically-disordered protein MEG-3 Ed J Ahringer. *eLife* **5**, e21337. doi:10.7554/eLife.21337

Snead WT, Gladfelter AS (2019). The Control Centers of Biomolecular Phase Separation: How Membrane Surfaces, PTMs, and Active Processes Regulate Condensation. *Molecular Cell* **76**, 295–305. doi:10.1016/j.molcel.2019.09.016

Sriramachandran AM, Meyer-Teschendorf K, Pabst S, Ulrich HD, Gehring NH, Hofmann K, Praefcke GJK, Dohmen RJ (2019). Arkadia/RNF111 is a SUMO-targeted ubiquitin ligase with preference for substrates marked with SUMO1-capped SUMO2/3 chain. *Nature Communications* **10**, 3678. doi:10.1038/s41467-019-11549-3

Steffan JS, Agrawal N, Pallos J, Rockabrand E, Trotman LC, Slepko N, Illes K, Lukacsovich T, Zhu Y-Z, Cattaneo E, Pandolfi PP, Thompson LM, Marsh JL (2004). SUMO Modification of Huntingtin and Huntington's Disease Pathology. *Science* **304**, 100–104. doi:10.1126/science.1092194

Steinacher R, Schär P (2005). Functionality of Human Thymine DNA Glycosylase Requires SUMO-Regulated Changes in Protein Conformation. *Current Biology* **15**, 616–623. doi:10.1016/j.cub.2005.02.054

Stelter P, Ulrich HD (2003). Control of spontaneous and damage-induced mutagenesis by SUMO and ubiquitin conjugation. *Nature* **425**, 188–191. doi:10.1038/nature01965

Sternburg EL, Silva LAG da, Dormann D (2022). Post-translational modifications on RNA-binding proteins: accelerators, brakes, or passengers in neurodegeneration? *Trends in Biochemical Sciences* **47**, 6–22. doi:10.1016/j.tibs.2021.07.004

Stewart MD, Ritterhoff T, Klevit RE, Brzovic PS (2016). E2 enzymes: more than just middle men. *Cell Research* **26**, 423–440. doi:10.1038/cr.2016.35

Suk TR, Part CE, Nguyen TT, Zhang JL, Heer MM, Caballero-Gómez A, Grybas VS, McKeever PM, Nguyen B, Callaghan SM, Woulfe JM, Robertson J, Rousseaux MWC (2024). A stress-dependent TDP-43 SUMOylation program preserves neuronal function. , 2024.04.12.589206. doi:10.1101/2024.04.12.589206

Suk TR, Rousseaux MWC (2020). The role of TDP-43 mislocalization in amyotrophic lateral sclerosis. *Molecular Neurodegeneration* **15**, 45. doi:10.1186/s13024-020-00397-1

Sulkowska JI (2020). On folding of entangled proteins: knots, lassos, links and θ<math><mi is="true">θ</mi></math>-curves. *Current Opinion in Structural Biology* **60**, 131–141. doi:10.1016/j.sbi.2020.01.007

Sun M, Zhang X (2022). Current methodologies in protein ubiquitination characterization: from ubiquitinated protein to ubiquitin chain architecture. *Cell & Bioscience* **12**, 126. doi:10.1186/s13578-022-00870-y

Tartari M, Gissi C, Lo Sardo V, Zuccato C, Picardi E, Pesole G, Cattaneo E (2008). Phylogenetic Comparison of Huntingtin Homologues Reveals the Appearance of a Primitive polyQ in Sea Urchin. *Molecular Biology and Evolution* **25**, 330–338. doi:10.1093/molbev/msm258

Taylor NO, Wei M-T, Stone HA, Brangwynne CP (2019). Quantifying Dynamics in Phase-Separated Condensates Using Fluorescence Recovery after Photobleaching. *Biophysical Journal* **117**, 1285–1300. doi:10.1016/j.bpj.2019.08.030

Tenno T, Fujiwara K, Tochio H, Iwai K, Morita EH, Hayashi H, Murata S, Hiroaki H, Sato M, Tanaka K, Shirakawa M (2004). Structural basis for distinct roles of Lys63- and Lys48-linked polyubiquitin chains. *Genes to Cells* **9**, 865–875. doi:10.1111/j.1365-2443.2004.00780.x

The UniProt Consortium (2024). UniProt: the Universal Protein Knowledgebase in 2025. *Nucleic Acids Research*, gkae1010. doi:10.1093/nar/gkae1010

Theillet F-X, Binolfi A, Frembgen-Kesner T, Hingorani K, Sarkar M, Kyne C, Li C, Crowley PB, Gierasch L, Pielak GJ, Elcock AH, Gershenson A, Selenko P (2014). Physicochemical Properties of Cells and Their Effects on Intrinsically Disordered Proteins (IDPs). *Chemical Reviews* **114**, 6661–6714. doi:10.1021/cr400695p

Tollervey JR, Curk T, Rogelj B, Briese M, Cereda M, Kayikci M, König J, Hortobágyi T, Nishimura AL, Župunski V, Patani R, Chandran S, Rot G, Zupan B, Shaw CE, Ule J (2011). Characterizing the RNA targets and position-dependent splicing regulation by TDP-43. *Nature Neuroscience* **14**, 452–458. doi:10.1038/nn.2778

Tran N-N, Lee B-H (2022). Functional implication of ubiquitinating and deubiquitinating mechanisms in TDP-43 proteinopathies. *Frontiers in Cell and Developmental Biology* **10**. doi:10.3389/fcell.2022.931968

Truant R, Atwal RS, Burtnik A (2007). Nucleocytoplasmic trafficking and transcription effects of huntingtin in Huntington's disease. *Progress in Neurobiology* **83**, 211–227. doi:10.1016/j.pneurobio.2006.11.004

Tziortzouda P, Van Den Bosch L, Hirth F (2021). Triad of TDP43 control in neurodegeneration: autoregulation, localization and aggregation. *Nature Reviews Neuroscience* **22**, 197–208. doi:10.1038/s41583-021-00431-1

Ulrich HD (2008). The Fast-Growing Business of SUMO Chains. *Molecular Cell* **32**, 301–305. doi:10.1016/j.molcel.2008.10.010

Varadan R, Walker O, Pickart C, Fushman D (2002). Structural properties of polyubiquitin chains in solution. *Journal of Molecular Biology* **324**, 637–647. doi:10.1016/s0022-2836(02)01198-1

Vaughan RM, Kupai A, Rothbart SB (2021). Chromatin Regulation through Ubiquitin and Ubiquitin-like Histone Modifications. *Trends in Biochemical Sciences* **46**, 258–269. doi:10.1016/j.tibs.2020.11.005

Waite KA, Vontz G, Lee SY, Roelofs J (2024). Proteasome condensate formation is driven by multivalent interactions with shuttle factors and ubiquitin chains. *Proceedings of the National Academy of Sciences* **121**, e2310756121. doi:10.1073/pnas.2310756121

Wang A, Conicella AE, Schmidt HB, Martin EW, Rhoads SN, Reeb AN, Nourse A, Ramirez Montero D, Ryan VH, Rohatgi R, Shewmaker F, Naik MT, Mittag T, Ayala YM, Fawzi NL (2018a). A single N-terminal phosphomimic disrupts TDP-43 polymerization, phase separation, and RNA splicing. *The EMBO Journal* **37**, e97452. doi:10.15252/embj.201797452

Wang J, Choi J-M, Holehouse AS, Lee HO, Zhang X, Jahnel M, Maharana S, Lemaitre R, Pozniakovsky A, Drechsel D, Poser I, Pappu RV, Alberti S, Hyman AA (2018b). A Molecular Grammar Governing the Driving Forces for Phase Separation of Prion-like RNA Binding Proteins. *Cell* **174**, 688-699.e16. doi:10.1016/j.cell.2018.06.006

Wang W, Matunis MJ (2023). Paralogue-Specific Roles of SUMO1 and SUMO2/3 in Protein Quality Control and Associated Diseases. *Cells* **13**, 8. doi:10.3390/cells13010008

Watanabe H (1999). Viscoelasticity and dynamics of entangled polymers. *Progress in Polymer Science* **24**, 1253–1403. doi:10.1016/S0079-6700(99)00029-5

Wegmann S, Meister C, Renz C, Yakoub G, Wollscheid H-P, Takahashi DT, Mikicic I, Beli P, Ulrich HD (2022). Linkage reprogramming by tailor-made E3s reveals polyubiquitin chain requirements in DNA-damage bypass. *Molecular Cell* **82**, 1589-1602.e5. doi:10.1016/j.molcel.2022.02.016

Wheeler JR, Matheny T, Jain S, Abrisch R, Parker R (2016). Distinct stages in stress granule assembly and disassembly Ed TW Nilsen. *eLife* **5**, e18413. doi:10.7554/eLife.18413

Winton MJ, Igaz LM, Wong MM, Kwong LK, Trojanowski JQ, Lee VM-Y (2008). Disturbance of Nuclear and Cytoplasmic TAR DNA-binding Protein (TDP-43) Induces Disease-like Redistribution, Sequestration, and Aggregate Formation *. *Journal of Biological Chemistry* **283**, 13302–13309. doi:10.1074/jbc.M800342200

Wood A, Gurfinkel Y, Polain N, Lamont W, Lyn Rea S (2021). Molecular Mechanisms Underlying TDP-43 Pathology in Cellular and Animal Models of ALS and FTLD. *International Journal of Molecular Sciences* **22**, 4705. doi:10.3390/ijms22094705

Wu J, Wu J, Chen T, Cai J, Ren R (2024). Protein aggregation and its affecting mechanisms in neurodegenerative diseases. *Neurochemistry International* **180**, 105880. doi:10.1016/j.neuint.2024.105880

Xu Y, Plechanovová A, Simpson P, Marchant J, Leidecker O, Kraatz S, Hay RT, Matthews SJ (2014). Structural insight into SUMO chain recognition and manipulation by the ubiquitin ligase RNF4. *Nature Communications* **5**, 4217. doi:10.1038/ncomms5217

Xu Z, Au SWN (2005). Mapping residues of SUMO precursors essential in differential maturation by SUMO-specific protease, SENP1. *Biochemical Journal* **386**, 325–330. doi:10.1042/BJ20041210

Xu Z, Wang W, Cao Y, Xue B (2023). Liquid-liquid phase separation: Fundamental physical principles, biological implications, and applications in supramolecular materials engineering. *Supramolecular Materials* **2**, 100049. doi:10.1016/j.supmat.2023.100049

Xue C, Lin TY, Chang D, Guo Z (2017). Thioflavin T as an amyloid dye: fibril quantification, optimal concentration and effect on aggregation. *Royal Society Open Science* **4**, 160696. doi:10.1098/rsos.160696

Yan X, Kuster D, Mohanty P, Nijssen J, Pombo-García K, Rizuan A, Franzmann TM, Sergeeva A, Passos PM, George L, Wang S-H, Shenoy J, Danielson HL, Honigmann A, Ayala YM, Fawzi NL, Mittal J, Alberti S, Hyman AA (2024). Intra-condensate demixing of TDP-43 inside stress granules generates pathological aggregates. *bioRxiv*, 2024.01.23.576837. doi:10.1101/2024.01.23.576837

Yang C, Qiao T, Yu J, Wang H, Guo Y, Salameh J, Metterville J, Parsi S, Yusuf I, Brown RH, Cai H, Xu Z (2022). Low-level overexpression of wild type TDP-43 causes late-onset, progressive neurodegeneration and paralysis in mice. *PloS One* **17**, e0255710. doi:10.1371/journal.pone.0255710

Yang J, Yang X (2020). Phase Transition of Huntingtin: Factors and Pathological Relevance. *Frontiers in Genetics* **11**. doi:10.3389/fgene.2020.00754

Yang M, Hsu C-T, Ting C-Y, Liu LF, Hwang J (2006). Assembly of a Polymeric Chain of SUMO1 on Human Topoisomerase I in Vitro. *Journal of Biological Chemistry* **281**, 8264–8274. doi:10.1074/jbc.M510364200

Yang P, Mathieu C, Kolaitis R-M, Zhang P, Messing J, Yurtsever U, Yang Z, Wu J, Li Y, Pan Q, Yu J, Martin EW, Mittag T, Kim HJ, Taylor JP (2020). G3BP1 Is a Tunable Switch that Triggers Phase Separation to Assemble Stress Granules. *Cell* **181**, 325-345.e28. doi:10.1016/j.cell.2020.03.046

Yang Q, Zhao J, Chen D, Wang Y (2021). E3 ubiquitin ligases: styles, structures and functions. *Molecular Biomedicine* **2**, 23. doi:10.1186/s43556-021-00043-2

Ye Y, Blaser G, Horrocks MH, Ruedas-Rama MJ, Ibrahim S, Zhukov AA, Orte A, Klenerman D, Jackson SE, Komander D (2012). Ubiquitin chain conformation regulates recognition and activity of interacting proteins. *Nature* **492**, 266–270. doi:10.1038/nature11722

Yunus AA, Lima CD (2006). Lysine activation and functional analysis of E2-mediated conjugation in the SUMO pathway. *Nature Structural & Molecular Biology* **13**, 491–499. doi:10.1038/nsmb1104

Zacco E, Graña-Montes R, Martin SR, de Groot NS, Alfano C, Tartaglia GG, Pastore A (2019). RNA as a key factor in driving or preventing self-assembly of the TAR DNA-binding protein 43. *Journal of Molecular Biology* **431**, 1671–1688. doi:10.1016/j.jmb.2019.01.028

Zbinden A, Pérez-Berlanga M, De Rossi P, Polymenidou M (2020). Phase Separation and Neurodegenerative Diseases: A Disturbance in the Force. *Developmental Cell* **55**, 45–68. doi:10.1016/j.devcel.2020.09.014

Zhang X-W, Yan X-J, Zhou Z-R, Yang F-F, Wu Z-Y, Sun H-B, Liang W-X, Song A-X, Lallemand-Breitenbach V, Jeanne M, Zhang Q-Y, Yang H-Y, Huang Q-H, Zhou G-B, Tong J-H, Zhang Y, Wu J-H, Hu H-Y, de Thé H, Chen S-J, Chen Z (2010). Arsenic Trioxide Controls the Fate of the PML-RARα Oncoprotein by Directly Binding PML. *Science* **328**, 240–243. doi:10.1126/science.1183424

Zhang Y-J, Xu Y-F, Cook C, Gendron TF, Roettges P, Link CD, Lin W-L, Tong J, Castanedes-Casey M, Ash P, Gass J, Rangachari V, Buratti E, Baralle F, Golde TE, Dickson DW, Petrucelli L (2009). Aberrant cleavage of TDP-43 enhances aggregation and cellular toxicity. *Proceedings of the National Academy of Sciences* **106**, 7607–7612. doi:10.1073/pnas.0900688106

Zhou Y, Liu S, Öztürk A, Hicks GG (2014). FUS-regulated RNA metabolism and DNA damage repair. *Rare Diseases* **2**, e29515. doi:10.4161/rdis.29515

Zhu J, Zhu S, Guzzo CM, Ellis NA, Sung KS, Choi CY, Matunis MJ (2008). Small Ubiquitin-related Modifier (SUMO) Binding Determines Substrate Recognition and Paralog-selective SUMO Modification∗. *Journal of Biological Chemistry* **283**, 29405–29415. doi:10.1074/jbc.M803632200

6 Appendix

6.1 Abbreviations

Amp	Ampicillin
ALS	Amyotrophic lateral sclerosis
ATP	Adenosine triphosphate
Cam	Chloramphenicol
CD	Circular dichroism
CF	Core facility
Cryo-EM	Cryogenic electron microscopy
CTF	C-terminal fragment
CV	Column volume
DIC	Differential interference contrast
DMEM	Dulbecco's modified eagle medium
DMSO	Dimethyl sulfoxide
DNA	Deoxyribonucleic acid
dNTP	Deoxynucleotide triphosphate
DPBS	Dulbecco's phosphate-buffered saline
DTT	Dithiothreitol
DUB	Deubiquitinating enzyme
E1	Activating enzyme
E2	Conjugating enzyme
E3	Ligating enzyme
EGFP	Enhanced green fluorescent protein
FBS	Fetal bovine serum
FKBP	FK506-binding protein
FP	Fluorescence polarization
FRET	Förster resonance energy transfer
FRET-AB	FRET acceptor bleaching
FTD	Frontotemporal dementia
FTLD	Frontotemporal lobar degeneration
FUS	Fused in sarcoma
GA	Gibson assembly
GFP	Green fluorescent protein

HD	Huntington's disease
HDX-MS	Hydrogen-Deuterium exchange mass spectrometry
HPLC	High-pressure liquid chromatography
Hyg	Hygromycin
Htt-Ex1	Huntingtin-exon1
IDR	Internally disordered region
IMAC	Immobilized metal affinity chromatography
IMB	Institute of Molecular Biology
Kan	Kanamycin
LB	Luria Broth
LCD	Low-complexity domain
LCST	Lower critical solution temperature
LLPS	Liquid-liquid phase separation
MBP	Maltose-binding protein
MLO	Membrane-less organelle
MS	Mass spectrometry
NES	Nuclear export sequence
NLS	Nuclear localization sequence
NMR	Nuclear magnetic resonance
NTD	N-terminal domain
o/n	overnight
PEG	Polyethylene glycol
PBS	Phosphate-buffered saline
PML-NB	Promyelocytic leukemia nuclear body
PRD	Prion-like domain
PTM	Post-translational modifier
RBR	RING between RING
RING	Really interesting new gene
RNA	Ribonucleic acid
RNP	Ribonucleoprotein
RRM	RNA recognition motif
RT	Room temperature
SCM	SUMO consensus motif
SDS-PAGE	Sodium dodecyl sulfate polyacrylamide gel electrophoresis
SEC	Size-exclusion chromatography
SDM	Site-directed mutagenesis
SENP	Sentrin-specific protease

SG	Stress granules
SIM	SUMO interaction motif
SPR	Surface plasmon resonance
STUbL	SUMO-targeted ubiquitin ligase
SUMO	Small ubiquitin-like modifier
TB	Terrific Broth
TDG	Thymine-DNA glycosylase
TDP-43	TAR DNA-binding protein 43
TEV	Tobacco etch virus
ThT	Thioflavin-T
Ub	Ubiquitin
UBD	Ubiquitin binding domain
UbL	Ubiquitin-like protein
UCST	Upper critical solution temperature
UHPLC	Ultra high-pressure liquid chromatography
UPS	Ubiquitin proteasome system
XL-MS	Crosslinking mass spectrometry
ZnF	Zinc finger

6.2 Supplementary data

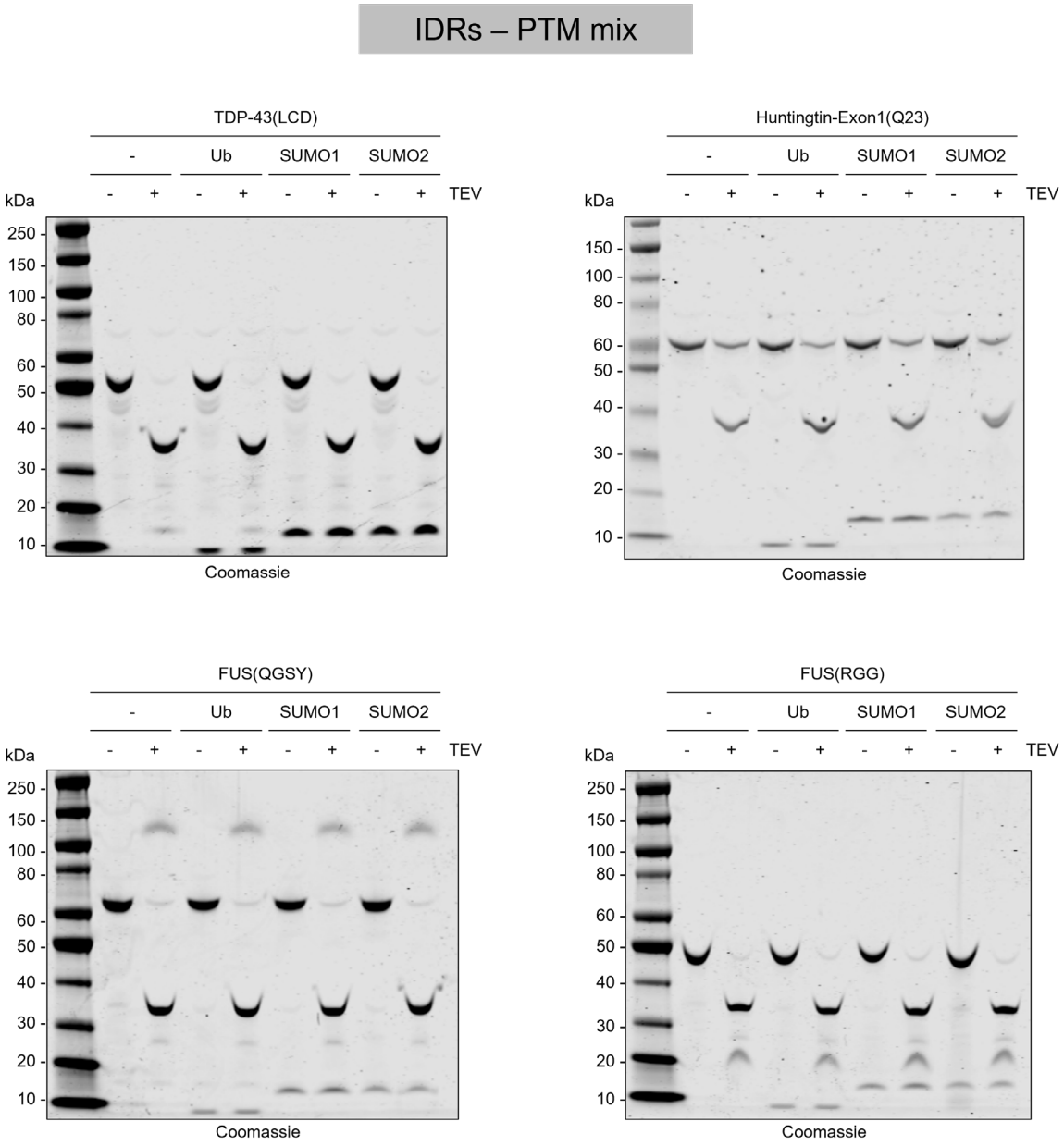

Appendix 1: Monitoring of IDR/modifier mix cleavage reactions. TEV-protease induced removal of MBP from IDRs mixed with ubiquitin, SUMO1 or SUMO2 was induced by the addition of TEV-protease. Reactions were analyzed by SDS-PAGE and Coomassie-staining.

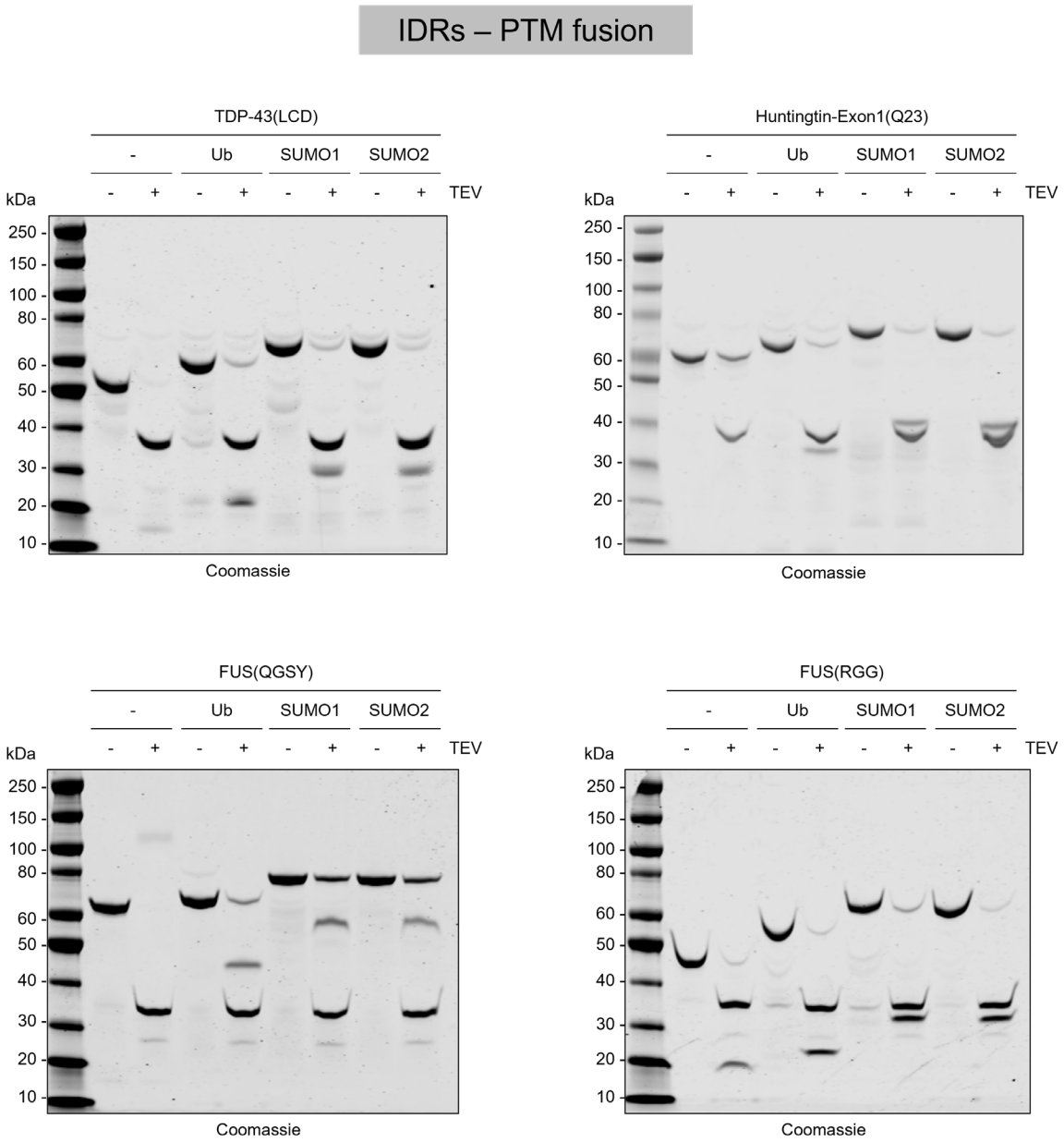

Appendix 2: Monitoring of IDR/modifier fusion cleavage reactions. TEV-protease induced removal of MBP from IDRs fused to ubiquitin, SUMO1 or SUMO2 was induced by the addition of TEV-protease. Reactions were analyzed by SDS-PAGE and Coomassie-staining.

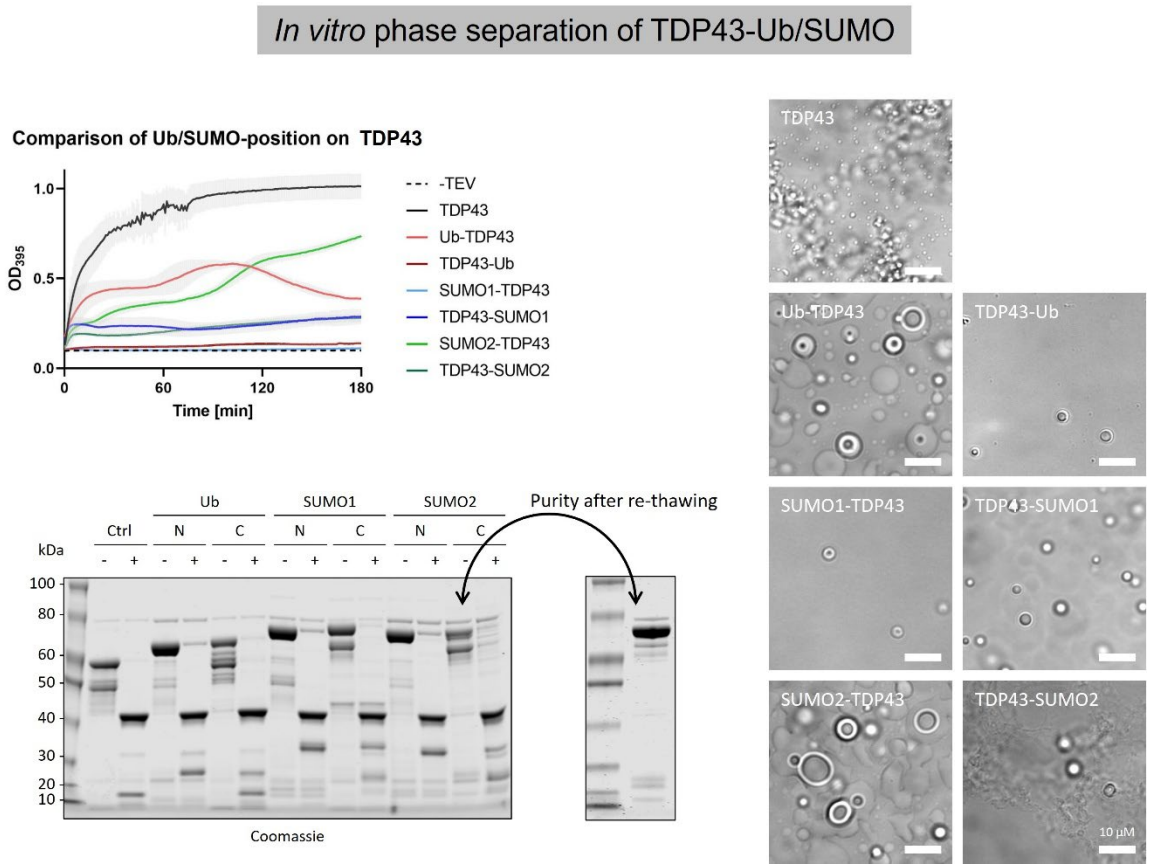

Appendix 3: In vitro phase separation of C-terminal Ub/SUMO fusions with TDP-43(LCD). Turbidity assay and exemplary DIC microscopy images of TDP-43(LCD)-Ub/SUMO after TEV-induced removal of MBP. Cleavage reactions were analyzed by SDS-PAGE and Coomassie-staining. The gel image on the bottom right shows the purity of all pooled fractions after the purification of TDP-43(LCD)-SUMO2-MBP.

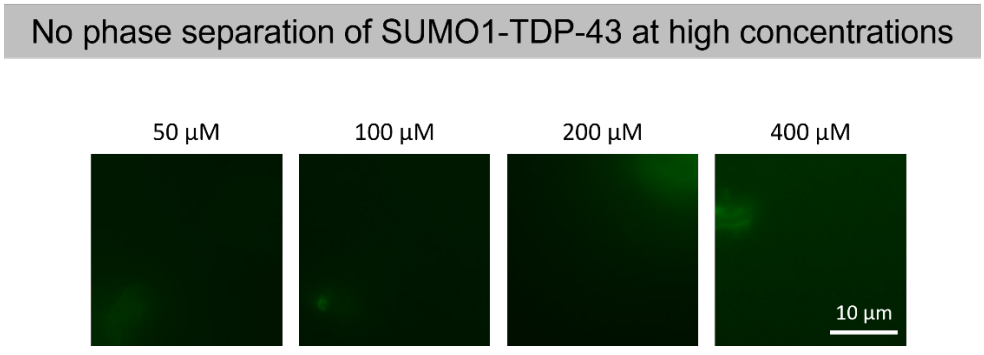

Appendix 4: Concentration-dependent inhibition of phase separation by SUMO1-TDP-43(LCD). Exemplary fluorescence microscopy images of different concentrations of AzDye488-labeled SUMO1-TDP-43(LCD) after TEV-induced removal of MBP.

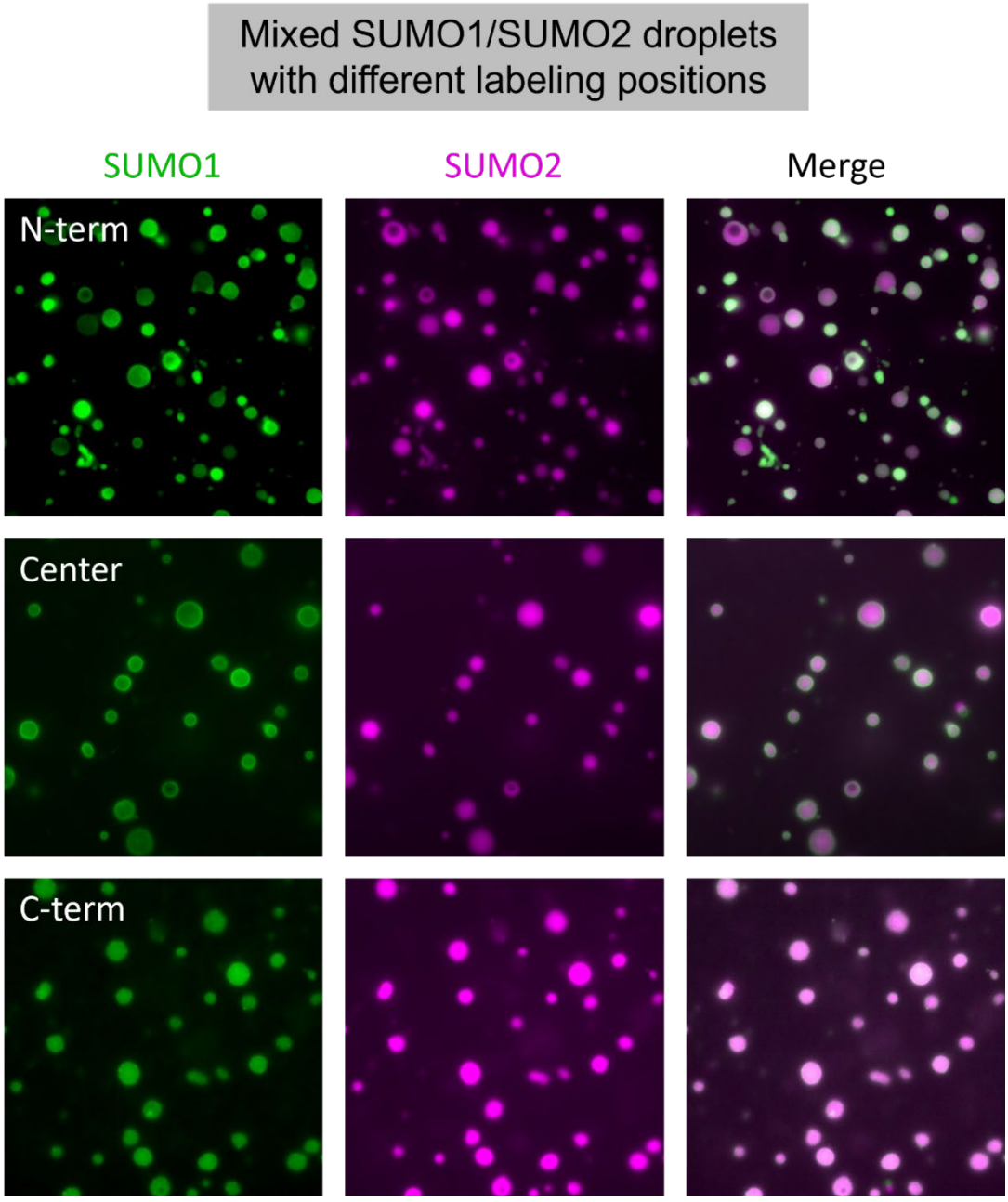

Appendix 5: Mixed condensates of site-specific AzDye488-labeled SUMO1- and Atto594-labeled SUMO2-TDP-43(LCD). SUMO1-TDP-43(LCD) was labeled with AzDye488 either at N-terminus, center or C-terminus and mixed 1:9 with Atto594-labeled SUMO2-TDP-43(LCD). Exemplary fluorescence microscopy images after TEV-induced removal of MBP, as similarly used for the FRET-AB experiment in **chapter 3.3.1**.

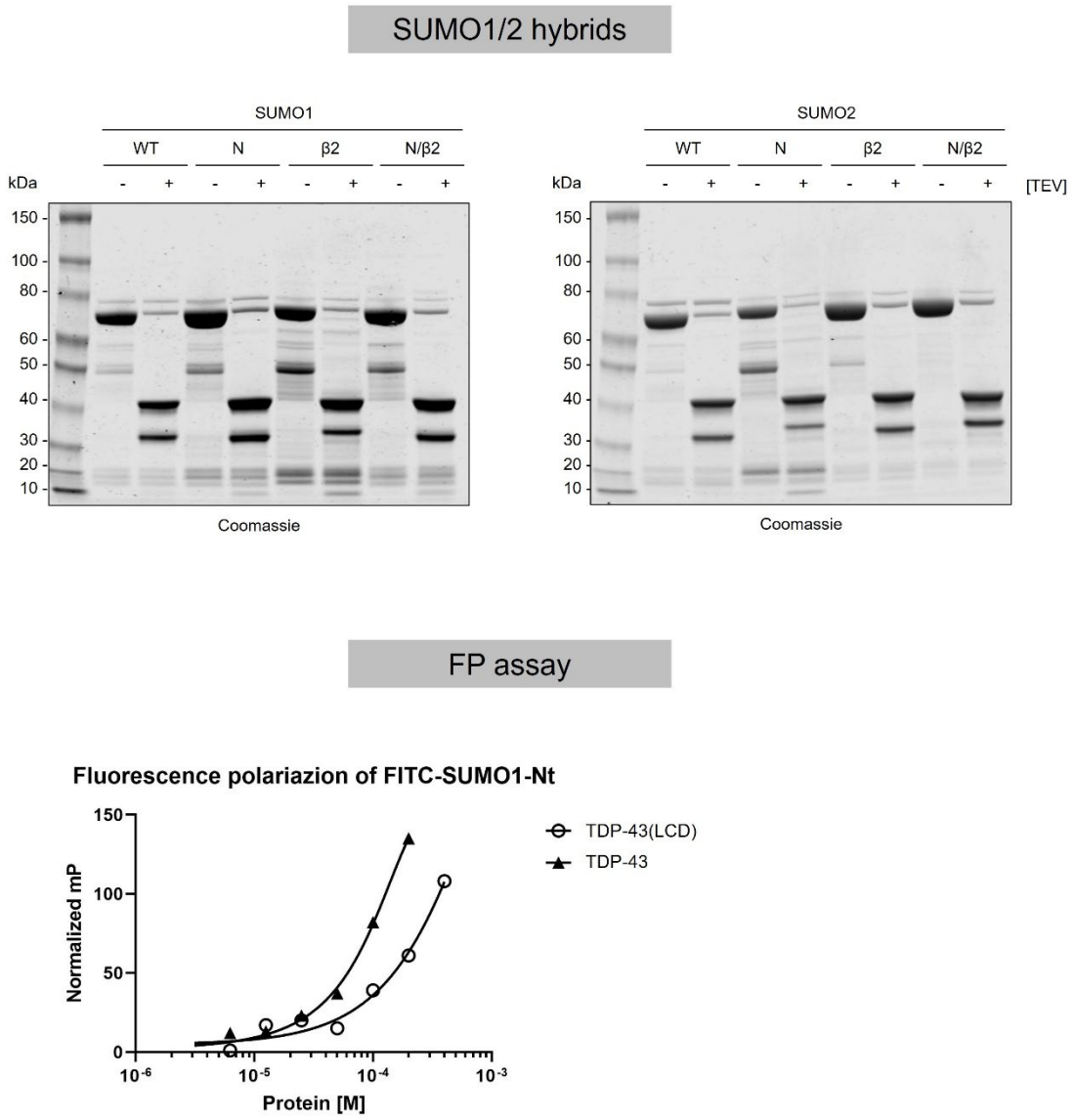

Appendix 6: Monitoring of chimeric SUMO-TDP-43(LCD) cleavage reactions and FP assay of TDP-43 and SUMO1 N-terminal peptide. (Upper) TEV-protease induced removal of MBP SUMO-TDP-43(LCD) with hybridized SUMO elements was induced by the addition of TEV-protease. Reactions were analyzed by SDS-PAGE and Coomassie-staining. (Lower) Fluorescence polarization of 5 nM FITC-SUMO1(N-terminus) in the presence of different concentrations of TDP-43(LCD)-MBP and full-length TDP-43-MBP.

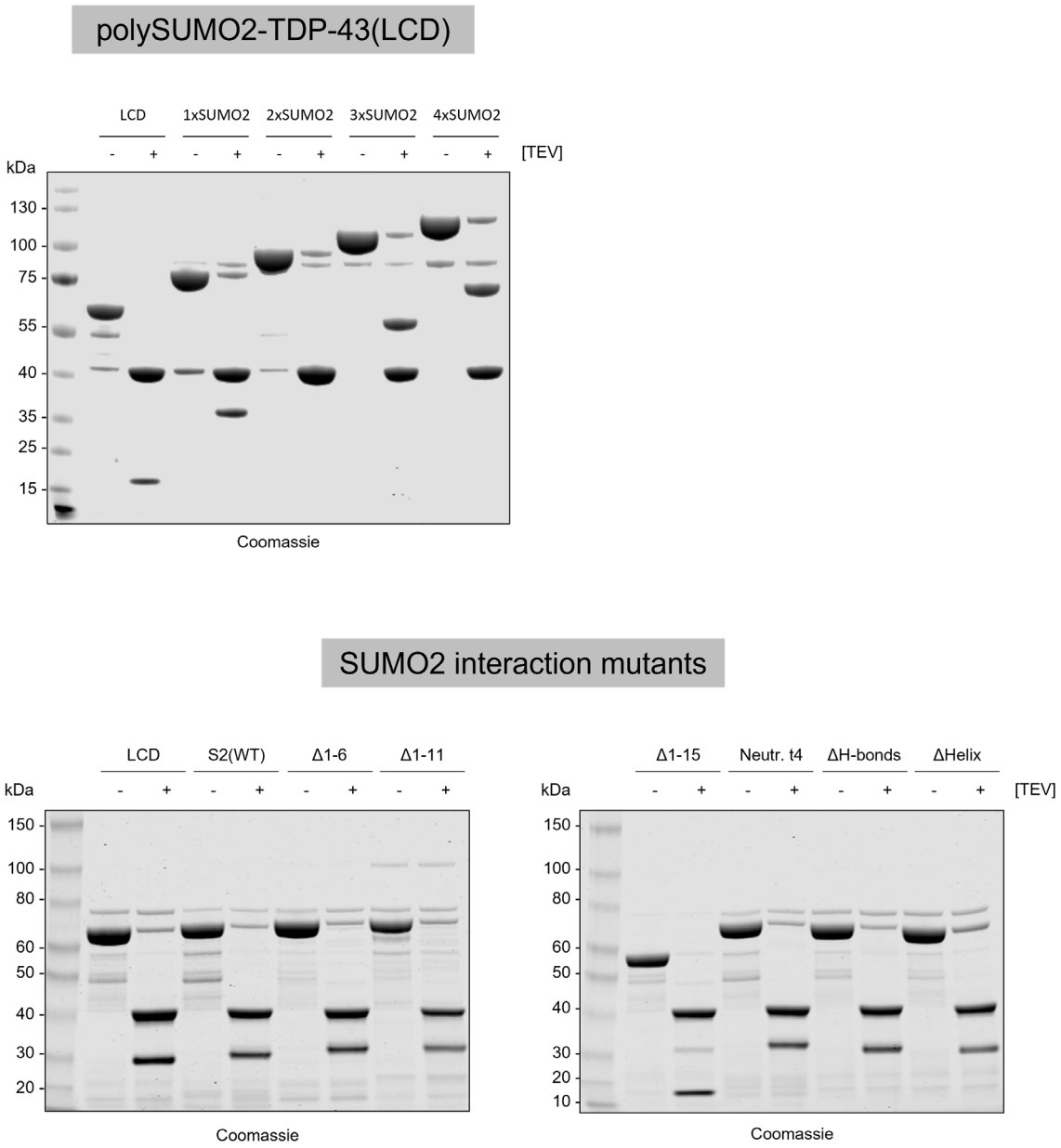

Appendix 7: Monitoring of polySUMO-TDP-43(LCD) and interaction-deficient SUMO2-TDP-43(LCD) cleavage reactions. TEV-protease induced removal of MBP from various mutated SUMO2-TDP-43(LCD) constructs was induced by the addition of TEV-protease. Reactions were analyzed by SDS-PAGE and Coomassie-staining.

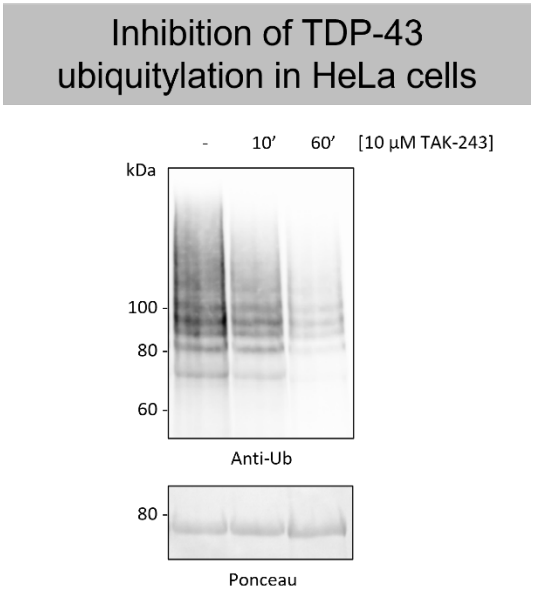

Appendix 8: Inhibition of TDP-43 ubiquitylation via TAK-243. HeLa cells transiently overexpressing His-TDP-43-EGFP were treated with 10 µM TAK-243 for the indicated time. Ubiquitylation was analyzed by denaturing NiNTA-pulldowns and western blotting.

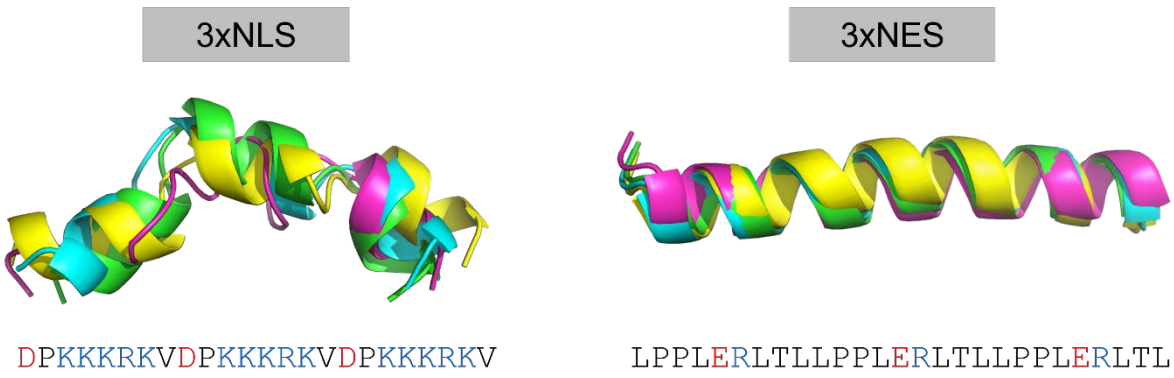

Appendix 9: AlphaFold3 simulations of cellular localization tags. Four models of each 3xNLS and 3xNES are shown in a carton representation with their respective query sequence.

Overexposure of Western-Blot in Figure 23 D

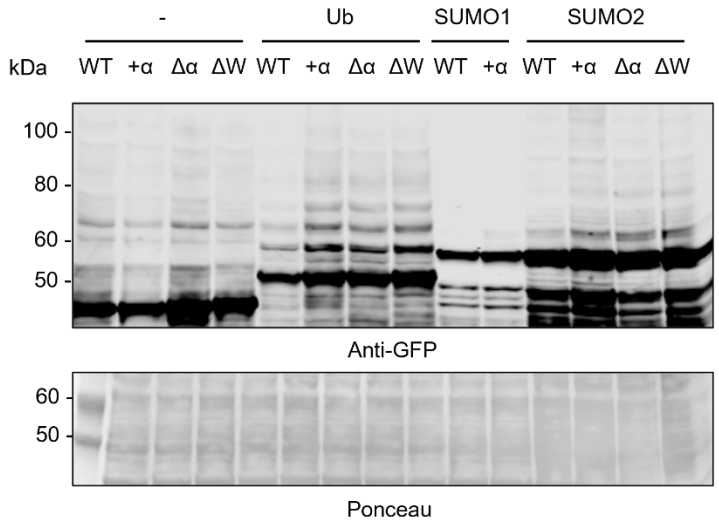

Appendix 10: PTM-patterns on overexpressed LLPS mutants of TDP-43(LCD). Alternative representation of the western blot showed in **Figure 23** D with increased contrast.